

Neural Network Based Adaptive Control for Nonlinear Dynamic Regimes

A Thesis
Presented to
The Academic Faculty

by

Yoonghyun Shin

In Partial Fulfillment
of the Requirements for the Degree
Doctor of Philosophy

George W. Woodruff School of Mechanical Engineering
Georgia Institute of Technology
December 2005

Copyright © 2005 by Yoonghyun Shin

Neural Network Based Adaptive Control for Nonlinear Dynamic Regimes

Approved by:

Dr. Nader Sadegh, Committee Chair
School of Mechanical Engineering
Georgia Institute of Technology

Dr. Anthony J. Calise, Co-Advisor
School of Aerospace Engineering
Georgia Institute of Technology

Dr. Wayne J. Book
School of Mechanical Engineering
Georgia Institute of Technology

Dr. J.V.R. Prasad
School of Aerospace Engineering
Georgia Institute of Technology

Dr. Kok-Meng Lee
School of Mechanical Engineering
Georgia Institute of Technology

Date Approved November 23, 2005

To my lovely wife, Hyunjeong

ℰ

my two sons, Mincheorl (Andy) and Woocheorl (Danny).

ACKNOWLEDGEMENTS

First I would like to thank Dr.Calise. He has let me have the chance to study for a Ph.D degree at Georgia Institute of Technology, guided my research, and supported me for last five years. I even got a nickname, "John", from him. He encouraged and helped me to overcome difficulties that I faced with. I also thank Dr.Sadegh. He has encouraged and guided me to finish my studies, too. I have learned much from him about discrete-time neural networks and other related control techniques. I believe that I was really fortunate in that I have had two great advisors, Dr.Calise and Dr.Sadegh. Without their guidance I could not finish my studies for my Ph.D degree at Georgia Tech.

I would also like to thank my thesis committee members for their good comments and suggestions that improved my dissertation.

I am grateful to many other people with whom my school life at Georgia Tech became much more enjoyable and plentiful; my lab mates, Bong-Jun ("Jun") Yang, Matthew Johnson, Ramachandra Sattigeri, Ali Kutay, Nakwan Kim, Venketesh Madyastha, Konstantin Volyansky, Suresh Kannan, Suraj Unnikrishnan, and Dr.Naira Hovakimyan at Virginia Tech, Seung-Min Oh, Jincheol Ha, and Dongwon Jung in the control group of AE, Hungsun Son and Sangil Lee in ME, and many others not written here. I would like to specially thank Dr.Bong-Jun Yang for nice discussions, and Matthew Johnson for his kind helps for last years. I will remember all the wonderful moments when we shared with together for last five years.

I can not thank enough my families, my wife and two sons. They have always been encouraging me and have been the very source of all my vitality on the long journey for last five years. Without their love, patience and supports, I could not continue and finish my Ph.D degree at Georgia Tech.

TABLE OF CONTENTS

DEDICATION	iii
ACKNOWLEDGEMENTS	iv
LIST OF TABLES	ix
LIST OF FIGURES	x
SUMMARY	xiv
I INTRODUCTION	1
1.1 Neural Network-based Adaptive Control	1
1.2 Nonlinear Dynamic Inversion	3
1.3 Adaptive Flight Control Design Using Neural Networks	4
1.4 Contributions of Thesis	7
1.5 Thesis Outline	8
II ARTIFICIAL NEURAL NETWORKS	10
2.1 Radial Basis Function (RBF) Neural Networks	10
2.2 Single Hidden Layer (SHL) Neural Networks	15
III ADAPTIVE NONLINEAR DYNAMIC INVERSION CONTROL USING NEURAL NETWORKS	18
3.1 Input-Output Feedback Linearization and Nonlinear Dynamic Inversion	18
3.2 Reformulation of Dynamic Inversion Error	25
3.3 Parametrization using Neural Networks	28
3.3.1 RBF Neural Networks	28
3.3.2 SHL Neural Networks	29
3.4 Nonlinear System and its Reference Model	31
3.5 Adaptive NDI Control Architecture	33
3.6 Linear Observer for the Error Dynamics	35
3.7 Stability Analysis using Lyapunov Theorems	35
3.7.1 RBF NN Adaptation	37

3.7.2	SHL NN Adaptation	39
3.8	Conclusion	41
IV	NEURAL NETWORK-BASED ADAPTIVE CONTROL OF F-15 AC-	
	TIVE AT NONLINEAR FLIGHT REGIMES	42
4.1	Introduction	42
4.2	Aircraft Model and Control Effectors	44
4.3	High Alpha Aerodynamics	46
4.3.1	Unsteady Aerodynamics	47
4.3.2	Lateral/Directional Aerodynamics at High-Alpha	48
4.4	Adaptive Control Structure	48
4.4.1	Two-stage Dynamic Inversion	49
4.4.2	Control Allocation with TV and DT	53
4.4.3	Thrust Vector Scheduling	54
4.4.4	Computation of the Effective Control (\mathbf{u}_e)	56
4.4.5	Adaptive Control	56
4.4.6	Pseudo-Control Hedging (PCH)	57
4.4.7	Neural Network Adaptation	57
4.5	Simulations	59
4.5.1	Control Design Parameters	59
4.5.2	Simulations and Evaluations	62
4.6	Conclusion	65
V	A COMPARISON STUDY OF CLASSICAL AND NEURAL NETWORK-	
	BASED ADAPTIVE CONTROL OF AIRCRAFT WING ROCK	76
5.1	Introduction	76
5.2	Aircraft Wing Rock Dynamics	77
5.3	Classical Adaptive Control	79
5.4	Adaptive Augmentation of a Linear Control Law	80
5.5	Simulation Results	83
5.5.1	Adaptive Controller Designs	84

5.5.2	Comparisons	85
5.5.3	Remarks on Stability	87
5.6	Conclusion	88
VI	ADAPTIVE AUTOPILOT DESIGNS FOR AN UNMANNED AERIAL VEHICLE, FQM-117B	96
6.1	Introduction	96
6.2	The UAV, FQM-117B	98
6.3	Control Design 1: Two-Stage Dynamic Inversion Based Adaptive Control Design	98
6.3.1	Two-stage Dynamic Inversion	100
6.3.2	Computation of the Control	101
6.3.3	Control Architecture	102
6.4	Control Design 2: Command Augmentation Based Adaptive Control Design	102
6.4.1	Outer-Loop Controller	103
6.4.2	Command Filter (Reference Model)	103
6.4.3	Dynamic Compensator and Control	103
6.4.4	Output Feedback Design	106
6.5	Pseudo-Control Hedging (PCH)	107
6.6	Neural Network Adaptation	108
6.7	Simulations	109
6.7.1	Model of Atmospheric Turbulence	109
6.7.2	Control Design 1: Two-Stage Dynamic Inversion Based Adaptive Control Design	110
6.7.3	Control Design 2: Command Augmentation Based Adaptive Control Design	111
6.8	Conclusion	114
VII	COMPOSITE MODEL REFERENCE ADAPTIVE OUTPUT FEED- BACK CONTROL OF MULTI-INPUT MULTI-OUTPUT NONLINEAR SYSTEMS USING NEURAL NETWORKS	131
7.1	Introduction	131

7.2	Control Problem Formulation	132
7.3	Input-Output Feedback Linearization and Nonlinear Dynamic Inversion . .	134
7.4	Nonlinear System and its Reference Model	137
7.5	Composite Adaptive Control Architecture	138
7.6	The System State Estimator	142
7.7	Stability Analysis using Lyapunov Theorems	142
	7.7.1 Composite RBF NN Adaptation	143
	7.7.2 Composite SHL NN Adaptation	146
7.8	Simulations and Evaluations	148
	7.8.1 Control Design Parameters	148
	7.8.2 Simulation Results	150
7.9	Conclusions	152
VIII	CONCLUSIONS	163
8.1	Future Research	164
	8.1.1 Relaxation of Assumption 7.2.3	164
	8.1.2 Relaxation of Assumption 7.4.1	164
APPENDIX A	— PROOF OF THEOREM 3.7.1	166
APPENDIX B	— PROOF OF THEOREM 3.7.2	169
APPENDIX C	— PROOF OF THEOREM 7.7.1	172
APPENDIX D	— PROOF OF THEOREM 7.7.2	175
APPENDIX E	— AIRCRAFT EQUATIONS OF MOTION	178
REFERENCES	190
VITA	200

LIST OF TABLES

1	F-15 ACTIVE neural network parameters	61
2	F-15 ACTIVE control effectors and their dynamic constraints	62
3	FQM-117B neural network parameters for Design 1	110
4	FQM-117B neural network parameters for Design 2	112
5	Neural network parameters for F-15 ACTIVE simulation	150
6	Adaptation gains for adaptive dynamic compensators	150

LIST OF FIGURES

1	Modern nonlinear maneuvers at highly nonlinear flight regimes	6
2	Radial Basis Function (RBF) Neural Network	13
3	Single Hidden Layer (SHL) Neural Network	14
4	Aircraft axis system and definitions	20
5	Adaptive nonlinear dynamic inversion control design architecture	24
6	Geometric representation of sets in the error space	37
7	NASA F-15 ACTIVE and its control effectors	45
8	Thrust vectoring angle limit and priority	47
9	Three dominant lateral/directional aerodynamic damping coefficients	48
10	Adaptive feedback control architecture	49
11	Two-stage dynamic inversion control law structure	50
12	Shape of thrust vector scheduling variables	55
13	Actuator estimator	58
14	Reference model with hedging in pitch channel	58
15	Structure of a second order relative degree pitch channel linear controller	60
16	Discretized control simulation environment in Matlab/Simulink	63
17	Aircraft α responses for a high α command with/without NN adaptation	66
18	Aircraft P_s and β responses for a high α command with/without NN adaptation	67
19	Aerodynamic control deflections for a high α command with/without NN adaptation	68
20	Thrust vector controls with/without NN adaptation	69
21	NN adaptation signal $\nu_{ad}(t)$ and $\Delta(t)$ in pitch, roll, and yaw channels	70
22	Aircraft α responses for α/p_s command with/without NN adaptation	71
23	Aircraft P_s and β responses for α/p_s command with/without NN adaptation	72
24	Aerodynamic control deflections for α/p_s command with/without NN adaptation	73
25	Thrust vector controls for α/p_s command with/without NN adaptation	74

26	NN adaptation signal $\nu_{ad}(t)$ and $\Delta(t)$ in pitch, roll, and yaw channels for α/p_s command	75
27	Three Adaptive Control Methods	79
28	Augmenting adaptive control architecture	81
29	Open loop system dynamics for the two initial conditions	84
30	Comparison of responses for a small initial condition	89
31	Comparison of classical adaptive and NN-based designs with σ -mod. for a small initial condition	89
32	Comparison of classical adaptive and NN-based designs with σ -mod. for a large initial condition	90
33	Gaussian basis functions for N=25	90
34	The effect that the number of RBF units has on the response for a small initial condition	91
35	The effect that the number of SHL neurons has on the response for a small initial condition	91
36	Responses for a square wave command	92
37	Comparison of ' $\Delta(t^*) - \nu_{ad}(t^*)$ '	92
38	3-dimensional view of ν_{ad} of SHL NN tracking Δ for a sinusoidal command	93
39	Final stage of σ - and e -modification responses to an initial condition for a zero command	94
40	σ - and e -modification responses of SHL NN for a step command of $\phi_c = -10$ degrees	94
41	e -modification response of RBF NN for a step command of $\phi_c = -10$ degrees	95
42	Projection responses for a step command of $\phi_c = -10$ degrees.	95
43	FQM-117B UAV	99
44	Adaptive feedback control architecture	100
45	Two-stage dynamic inversion control law structure	100
46	Command augmentation based adaptive control design using neural networks	104
47	Actuator estimator	108
48	Reference model with hedging in pitch channel	108
49	Aircraft responses for an α -command with/without NN adaptation	115

50	Aerodynamic control deflections	116
51	NN adaptation signal $\nu_{ad}(t)$ and $\Delta(t)$	116
52	Aircraft responses for a p_s -command with/without NN adaptation	117
53	Aerodynamic control deflections	118
54	NN adaptation signal $\nu_{ad}(t)$ and $\Delta(t)$	118
55	Aircraft responses for a normal acceleration (a_n) command using state feedback with/without NN adaptation	119
56	Pitch rate, q and yaw rate, r	120
57	Angle of attack and sideslip angle	120
58	Aerodynamic control deflections	121
59	NN adaptation signal $\nu_{ad}(t)$ and $\Delta(t)$	121
60	Aircraft responses for a roll rate (p) command using state feedback with/without NN adaptation	122
61	Pitch rate, q and yaw rate, r	123
62	Angle of attack and sideslip angle	123
63	Aerodynamic control deflections	124
64	NN adaptation signal $\nu_{ad}(t)$ and $\Delta(t)$	124
65	Aircraft responses for a normal acceleration (a_n) command using output feedback with/without NN adaptation	125
66	Pitch Rate, q and Yaw Rate, r	126
67	Angle of attack and sideslip angle	126
68	Aerodynamic control deflections	127
69	NN adaptation signal $\nu_{ad}(t)$ and $\Delta(t)$	127
70	Aircraft responses for a roll rate (p) command using output feedback with/without NN adaptation	128
71	Pitch rate, q and yaw rate, r	129
72	Angle of attack and sideslip angle	129
73	Aerodynamic control deflections	130
74	NN adaptation signal $\nu_{ad}(t)$ and $\Delta(t)$	130
75	Composite model reference adaptive control architecture	141

76	Geometric representation of sets in the error space	144
77	NASA F-15 ACTIVE in flight	149
78	Aircraft responses for a high α command with Adaptive NDI and Composite adaptive control	153
79	Aerodynamic control deflections for a high α command with Adaptive NDI and Composite adaptive control	154
80	Thrust vector controls with Adaptive NDI and Composite adaptive control .	155
81	NN adaptation signal $\boldsymbol{\nu}_{ad}(t)$ and $\boldsymbol{\Delta}(t)$ in each channel with Adaptive NDI and Composite adaptive control	156
82	Time history of adaptive DC gains \hat{K}_e, \hat{K}_r in each channel of Composite adaptive control	157
83	Aircraft responses for a high α command with Adaptive NDI and Composite adaptive control	158
84	Aerodynamic control deflections for a high α command with Adaptive NDI and Composite adaptive control	159
85	Thrust vector controls with Adaptive NDI and Composite adaptive control .	160
86	NN adaptation signal $\boldsymbol{\nu}_{ad}(t)$ and $\boldsymbol{\Delta}(t)$ in each channel with Adaptive NDI and Composite adaptive control	161
87	Time history of adaptive DC gains \hat{K}_e, \hat{K}_r in each channel of Composite adaptive control	162

SUMMARY

Adaptive control designs using neural networks (NNs) based on dynamic inversion are investigated for aerospace vehicles which are operated at highly nonlinear dynamic regimes. NNs play a key role as the principal element of adaptation to approximately cancel the effect of inversion error, which subsequently improves robustness to parametric uncertainty and unmodeled dynamics in nonlinear regimes.

An adaptive control scheme previously named 'composite model reference adaptive control' is further developed so that it can be applied to multi-input multi-output output feedback dynamic inversion. It can have adaptive elements in both the dynamic compensator (linear controller) part and/or in the conventional adaptive controller part, also utilizing state estimation information for NN adaptation. This methodology has more flexibility and thus hopefully greater potential than conventional adaptive designs for adaptive flight control in highly nonlinear flight regimes. The stability of the control system is proved through Lyapunov theorems, and validated with simulations.

The control designs in this thesis also include the use of 'pseudo-control hedging' techniques which are introduced to prevent the NNs from attempting to adapt to various actuation nonlinearities such as actuator position and rate saturations. Control allocation is introduced for the case of redundant control effectors including thrust vectoring nozzles. A thorough comparison study of conventional and NN-based adaptive designs for a system under a limit cycle, wing-rock, is included in this research, and the NN-based adaptive control designs demonstrate their performances for two highly maneuverable aerial vehicles, NASA F-15 ACTIVE and FQM-117B unmanned aerial vehicle (UAV), operated under various nonlinearities and uncertainties.

CHAPTER I

INTRODUCTION

1.1 Neural Network-based Adaptive Control

Artificial neural networks (NNs) are any computing architecture that consists of massively parallel interconnections of simple computing elements. NNs have been implemented in various fields such as system identification and control, image processing, speech recognition, etc. The fundamental and core property of NNs for their superiority over other approximation methods is based on the fact that NNs are able to universally approximate smooth but otherwise arbitrary nonlinear functions on a wide range of complex nonlinear functions on a compact set, using fewer parameters and requiring less computation time. This property was proved and demonstrated in the late 80's and early 90's [20, 24, 28, 95, 96, 98].

In the 80's important results that guarantee the closed-loop stability of adaptive control were presented [74, 79, 80]. Since that time a great deal of progress has been made in the area of adaptive control. Stability analysis of adaptive control design involves the use of Lyapunov stability theory [41, 43, 107, 123], along with LaSalle's theorem which allows less restrictive conditions [52, 53]. Among the suggested adaptation laws, two methods will be discussed in this thesis: σ -modification, introduced by Ioannou and Kokotovic [33] to prevent instability and to improve robustness, and e -modification, suggested by Narendra and Annaswamy [77, 78] to eliminate the need for the persistent excitation (PE) condition in stability analysis of adaptive systems. There has also been a great deal of literature treating advanced topics related to stability analysis and other aspects of adaptive control [3, 34, 43, 77, 100, 115].

Usually adaptive control methodologies are categorized into two classes: direct and indirect. In direct adaptive control, the parameters defining the controller rather than describing

the system itself are updated directly, while indirect adaptive control relies on *on-line* identification of plant parameters with an assumption that a suitable controller is implemented. Robustness to disturbances and unmodeled dynamics is one of main goals of adaptive control system design, leading to the introduction of several methods, some of which are: parameter projection techniques [76] and backstepping to improve robustness of adaptive nonlinear controllers [124].

For nonlinear control design, several novel approaches have been introduced. One approach is known as feedback linearization which depends on nonlinear transformation techniques and differential geometry [36,37,42,43,99,100]. In this approach, the nonlinear dynamics are first transformed into a linear, time-invariant form through the definition of the state and control of the nonlinear system. The transformed linear system can then be treated using well known methods for linear control design. Another approach is backstepping [47–49]. This approach employs Lyapunov function to recursively determine nonlinear controls for nonlinear systems. For NN-based adaptive control of nonlinear systems, we employ the first approach in this thesis.

In recent decades, there have been research efforts to implement neural nets as adaptive elements in nonlinear adaptive control designs to achieve desired system performance using NN's guaranteed universal approximation ability which offers outstanding advantages over most other conventional linear parameter adaptive controllers [27,62,84,97,119]. In the early 90's, Narendra studied identification and control of linear and nonlinear Dynamical Systems using NNs [81–83]. Lewis *et al.* studied a state feedback linearly parameterized NN adaptive controller [60] and later studied multi-layer NN structures with improved update laws [61,62]. Recently, Hovakimian and Calise *et al.* developed Single-Hidden-Layer (SHL) NN-based adaptive output feedback control of uncertain nonlinear systems through Lyapunov's direct method by building an observer for the output tracking error, assuming both the dynamics and the dimension of the regulated system may be unknown, while the relative degree of the regulated output is assumed to be known [29]. In addition, they developed an adaptive

output feedback control methodology for multi-input multi-output nonlinear systems using linearly parameterized NNs [30]. All the applications using neural networks have shown remarkable results in areas such as robotics, process control and flight control. Therefore NNs are becoming the leading method of adaptive control design in various fields.

Composite adaptive control design was introduced by Slotine and Li [107], in which the adaptation law is a combination of the classical adaptation law and a prediction/estimation-error-based adaptation law. They showed that for a simple system, composite design improves the performance of an adaptive controller and results in a faster parameter convergence and smaller tracking errors. A class of conventional adaptive control design based on the form of the linear controller, assuming what is referred to as matching conditions, is introduced and developed in [34, 77, 114] for known- or unknown-parameter systems. In this thesis both the composite and linear controller-based adaptive designs are synthesized and analyzed for multi-input multi-output (MIMO) output feedback control of uncertain systems with external disturbance, and applied to the problem of flight control in nonlinear dynamic regimes.

1.2 Nonlinear Dynamic Inversion

Flight control law design methods have evolved immensely due to advances in both hardware and theoretical development over the past decades. They have progressed from very simple fixed-feedback structures for providing stability augmentation to complicated multi-variable feedback laws with the help of modern well-organized design tools that optimally tune command responses, robustness characteristics, and disturbance responses of the final closed-loop airframe/controller integration. Recently control researchers have developed an advanced flight control design called nonlinear dynamic inversion (NDI) based on feedback linearization [10, 14, 23, 44, 51, 105, 109].

Conventional flight control designs assume the aircraft dynamics are linear and time invariant about some nominal flight condition, and they feature stability and command augmentation systems to meet required flying/handling qualities, with gains scheduled as

functions of nominal flight conditions. In extreme flight conditions the performance of these systems begins to deteriorate due to the unmodelled effects of strong nonlinearities inherent in the flight dynamics, which become significant at high angle of attack or high angular rates.

The chief advantage of the NDI methodology is that it avoids the gain-scheduling process of other methods, which is time consuming, costly, iterative, and labor intensive. The NDI technique offers greater reusability across different airframes, greater flexibility for handling changed models as an airframe evolves during its design cycle, and greater power to address non-standard flight regimes such as supermaneuver. Control laws based on NDI offer the potential for providing improved levels of performance over conventional flight control designs in these extreme flight conditions. This is due to the NDI controllers' more accurate representation of forces and moments that arise in response to large state and control perturbations. These control laws also allow specific state variables to be commanded directly [23, 51]. Because of the superior performance of NDI methodology, many designs of modern, advanced aerospace vehicles are based on this technique.

Successful flight control designs using nonlinear dynamic inversions were developed in [21,44,51,72,91,116,122]. A two-time scale, or two-stage dynamic inversion approach has been widely applied for highly maneuverable fighter aircraft [1,6,9,10,73,92,105,109], missiles [102], and UAVs [104]. These studies demonstrated that nonlinear dynamic inversions is an effective method for highly maneuverable air vehicles. However, as noted by Brinker and Wise [6], dynamic inversion can be vulnerable to modeling and inversion errors. So NN-based adaptive control design can be introduced to compensate for the inversion errors, unmodeled dynamics and parametric uncertainty which are quite common in highly nonlinear regimes [14,104,105].

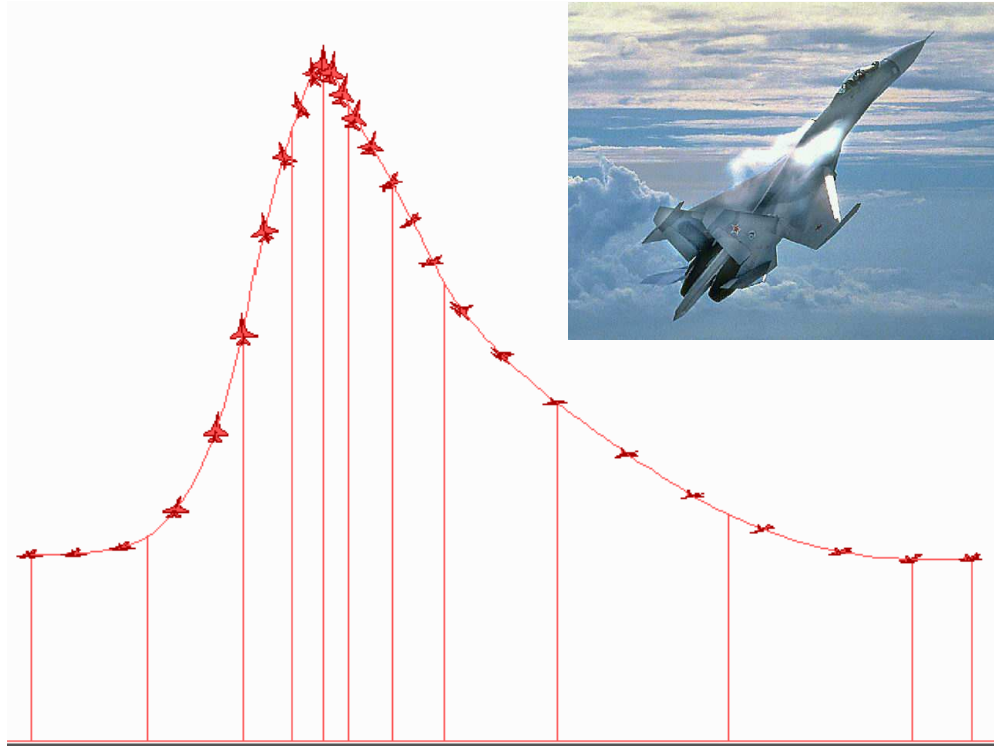
1.3 Adaptive Flight Control Design Using Neural Networks

Today newly emerging advanced aerial vehicles are extending their flight envelopes greatly over traditional flight regimes, leading to a need for substantially higher performance adaptive

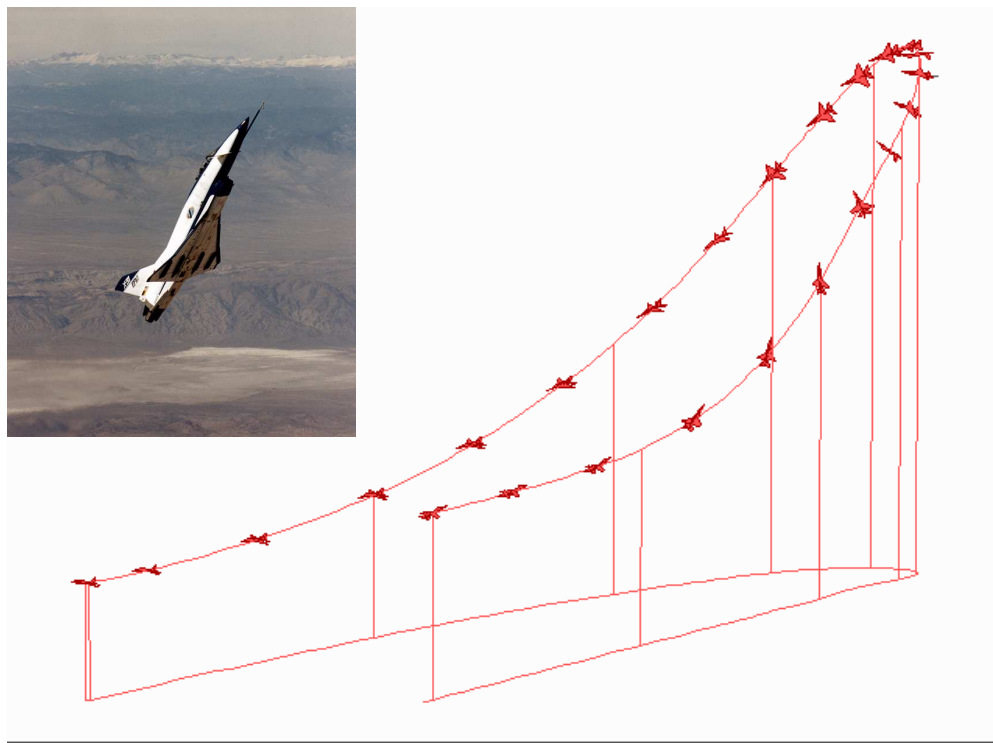
controls. Among these vehicles are the advanced supermaneuverable tactical fighters which are operated at extremely nonlinear dynamic regimes or at high angle of attack. At these flight conditions both unmodeled parameter variations and unmodeled vehicle dynamics such as nonlinear, unsteady aerodynamic effects, saturation of aerodynamic effectors and highly coupled vehicle dynamics occur. Two examples among such maneuvers are presented in Figure 1. Unconventionally configured aerial vehicles such as stealth fighters or bombers need more active controls to compensate for the unmodeled dynamic phenomena which possibly come from their unusual configurations themselves. These can potentially benefit from having adaptive elements in the control system. Other potential beneficiaries of these advanced control designs are unmanned aerial vehicles which are now rapidly extending their missions beyond target drone and air reconnaissance toward air combat and air-to-ground combat roles. These vehicles usually contain simpler and cheaper systems with substantially smaller mass compared to manned vehicles, and in addition minimal or no aerodynamic data are available for control design. Hence adaptive flight control systems should be designed to achieve required performance by dealing with uncertainties in the systems and environment. Newly emerging guided munitions may be classified in this category. There will therefore be a greater need for adaptive control design methods in the future, and NN-based designs are best suited for this purpose.

Stengel summarized and proposed intelligent flight control architectures including expert systems and procedural algorithms as well as neural networks [113]. Flight control design and improvement using NNs are described in [4, 93, 110–112, 117, 118]. Since the early 90's, lots of research has been performed for improving air vehicles' performance by designing control systems using neural networks. This research has included high performance fighters [26, 44, 56, 63, 64, 105], tailless aircraft [14, 122], missiles [67–71], tilt-rotor aircraft [94], UAVs [7, 13, 104], guided munitions [103], and helicopters [12, 15, 19, 57–59, 89].

Pseudo-control hedging (PCH) is a methodology to protect an NN's adaptive process when control nonlinearities such as actuator saturation and rate limits are present [38, 40].



(a) Su-27 Cobra Maneuver



(b) X-31 Herbst Maneuver

Figure 1: Modern nonlinear maneuvers at highly nonlinear flight regimes

NASA has performed a series of adaptive flight control studies since the 70's, and recently, NASA studied the verification and validation of neural networks for aerospace systems [66], and it has performed several research projects on intelligent adaptive flight control implementations which incorporate innovative real-time NN technologies to demonstrate NN's capability to enhance aircraft performance under nominal conditions and to stabilize the aircraft under various critical flight conditions [120]. Today NASA is still seeking further development of NNs for the purposes addressed above.

1.4 Contributions of Thesis

The research in this thesis is focused on NN-based adaptive control designs for systems at highly nonlinear dynamic regimes which have severe parametric uncertainties and disturbances. The contributions of the research can be summarized as:

- A new model reference adaptive control design methodology that combines the composite adaptive design and dynamic compensator-based adaptive design in addition to NN-based adaptive elements is developed for output feedback MIMO nonlinear systems, and its stability is proved through Lyapunov theorems. The performance is validated through simulations.
- NN-based model reference adaptive control design for nonlinear systems is introduced and stability is proved. The design was successfully implemented and demonstrated for an accurate nonlinear model of NASA F-15 ACTIVE (Advanced Control Technology for Integrated Vehicles), equipped with thrust vectored nozzles [16, 105], which is operated at extremely nonlinear dynamic regimes where there exist unmodeled parameter variations and unmodeled vehicle dynamics such as highly nonlinear, unsteady aerodynamic effects, saturation of aerodynamic effectors, and highly coupled vehicle dynamics [17, 105].

The pseudo-control hedging (PCH) technique was implemented to protect NN adaptation from various actuation nonlinearities such as actuator position and rate saturation, while not hindering the NN's adaptation to other sources of inversion error. Thrust vector and differential stabilator were added to the vehicle model to increase control authority at high angles of attack, and its static stability was relaxed in order to achieve greater pitch maneuverability. A control allocation methodology was introduced and implemented for effective operation of the redundant control effectors of F-15 ACTIVE.

- A thorough comparison study is performed on the performance of a classical adaptive control design and two different classes of neural networks: linearly parameterized Radial Basis Functional (RBF) NN and nonlinearly parameterized Single Hidden Layer (SHL) NN for stabilizing the unsteady lateral dynamics, or wing rock, of a delta wing [17, 18].
- A command augmentation-based adaptive control design using NNs is developed and implemented for a vehicle, FQM-117B UAV which is built with simple and inexpensive subsystems, having little aerodynamic data for control design. Its control system is designed to achieve high maneuverability without requiring accurate modeling of the vehicle, and the UAV's adaptive flight control design provides a way to deal with the uncertainties in the system and environment [104].

1.5 Thesis Outline

The thesis is organized as follows.

Chapter 2 presents structure and synthesis of linearly and nonlinearly parameterized neural networks which are used in the remaining chapters.

Chapter 3 illustrates adaptive nonlinear dynamic inversion control design for MIMO output feedback systems. Feedback linearization and inversion control of aircraft are discussed, and the stability of the closed-loop system is proved using Lyapunov theorems.

Chapter 4 presents a NN-based adaptive control design, based on the theoretical approach in Chapter 3, and application to a highly maneuverable aircraft, NASA F-15 ACTIVE, which has redundant control effectors including thrust vector nozzles. PCH technique is implemented in order to protect NN's adaptation from control nonlinearities of the actuators. To manage control redundancy, a control allocation scheme is applied along with a thrust vector scheduling algorithm. Simulation results validate the NN-based adaptive control design.

Chapter 5 describes a thorough comparison study of classical adaptive control design and two different NN-based adaptive control designs for an aircraft wing rock model at high angle of attack.

Chapter 6 presents an application of NN-based control design for a UAV, NASA FQM-117B, which is operated under several kinds of nonlinearities and uncertainties. A command augmentation based adaptive control design is developed for the vehicle, and simulation results show the effectiveness of the design.

Chapter 7 introduces the composite model reference adaptive control design and analysis for output feedback MIMO nonlinear systems, in which input-output feedback linearization and nonlinear dynamic inversion, and additional adaptive elements in both the dynamic compensator and the NN-based adaptive element are synthesized. The stability of the composite adaptive design is proved through Lyapunov theorems. The performances of the design are validated through simulations using F-15 ACTIVE.

Chapter 8 summarizes the results of all research efforts, and concludes the thesis along with some future research direction.

CHAPTER II

ARTIFICIAL NEURAL NETWORKS

Neural networks (NNs) have a well-proved property that they are able to approximate smooth nonlinear functions on a compact set to any desired degree of accuracy using a sufficiently large number of NN elements. Hence they are called universal approximators. This property has been proved and demonstrated since the late 80's [24, 27, 96, 98, 101]. For the purpose of adaptive control design, we can use the property of neural networks to approximate any continuous, unknown nonlinear functions, which we will call $\mathbf{f}(\mathbf{x})$.

The mathematical description of the approximation of $\mathbf{f}(\mathbf{x})$ by NNs can be written as:

$$\mathbf{f}(\mathbf{x}) = \mathbf{f}_{NN}(\mathbf{x}) + \boldsymbol{\varepsilon}(\mathbf{x}) \quad (2.0.1)$$

where $\mathbf{f}_{NN}(\mathbf{x})$ is the approximation of $\mathbf{f}(\mathbf{x})$ by any NN using its *ideal* weights and $\boldsymbol{\varepsilon}(\mathbf{x})$ is called the function approximation, or reconstruction error.

In this chapter, we introduce and discuss the mechanisms and structures of two representative classes of Neural networks which are used throughout this thesis. One is the Radial Basis Function (RBF) NNs which are also referred to as linearly parameterized NNs and the other is the Single Hidden Layer (SHL) NNs which is also referred to as nonlinearly parameterized NN. Both are feed-forward networks.

2.1 Radial Basis Function (RBF) Neural Networks

As noted earlier it is assumed that a nonlinear function is completely unknown to the control designer, and that there exists a set of NN weights such that the output $\boldsymbol{\nu}_{ad}(\mathbf{x})$ of an RBF NN approximates the function $\mathbf{f}(\mathbf{x})$. The following theorem describes the approximation for the RBF-class NNs.

Theorem 2.1.1 (Universal Approximation Theorem for RBF NN). *Let $\Psi(\mathbf{x}) : \mathfrak{R}^n \rightarrow \mathfrak{R}$ be an bounded integrable, continuous function; then for any continuous function $f(\mathbf{x})$ and any ε there is an RBF NN with N neurons, a set of centers $\{c_i\}_{i=1}^N$ and a width $\sigma > 0$, and*

$$\mathbf{f}_{NN}(\mathbf{x}) = \sum_{i=1}^N w_i \psi((\mathbf{x} - c_i)/\sigma) = W^T \Psi(\mathbf{x}) \quad (2.1.1)$$

such that

$$\|\mathbf{f}(\mathbf{x}) - \mathbf{f}_{NN}(\mathbf{x})\|_{L_2}^2 \triangleq \int_{\|\mathbf{x}\| \leq r} [\mathbf{f}(\mathbf{x}) - \mathbf{f}_{NN}(\mathbf{x})]^2 d\mathbf{x} \leq \varepsilon \quad (2.1.2)$$

Proof. See [87] □

A nonlinear function $\mathbf{f}(\mathbf{x}) : \mathfrak{R}^n \rightarrow \mathfrak{R}^m$ is assumed to be linearly parameterized by RBF NN over a sufficiently large compact region of interest $\mathcal{D}_x \subset \mathfrak{R}^n$ in the state space such that

$$\mathbf{f}(\mathbf{x}) = \boldsymbol{\nu}_{ad}(\mathbf{x}) + \boldsymbol{\varepsilon}(\mathbf{x}) \quad (2.1.3)$$

where

$$\nu_{ad_i}(\mathbf{x}) = w_{0,i} + \sum_{j=1}^N w_{i,j} \psi_j(\mathbf{x}) \quad i = 1, \dots, m \quad (2.1.4)$$

for all $\mathbf{x} \in \mathcal{D}_x$ and $\boldsymbol{\varepsilon}(\mathbf{x})$ is the function approximation error which is bounded as

$$\|\boldsymbol{\varepsilon}(\mathbf{x})\| \leq \varepsilon_m \quad (2.1.5)$$

where ε_m is a positive number. The radial basis functions of NNs are defined by

$$\psi_j(\mathbf{x}) = \exp(-\|\mathbf{x} - c_j\|^2 / \sigma_j^2), \quad j = 1, \dots, N \quad (2.1.6)$$

where $\|\cdot\|$ denotes the Euclidian norm and c_k and σ_k are the center and width of the k^{th} kernel unit, respectively. The functions in (2.1.6) are known as Gaussian basis functions.

The output of the RBF NNs is calculated according to

$$\boldsymbol{\nu}_{ad} = \hat{W}^T \Psi(\mathbf{x}) \quad (2.1.7)$$

where

$$\hat{W} = \begin{bmatrix} w_{0,1} & \cdots & w_{0,m} \\ w_{1,1} & \cdots & w_{1,m} \\ \vdots & \ddots & \vdots \\ w_{N,1} & \cdots & w_{N,m} \end{bmatrix} \in \mathfrak{R}^{(N+1) \times m} \quad (2.1.8)$$

$$\Psi(\mathbf{x}) = [1 \ \psi_1(\mathbf{x}) \ \psi_2(\mathbf{x}) \ \cdots \ \psi_N(\mathbf{x})]^T \in \mathfrak{R}^{N+1} \quad (2.1.9)$$

The NN weight matrix \hat{W} is an approximation of the ideal weight W which is unknown but bounded as

$$\|W\|_F \leq w_m \quad (2.1.10)$$

where $\|\cdot\|_F$ is the Frobenius norm and w_m is a positive number. Figure 2 depicts an RBF NN generating the control input given by (2.1.7). A proof that RBF NNs satisfy the universal approximation property described above is given in [87, 96, 98].

The adaptation law is chosen as:

$$\dot{\hat{W}} = -\Gamma \left[\mathbf{E}^T P B \Psi(\mathbf{x}) + \kappa \cdot (\hat{W} - W_0) \right] \quad (2.1.11)$$

or

$$\dot{\hat{W}} = -\Gamma \left[\mathbf{E}^T P B \Psi(\mathbf{x}) + \kappa \cdot \|\mathbf{E}\| \cdot (\hat{W} - W_0) \right] \quad (2.1.12)$$

where $\Gamma, \kappa > 0$ are adaptation gains, W_0 is an initial guess (or guess) of W , and P is a solution of the Lyapunov equation

$$A^T P + P A = -Q, \quad Q > 0 \quad (2.1.13)$$

The first form in (2.1.11) employs a so-called 'σ-modification' term, while the second form in (2.1.12) uses an 'e-modification' term [62, 78]. It is also noted that there are always NN approximation errors described as:

$$\begin{aligned} \mathbf{f}(\mathbf{x}) - \boldsymbol{\nu}_{ad} &= W^T \Psi(\mathbf{x}) - \hat{W}^T \Psi(\mathbf{x}) + \boldsymbol{\varepsilon}(\mathbf{x}) \\ &= \tilde{W}^T \Psi(\mathbf{x}) + \boldsymbol{\varepsilon}(\mathbf{x}) \end{aligned} \quad (2.1.14)$$

where $\tilde{W} = W - \hat{W}$ is NN estimation error.

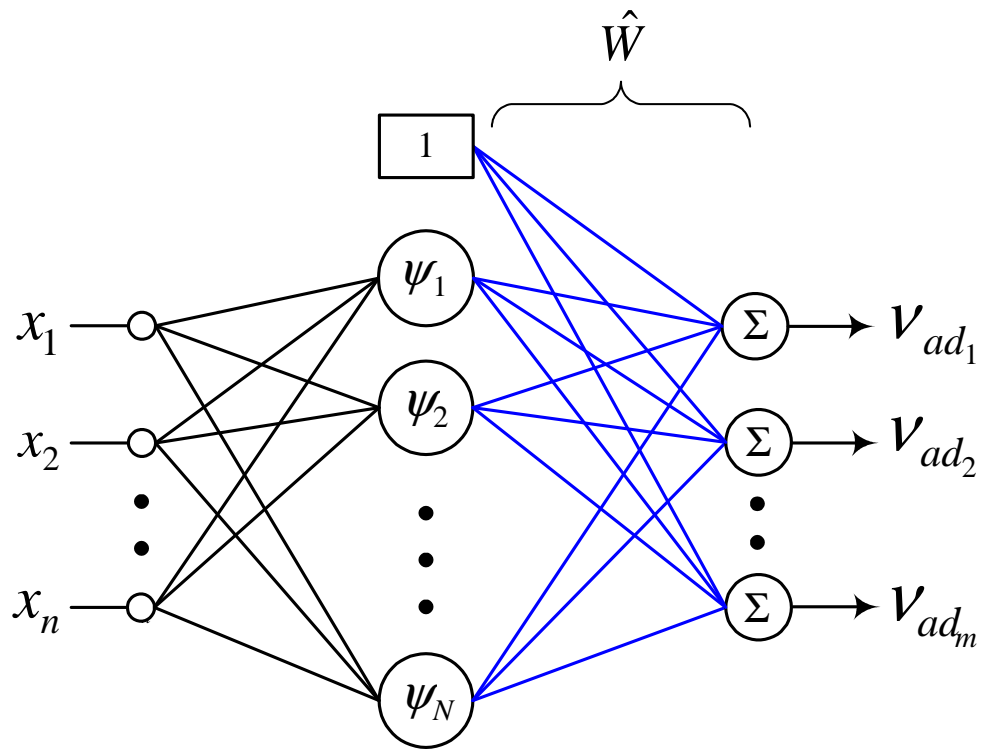


Figure 2: Radial Basis Function (RBF) Neural Network

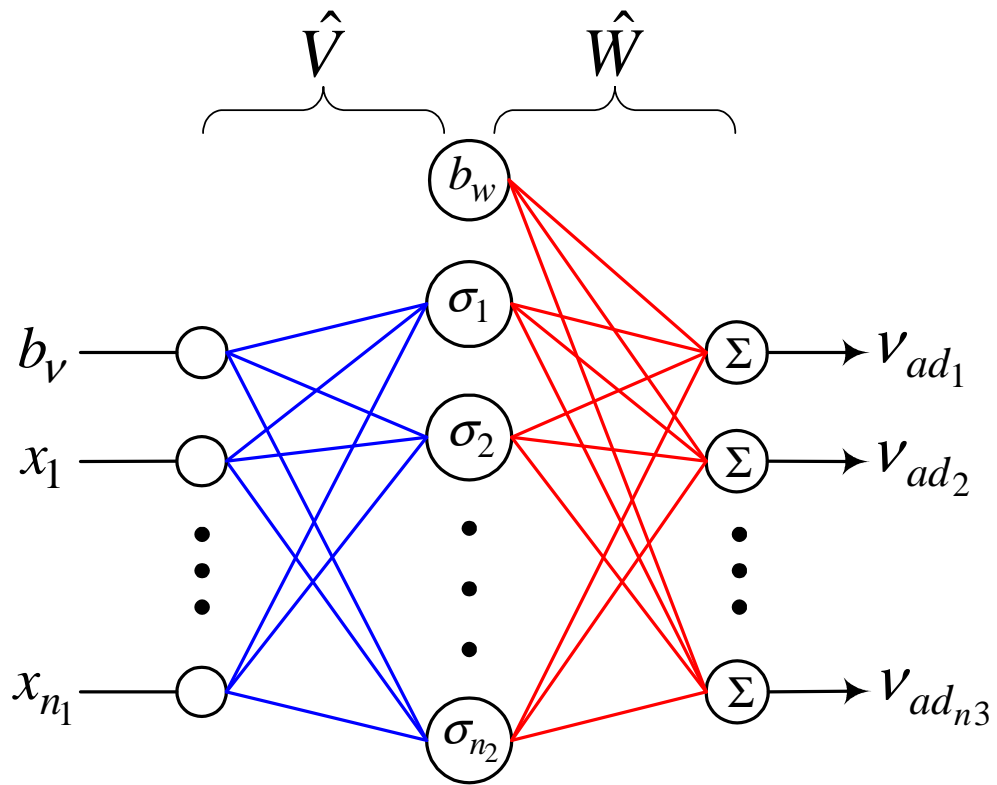


Figure 3: Single Hidden Layer (SHL) Neural Network

2.2 Single Hidden Layer (SHL) Neural Networks

Single Hidden Layer (SHL) Perceptron NNs are also universal approximators [27] in that they can approximate any smooth nonlinear function to within arbitrary accuracy, given a sufficient number of hidden layer neurons and sufficient input information. Figure 3 shows the structure of a generic SHL NN. Below is a theorem that describes the approximation of the SHL-class neural networks.

Theorem 2.2.1 (Universal Approximation Theorem for SHL NN). *Any continuous function $\mathbf{f}(\mathbf{x}) : \mathbb{R}^n \rightarrow \mathbb{R}$ can be uniformly approximated by a single hidden layer NN with a bounded monotonically increasing continuous activation function and on a compact domain $\mathcal{D}_x \in \mathbb{R}^n$; that is, for all $\varepsilon > 0$ and $x \in \mathcal{D}_x$, there exist N , W , V , b , and θ such that*

$$\|\mathbf{f}(\mathbf{x}) - \mathbf{f}_{NN}(\mathbf{x})\|_\infty \triangleq \|\mathbf{f}(\mathbf{x}) - \{W^T \bar{\sigma}(V^T \mathbf{x} + \theta) + b\}\|_\infty \leq \varepsilon \quad (2.2.1)$$

Proof. See [20] □

Similar to the RBF NN, the input-output map of SHL NN can be expressed as [61]

$$\nu_{ad_k} = b_w \theta_{w,k} + \sum_{j=1}^{n_2} w_{j,k} \sigma_j \quad (2.2.2)$$

where $k = 1, \dots, n_3$ and

$$\sigma_j = \sigma \left(b_w \theta_{v,j} + \sum_{i=1}^{n_1} v_{i,j} x_i \right) \quad (2.2.3)$$

Here n_1 , n_2 , and n_3 are the number of input nodes, hidden layer nodes, and outputs respectively. The scalar function $\sigma(\cdot)$ is a sigmoidal activation function that represents the 'firing' characteristics of the neuron. Typically, these basis functions are selected as squashing functions. A typical form employed is

$$\sigma(z) = \frac{1}{1 + e^{-az}} \quad (2.2.4)$$

The factor a is known as the activation potential, and can be a distinct value for each neuron.

The input-output map of the SHL NN in the controller architecture can be conveniently written in matrix form as

$$\boldsymbol{\nu}_{ad} = \hat{W}^T \overline{\boldsymbol{\sigma}} \left(\hat{V}^T \boldsymbol{\mu} \right) \quad (2.2.5)$$

where the two NN weight matrices \hat{V} , \hat{W} are estimates of ideal weights V , W and they are defined as follows.

The inner-layer synaptic weight matrix V is written as

$$\hat{V} = \begin{bmatrix} \theta_{v,1} & \cdots & \theta_{v,n_2} \\ v_{1,1} & \cdots & v_{1,n_2} \\ \vdots & \ddots & \vdots \\ v_{n_1,1} & \cdots & v_{n_1,n_2} \end{bmatrix} \in \mathfrak{R}^{(n_1+1) \times n_2} \quad (2.2.6)$$

with a sigmoid vector defined as

$$\overline{\boldsymbol{\sigma}}(z) = [b_w \ \sigma(z_1) \ \sigma(z_2) \ \cdots \ \sigma(z_{n_2})]^T \in \mathfrak{R}^{n_2+1} \quad (2.2.7)$$

where b_w is a bias term. The outer-layer weight matrix W is defined as

$$\hat{W} = \begin{bmatrix} \theta_{w,1} & \cdots & \theta_{w,n_3} \\ w_{1,1} & \cdots & w_{1,n_3} \\ \vdots & \ddots & \vdots \\ w_{n_2,1} & \cdots & w_{n_2,n_3} \end{bmatrix} \in \mathfrak{R}^{(n_2+1) \times n_3} \quad (2.2.8)$$

Note that $\theta_{v,j}$ in V acts as a threshold for each neuron, and that $\theta_{w,j}$ in W allows the bias term, b_w , to be weighted in each output channel.

Define the input vector

$$\boldsymbol{\mu} = \begin{bmatrix} b_v & x_1 & x_2 & \cdots & x_{n_1} \end{bmatrix}^T \in \mathfrak{R}^{n_1+1} \quad (2.2.9)$$

where $b_v \geq 0$ is an input bias. The weight matrices V , W are updated according to the following adaptation laws:

$$\begin{aligned}\dot{\hat{V}} &= -\Gamma_v \cdot \left[\boldsymbol{\mu} \mathbf{E}^T P B \hat{W}^T \hat{\boldsymbol{\sigma}}' + \kappa_v \cdot (\hat{V} - V_0) \right] \\ \dot{\hat{W}} &= -\Gamma_w \cdot \left[(\hat{\boldsymbol{\sigma}} - \hat{\boldsymbol{\sigma}}' \hat{V}^T \boldsymbol{\mu}) \mathbf{E}^T P B + \kappa_w \cdot (\hat{W} - W_0) \right]\end{aligned}\tag{2.2.10}$$

or

$$\begin{aligned}\dot{\hat{V}} &= -\Gamma_v \cdot \left[\boldsymbol{\mu} \mathbf{E}^T P B \hat{W}^T \hat{\boldsymbol{\sigma}}' + \kappa_v \cdot \|\mathbf{E}\| \cdot (\hat{V} - V_0) \right] \\ \dot{\hat{W}} &= -\Gamma_w \cdot \left[(\hat{\boldsymbol{\sigma}} - \hat{\boldsymbol{\sigma}}' \hat{V}^T \boldsymbol{\mu}) \mathbf{E}^T P B + \kappa_w \cdot \|\mathbf{E}\| \cdot (\hat{W} - W_0) \right]\end{aligned}\tag{2.2.11}$$

where $\hat{\boldsymbol{\sigma}} = \boldsymbol{\sigma}(\hat{V}^T \boldsymbol{\mu})$ and $\boldsymbol{\sigma}' = \text{diag}(d\sigma_i/dz_i)$ denotes the Jacobian matrix. W_0 and V_0 are initial guesses (or guesses), Γ_v , Γ_w , κ_v , and $\kappa_w > 0$ are adaptation gains, and P is a solution of the Lyapunov equation

$$A^T P + P A = -Q, \quad Q > 0\tag{2.2.12}$$

It is noted that the first form in (2.2.10) employs a ' σ -modification' term, while the second form in (2.2.11) uses ' e -modification'. It has been proven that both forms of the weight adaptation laws for the SHL NN guarantee that all error signals are uniformly bounded [11, 29, 61, 62].

Similar to the RBF NNs, there are always NN approximation errors described as [29]:

$$\begin{aligned}\mathbf{f}(\mathbf{x}) - \boldsymbol{\nu}_{ad} &= W^T \bar{\boldsymbol{\sigma}}(V^T \boldsymbol{\mu}) - \hat{W}^T \bar{\boldsymbol{\sigma}}(\hat{V}^T \boldsymbol{\mu}) + \boldsymbol{\varepsilon}(\mathbf{x}) \\ &= \tilde{W}^T (\hat{\boldsymbol{\sigma}} - \hat{\boldsymbol{\sigma}}' \hat{V}^T \boldsymbol{\mu}) + \hat{W}^T \hat{\boldsymbol{\sigma}}' \tilde{V}^T \boldsymbol{\mu} + \boldsymbol{\varepsilon}(\mathbf{x}) - \mathbf{w}\end{aligned}\tag{2.2.13}$$

where $\tilde{W} \triangleq W - \hat{W}$, $\tilde{V} \triangleq V - \hat{V}$ are NN estimation errors.

CHAPTER III

ADAPTIVE NONLINEAR DYNAMIC INVERSION CONTROL USING NEURAL NETWORKS

As noted in Chapter 1, nonlinear dynamic inversion (NDI) control is one of the most advanced control design methodologies. It offers the potential for high performance in extreme flight conditions such as high angle of attack and/or high rotational rates, in which uncertainties are common.

This section reviews the adaptive NDI control of aircraft, emphasizing characteristics particular to aircraft control rather than general description of arbitrary nonlinear systems, and describes how adaptive elements can be introduced to augment the NDI design to achieve the desired high performance.

3.1 Input-Output Feedback Linearization and Nonlinear Dynamic Inversion

Rigid body dynamics of aircraft are described globally over the full flight envelope by a set of n nonlinear differential equations as

$$\begin{aligned}\dot{\mathbf{x}}(t) &= \mathbf{f}(\mathbf{x}, \mathbf{u}) \\ \mathbf{y}(t) &= \mathbf{g}(\mathbf{x})\end{aligned}\tag{3.1.1}$$

where $\mathbf{x} \in \mathcal{D}_x \subset \mathbb{R}^n$ is the state vector, $\mathbf{u} \in \mathcal{D}_u \subset \mathbb{R}^m$ is the system control vector, and $\mathbf{y} \in \mathcal{D}_y \subset \mathbb{R}^m$ is the system output vector. It is assumed that the system (3.1.1) is stabilizable and observable, and that $\mathbf{f}(\cdot, \cdot)$ and $\mathbf{g}(\cdot)$ are sufficiently smooth functions known to us reasonably precisely as a mix of analytical expressions and tabular data.

Assumption 3.1.1. *The nonlinear dynamical system in (3.1.1) satisfies the conditions for output feedback linearization with well-defined vector relative degree r .*

By selecting the appropriate controlled variables for input-output feedback linearization, it is possible to rewrite (3.1.1) in the following general normal form :

$$\begin{aligned}
\dot{\boldsymbol{\chi}} &= \mathbf{f}_o(\boldsymbol{\chi}, \boldsymbol{\xi}) \\
\dot{\xi}_i^1 &= \xi_{i+1}^2 \\
&\vdots \\
\dot{\xi}_i^{r_i-1} &= \xi_i^{r_i} \\
\dot{\xi}_i^{r_i} &= h_i(\boldsymbol{\xi}, \boldsymbol{\chi}, u_i) \\
y_i &= \xi_i^1, \quad i = 1, \dots, m
\end{aligned} \tag{3.1.2}$$

where $\boldsymbol{\xi} \triangleq [\xi_1^1 \ \xi_1^2 \ \dots \ \xi_1^{r_1} \ \dots \ \xi_m^1 \ \xi_m^2 \ \dots \ \xi_m^{r_m}]^T \in \mathfrak{R}^r$, $h_i(\boldsymbol{\xi}, \boldsymbol{\chi}, u_i) \triangleq L_{\mathbf{f}}^{(r_i)} \mathbf{g}|_{u_i}, i = 1, \dots, m$ being the Lie derivatives, $\boldsymbol{\chi} \in \mathcal{D}_{\boldsymbol{\chi}} \subset \mathfrak{R}^{n-r}$ are the state vector associated with the internal, or zero dynamics

$$\dot{\boldsymbol{\chi}} = \mathbf{f}_o(\boldsymbol{\chi}, \boldsymbol{\xi}) \tag{3.1.3}$$

The overall relative degree r is defined as $r \triangleq r_1 + r_2 + \dots + r_m \leq n$, in which r_i is the relative degree of the i^{th} output, or controlled variable. The function $\mathbf{f}_o(\boldsymbol{\xi}, \boldsymbol{\chi})$ and $h_i(\boldsymbol{\xi}, \boldsymbol{\chi}, u_i)$ are partially known continuous functions. In other words, in order to obtain this normal form (3.1.2), we differentiate the individual elements of $\mathbf{y}(\mathbf{x})$ a sufficient number of times until the control variables \mathbf{u} appear explicitly.

Assumption 3.1.2. *$\partial h_i(\mathbf{x}, u_i)/\partial u_i$ is continuous and non-zero for every $(\mathbf{x}, u_i) \in \mathcal{D}_x \times \mathfrak{R}$.*

Aircraft Equations of Motion

For aerospace vehicles, the equations of motion are typically described using the state vector \mathbf{x} which consists of following components:

1. (p, q, r) : 3 rotational rate about body axes

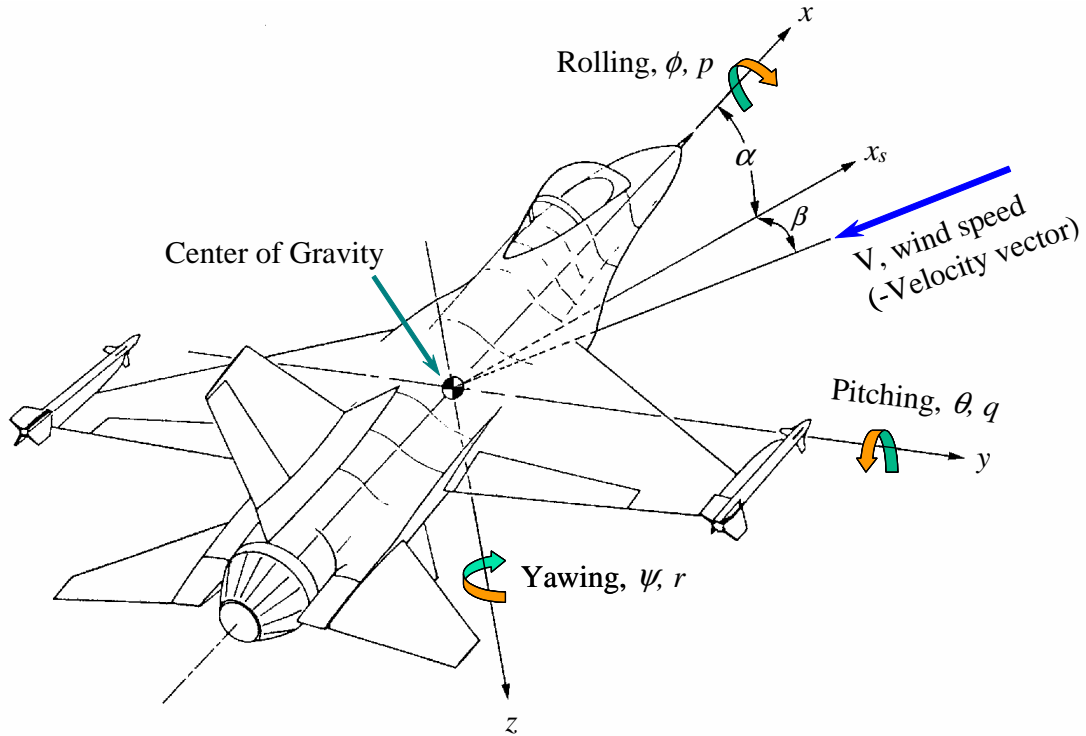


Figure 4: Aircraft axis system and definitions

2. (α, β, μ) : 3 attitudes, measured with respect to the airstream
3. (V, γ, ψ) : 3 velocity components, described by total velocity, flight path angle, and heading angle
4. (X, Y, H) : 3 inertial position coordinates

The control vector $\mathbf{u} \triangleq [u_1 \ u_2 \ \cdots \ u_m]^T$ denotes the positions of all control effectors. This includes the conventional aerodynamic control surfaces such as stabilator (elevator), aileron, and rudder. For nonconventional aircraft configurations, it may also include any other additional control effectors such as canards, leading edge devices, and thrust vectoring nozzles. The output $\mathbf{y} \triangleq [y_1 \ y_2 \ \cdots \ y_m]^T$ denotes selected variables to be controlled. These variables are chosen according to the purpose of control. Figure 4 presents the aircraft axis system and several fundamental definitions.

In the field of aerospace dynamics and control problems, the equations of motion (3.1.1)

can be written in the matrix form as [51]:

$$\begin{aligned}\dot{\mathbf{x}}(t) &= F(\mathbf{x}) + G(\mathbf{x})\mathbf{u} \\ \mathbf{y}(t) &= C(\mathbf{x})\end{aligned}\tag{3.1.4}$$

Recalling that $\dim(\mathbf{y}) = \dim(\mathbf{u})$ and the Lie derivative as

$$\begin{aligned}L_F^k(\mathbf{x}) &= \left[\frac{\partial}{\partial \mathbf{x}} L_F^{k-1}(\mathbf{x}) \right] F(\mathbf{x}) \\ L_F^0(\mathbf{x}) &= \mathbf{x}\end{aligned}\tag{3.1.5}$$

we can write the differentiation of the i^{th} component of \mathbf{y} as:

$$\begin{aligned}\dot{y}_i &= C_i \dot{\mathbf{x}} = C_i F(\mathbf{x}) + C_i G(\mathbf{x})\mathbf{u} = C_i L_F^1(\mathbf{x}) \\ \ddot{y}_i &= C_i \ddot{\mathbf{x}} = C_i [L_F^1(\mathbf{x})] F(\mathbf{x}) + C_i [L_F^1(\mathbf{x})] G(\mathbf{x})\mathbf{u} = C_i L_F^2(\mathbf{x}) \\ &\vdots \\ y_i^{r_i} &= C_i \mathbf{x}^{r_i} = C_i [L_F^{r_i-1}(\mathbf{x})] F(\mathbf{x}) + C_i [L_F^{r_i-1}(\mathbf{x})] G(\mathbf{x})\mathbf{u}\end{aligned}\tag{3.1.6}$$

where r_i is the order of the derivative of y_i necessary to ensure that

$$C_i [L_F^{r_i-1}(\mathbf{x})] G(\mathbf{x}) \neq 0\tag{3.1.7}$$

After differentiating the m elements of \mathbf{y} the appropriate number of times such that each will satisfy (3.1.7), the output dynamics can be written as:

$$\begin{aligned}\mathbf{y}^{(r)} &= \begin{bmatrix} y_1^{(r_1)} \\ y_2^{(r_2)} \\ \vdots \\ y_m^{(r_m)} \end{bmatrix} \\ &= \begin{bmatrix} C_1 L_F^{r_1}(\mathbf{x}) \\ C_2 L_F^{r_2}(\mathbf{x}) \\ \vdots \\ C_m L_F^{r_m}(\mathbf{x}) \end{bmatrix} + \begin{bmatrix} C_1 \frac{\partial}{\partial \mathbf{x}} L_F^{r_1-1}(\mathbf{x}) \\ C_2 \frac{\partial}{\partial \mathbf{x}} L_F^{r_2-1}(\mathbf{x}) \\ \vdots \\ C_m \frac{\partial}{\partial \mathbf{x}} L_F^{r_m-1}(\mathbf{x}) \end{bmatrix} G(\mathbf{x})\mathbf{u}\end{aligned}\tag{3.1.8}$$

By defining the notations as:

$$\begin{aligned}\bar{F}_i &= C_i [L_F^{r_i}(\mathbf{x})], \quad i = 1, \dots, r \\ \bar{G}_i &= C_i \left[\frac{\partial}{\partial \mathbf{x}} L_F^{r_i-1}(\mathbf{x}) \right] G(\mathbf{x}) \in \mathfrak{R}^{r \times m}\end{aligned}\tag{3.1.9}$$

the equation (3.1.8) can then be written in a compact form as

$$\mathbf{y}^{(r)} = \bar{F}(\mathbf{x}) + \bar{G}(\mathbf{x})\mathbf{u}\tag{3.1.10}$$

It can be easily seen that the sufficient condition for the existence of an inverse model to the system (3.1.4) is that the control effective matrix $\bar{G}(\mathbf{x})$ in (3.1.10) be nonsingular. This condition is fully satisfied in the normal flight envelope of the aircraft [51].

Now assign the pseudo-control $\boldsymbol{\nu}$ such that $\boldsymbol{\nu} = \mathbf{y}^{(r)}$, then the *inverse system model* takes the form:

$$\begin{aligned}\dot{\mathbf{x}}(t) &= [F(\mathbf{x}) - G(\mathbf{x})Q(\mathbf{x})] + G(\mathbf{x})R(\mathbf{x})\boldsymbol{\nu} \\ \mathbf{u} &= -Q(\mathbf{x}) + R(\mathbf{x})\boldsymbol{\nu}\end{aligned}\tag{3.1.11}$$

where $\boldsymbol{\nu}$ is the *input* to the inverse system, and \mathbf{u} is the *output*, and

$$\begin{aligned}Q(\mathbf{x}) &= [\bar{G}(\mathbf{x})]^{-1} \bar{F}(\mathbf{x}) \\ R(\mathbf{x}) &= [\bar{G}(\mathbf{x})]^{-1}\end{aligned}\tag{3.1.12}$$

Applying the NDI control law

$$\mathbf{u} = -Q(\mathbf{x}) + R(\mathbf{x})\boldsymbol{\nu}\tag{3.1.13}$$

to the original system (3.1.4) yields the so-called integrator-decoupled form

$$\mathbf{y}^{(r)} = \boldsymbol{\nu}\tag{3.1.14}$$

Usually we set

$$\boldsymbol{\nu} = - \sum_{j=0}^{r-1} K_j \mathbf{y}^{(j)} + K_0 \mathbf{y}_c\tag{3.1.15}$$

with $\mathbf{y}^{(j)}$ is the j^{th} derivatives of the output vector \mathbf{y} , the matrix K is chosen as $(r \times r)$ constant diagonal matrix, \mathbf{y}_c is the external input, and $\boldsymbol{\nu}_{dc}$ is usually called the dynamic compensator. The pseudo-control (3.1.15) yields the decoupled linear, time-invariant dynamics as

$$\mathbf{y}^{(r)} + K_{r-1}\mathbf{y}^{(r-1)} + \dots + K_0\mathbf{y} = K_0\mathbf{y}_c \quad (3.1.16)$$

Figure 5 presents the process described above to develop the nonlinear dynamic inversion control law, along with NN adaptive element and pseudo-control hedging.

Remark 3.1.1 (Zero dynamics). Theoretically the maximum number of poles that can be placed with the NDI control law is dependent on the selection of the controlled variables shown in the output vector \mathbf{y} . For the case $r = n$ all the considered system poles can be placed by choosing K , and the closed-loop stability can be guaranteed if closed-loop observability is assumed, while for the case $r \leq n$, closed-loop stability can be guaranteed only locally by showing that the modes, namely the zero dynamics in (3.1.3), which are unobservable by the NDI control law, have stable dynamics over the region of interest in the state space. These dynamics are implicitly defined by the selection of controlled variables. Usually an unstable zero shows up in the aircraft pitch axis mode, for example in the phugoid mode which has a slightly unstable zero (for example [23], time to double $\cong 150sec$). These kinds of conditions can be overcome by adding an appropriate term to the controlled variable, or adding a control term to handle them in the outer loop of the control system. \diamond

Like most other nonlinear systems, in real flights there are unmodelled dynamics and uncertainties, which can cause significant inversion errors in the NDI control design approach discussed so far. This situation is highly common and severe at the extremely nonlinear flight regimes such as high angle of attack and/or high rate rotational maneuvers which is the main interest of this research. This condition can be described by adding uncertainty terms in the nominal aircraft model (3.1.10) as

$$\mathbf{y}^{(r)} = [\overline{F}(\mathbf{x}) + \boldsymbol{\Delta}_f(\mathbf{x})] + [\overline{G}(\mathbf{x}) + \boldsymbol{\Delta}_g(\mathbf{x})] \mathbf{u} \quad (3.1.17)$$

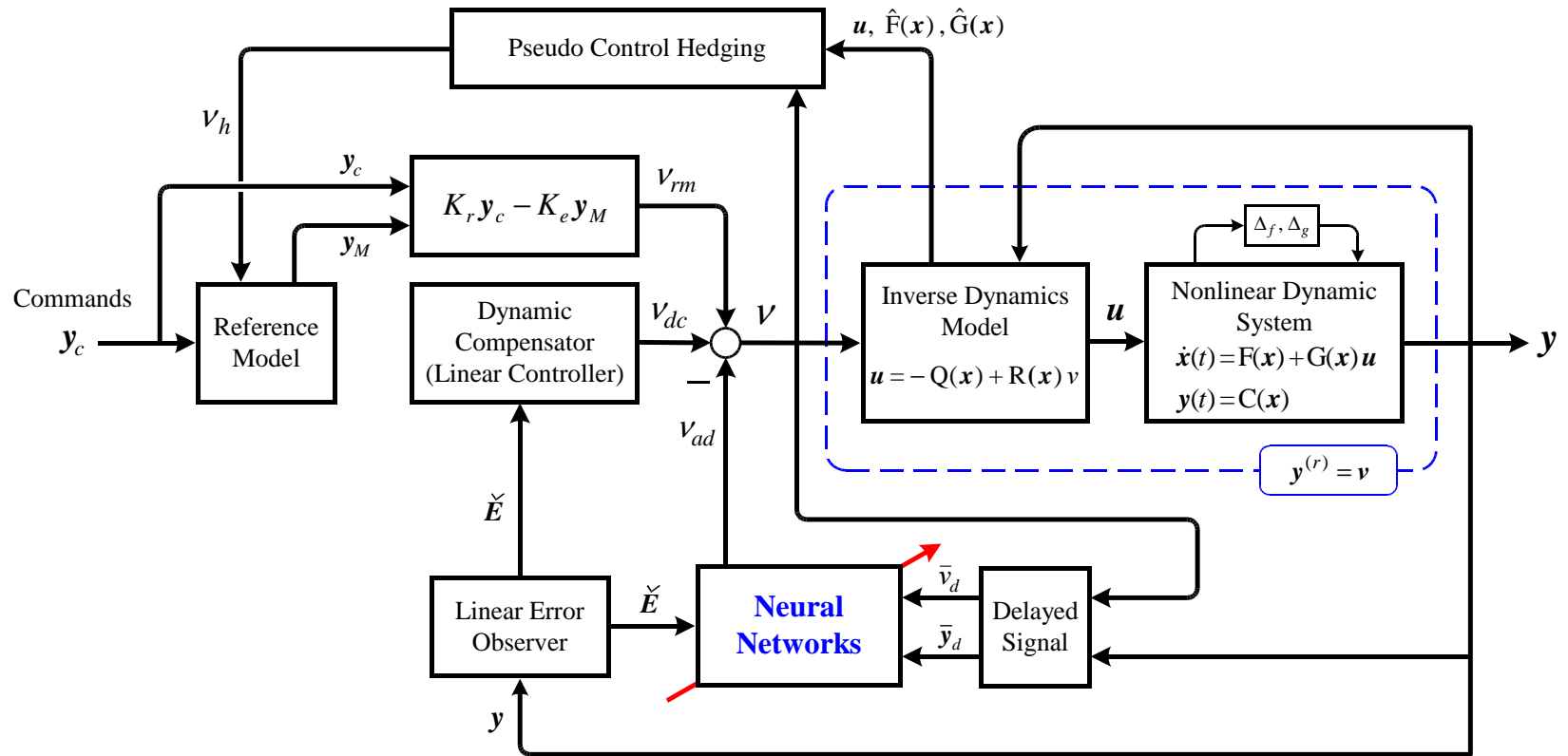


Figure 5: Adaptive nonlinear dynamic inversion control design architecture

where $\Delta_f(\mathbf{x}, \mathbf{u})$, $\Delta_g(\mathbf{x}, \mathbf{u})$ are unknown, unmodelled dynamics, or uncertainty, which are possibly nonlinear functions, and by placing an uncertainty upon the ideal NDI control law \mathbf{u} in (3.1.18) in the form as [23]

$$\mathbf{u} = -(I + \Delta_u)Q(\mathbf{x}) + (I + \Delta_u)R(\mathbf{x})\boldsymbol{\nu} \quad (3.1.18)$$

where $\Delta_u(\mathbf{x}, \mathbf{u})$ is assumed to have an arbitrary stable dynamics. Applying this control \mathbf{u} into (3.1.17) yields a dynamic model such as

$$\mathbf{y}^{(r)} = \tilde{F}(\mathbf{x}) + \tilde{G}(\boldsymbol{\nu} + \Delta(\mathbf{x}, \mathbf{u})) \quad (3.1.19)$$

The uncertainty $\Delta(\mathbf{x}, \mathbf{u})$ will show up in (3.1.16) as an inversion error such that

$$\mathbf{y}^{(r)} + K_{r-1}\mathbf{y}^{(r-1)} + \dots + K_0\mathbf{y} = K_0\mathbf{y}_c + \Delta(\mathbf{x}, \mathbf{u}) - \boldsymbol{\nu}_{ad} \quad (3.1.20)$$

Hence in order to achieve the required performance at the flight regimes that result in significant uncertainties, we definitely need to introduce an adaptive element $\boldsymbol{\nu}_{ad}$, which is the output of properly-trained neural networks for canceling out the nonlinear uncertainties $\Delta(\mathbf{x}, \mathbf{u})$. Therefore the neural networks play a key role in the adaptive control design.

3.2 Reformulation of Dynamic Inversion Error

A linearizing feedback control law is approximated by introducing the following signal:

$$u_i = \hat{h}_i^{-1}(\mathbf{y}, \nu_i), \quad i = 1, \dots, m \quad (3.2.1)$$

where ν_i , commonly referred to as pseudo-control, is defined as

$$\nu_i = \hat{\mathbf{h}}(\mathbf{y}, u_i), \quad i = 1, \dots, m \quad (3.2.2)$$

The function $\hat{\mathbf{h}}(\mathbf{y}, \mathbf{u}) = [\hat{h}_1(\mathbf{x}, u_1) \cdots \hat{h}_m(\mathbf{x}, u_m)]^T$ can be determined by using a possibly simplified model of the system dynamics. It is assumed that $\hat{h}_i(\mathbf{x}, u_i)$, an approximation of $h_i(\boldsymbol{\xi}, \boldsymbol{\chi}, u_i)$, is invertible with respect to its second argument and satisfies the following assumption:

Assumption 3.2.1. $\partial h_i(\mathbf{y}, u_i)/\partial u_i$ is continuous and non-zero for every $(\mathbf{y}, u_i) \in \mathcal{D}_y \times \mathfrak{R}$, and

$$\frac{\partial \hat{h}_i(\mathbf{y}, u_i)}{\partial u_i} \frac{\partial h_i(\mathbf{x}, u_i)}{\partial u_i} > 0, \quad i = 1, \dots, m \quad (3.2.3)$$

for every $(\mathbf{x}, \mathbf{y}, u_i) \in \mathcal{D}_x \times \mathcal{D}_y \times \mathfrak{R}$.

Defining $\boldsymbol{\nu} = [\nu_1 \ \dots \ \nu_m]^T$, we rewrite (3.2.2) in a compact form as

$$\boldsymbol{\nu} = \hat{\mathbf{h}}(\mathbf{y}, \mathbf{u}) \quad (3.2.4)$$

With this definition of pseudo-control (3.2.4), the output dynamics can be expressed as

$$\mathbf{y}^{(r)} = \boldsymbol{\nu} + \boldsymbol{\Delta} \quad (3.2.5)$$

where $\mathbf{y}^{(r)} = [y_1^{(r_1)} \ \dots \ y_m^{(r_m)}]^T$ and

$$\begin{aligned} \boldsymbol{\Delta}(\mathbf{x}, \mathbf{u}) &= \boldsymbol{\Delta}(\boldsymbol{\xi}, \boldsymbol{\chi}, \mathbf{u}) \\ &= \mathbf{h}(\boldsymbol{\xi}, \boldsymbol{\chi}, \hat{\mathbf{h}}^{-1}(\mathbf{y}, \boldsymbol{\nu})) - \hat{\mathbf{h}}(\mathbf{y}, \hat{\mathbf{h}}^{-1}(\mathbf{y}, \boldsymbol{\nu})) \end{aligned} \quad (3.2.6)$$

which is the difference between the function $\mathbf{h}(\mathbf{x}, \mathbf{u})$ and its approximation $\hat{\mathbf{h}}(\mathbf{y}, \mathbf{u})$, and it is usually referred to as modeling error.

The pseudo-control $\boldsymbol{\nu}$ is usually chosen to have the form

$$\boldsymbol{\nu} = \boldsymbol{\nu}_{dc} + \boldsymbol{\nu}_{rm} - \boldsymbol{\nu}_{ad} \quad (3.2.7)$$

where $\boldsymbol{\nu}_{dc}$ is the output of a linear dynamic compensator, $\boldsymbol{\nu}_{rm} = \mathbf{y}_c^{(r)} = [y_c^{(r_1)} \ \dots \ y_c^{(r_m)}]^T$ is a vector of the r_i^{th} derivative of the command signal $y_{c_i}(t)$, and $\boldsymbol{\nu}_{ad}$ is the adaptive control signal designed to cancel $\boldsymbol{\Delta}(\mathbf{x}, \mathbf{u})$. Figure 5 illustrates the overall architecture of the adaptive control design.

Using (3.2.7), the output dynamics in (3.2.5) becomes

$$\mathbf{y}^{(r)} = \boldsymbol{\nu}_{dc} + \boldsymbol{\nu}_{rm} - \boldsymbol{\nu}_{ad} + \boldsymbol{\Delta} \quad (3.2.8)$$

It can be seen from (3.2.6) that Δ depends on $\boldsymbol{\nu}_{ad}$ through $\boldsymbol{\nu}$, whereas $\boldsymbol{\nu}_{ad}$ has to be designed to cancel Δ . Define the following signals,

$$\begin{aligned}\nu_{l_i} &\triangleq \mathbf{y}_{c_i}^{(r_i)} + \nu_{dc_i} \\ \nu_i^* &\triangleq \hat{h}_i(\mathbf{y}, h_i^{-1}(\mathbf{y}, \nu_{l_i}))\end{aligned}\tag{3.2.9}$$

where ν_{dc_i} is the i^{th} component of $\boldsymbol{\nu}_{dc}$. Invertibility of $h_i(\cdot, \cdot)$ with respect to its second argument is guaranteed by Assumption 3.1.2. From (3.2.9), it follows that ν_{l_i} can be written as

$$\nu_{l_i} = h_i(\mathbf{x}, \hat{h}_i^{-1}(\mathbf{y}, \nu_i^*))\tag{3.2.10}$$

and thus $\boldsymbol{\nu}_{ad} - \Delta$ can be expressed componentwise as

$$\begin{aligned}\nu_{ad_i} - \Delta_i(\mathbf{x}, u_i) &= \nu_{ad_i} - h_i(\mathbf{x}, u_i) + \hat{h}_i(\mathbf{y}, u_i) \\ &= \nu_{ad_i} - h_i(\mathbf{x}, \hat{h}_i^{-1}(\mathbf{y}, \nu_i)) + \nu_{l_i} - \nu_{ad_i} \\ &= h_i(\mathbf{x}, \hat{h}_i^{-1}(\mathbf{y}, \nu_i^*)) - h_i(\mathbf{x}, \hat{h}_i^{-1}(\mathbf{y}, \nu_i))\end{aligned}\tag{3.2.11}$$

Applying the mean value theorem to $h_i(\mathbf{x}, \hat{h}_i^{-1}(\mathbf{y}, \nu_i))$

$$\begin{aligned}h_i(\mathbf{x}, \hat{h}_i^{-1}(\mathbf{y}, \nu_i)) &= h_i(\mathbf{x}, \hat{h}_i^{-1}(\mathbf{y}, \nu_i^*)) + h_{\bar{\nu}_i}(\nu^* - \nu) \\ &= \nu_{l_i} + h_{\bar{\nu}_i}(\nu^* - \nu)\end{aligned}\tag{3.2.12}$$

where

$$h_{\bar{\nu}_i} \triangleq \left. \frac{\partial h_i}{\partial u_i} \frac{\partial u_i}{\partial \nu_i} \right|_{\nu_i = \bar{\nu}_i} > 0, \quad \bar{\nu}_i = \eta_i \nu_i + (1 - \eta_i) \nu_i^*, \quad \text{and } 0 \leq \eta_i \leq 1\tag{3.2.13}$$

Applying (3.2.9) and (3.2.12) into (3.2.11) yields

$$\begin{aligned}\nu_{ad_i} - \Delta_i(\mathbf{x}, u_i) &= h_{\bar{\nu}_i}(\nu_i^* - \nu_i) \\ &= h_{\bar{\nu}_i} \left[\hat{h}_i(\mathbf{y}, h_i^{-1}(\mathbf{x}, \nu_{l_i})) - \nu_{l_i} + \nu_{ad_i} \right] \\ &= h_{\bar{\nu}_i} \left[\nu_{ad_i} - \bar{\Delta}_i(\mathbf{x}, \nu_{l_i}) \right]\end{aligned}\tag{3.2.14}$$

where the redefined modeling error $\bar{\Delta}_i(\mathbf{x}, \nu_{l_i}) = \nu_{l_i} - \hat{h}_i(\mathbf{y}, h_i^{-1}(\mathbf{x}, \nu_{l_i}))$ is rendered independent of the control \mathbf{u} . This can be written in the matrix form

$$\boldsymbol{\nu}_{ad} - \Delta(\mathbf{x}, \mathbf{u}) = H \left[\boldsymbol{\nu}_{ad} - \bar{\Delta}(\mathbf{x}, \boldsymbol{\nu}_l) \right]\tag{3.2.15}$$

where

$$H = \begin{bmatrix} h_{\bar{\nu}_1} & 0 & \cdots & 0 & 0 \\ 0 & h_{\bar{\nu}_2} & \cdots & 0 & 0 \\ \vdots & \vdots & \ddots & \vdots & \vdots \\ 0 & 0 & \cdots & h_{\bar{\nu}_{m-1}} & 0 \\ 0 & 0 & \cdots & 0 & h_{\bar{\nu}_m} \end{bmatrix} \in \mathfrak{R}^{m \times m} \quad (3.2.16)$$

The positive sign of $h_{\bar{\nu}_i}$ is guaranteed by Assumption 3.1.2 and 3.2.1, so is this matrix H having them as its diagonal components. Now using (3.2.15) the dynamics in (3.1.10) can be rewritten as

$$\tilde{\mathbf{y}}^{(r)} = -\boldsymbol{\nu}_{dc} + H [\boldsymbol{\nu}_{ad} - \bar{\Delta}(\mathbf{x}, \boldsymbol{\nu}_l)] \quad (3.2.17)$$

The main difference between the dynamics in (3.1.10) and (3.2.17) lies in the functional structure of the modeling error. In (3.2.17) the modeling error is independent of the actual control variable.

3.3 Parametrization using Neural Networks

3.3.1 RBF Neural Networks

It is assumed that the nonlinear function Δ in (3.2.15) is linearly parameterized by the RBF NN which is discussed in Chapter 2 such that

$$\Delta(\mathbf{x}, \mathbf{u}) = W^T \Psi(\mathbf{x}) + \boldsymbol{\varepsilon}(\mathbf{x}), \quad \|\boldsymbol{\varepsilon}(\mathbf{x})\| \leq \varepsilon_m \quad (3.3.1)$$

Using this fact and the results obtained in the previous section, we consider parametrization of the modeling error on a compact set $(\mathbf{x}, \boldsymbol{\nu}_l) \in \mathcal{D}_l \subset \mathcal{D}_x \times \mathfrak{R}^m$ [30]

$$\bar{\Delta}(\mathbf{x}, \boldsymbol{\nu}_l) = W^T \Psi(\mathbf{x}, \boldsymbol{\nu}_l) + \boldsymbol{\varepsilon}(\mathbf{x}, \boldsymbol{\nu}_l) \quad (3.3.2)$$

The adaptive controller is designed to approximate the nonlinear function $\bar{\Delta}(\mathbf{x}, \boldsymbol{\nu}_l)$. Since our control design is based on output feedback, we cannot use states \mathbf{x} as inputs to the NN.

Instead of $\hat{W}^T \Psi(\mathbf{x})$ in (2.1.7) we build our adaptive controller using a tapped-delay line of memory units as

$$\boldsymbol{\nu}_{ad} \triangleq \hat{W}^T \Psi(\boldsymbol{\mu}) \quad (3.3.3)$$

where $\boldsymbol{\mu}$ is a vector of tapped delay line of memory unit [30, 55]

$$\boldsymbol{\mu}(t) = [1 \ \boldsymbol{\nu}_l^T \ \bar{\boldsymbol{\nu}}_d^T(t) \ \bar{\mathbf{y}}_d^T(t)]^T \quad (3.3.4)$$

Here $\bar{\mathbf{y}}_d^T(t)$ and, similarly, $\bar{\boldsymbol{\nu}}_d^T(t)$, are vectors of difference quotients of the measurement and control variables, respectively:

$$\begin{aligned} \bar{\mathbf{y}}_d^T(t) &= [\Delta_d^{(0)} y_1(t) \ \Delta_d^{(1)} y_1(t) \ \cdots \Delta_d^{(n-1)} y_1(t) \ \cdots \Delta_d^{(0)} y_m(t) \ \Delta_d^{(1)} y_m(t) \ \cdots \Delta_d^{(n-1)} y_m(t)]^T \\ \Delta_d^{(0)} y_i(t) &\triangleq y_i(t) \\ \Delta_d^{(k)} y_i(t) &\triangleq \frac{\Delta_d^{(k-1)} y_i(t) - \Delta_d^{(k-1)} y_i(t-d)}{d}, \quad k = 1, \dots, n-1 \end{aligned} \quad (3.3.5)$$

The difference $\boldsymbol{\nu}_{ad} - \bar{\boldsymbol{\Delta}}(\mathbf{x}, \boldsymbol{\nu}_l)$ in (3.2.17) can be expressed as

$$\begin{aligned} \boldsymbol{\nu}_{ad} - \bar{\boldsymbol{\Delta}}(\mathbf{x}, \boldsymbol{\nu}_l) &= \hat{W}^T \Psi(\boldsymbol{\mu}) - W^T \Psi(\mathbf{x}, \boldsymbol{\nu}_l) - \boldsymbol{\varepsilon} \\ &= \hat{W}^T \Psi(\boldsymbol{\mu}) - W^T \Psi(\boldsymbol{\mu}) + W^T \Psi(\boldsymbol{\mu}) - W^T \Psi(\mathbf{x}, \boldsymbol{\nu}_l) - \boldsymbol{\varepsilon} \\ &= -\tilde{W}^T \Psi(\boldsymbol{\mu}) + W^T (\Psi(\boldsymbol{\mu}) - \Psi(\mathbf{x}, \boldsymbol{\nu}_l)) - \boldsymbol{\varepsilon} \end{aligned} \quad (3.3.6)$$

where $W^T (\Psi(\boldsymbol{\mu}) - \Psi(\mathbf{x}, \boldsymbol{\nu}_l))$ can be upper bounded

$$\|W^T (\Psi(\boldsymbol{\mu}) - \Psi(\mathbf{x}, \boldsymbol{\nu}_l))\| \leq 2w_m p_m \quad (3.3.7)$$

In [55], it has been shown that if the system dynamics evolve on a bounded set, then $\|\Psi(\boldsymbol{\mu}) - \Psi(\mathbf{x}, \boldsymbol{\nu}_l)\| \approx \mathcal{O}(d)$, where d is introduced in (3.3.5), and hence, tends to zero, as $d \rightarrow 0$.

3.3.2 SHL Neural Networks

It is now assumed that the nonlinear function $\boldsymbol{\Delta}$ in (3.2.15) is nonlinearly parameterized by the SHL NN which is also described in Chapter 2 such that

$$\boldsymbol{\Delta}(\mathbf{x}, \mathbf{u}) = \hat{W}^T \boldsymbol{\sigma}(\hat{V}^T \boldsymbol{\mu}) + \boldsymbol{\varepsilon}(\mathbf{x}) \quad (3.3.8)$$

The following theorem re-defines Theorem 2.2.1 in Section 2.2 for the output feedback case when the system is observable from input-output history

Theorem 3.3.1. *Given $\varepsilon^* > 0$ and the compact set $\mathcal{D} \subset \mathcal{D}_x \times \mathfrak{R}$, there exists a set of bounded weights V , W and n_2 sufficiently large such that a continuous function $\bar{\Delta}(\mathbf{x}, \nu_l)$ can be approximated by a nonlinearly parameterized SHL NN*

$$\begin{aligned} \bar{\Delta}(\mathbf{x}, \nu_l) &= W^T \boldsymbol{\sigma}(V^T \boldsymbol{\mu}) + \boldsymbol{\varepsilon}(\boldsymbol{\mu}, \mathbf{d}), \\ \|W\|_F &< W^*, \quad \|V\|_F < V^*, \quad \|\boldsymbol{\varepsilon}(\boldsymbol{\mu}, \mathbf{d})\| < \varepsilon^* \end{aligned} \quad (3.3.9)$$

where the input vector is

$$\boldsymbol{\mu}(t) = \begin{bmatrix} 1 & \boldsymbol{\nu}_l^T & \boldsymbol{\nu}_d^T(t) & \mathbf{y}_d^T(t) \end{bmatrix}^T \in \mathfrak{R}^{2N_1-r+2}, \quad \|\boldsymbol{\mu}\| \leq \mu^* \quad (3.3.10)$$

and

$$\begin{aligned} \boldsymbol{\nu}_d(t) &= \begin{bmatrix} \nu(t) & \nu(t-d) & \cdots & \nu(t - (N_1 - r - 1)d) \end{bmatrix}^T \\ \mathbf{y}_d(t) &= \begin{bmatrix} y(t) & y(t-d) & \cdots & y(t - (N_1 - 1)d) \end{bmatrix}^T \end{aligned} \quad (3.3.11)$$

with $N_1 \geq n$ and $d > 0$.

Proof. see [55] □

According to [55], for this output feedback control design an important concept in order to find the bound of approximation error is to model $\bar{\Delta}(\mathbf{x}, \mathbf{u})$ with NN in terms of delayed values of \mathbf{y} and \mathbf{u} . To this end, let r denote the relative degree of the system output. If $r = n$, then the first through $(n - 1)$ derivatives of the system y do not explicitly depend upon the input. If $r < n$, then the $(n - 1)$ derivatives of the system y will contain no more than $n - r - 1$ derivatives of the system input u . By following the processes in [55], with (3.2.15), the SHL NN approximation upper bound can be written as

$$\begin{aligned} \|\boldsymbol{\nu}_{ad} - \boldsymbol{\Delta}(\mathbf{x}, \boldsymbol{\nu}_l)\| &= \|H \left(\hat{W}^T \hat{\boldsymbol{\sigma}}(\hat{V}^T \boldsymbol{\mu}) - \bar{\Delta}(\mathbf{x}, \boldsymbol{\nu}_l) \right)\| \\ &\leq k_1 \sqrt{\frac{2n-r}{\min_{1 \leq k \leq n} N_k}} + k_2 \frac{d}{2} M \end{aligned} \quad (3.3.12)$$

where k_1, k_2 are constants, and

$$M = \left(2n - r - 1\right)^{3/2} \max_{t \geq 0} \left\{ \max_{1 \leq k \leq n-1} |y^{(k+1)}(t)|, \max_{1 \leq k \leq (n-r-1)} |\nu^{(k+1)}(t)| \right\} \quad (3.3.13)$$

As shown in Chapter 2, $\Delta - \nu_{ad}$ with SHL NNs can be written by:

$$\Delta - \nu_{ad} = \tilde{W}^T \left(\hat{\sigma} - \hat{\sigma}' \hat{V}^T \mu \right) + \hat{W}^T \hat{\sigma}' \tilde{V}^T \mu + \varepsilon(\mathbf{x}) - \mathbf{w} \quad (3.3.14)$$

where $\tilde{W} \triangleq W - \hat{W}$, $\tilde{V} \triangleq V - \hat{V}$ are NN estimation errors, and the error $\varepsilon(\mathbf{x}) - \mathbf{w}$ is bounded such that [29]

$$\|\varepsilon(\mathbf{x}) - \mathbf{w}\| \leq \gamma_1 \|\tilde{Z}\|_F + \gamma_2 \quad (3.3.15)$$

and γ_1, γ_2 are positive computable constants, and matrix \tilde{Z} is defined as

$$\tilde{Z} \triangleq \begin{bmatrix} \tilde{W} & 0 \\ 0 & \tilde{V} \end{bmatrix} \quad (3.3.16)$$

Further the modeling error $\Delta - \nu_{ad}$ is known to be bounded by [29]:

$$\begin{aligned} \|\Delta - \nu_{ad}\| &= \|W^T \sigma(V^T \mu) - \hat{W}^T \sigma(\hat{V}^T \mu) + \varepsilon(\mathbf{x}) - \mathbf{w}\| \\ &\leq \alpha_1 \|\tilde{Z}\|_F + \alpha_2 \end{aligned} \quad (3.3.17)$$

where $\alpha_1 = \sqrt{n_2 + 1}$, and $\alpha_2 = 2\sqrt{n_2 + 1} W + \varepsilon_m$.

3.4 Nonlinear System and its Reference Model

We rewrite the output equation (3.1.19) or (3.2.5) in a matrix form, considering the external disturbance $\mathbf{d}(t)$ as well as the modeling error $\Delta(\mathbf{x}, \mathbf{u})$:

$$\dot{\mathbf{y}}(t) = A\mathbf{y}(t) + B[\nu(t) + \Delta(\mathbf{x}, \mathbf{u}) + \mathbf{d}(t)] \quad (3.4.1)$$

where

$$\begin{aligned} \mathbf{y} &\triangleq [\mathbf{y}_1^T \ \mathbf{y}_2^T \ \cdots \ \mathbf{y}_m^T]^T \in \mathfrak{R}^r \\ \mathbf{y}_i &\triangleq [y_i \ \dot{y}_i \ \cdots \ y_i^{(r_i-1)}]^T \in \mathfrak{R}^{r_i}, \quad i = 1, \dots, m \\ A &\triangleq \text{block-diag}(A_1 \ A_2 \ \cdots \ A_m) \in \mathfrak{R}^{r \times r} \\ B &\triangleq \text{block-diag}(B_1 \ B_2 \ \cdots \ B_m) \in \mathfrak{R}^{r \times m} \end{aligned} \quad (3.4.2)$$

and

$$A_i = \begin{bmatrix} 0 & 1 & 0 & \cdots & 0 & 0 \\ 0 & 0 & 1 & \cdots & 0 & 0 \\ \vdots & \vdots & \vdots & \ddots & \vdots & \vdots \\ 0 & 0 & 0 & \cdots & 0 & 1 \\ 0 & 0 & 0 & \cdots & 0 & 0 \end{bmatrix} \in \mathfrak{R}^{r_i \times r_i}, \quad B_i = \begin{bmatrix} 0 \\ 0 \\ \vdots \\ 0 \\ 1 \end{bmatrix} \in \mathfrak{R}^{r_i \times 1} \quad (3.4.3)$$

where $\mathbf{d}(t) \in \mathfrak{R}^{m \times 1}$ is the bounded external disturbance such that

$$\|\mathbf{d}(t)\| \leq d_m \quad (3.4.4)$$

A reference model is described by an equation which is composed of m -ordinary differential equations having $r_i^{th}, i = 1, \dots, m$ order, respectively. The equation can be written in a compact state-space form as:

$$\dot{\mathbf{y}}_M(t) = A_M \mathbf{y}_M(t) + B_M \cdot \mathbf{y}_c(t) \quad (3.4.5)$$

where

$$\begin{aligned} \mathbf{y}_M &\triangleq [\mathbf{y}_{M_1}^T \quad \mathbf{y}_{M_2}^T \quad \cdots \quad \mathbf{y}_{M_m}^T]^T \in \mathfrak{R}^r \\ \mathbf{y}_{M_i} &\triangleq [y_{M_i} \quad \dot{y}_{M_i} \quad \cdots \quad y_{M_i}^{(r_i-1)}]^T \in \mathfrak{R}^{r_i}, \quad i = 1, \dots, m \\ \mathbf{y}_c &\triangleq [y_{c_1} \quad y_{c_2} \quad \cdots \quad y_{c_m}]^T \in \mathfrak{R}^m \\ A_M &\triangleq \text{block-diag}(A_{M_1} \quad A_{M_2} \quad \cdots \quad A_{M_m}) \in \mathfrak{R}^{r \times r} \\ B_M &\triangleq \text{block-diag}(B_{M_1} \quad B_{M_2} \quad \cdots \quad B_{M_m}) \in \mathfrak{R}^{r \times m} \end{aligned} \quad (3.4.6)$$

and

$$A_{M_i} = \begin{bmatrix} 0 & 1 & 0 & \cdots & 0 & 0 \\ 0 & 0 & 1 & \cdots & 0 & 0 \\ \vdots & \vdots & \vdots & \ddots & \vdots & \vdots \\ 0 & 0 & 0 & \cdots & 0 & 1 \\ -a_{i1} & -a_{i2} & -a_{i3} & \cdots & -a_{i(r_i-1)} & -a_{ir_i} \end{bmatrix} \in \mathfrak{R}^{r_i \times r_i}, \quad B_{M_i} = \begin{bmatrix} 0 \\ 0 \\ \vdots \\ 0 \\ a_{i1} \end{bmatrix} \in \mathfrak{R}^{r_i \times 1} \quad (3.4.7)$$

and $\mathbf{y}_M \in \mathbb{R}^r$ is the reference model state vector, $\mathbf{y}_c(t) \in \mathbb{R}^m$ is a bounded piecewise continuous reference command, and A_M is Hurwitz.

The r^{th} -order reference model (RM) can usually be factored into a combination of the first order and the second order reference models such that

$$r^{\text{th}} - \text{order RM} = \sum_{i=1}^{m_1} (1^{\text{st}} \text{ order RM})_i + \sum_{j=1}^{m_2} (2^{\text{nd}} \text{ order RM})_j, \quad r = m_1 + m_2 \quad (3.4.8)$$

where the parameters in each reference model contain the requirements of the closed-loop system. In aerospace control problems, these parameters are chosen to ensure that flying quality specifications are met. For a first-order reference model one chooses the time constant of the system, while for a second-order reference model the parameters are chosen to yield the desired natural frequency and damping ratio.

A first-order reference model can be written as

$$y_M = \frac{1}{\tau s + 1} y_c \quad (3.4.9)$$

where τ is the time constant, and the second order reference model is written as

$$y_M = \frac{\omega_n^2}{s^2 + 2\zeta\omega_n s + \omega_n^2} y_c \quad (3.4.10)$$

where ω_n is the natural frequency and ζ is the damping ratio.

Now it is desired to design a control law such that the output tracking error

$$\mathbf{E}(t) = \mathbf{y}_M(t) - \mathbf{y}(t) \quad (3.4.11)$$

tends to zero and all the signals in the system remain bounded as $t \rightarrow \infty$.

3.5 Adaptive NDI Control Architecture

In this section we design an adaptive control based on the Lyapunov theorems. Based on (3.2.7), the pseudo-control $\boldsymbol{\nu}$ is chosen to have feedback and feedforward elements such that

$$\boldsymbol{\nu}(t) \triangleq \underbrace{K_e \cdot \check{\mathbf{E}}(t)}_{\boldsymbol{\nu}_{dc}} + \underbrace{K_r \cdot \mathbf{y}_c(t) - K_e \cdot \mathbf{y}_M(t)}_{\boldsymbol{\nu}_{rm}} - \boldsymbol{\nu}_{ad} \quad (3.5.1)$$

where $\check{\mathbf{E}}(t) \triangleq \mathbf{E}(t) - \tilde{\mathbf{E}}(t)$ is the output of linear observer for the tracking error $\mathbf{E}(t)$, and the feedback gain $K_e \in \mathfrak{R}^{m \times r}$ and the feedforward gain $K_r \in \mathfrak{R}^{m \times m}$ are fixed and bounded such that

$$\begin{aligned} \|K_e\| &< k_{em} \\ \|K_r\| &< k_{rm} \end{aligned} \tag{3.5.2}$$

with positive numbers k_{em} and k_{rm} , respectively. Substituting (3.5.1) into the system dynamics (3.4.1) results in the closed-loop system

$$\dot{\mathbf{y}}(t) = (A - BK_e)\mathbf{y}(t) + BK_r\mathbf{y}_c(t) + B \left(\Delta - \boldsymbol{\nu}_{ad} + \mathbf{d} - K_e\tilde{\mathbf{E}} \right) \tag{3.5.3}$$

Therefore if $\boldsymbol{\nu}_{ad}$ cancels out $\Delta(\mathbf{x}, \mathbf{u})$, and there are no external disturbance \mathbf{d} and observation error $\tilde{\mathbf{E}}$, then by choosing K_e such that $(A - BK_e)$ is Hurwitz, we get a stable closed-loop system response.

It is noted that in [30] the dynamic compensator $\boldsymbol{\nu}_{dc_i}$ is an output of a dynamic equation with the i^{th} error as an input, while in (3.5.1), K_e of $\boldsymbol{\nu}_{dc}$ is updated through an adaptation law introduced later and the estimation error $\tilde{\mathbf{E}}$ is introduced in (3.5.3). A stability analysis will be provided for this new architecture.

Here for a convenience we set the gains K_e and K_r such that

$$\begin{aligned} A - BK_e &= A_M \\ BK_r &= B_M \end{aligned} \tag{3.5.4}$$

Applying (3.5.4) into (3.5.3) yields

$$\dot{\mathbf{y}}(t) = A_M\mathbf{y}(t) + B_M\mathbf{y}_c(t) + B \left(\Delta - \boldsymbol{\nu}_{ad} + \mathbf{d} - K_e\tilde{\mathbf{E}} \right) \tag{3.5.5}$$

According to the definition of tracking error (3.4.11), the closed-loop dynamics of the tracking error signal $\mathbf{E}(t)$ can be obtained by subtracting (3.5.5) from (3.4.5)

$$\begin{aligned} \dot{\mathbf{E}}(t) &= A_M\mathbf{E}(t) - B \left(\Delta - \boldsymbol{\nu}_{ad} + \mathbf{d} - K_e\tilde{\mathbf{E}} \right) \\ \mathbf{z} &= C\mathbf{E}(t) \end{aligned} \tag{3.5.6}$$

where $\mathbf{z} = [z_1 \ z_2 \ \cdots \ z_m] \in \mathfrak{R}^m$, $\mathbf{z}_i = [1 \ 0 \ \cdots \ 0] \in \mathfrak{R}^{1 \times r_i}$, is the vector of available measurements. Since A_M is Hurwitz, there exists a unique and positive definite matrix $P = P^T > 0$ for an arbitrary matrix $Q = Q^T > 0$ satisfying the Lyapunov equation

$$A_M^T P + P A_M = -Q \quad (3.5.7)$$

3.6 Linear Observer for the Error Dynamics

We consider the case of a full-order observer of dimension r . To this end, consider the following linear observer for the tracking error dynamics in (3.5.6)

$$\begin{aligned} \dot{\check{\mathbf{E}}}(t) &= A_M \check{\mathbf{E}}(t) + F(\mathbf{z} - \check{\mathbf{z}}) \\ \check{\mathbf{z}} &= C \check{\mathbf{E}} \end{aligned} \quad (3.6.1)$$

where F is a gain matrix, and should be chosen such that $A_M - FC$ is asymptotically stable, and \mathbf{z} is defined in (3.5.6). Let

$$\begin{aligned} \tilde{A} &\triangleq A_M - FC \\ \tilde{\mathbf{E}} &\triangleq \mathbf{E} - \check{\mathbf{E}} \end{aligned} \quad (3.6.2)$$

Then the error observer dynamics can be written as

$$\dot{\tilde{\mathbf{E}}}(t) = \tilde{A} \tilde{\mathbf{E}}(t) - B \left(\Delta - \nu_{ad} + \mathbf{d} - K_e \tilde{\mathbf{E}} \right) \quad (3.6.3)$$

Since \tilde{A} is Hurwitz, there exists a unique and positive definite matrix $\tilde{P} = \tilde{P}^T > 0$ for an arbitrary matrix $\tilde{Q} = \tilde{Q}^T > 0$ satisfying the Lyapunov equation

$$\tilde{A}^T \tilde{P} + \tilde{P} \tilde{A} = -\tilde{Q} \quad (3.6.4)$$

3.7 Stability Analysis using Lyapunov Theorems

Using Lyapunov's direct method we show that all the errors are ultimately bounded. They are the tracking error \mathbf{E} , the observation error $\tilde{\mathbf{E}}$, and the NN weight errors. To this end we consider one of following vectors:

a) RBF NN:

$$\zeta = \begin{bmatrix} \mathbf{E}^T & \tilde{\mathbf{E}}^T & \tilde{W}^T \end{bmatrix}^T \quad (3.7.1)$$

b) SHL NN:

$$\zeta = \begin{bmatrix} \mathbf{E}^T & \tilde{\mathbf{E}}^T & \tilde{W}^T & \tilde{V}^T \end{bmatrix}^T \quad (3.7.2)$$

and one of following positive definite Lyapunov function candidates:

a) RBF NN:

$$V(\zeta) = \mathbf{E}^T P \mathbf{E} + \tilde{\mathbf{E}}^T \tilde{P} \tilde{\mathbf{E}} + tr \left(H \cdot \tilde{W}^T \Gamma_w^{-1} \tilde{W} \right) \quad (3.7.3)$$

b) SHL NN:

$$\mathcal{L}(\zeta) = \mathbf{E}^T P \mathbf{E} + \tilde{\mathbf{E}}^T \tilde{P} \tilde{\mathbf{E}} + tr \left(\tilde{W}^T \Gamma_w^{-1} \tilde{W} + \tilde{V}^T \Gamma_v^{-1} \tilde{V} \right) \quad (3.7.4)$$

In the expanded space of the compound error variable, consider the largest level set of $V(\zeta)$ or $\mathcal{L}(\zeta)$ in \mathcal{D}_ζ such that its projection on the subspace of the NN input variables completely lies in \mathcal{D}_l . As shown in Figure 6, define the largest ball that lies inside that level set as

$$B_R \triangleq \{ \zeta \mid \|\zeta\| \leq R \} \quad (3.7.5)$$

and let α be the minimum value of $V(\zeta)$ on the boundary of B_R

$$\begin{aligned} \alpha &\triangleq \min_{\|\zeta\|=R} V(\zeta) \quad \text{for RBF NN} \\ \text{or } \alpha &\triangleq \min_{\|\zeta\|=R} \mathcal{L}(\zeta) \quad \text{for SHL NN} \end{aligned} \quad (3.7.6)$$

Introduce the set

$$\begin{aligned} \Omega_\alpha &\triangleq \{ \zeta \in B_R \mid V(\zeta) \leq \alpha \} \quad \text{for RBF NN} \\ \text{or } \Omega_\alpha &\triangleq \{ \zeta \in B_R \mid \mathcal{L}(\zeta) \leq \alpha \} \quad \text{for SHL NN} \end{aligned} \quad (3.7.7)$$

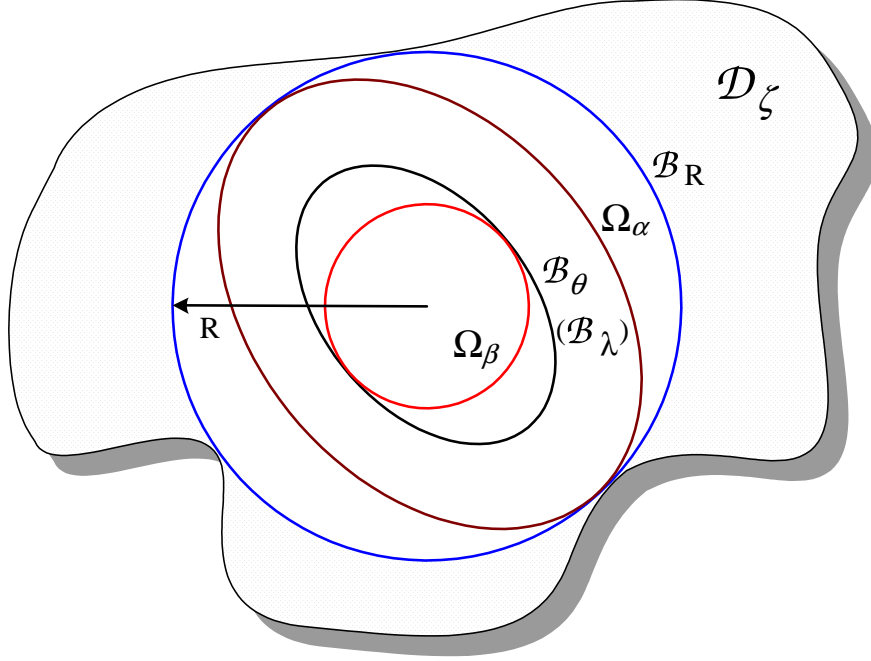


Figure 6: Geometric representation of sets in the error space

3.7.1 RBF NN Adaptation

Through Lyapunov theorems we show that \mathbf{E} , $\tilde{\mathbf{E}}$, and \tilde{W} are all uniformly bounded using RBF NN with σ -modification.

Since $h_{\bar{\nu}_i}, i = 1, \dots, m$ in (3.2.13) are positive continuous functions over the compact set \mathcal{D}_l , we can define the minimum/maximum values of the functions as

$$\begin{aligned} \underline{h} &\triangleq \min \left[\min_{(\mathbf{x}, \nu_1) \in \mathcal{D}_1} h_{\bar{\nu}_1}, \min_{(\mathbf{x}, \nu_1) \in \mathcal{D}_1} h_{\bar{\nu}_2}, \dots, \min_{(\mathbf{x}, \nu_1) \in \mathcal{D}_1} h_{\bar{\nu}_m} \right] \\ \bar{h} &\triangleq \max \left[\max_{(\mathbf{x}, \nu_1) \in \mathcal{D}_1} h_{\bar{\nu}_1}, \max_{(\mathbf{x}, \nu_1) \in \mathcal{D}_1} h_{\bar{\nu}_2}, \dots, \max_{(\mathbf{x}, \nu_1) \in \mathcal{D}_1} h_{\bar{\nu}_m} \right] \end{aligned} \quad (3.7.8)$$

Assumption 3.7.1. *It is assumed that the time derivative of the control effectiveness matrix H in (3.2.16) is bounded such that [25, 30, 45]:*

$$\|\dot{H}\| \leq h_m \quad (3.7.9)$$

From the definition of the candidate Lyapunov function in (3.7.3), there exist class \mathcal{K}

functions η_1 and η_2 such that

$$\eta_1(\zeta) \leq V(\|\zeta\|) \leq \eta_2(\zeta) \quad (3.7.10)$$

where

$$\begin{aligned} \eta_1(\|\zeta\|) &= \lambda_{\min}(P)\|\mathbf{E}\|^2 + \lambda_{\min}(\tilde{P})\|\tilde{\mathbf{E}}\|^2 + \lambda_{\min}(\Gamma_w^{-1})\underline{h}\|\tilde{W}\|_F^2 \\ \eta_2(\|\zeta\|) &= \lambda_{\max}(P)\|\mathbf{E}\|^2 + \lambda_{\max}(\tilde{P})\|\tilde{\mathbf{E}}\|^2 + \lambda_{\max}(\Gamma_w^{-1})\bar{h}\|\tilde{W}\|_F^2 \end{aligned} \quad (3.7.11)$$

Assumption 3.7.2. *Assume that*

$$R > \eta_1^{-1}(\eta_2(\theta)) \quad (3.7.12)$$

where θ is defined as

$$\theta \triangleq \frac{\sqrt{\left(\|PB\|^2 + \|\tilde{P}B\|^2\right) \left(2w_m p_m \bar{h} + \varepsilon_m \bar{h} + d_m\right)^2 + \kappa \bar{h} \|W - W_0\|_F^2}}{\min(\Theta_1, \Theta_2, \Theta_3)} \quad (3.7.13)$$

and

$$\begin{aligned} \Theta_1 &= \sqrt{\lambda_{\min}(Q) - 1 - k_{em}^2 \|PB\|^2} \\ \Theta_2 &= \sqrt{\lambda_{\min}(\tilde{Q}) - 3 - 2k_{em} \|\tilde{P}B\|} \\ \Theta_3 &= \sqrt{\kappa \bar{h} - \bar{h}^2 p_m^2 (\|PB\| + \|\tilde{P}B\|)^2 - \frac{h_m}{\lambda_{\min}(\Gamma_w)}} \end{aligned} \quad (3.7.14)$$

Remark 3.7.1 (Boundedness of RBF NN with Backpropagation *alone*). It is noted that the update law of adaptive control element with *back-propagation* alone, shown below, results in the proof of the boundedness of \mathbf{E} , $\tilde{\mathbf{E}}$ only,

$$\dot{\tilde{W}} = -\Gamma \Psi(\boldsymbol{\mu}) \check{\mathbf{E}}^T PB \quad (3.7.15)$$

where the matrix $\Gamma = \Gamma^T > 0$ is the rate of adaptation, or adaptation gain. Therefore in order to prove the boundedness of all parameters including \tilde{W} , we need to introduce a modification such as σ -modification or e -modification to the adaptation law (3.7.15). A similar remark is applicable to SHL NNs in Section 3.7.2. \diamond

Theorem 3.7.1. *Let assumptions 3.1.1 - 3.7.2 hold. Then, if the initial error $\zeta(0) \in \Omega_\alpha$, the control law given by (3.5.1), along with RBF NN shown below, guarantees that the signals \mathbf{E} , $\tilde{\mathbf{E}}$, and \tilde{W} in the closed loop system are all ultimately bounded.*

$$\dot{W} = -\Gamma \left[\Psi(\boldsymbol{\mu}) \tilde{\mathbf{E}}^T P B + \kappa (\hat{W} - W_0) \right] \quad (3.7.16)$$

where the matrix $\Gamma = \Gamma^T > 0$, the constant $\kappa > 0$ are the adaptation gains, and W_0 is a initial guess (or a guess).

Proof. See Appendix A □

From the result of Theorem 3.7.1, we can see that the overall control architecture of adaptive NDI scheme using RBF NNs developed in this chapter results in stable closed-loop systems for output feedback, NDI-based MIMO nonlinear systems.

3.7.2 SHL NN Adaptation

In this section, through Lyapunov theorems, we show that \mathbf{E} , $\tilde{\mathbf{E}}$, \tilde{V} , and \tilde{W} are all uniformly bounded using SHL NN with σ -modification.

From the definition of the candidate Lyapunov function \mathcal{L} in (3.7.4), there exist class \mathcal{K} functions φ_1 and φ_2 such that

$$\varphi_1(\zeta) \leq \mathcal{L}(\|\zeta\|) \leq \varphi_2(\zeta) \quad (3.7.17)$$

where

$$\begin{aligned} \varphi_1(\|\zeta\|) &= \lambda_{\min}(P) \|\mathbf{E}\|^2 + \lambda_{\min}(\tilde{P}) \|\tilde{\mathbf{E}}\|^2 + \lambda_{\min}(\Gamma_w^{-1}) \|\tilde{W}\|_F^2 + \lambda_{\min}(\Gamma_v^{-1}) \|\tilde{V}\|_F^2 \\ \varphi_2(\|\zeta\|) &= \lambda_{\max}(P) \|\mathbf{E}\|^2 + \lambda_{\max}(\tilde{P}) \|\tilde{\mathbf{E}}\|^2 + \lambda_{\max}(\Gamma_w^{-1}) \|\tilde{W}\|_F^2 + \lambda_{\max}(\Gamma_v^{-1}) \|\tilde{V}\|_F^2 \end{aligned} \quad (3.7.18)$$

Assumption 3.7.3. *Assume that*

$$R > \varphi_1^{-1}(\varphi_2(\lambda)) \quad (3.7.19)$$

where λ is defined as

$$\lambda \triangleq \frac{\sqrt{2\alpha_1 p_a + 2\gamma_1(\gamma_2 + d_m)\|PB\| + \kappa_w\|W - W_0\|_F^2 + \kappa_v\|V - V_0\|_F^2}}{\min(\Lambda_1, \Lambda_2, \Lambda_3)} \quad (3.7.20)$$

and

$$\begin{aligned} \Lambda_1 &= \sqrt{\lambda_{\min}(Q) - \gamma_1\|PB\|(1 + \gamma_2 + d_m) - 2p_a k_{em}} \\ \Lambda_2 &= \sqrt{\lambda_{\min}(\tilde{Q}) - 2p_a(\alpha_1 + \alpha_2) - \gamma_1\|PB\|(1 + \gamma_2 + d_m) - 6p_a k_{em}} \\ \Lambda_3 &= \sqrt{\kappa_a - 2\alpha_1 p_a - 2\gamma_1\|PB\|} \end{aligned} \quad (3.7.21)$$

Theorem 3.7.2. *Let assumptions 3.1.1 - 3.7.3 hold. Then, if the initial error $\zeta(0) \in \Omega_\alpha$, the control law given by (3.5.1), along with SHL NN shown below, guarantees that the signals \mathbf{E} , $\tilde{\mathbf{E}}$, \tilde{V} , and \tilde{W} in the closed loop system are all ultimately bounded.*

$$\begin{aligned} \dot{\hat{V}} &= -\Gamma_v \cdot \left[\boldsymbol{\mu} \check{\mathbf{E}}^T PB \hat{W}^T \hat{\boldsymbol{\sigma}}' + \kappa_v \cdot (\hat{V} - V_0) \right] \\ \dot{\hat{W}} &= -\Gamma_w \cdot \left[(\hat{\boldsymbol{\sigma}} - \hat{\boldsymbol{\sigma}}' \hat{V}^T \boldsymbol{\mu}) \check{\mathbf{E}}^T PB + \kappa_w \cdot (\hat{W} - W_0) \right] \end{aligned} \quad (3.7.22)$$

where $\hat{\boldsymbol{\sigma}} = \boldsymbol{\sigma}(\hat{V}^T \boldsymbol{\mu})$ and $\boldsymbol{\sigma}' = \text{diag}(d\sigma_i/dz_i)$ denotes the Jacobian matrix. Γ_v , Γ_w , κ_v , and $\kappa_w > 0$ are adaptation gains. W_0 and V_0 are initial guesses (or guesses).

Proof. See Appendix B □

From the result of Theorem 3.7.2, we can also conclude that the overall control architecture of adaptive NDI scheme using SHL NNs developed in this chapter results in stable closed-loop systems for output feedback, NDI-based MIMO nonlinear systems.

3.8 Conclusion

A systematic approach of adaptive output feedback control design for MIMO nonlinear systems is formulated by introducing feedback input-output linearization of nonlinear MIMO systems, nonlinear dynamic inversion, reference model, NNs and their parametrization, and linear observer.

Stability analysis with RBF NNs or SHL NNs using Lyapunov theorems is performed to show the boundedness of all errors of the closed-loop system.

Applications of this adaptive NDI control design follow in Chapters 4 – 6, where various aerial vehicles operated in nonlinear dynamic regimes are controlled.

CHAPTER IV

NEURAL NETWORK-BASED ADAPTIVE CONTROL OF F-15 ACTIVE AT NONLINEAR FLIGHT REGIMES

When advanced fighter aircraft fly at high angles of attack, unsteady aerodynamic effects, wing rock, and saturation of aerodynamic effectors can lead to difficulty in control and maneuverability. This chapter will illustrate the use of a neural network-based adaptive feedback control design applied to an advanced variant of the F-15 aircraft, the F-15 ACTIVE model with thrust vectoring capability and relaxed static stability. The effects of control saturation are directly accounted for in the design of the adaptive controller. The main objective of the control design is to demonstrate adaptation to aerodynamic uncertainty in the form of both unmodeled parameter variations and unmodeled dynamics not present in the nominal inverting control design. Hypothetical aerodynamic models are implemented to test the design approach at high angles of attack.

4.1 Introduction

Future aircraft are expected to have enhanced performance and maneuverability, which will require them to routinely operate in nonlinear aerodynamic flight regimes. Operation in near- and post-stall high angle of attack (high-alpha) regimes is important for air superiority of next-generation fighter aircraft as well as uninhabited combat aerial vehicles. Novel advanced control design methodologies are required to address the complex nonlinear dynamic characteristics of such vehicles. Uncertainty associated with modeling, and the complexity of the nonlinear and unsteady phenomena associated with high-alpha flight present the main

challenges in designing flight control systems for these regimes.

Conventional flight control design methods make use of linearized models and gain scheduling. Models at high alpha conditions are usually obtained using computational fluid dynamics (CFD) techniques or high-alpha wind tunnel test techniques, leading to complex representations of the aerodynamic characteristics of the aircraft. Linearized aerodynamic models do not reliably predict many of the well-known nonlinear, unsteady characteristics at these angles of attack, such as wing rock, roll reversal, and yaw departure, among others. Moreover, such aggressive flight maneuvers are likely to occur under highly dynamic flight conditions, implying that aeroelastic effects will also be significant. In addition, it should also be recognized that novel actuation devices with highly nonlinear characteristics are currently under development (for example, synthetic jet devices for active flow control and virtual shape control devices) that could prove to be effective for control at high alpha conditions. These devices may be either continuous or discrete in their characteristics. This combination of factors suggests that a new flight control design paradigm is needed to address the following challenges:

- The vehicle may encounter a high degree of both parametric and dynamic uncertainty at high angle of attack.
- Both the aircraft dynamics and its actuation devices may be highly nonlinear.
- Some or all of the actuation devices may become saturated.
- There may be a combination of both discrete (on-off or bang-bang) and continuous actuation.

This chapter suggests a design paradigm building on past results in the area of NN-based adaptive flight control which have been successfully utilized for a variety of aerospace applications [14, 105], while incorporating recent advances in the areas of output feedback and adaptation under saturated control conditions. The paradigm is based on approximate

feedback linearization and synthesis of a *fixed-gain* dynamic compensator, while incorporating a NN to compensate for model inversion error. The adaptive nonlinear dynamic inversion output feedback formulation developed in Chapter 3 is applied to compensate for the full dynamic characteristics of the plant. Treatment of control saturation is described in [38,39].

The F-15 ACTIVE and its control effectors are described in Section 4.2. Mathematical modeling of high angle of attack aerodynamics is discussed in Section 4.3. Section 4.4 illustrates the adaptive control structure along with its elements: two-stage dynamic inversion, control allocation, thrust vector scheduling. Pseudo-control hedging (PCH) to handle control input nonlinearities is described in Section 4.4.6, and NNs are briefly discussed in Section 4.4.7. Simulation results are presented in Section 4.5. Conclusions are given in Section 4.6.

4.2 Aircraft Model and Control Effectors

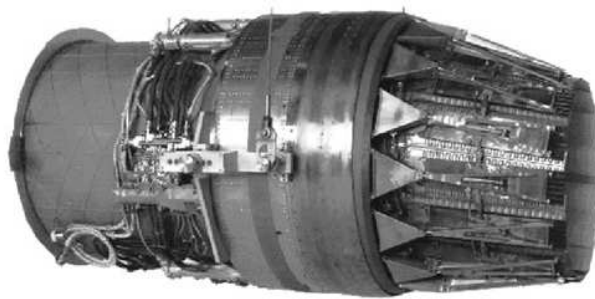
The basic F-15 aircraft dynamic model used for this research is obtained from [8]. The 6-DOF F-15 model has a complete set of look-up tables of aerodynamic coefficients as functions of Mach, α , β , altitude and aerodynamic control deflections, which is useful up to 60° angle of attack.

Maneuvering an aircraft in highly nonlinear dynamic regimes or at high angles of attack requires an abundance of control authority. In order to enhance the maneuverability of the vehicle, we incorporate models for advanced aerodynamic actuators, differential stabilator, and thrust vector control (TVC) nozzles [17] of the F-15 ACTIVE aircraft as shown in Figure 77, as well as application of relaxed static stability (RSS).

TVC nozzles are to increase the control power of the F-15 aircraft in all axes at high angles of attack, where aerodynamic controls have little contribution. The nozzles are modeled by the Pitch/Yaw Balance Beam Nozzles (P/YBBN) of the F-15 ACTIVE aircraft, which allow at most 20 degrees of nozzle deflection in any direction. TVC nozzle angle limiters are implemented in the model to keep their movements within their own physical constraints. Each nozzle model is also rate limited. Rolling moment can be produced by differential pitch



(a) F-15 ACTIVE and its aerodynamic controls



(b) Thrust Vector Nozzle: P/YBBN

Figure 7: NASA F-15 ACTIVE and its control effectors

thrust vectoring of the left and right nozzles. Thus, vectoring the thrust lines can generate pitching, yawing and rolling moments by deflecting the nozzles synchronously or differentially as required. Because full deflection of TVC in one direction is only achievable when the other direction has zero deflection, a need to set a priority strategy among these movements along 3 axes arises. As depicted in Figure 8, priority is given to the pitch/roll angle direction, i.e. it first follows the pitch/roll command to the extent possible and then follows the yaw command to the extent possible. Control activation scheduling of TV nozzles is described in Section 4.4.

To maximize the rolling moment achievable by aerodynamic controls, differential deflection of two horizontal stabilators, defined by $\delta_{DT} = (\delta_{e_{right}} - \delta_{e_{left}}) / 2$, is introduced. The mathematical modeling of force and moment coefficients including differential stabilator δ_{DT} are described in [86].

To achieve higher angle of attack responses, the aircraft model is destabilized in pitch to become a RSS aircraft. This destabilization was carried out by moving the CG point of the model backward. Coupling the effects of this RSS modification along with thrust vector nozzles and differential stabilators, a much more agile aircraft model is developed, enabling maneuvers at high angles of attack.

4.3 High Alpha Aerodynamics

It is well known that aerodynamic derivatives at high angle of attack are highly nonlinear, complex and even unstable. Thus in addition to the basic aerodynamic data from wind tunnel tests, we need to investigate additional nonlinear aerodynamic effects by including or altering the damping derivatives of the vehicle at high alpha flight conditions. In this research, an unsteady aerodynamic model is implemented in pitch axis, while nonlinear, unstable effects of significant damping derivatives are added in lateral/directional axes.

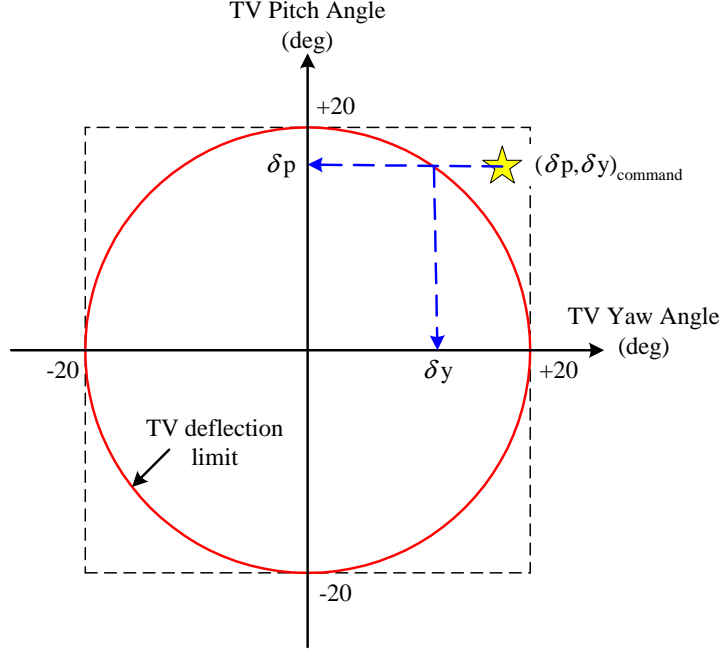


Figure 8: Thrust vectoring angle limit and priority

4.3.1 Unsteady Aerodynamics

High angle-of-attack flight with large amplitude maneuvers is affected by unsteady aerodynamic effects such as aerodynamic lag on the wings especially in the post-stall region. Thus we incorporated an unsteady aerodynamic model in the pitch axis to test the robustness of the adaptive controller to these effects. To this end, a modified version of an unsteady aerodynamic model based on indicial functions was adopted [46]. The unsteady aerodynamic model in longitudinal axis can be expressed as:

$$\begin{bmatrix} \dot{\alpha} \\ \dot{q} \\ \dot{x}_\alpha \end{bmatrix} = \begin{bmatrix} Z_\alpha & Z_q & 0 \\ C & M_q & B \\ 1 & 0 & -b_1 \end{bmatrix} \begin{bmatrix} \alpha \\ q \\ x_\alpha \end{bmatrix} + \begin{bmatrix} Z_\delta \\ M_\delta \\ 0 \end{bmatrix} \cdot \delta \quad (4.3.1)$$

where

$$B = \frac{\rho V^2 S \bar{c}}{2I_{yy}} a b_1, \quad C = \frac{\rho V^2 S \bar{c}}{2I_{yy}} c \quad (4.3.2)$$

and $a = 0.25$, $c = -0.23$, $b_1 = 1.0$.

4.3.2 Lateral/Directional Aerodynamics at High-Alpha

The three significant lateral/directional aerodynamic damping coefficients used in the aircraft model are presented in Figure 9, where positiveness of C_{l_p} and C_{n_r} at high α implies instability.

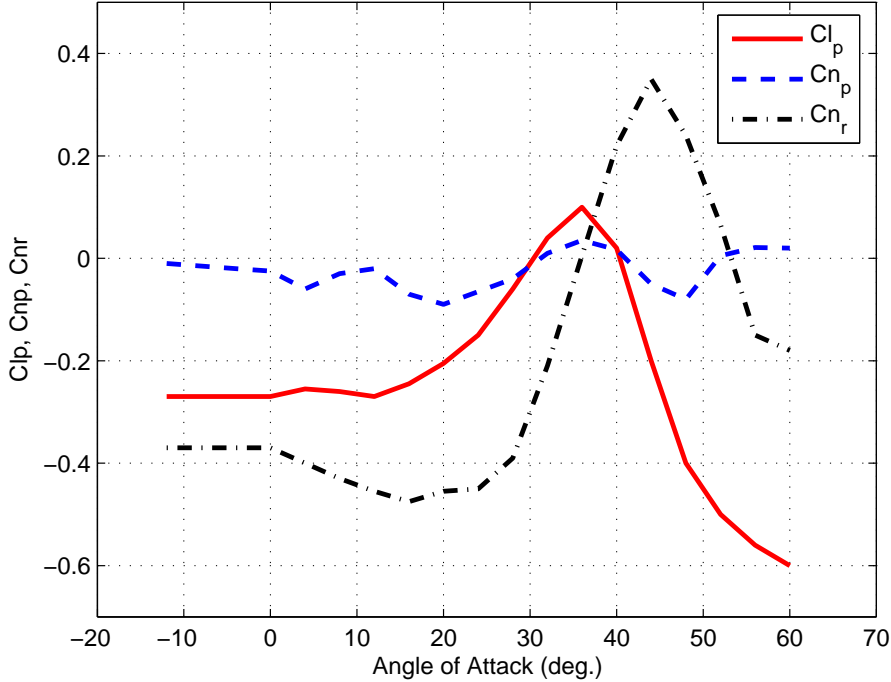


Figure 9: Three dominant lateral/directional aerodynamic damping coefficients

4.4 Adaptive Control Structure

In this design approach based on the formulation in Chapter 3, angle of attack (α), sideslip angle (β) and stability axis roll rate (p_s) are commanded. As shown in Figure 10, the pilot's command is input to the command filters to generate reference signals, while employing PCH to protect the adaptive process from control saturation nonlinearities. Next, proportional and derivative (PD) controllers are used to follow the reference commands. The control commands are obtained by a two-stage dynamic inversion. Since there are not α and β sensors, the required feedbacks are assumed to be computed by integration of IMU sensor

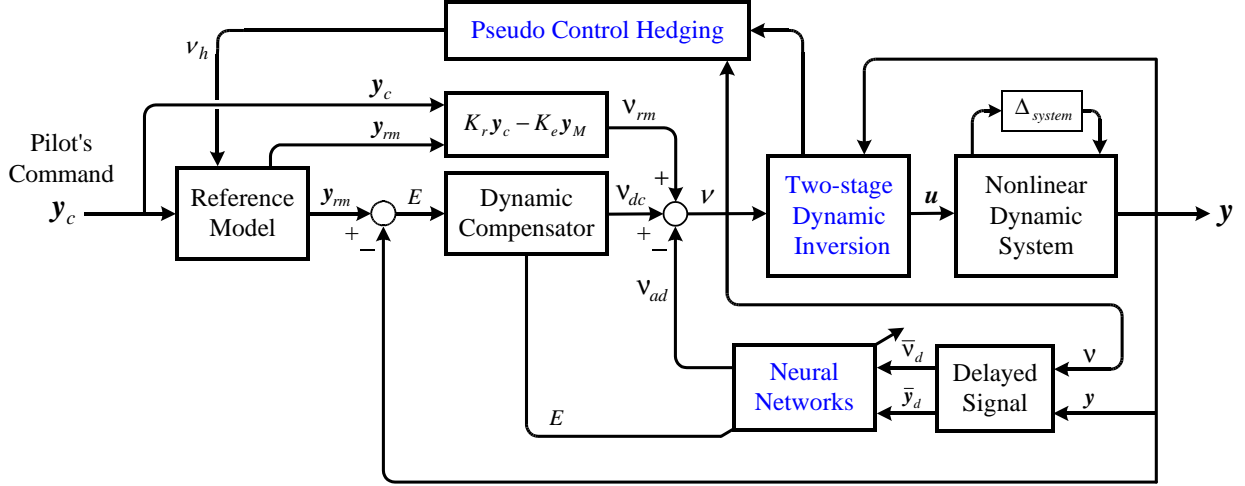


Figure 10: Adaptive feedback control architecture

outputs. The PCH and the NN signals shown in Figure 10 are discussed later.

4.4.1 Two-stage Dynamic Inversion

A two-stage approach for dynamic inversion has been developed for designing a flight control system that regulates $[p_s \ \alpha \ \beta]$. It assumes that the state dynamics can be decomposed in stages as follows [2, 6, 105]:

- Stage 1 dynamics, $\mathbf{x}_1 = [\alpha \ \dot{\alpha} \ \beta \ \dot{\beta} \ \phi \ \theta \ V]^T$
- Stage 2 dynamics, $\mathbf{x}_2 = [p_s \ q \ r_s]^T$

It should be noted that the references use the terminology *slow* and *fast*, which is not strictly appropriate as the dynamics are not separable according to the definitions given above. However, the inverting solution does not rely on a separation in dynamics to be valid. Therefore it is more appropriate to say that the inversion is done in two stages, which is the terminology we will use.

The structure of the inverting law and its implementation is displayed in Figure 11. In both stages of the inversion, the equations of motion are expressed in the form

$$\begin{aligned} \dot{\mathbf{x}} &= a(\mathbf{x}) + b(\mathbf{x})\mathbf{u} \\ \mathbf{y} &= C\mathbf{x} \end{aligned} \tag{4.4.1}$$

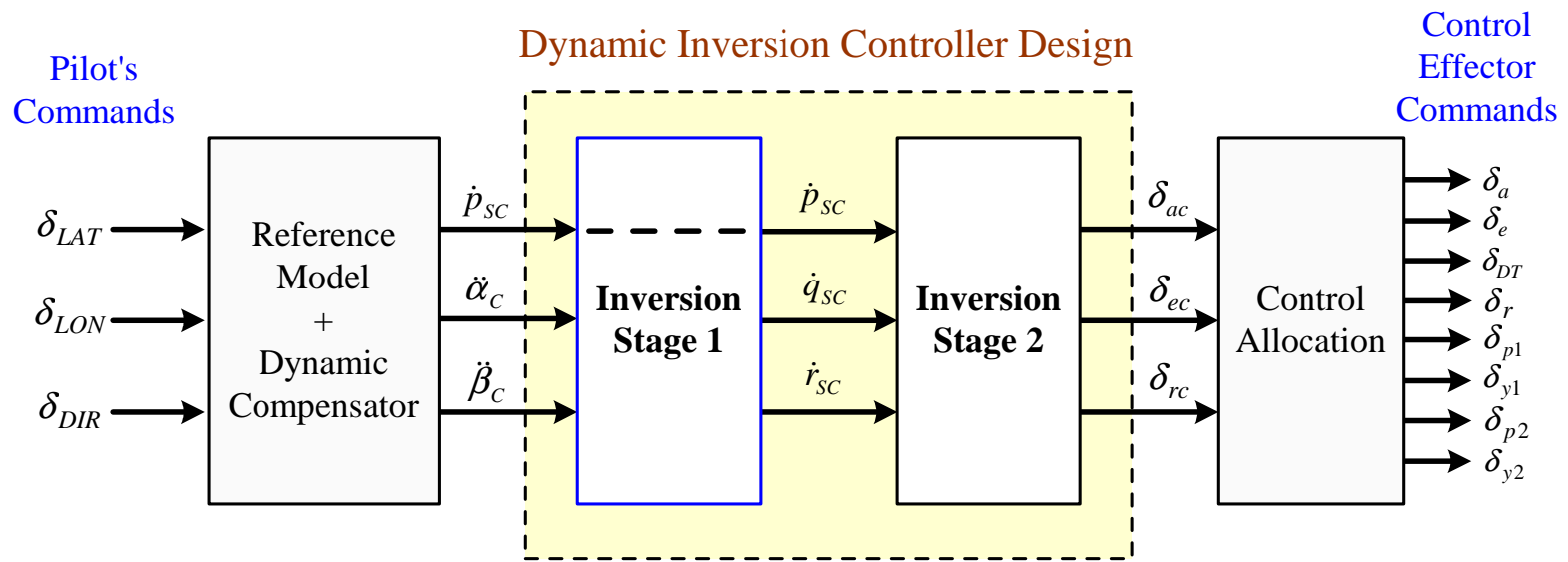


Figure 11: Two-stage dynamic inversion control law structure

where \mathbf{y} defines the regulated variables and \mathbf{u} defines the control variables, which are the output variables of the inverting blocks in the figure.

The control variables for the stage 1 dynamics are the angular accelerations in the roll, pitch and yaw stability axis frame

$$\mathbf{u}_1 = [\dot{p}_{sc} \ \dot{q}_{sc} \ \dot{r}_{sc}]^T \quad (4.4.2)$$

and the control variables for the stage 2 dynamics are the effective control displacement commands in each axis

$$\mathbf{u}_2 = [\delta_{ac} \ \delta_{ec} \ \delta_{rc}]^T \quad (4.4.3)$$

Assuming $Cb(\mathbf{x})$ is invertible, then the inverting design in each stage is based on

$$\begin{aligned} \dot{\mathbf{y}} &= Ca(\mathbf{x}) + Cb(\mathbf{x})\mathbf{u} \\ &= \boldsymbol{\nu} \end{aligned} \quad (4.4.4)$$

where $\boldsymbol{\nu}$ is the pseudo-control. The pseudo-control is a linear control law designed to regulate \mathbf{y} , and corresponds to the inputs to each inverting block in Figure 11.

The regulated variables in each stage are:

$$\begin{aligned} \mathbf{y}_1 &= [p_s \ \dot{\alpha} \ \dot{\beta}]^T \\ \mathbf{y}_2 &= [p_s \ q \ r_s]^T \end{aligned} \quad (4.4.5)$$

Note that the regulated variables of the stage 1 dynamics are related to regulated variables $[p_s \ \alpha \ \beta]$ according to the relative degree of each regulated variable. The variable p_s has relative degree one, while α and β each have relative degree two (it is necessary to differentiate these variables twice before a control term appears). Therefore \mathbf{y}_1 is defined so that the control appears in the first derivative of each of its elements. The same is true for stage 2. Complete equations of motion of the aircraft are simplified through reasonable assumptions for implementation. Refer to Appendix E for details.

4.4.1.1 Stage 1 Dynamics

Subject to a set of approximations [17] the stage 1 dynamics can be expressed in the following form:

$$\begin{bmatrix} \dot{\alpha} \\ \ddot{\alpha} \\ \dot{\beta} \\ \ddot{\beta} \\ \dot{\phi} \\ \dot{\theta} \\ \dot{V} \\ \ddot{V} \end{bmatrix} = \begin{bmatrix} f_1(\mathbf{x}) \\ f_2(\mathbf{x}, \boldsymbol{\delta}) \\ f_3(\mathbf{x}) \\ f_4(\mathbf{x}, \boldsymbol{\delta}) \\ f_5(\mathbf{x}, \boldsymbol{\delta}) \\ f_6(\mathbf{x}, \boldsymbol{\delta}) \\ f_7(\mathbf{x}, \boldsymbol{\delta}) \\ f_8(\mathbf{x}, \boldsymbol{\delta}, \dot{\boldsymbol{\delta}}) \end{bmatrix} + \begin{bmatrix} 0 & 0 & 0 \\ -\tan(\beta) & 1 & 0 \\ 0 & 0 & 0 \\ 0 & 0 & -1 \\ 0 & 0 & 0 \\ 0 & 0 & 0 \\ 0 & 0 & 0 \\ 0 & 0 & 0 \end{bmatrix} \begin{bmatrix} \dot{p}_s \\ \dot{q} \\ \dot{r}_s \end{bmatrix} \quad (4.4.6)$$

where p_s and r_s denote the stability axis roll and yaw rates. For purposes of inverting design, we can eliminate the states associated with zero dynamics, and reduce (4.4.6) to the following:

$$\begin{aligned} \begin{bmatrix} \dot{p}_s \\ \ddot{\alpha} \\ \ddot{\beta} \end{bmatrix} &= \begin{bmatrix} 0 \\ f_2(\mathbf{x}, \boldsymbol{\delta}) \\ f_4(\mathbf{x}, \boldsymbol{\delta}) \end{bmatrix} + \begin{bmatrix} 1 & 0 & 0 \\ -\tan(\beta) & 1 & 0 \\ 0 & 0 & -1 \end{bmatrix} \begin{bmatrix} \dot{p}_s \\ \dot{q} \\ \dot{r}_s \end{bmatrix} \\ &= F(\mathbf{x}, \boldsymbol{\delta}) + G(\mathbf{x}) \cdot \mathbf{u}_1 \end{aligned} \quad (4.4.7)$$

4.4.1.2 Stage 2 Dynamics

Similarly, the stage 2 dynamics can be expressed as:

$$\begin{bmatrix} \dot{p}_s \\ \dot{q} \\ \dot{r}_s \end{bmatrix} = \begin{bmatrix} f_9(\mathbf{x}) \\ f_{10}(\mathbf{x}) \\ f_{11}(\mathbf{x}) \end{bmatrix} + \begin{bmatrix} \overline{L}_{\delta_a} & 0 & 0 \\ 0 & M_{\delta_e} & 0 \\ 0 & 0 & \overline{N}_{\delta_r} \end{bmatrix} \begin{bmatrix} \delta_{ac} \\ \delta_{ec} \\ \delta_{rc} \end{bmatrix} \quad (4.4.8)$$

where $\bar{L}_{\delta_a}, M_{\delta_e}, \bar{N}_{\delta_r}$ are control effectiveness functions which are described in detail in Appendix E.

4.4.2 Control Allocation with TV and DT

As we saw in the previous section, the aircraft has redundant control effectors in each axis. Therefore we need a policy to manage this redundancy effectively. In this section, we consider how to allocate the controls including thrust vector nozzles and differential stabilators.

Consider the stage 2 dynamic equation (4.4.8) expressed as

$$\begin{aligned}\dot{\mathbf{x}}_2 &= A(\mathbf{x}) + B(\mathbf{x})\mathbf{u}_2 \\ \mathbf{y}_2 &= \mathbf{x}_2\end{aligned}\tag{4.4.9}$$

where

$$A(\mathbf{x}) = \begin{bmatrix} f_9(\mathbf{x}) & f_{10}(\mathbf{x}) & f_{11}(\mathbf{x}) \end{bmatrix}^T\tag{4.4.10}$$

$$B(\mathbf{x}) = \begin{bmatrix} \bar{L}_{\delta_a} & 0 & L_{DT} & 0 & \bar{L}_{TV} & 0 & \bar{L}_{TV} & 0 \\ 0 & M_{\delta_e} & 0 & 0 & \bar{M}_{DT} & 0 & \bar{M}_{TV} & 0 \\ 0 & 0 & N_{DT} & \bar{N}_{\delta_r} & 0 & \bar{N}_{TV} & 0 & \bar{N}_{TV} \end{bmatrix}\tag{4.4.11}$$

$$\mathbf{x}_2 = \begin{bmatrix} p_s & q & r_s \end{bmatrix}^T\tag{4.4.12}$$

$$\mathbf{u}_2 = \begin{bmatrix} \delta_a & \delta_e & \delta_{DT} & \delta_r & \delta_{p1} & \delta_{y1} & \delta_{p2} & \delta_{y2} \end{bmatrix}^T\tag{4.4.13}$$

δ_a is aileron deflection, δ_e is elevator deflection, δ_{DT} is differential stabilator, δ_r is rudder deflection, δ_{p1}, δ_{y1} are the pitch and yaw vectoring angles of the left engine, and δ_{p2}, δ_{y2} are the pitch and yaw vectoring angles of the right engine.

A control allocation matrix is introduced in order to relate the effective control demand associated with each axis to the actual controls. Letting $\mathbf{u}_e = \begin{bmatrix} \delta_a & \delta_e & \delta_r \end{bmatrix}^T$ denote the effective control demand, then

$$\mathbf{u}_2 = T_a \cdot \mathbf{u}_e\tag{4.4.14}$$

where

$$T_a = \begin{bmatrix} 1 & 0 & 0 \\ 0 & 1 & 0 \\ 0.5 & 0 & 0 \\ 0 & 0 & 1 \\ S_p & S_\alpha & 0 \\ 0 & 0 & S_\beta \\ -S_p & S_\alpha & 0 \\ 0 & 0 & S_\beta \end{bmatrix} \quad (4.4.15)$$

From (4.4.15) and (4.4.14), it can be seen that the roll component of \mathbf{u}_e is allocated to aileron, differential tail (DT), and differential pitch thrust vector deflections, the pitch component of \mathbf{u}_e is allocated to symmetric tail (elevator) and symmetric pitch thrust vector deflections, and the yaw component of \mathbf{u}_e is allocated to rudder and symmetric yaw thrust vector deflections. Therefore control redundancy exists in all three channels.

4.4.3 Thrust Vector Scheduling

Thrust vector scheduling variables S_p , S_α and S_β in (4.4.15) depend on the ratio of the peak moments available from aerodynamic and thrust vector control according to:

$$S_p = \begin{cases} 0 & , \quad L_{TV} < \frac{1}{2}L_{aero} \\ 2 - \frac{L_{aero}}{L_{TV}} & , \quad \frac{1}{2}L_{aero} \leq L_{TV} \leq L_{aero} \\ 1 & , \quad L_{TV} > L_{aero} \end{cases} \quad (4.4.16)$$

$$S_\alpha = \begin{cases} 0 & , \quad M_{TV} < \frac{1}{2}M_{aero} \\ 2 - \frac{M_{aero}}{M_{TV}} & , \quad \frac{1}{2}M_{aero} \leq M_{TV} \leq M_{aero} \\ 1 & , \quad M_{TV} > M_{aero} \end{cases} \quad (4.4.17)$$

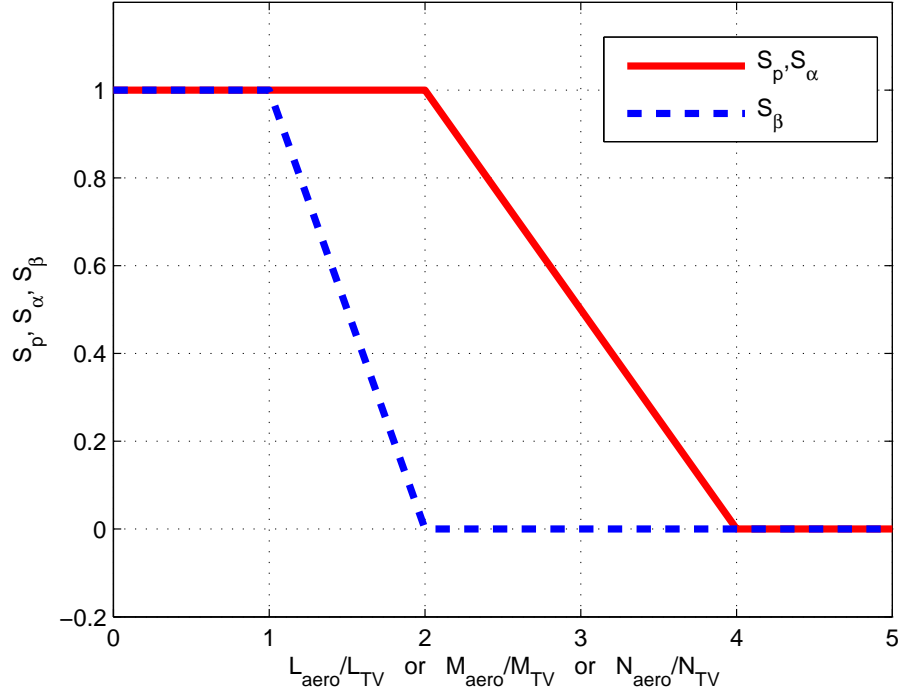


Figure 12: Shape of thrust vector scheduling variables

$$S_\beta = \begin{cases} 0 & , \quad N_{TV} < \frac{1}{4}N_{aero} \\ 2 - \frac{N_{aero}}{N_{TV}} & , \quad \frac{1}{4}N_{aero} \leq N_{TV} \leq N_{aero} \\ 1 & , \quad N_{TV} > N_{aero} \end{cases} \quad (4.4.18)$$

where L_{aero} , M_{aero} and N_{aero} are the rolling, pitching and yawing moment margins available from aerodynamic controls, and L_{TV} , M_{TV} and N_{TV} are the marginal rolling, pitching and yawing moment available from thrust vector controls [50]. Thrust vector scheduling is depicted in Figure 12.

4.4.4 Computation of the Effective Control (\mathbf{u}_e)

From (4.4.9) it follows that

$$\begin{aligned}
 \dot{\mathbf{y}}_2 &= \dot{\mathbf{x}}_2 \\
 &= A(\mathbf{x}) + B(\mathbf{x})\mathbf{u}_2 \\
 &= A(\mathbf{x}) + B(\mathbf{x}) \cdot T_a \mathbf{u}_e \\
 &= \mathbf{u}_1
 \end{aligned} \tag{4.4.19}$$

The stage 1 dynamic equation is given as

$$\begin{aligned}
 \dot{\mathbf{y}}_1 &= F(\mathbf{x}) + G(\mathbf{x})\mathbf{u}_1 \\
 &= \boldsymbol{\nu}
 \end{aligned} \tag{4.4.20}$$

where $\boldsymbol{\nu}$ is the pseudo-control. Combining (4.4.19) and (4.4.20), we have

$$\mathbf{u}_e = (\hat{G}(\mathbf{x})\hat{B}(\mathbf{x})T_a)^{-1} \left[\boldsymbol{\nu} - \left(\hat{F}(\mathbf{x}) + \hat{G}(\mathbf{x})\hat{A}(\mathbf{x}) \right) \right] \tag{4.4.21}$$

where $\hat{G}(\mathbf{x})$, $\hat{B}(\mathbf{x})$, $\hat{F}(\mathbf{x})$ and $\hat{A}(\mathbf{x})$ denote estimates of $G(\mathbf{x})$, $B(\mathbf{x})$, $F(\mathbf{x})$ and $A(\mathbf{x})$. Substitution of (4.4.21) into (4.4.14) provides the commanded control that is applied to the aircraft.

4.4.5 Adaptive Control

The pseudo-control for feedback control design, depicted in Figure 10, has the form

$$\boldsymbol{\nu} = \boldsymbol{\nu}_{dc} + \boldsymbol{\nu}_{rm} - \boldsymbol{\nu}_{ad} \tag{4.4.22}$$

where $\boldsymbol{\nu}_{rm} = \mathbf{x}_c^{(r)}$ is output of an r^{th} -order reference model that is used to define the desired closed loop response, $\boldsymbol{\nu}_{dc}$ is the output of a dynamic compensator, and $\boldsymbol{\nu}_{ad}$ is the adaptive signal. The error dynamics for the state feedback can be expressed as

$$\begin{aligned}
 \tilde{\mathbf{x}}_c^{(r)} &= \mathbf{x}_c^{(r)} + \mathbf{x}^{(r)} \\
 &= -\boldsymbol{\nu}_{dc} + \boldsymbol{\nu}_{ad} - \boldsymbol{\Delta}
 \end{aligned} \tag{4.4.23}$$

It is apparent that the dynamic compensator should be designed to stabilize (4.4.23), and that the role of $\boldsymbol{\nu}_{ad}$ is to cancel $\boldsymbol{\Delta}$.

4.4.6 Pseudo-Control Hedging (PCH)

PCH is used to address NN adaptation difficulties arising from various actuation nonlinearities, including actuator position and/or rate saturation, discrete (magnitude quantized) control, time delays and actuator dynamics [39]. NN training difficulties occur when unmodeled actuator characteristics are encountered. For example, the NN adaptive element will attempt to adapt to these nonlinearities, even when it is impossible to do so. The goal of PCH is to prevent the adaptive element from attempting to adapt to these characteristics, while not affecting NN adaptation to other sources of inversion error. Conceptually, PCH "moves the reference model backwards" by an estimate of the amount the controlled system did not move due to selected actuator characteristics (such a position and rate limits, time delays, etc). The reference model is hedged according to an estimate of the difference between the commanded and achieved pseudo-control.

The hedge signal is defined as

$$\boldsymbol{\nu}_h = \boldsymbol{\nu} - \hat{\boldsymbol{\nu}} \quad (4.4.24)$$

where $\boldsymbol{\nu}$ is the commanded pseudo-control as defined in (4.4.20), and $\hat{\boldsymbol{\nu}}$ is an estimate for the achieved pseudo-control. The estimate is obtained by combining (4.4.14), (4.4.19) and (4.4.20) and replacing the elements of \mathbf{u}_2 by estimates obtained from actuator models of the form in Figure 13. Thus,

$$\boldsymbol{\nu}_h = \boldsymbol{\nu} - \left[\hat{F}(\mathbf{x}) + \hat{G}(\mathbf{x})\hat{A}(\mathbf{x}) + \hat{G}(\mathbf{x})\hat{B}(\mathbf{x}) \cdot \hat{\mathbf{u}}_2 \right] \quad (4.4.25)$$

The elements of the hedge signal are then subtracted in the reference models for each respective axis (roll, pitch and yaw). The manner in which this is done for a second order reference model is depicted in Figure 14.

4.4.7 Neural Network Adaptation

The properties of NNs described in Chapter 2 are used for adaptive control design. According to (4.4.23) and (4.4.25), Δ depends on the states and the pseudo-control. As described in

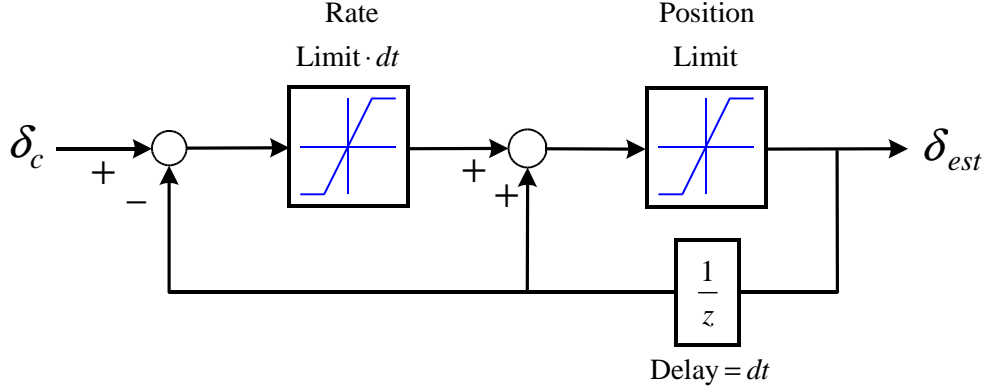


Figure 13: Actuator estimator

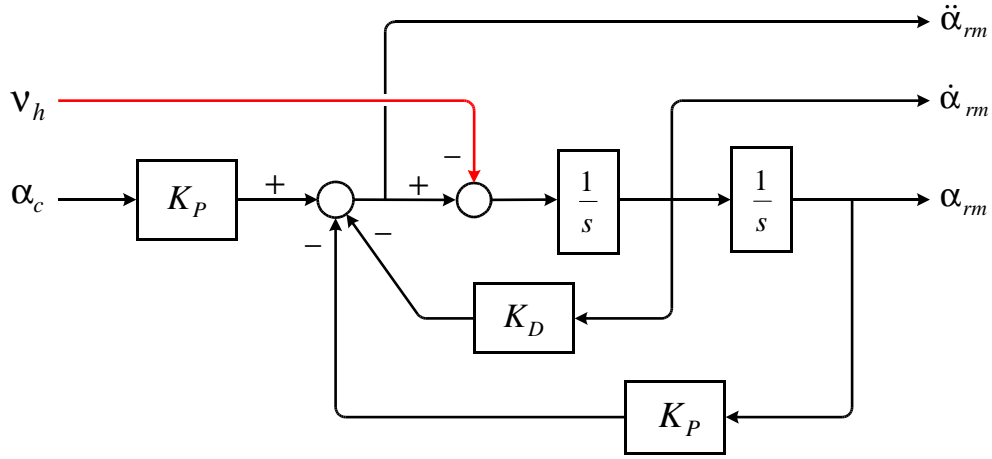


Figure 14: Reference model with hedging in pitch channel

Chapter 2, it has been shown that this error can be approximated, in a bounded region, to any desired degree of accuracy using a neural network (NN) with a sufficient number of hidden layer neurons, having the following input vector [11, 29]:

$$\boldsymbol{\mu}(t) = [1 \quad \bar{\boldsymbol{v}}_d^T(t) \quad \bar{\boldsymbol{y}}_d^T(t)] \quad (4.4.26)$$

where

$$\begin{aligned} \bar{\boldsymbol{v}}_d(t) &= [\nu(t) \quad \nu(t-d) \quad \cdots \quad \nu(t-(n_1-r-1)d)]^T \\ \bar{\boldsymbol{y}}_d(t) &= [y(t) \quad y(t-d) \quad \cdots \quad y(t-(n_1-r-1)d)]^T \end{aligned} \quad (4.4.27)$$

with $n_1 \geq n$ and $d > 0$ denotes time delay.

In the case of SHL NNs shown in Figure 3, we have

$$\boldsymbol{\nu}_{ad}(t) = \hat{W}^T \boldsymbol{\sigma} \left(\hat{V}^T \boldsymbol{\mu} \right) \quad (4.4.28)$$

where $\boldsymbol{\sigma}$ is a vector whose elements, $\sigma_i(z_i)$, are the basis functions of the NN. Typically, these basis functions are selected as so-called squashing functions. The form we employed is $\sigma_i(z_i) = 1 / (e^{-a_i z_i} + 1)$, where a_i is the activation potential. The network weights are updated according to the following adaptation laws:

$$\begin{aligned} \dot{\hat{V}} &= -\Gamma_v \left[2\boldsymbol{\mu} \mathbf{E}^T P B \hat{W}^T \hat{\boldsymbol{\sigma}}' + \kappa_v \left(\hat{V} - V_0 \right) \right] \\ \dot{\hat{W}} &= -\Gamma_w \left[2 \left(\hat{\boldsymbol{\sigma}} - \hat{\boldsymbol{\sigma}}' \hat{V}^T \boldsymbol{\mu} \right) \mathbf{E}^T P B + \kappa_w \left(\hat{W} - W_0 \right) \right] \end{aligned} \quad (4.4.29)$$

where $\hat{\boldsymbol{\sigma}} = \boldsymbol{\sigma} \left(\hat{V}^T \boldsymbol{\mu} \right)$ and $\boldsymbol{\sigma}' = \text{diag} (d\sigma_i/dz_i)$. P is the positive definite solution to the Lyapunov equation $A^T P + P A^T = -Q$ with $Q = Q^T > 0$, Γ_v , Γ_w , κ_v , and κ_w are adaptation gains, \mathbf{E} is the tracking error, and W_0 and V_0 are initial guesses (or guesses). It has been shown in Appendix B that the adaptive laws given in (4.4.29) guarantee that all error signals and network weights are uniformly bounded.

4.5 Simulations

4.5.1 Control Design Parameters

The control design was carried out assuming that the pilot commands α , β , and p_s . The roll channel is relative degree one ($r = 1$) with respect to the control, while both the α and β channels are relative degree two as shown in Figure 15. The design for the α -channel control architecture is described here.

A dynamic compensator or linear controller is designed for each degree of freedom assuming perfect inversion. The linear controller is designed so that the error dynamics are stabilized. In the case of state feedback, this can be achieved using a standard proportional and derivative (PD) controller, although additional integral action can be incorporated to

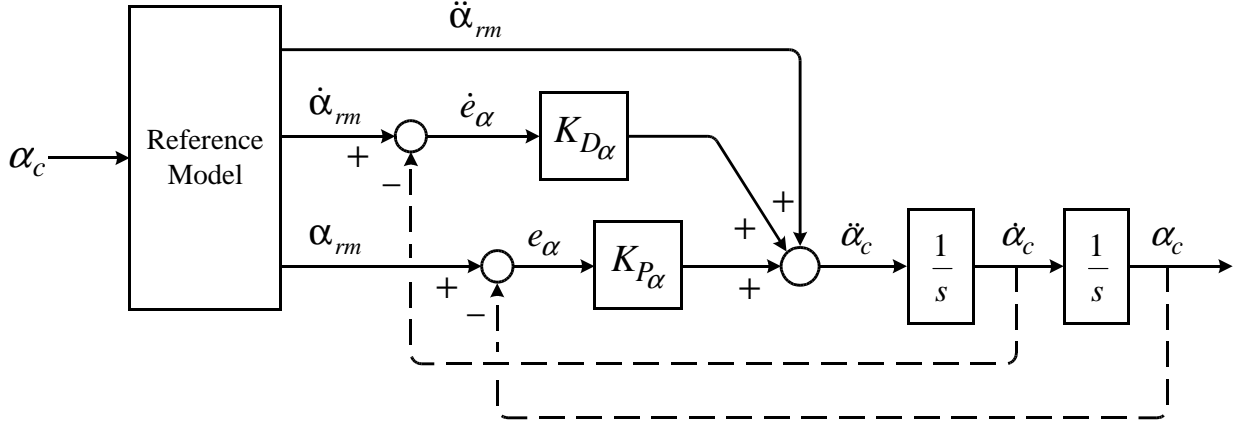


Figure 15: Structure of a second order relative degree pitch channel linear controller

improve steady state performance. In general, the linear controller can be designed using any technique as long as the linearized closed-loop system is stable.

With reference to (4.4.22), we have a dynamic compensator as

$$\begin{aligned} \boldsymbol{\nu}_{dc} &= K_e \cdot \mathbf{E} \\ &= [K_P \ K_D] \cdot \mathbf{E} \end{aligned} \quad (4.5.1)$$

where the tracking error vector is defined by

$$\mathbf{E} = \begin{bmatrix} y_{rm} - y \\ \dot{y}_{rm} - \dot{y} \end{bmatrix} \quad (4.5.2)$$

The tracking error dynamics are given by

$$\begin{aligned} \dot{\mathbf{E}} &= A_e \mathbf{E} + B_e (\boldsymbol{\nu} - \Delta) \\ A_e &= \begin{bmatrix} 0 & 1 \\ -K_P & -K_D \end{bmatrix}, \quad B_e = \begin{bmatrix} 0 \\ 1 \end{bmatrix}, \end{aligned} \quad (4.5.3)$$

The gains are related to the natural frequency and damping ratio by:

$$K_P = \omega_n^2, \quad K_D = 2\zeta\omega_n \quad (4.5.4)$$

Note that, as shown in Chapter 3, dynamic compensators $\boldsymbol{\nu}_{dc}$ and $\boldsymbol{\nu}_{rm}$ of the adaptive NDI design have fixed gains, using (3.5.4) we set them to make the tracking error dynamics in

(3.5.6), or (4.5.3) for this case, have the same stable pole locations as those of the reference model.

Since $r = 1$ in the roll channel, a first order reference model is employed for that channel, with a time constant of 0.3. Likewise, second order reference models are employed in the pitch and directional channels, with $\omega_n = 3 \text{ rad/sec}$ and $\zeta = 1.5$. The values selected for the NN gains, defined in (4.4.29), the number of hidden layer neurons(n_2), and the number of inputs(n_1), including input/output delays, to NN update laws are given in Table 1.

Table 1: F-15 ACTIVE neural network parameters

Channel	Γ_V	Γ_W	κ_v, κ_w	n_1	n_2	d
p_s	3.0	3.0	0.5	23	10	0.01
α	5.0	4.0	0.1	23	10	0.01
β	3.0	3.0	0.1	23	10	0.01

Following the approach suggested in Appendix B of [38], we choose

$$Q = \begin{bmatrix} \zeta\omega_n^5 & 0 \\ 0 & \zeta\omega^3 \end{bmatrix} = \begin{bmatrix} 364.3 & 0 \\ 0 & 40.5 \end{bmatrix} \quad (4.5.5)$$

The activation potentials (a_i) were uniformly distributed between 0.1 and 0.5. In addition, the first NN basis function was used to provide a bias term ($a_0 = 0$).

All control effectors have their own dynamic constraints or nonlinearities such as magnitude limit and rate limit, as shown in Table 2. When any of these nonlinearities occurs, PCH works to protect the adaptive process from it.

The unsteady aerodynamic effect described earlier was also implemented in the pitch axis. Consequently, this effect has little impact on the lateral modes such as sideslip angle and roll rate, which is to be expected. The unstable lateral/directional aerodynamic damping coefficients were used and they have significant impact on the responses of the aircraft during high- α maneuvers.

Table 2: F-15 ACTIVE control effectors and their dynamic constraints

Name	Symbol	Magnitude limits (deg.)	Rate limits (deg/sec)	Remark
Aileron	δ_a	-20 to +20	± 100	
Stabilator (Elevator)	δ_e	-25 to +25	± 46	
Differential Stabilator	δ_{DT}	-25 to +25	± 46	$\delta_{DT} = (\delta_{e_{right}} - \delta_{e_{left}})/2$
Rudder	δ_r	-30 to +30	± 105	
TV Nozzle	δ_p, δ_y	20 in any direction with $(\delta_p^2 + \delta_y^2)^{1/2} \leq 20$	± 80	

4.5.2 Simulations and Evaluations

The simulation model was constructed using Matlab/Simulink using the vehicle's configuration data, mass properties, wind tunnel data, and control effectors' dynamics [90]. All simulations begin from the trim condition: a Mach number of 0.32 at 5000 m altitude, and it is assumed that the magnitude of the thrust is constant.

Figure 16 illustrates the simulation model in Matlab/Simulink. As shown in the figure, the commands and the aircraft's response are discretized using zero-order-hold (ZOH). Thus the controller is implemented in digital form. The term D/A in the figure indicates a digital to analog converter. This discretization provides a good environment to fully synthesize the NN parametrization theory introduced in Section 3.3, in which inputs to NNs consist of tapped-delay line of memory units, or delayed signals, which are realizable only through discretization. This also models almost the same control system environment as that of real-world advanced aircraft which are equipped with digital fly-by-wire (FBW) or fly-by-light (FBL) flight control systems. Note that all control simulations in this thesis are performed in this environment and the sampling time of ZOH is set to 0.01 sec.

4.5.2.1 High- α Maneuver

Simulation results are presented in Figures 17 – 21 for a 40° angle of attack command with a small amplitude ($5^\circ/\text{sec}$) doublet in p_s . Figure 17 presents the α responses for various

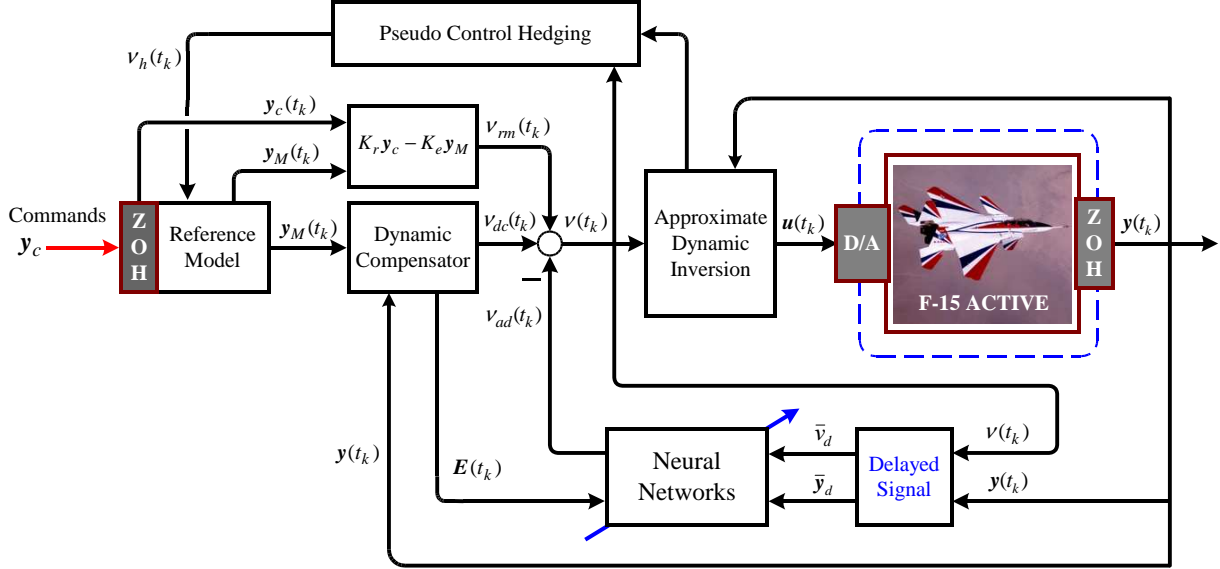


Figure 16: Discretized control simulation environment in Matlab/Simulink

conditions: with or without RSS, thrust vectors as well as adaptation (NN/PCH). Figure 18 depicts p_s and β responses with/without adaptation. At time 0, α begins from its trim value 11.5° and initially follows the reference signal to the commanded value of 0° . Subsequently at 5 seconds, a command of 40° is applied. The large α -command results in position and rate saturation of the actuators, which lead to a response with about 5° overshoot in α -response.

For the system with adaptation, excellent tracking is achieved by about 7 – 8 seconds, even though the actuators have periods of rate saturation for several more seconds. The hedged reference signal cannot be distinguished from the response at this scale. With no adaptation, the aircraft exhibits slightly oscillatory error at high alpha, and has difficulty returning to $\alpha = 0$. The response without RSS shows the motivation for relaxing the static stability, namely that the aircraft doesn't have enough control authority to reach high angles of attack without this relaxation. It is also interesting to note that, without TV, the aircraft has great difficulty returning from 40° to 0° due to lack of control power.

The p_s response in Figure 18(a) exhibits an oscillatory divergence without adaptation, while with adaptation the response is stable and accurately follows the hedged reference command in both p_s and β responses. Figure 18(b) shows that there are large errors in β

when no adaptation is present. The oscillation and hedging that appears in the roll channel around 6 – 10 seconds is due to the rate and position limiting that is occurring in the TV pitch control. This can be seen from Figure 20 which shows that the differential TV control is zero. It can be seen from Figures 19 and 20 that the small oscillations in sideslip are due to rate and position limiting in rudder and TV yaw control. In general, all of the oscillations that appear in Figure 17 and 18 are due to actuator limiting in one form or another. The role that hedging plays in maintaining a stable response is very apparent from these figures.

Time histories of aerodynamic and thrust vector controls for cases with and without adaptation are depicted in Figures 19 and 20. Note that lateral deflections are not commanded in the without adaptation case, whereas they play a significant role in the with adaptation case. The NN adaptation signal $\nu_{ad}(t)$ and inversion error $\Delta(t)$ for all channels are compared in Figure 21. This represents a measure of the degree that adaptation is able to compensate for inversion error, even during periods of control saturation.

4.5.2.2 *Simultaneous α and p_s Maneuver*

Simulation results for simultaneous commands of $\alpha = 30^\circ$ and $p_s = 25^\circ/sec$ are depicted in Figures 22–26. Figure 22 shows the aircraft angle of attack responses for cases with and without adaptation, and 23 depicts p_s and β responses. It can be seen that with adaptation good tracking is maintained, except for the oscillation in roll response. Like the previous simulation, the significant effects of unstable lateral/directional aerodynamic coefficients at high angle of attack regime induce the overshoot of p_s channel. Actuator limiting is most apparent in the time period between 6 and 8 seconds. However the combination of TV pitch and yaw control, seen in Figure 25, is causing saturation at several points. Without adaptation, there are large tracking errors, with nearly 10° steady state error in α , a large error in β response, and there is a total lack of command following in the p_s channel.

From the time histories of aerodynamic and thrust vector controls in Figures 24 and 25 it can be seen that the nonadaptive controller saturates the control effectors for long portions

of the maneuver. Figure 26 compares $\nu_{ad}(t)$ and $\Delta(t)$ for all three channels. In all cases, the NN shows correct adaptation.

4.6 Conclusion

An adaptive nonlinear dynamic inversion approach for control of high-performance aircraft in unsteady and high-alpha flight conditions is presented. The adaptive approach is robust to both parametric uncertainty and unmodeled dynamics. Control allocation for redundant control effectors, including thrust vector nozzles and differential stabilators, was also implemented.

Pseudo-control hedging is used to protect the adaptive process during periods of control saturation. Simulation results obtained using a modified F-15 ACTIVE model in the presence of unsteady aerodynamics at high angle of attack show reasonable responses using NN adaptation.

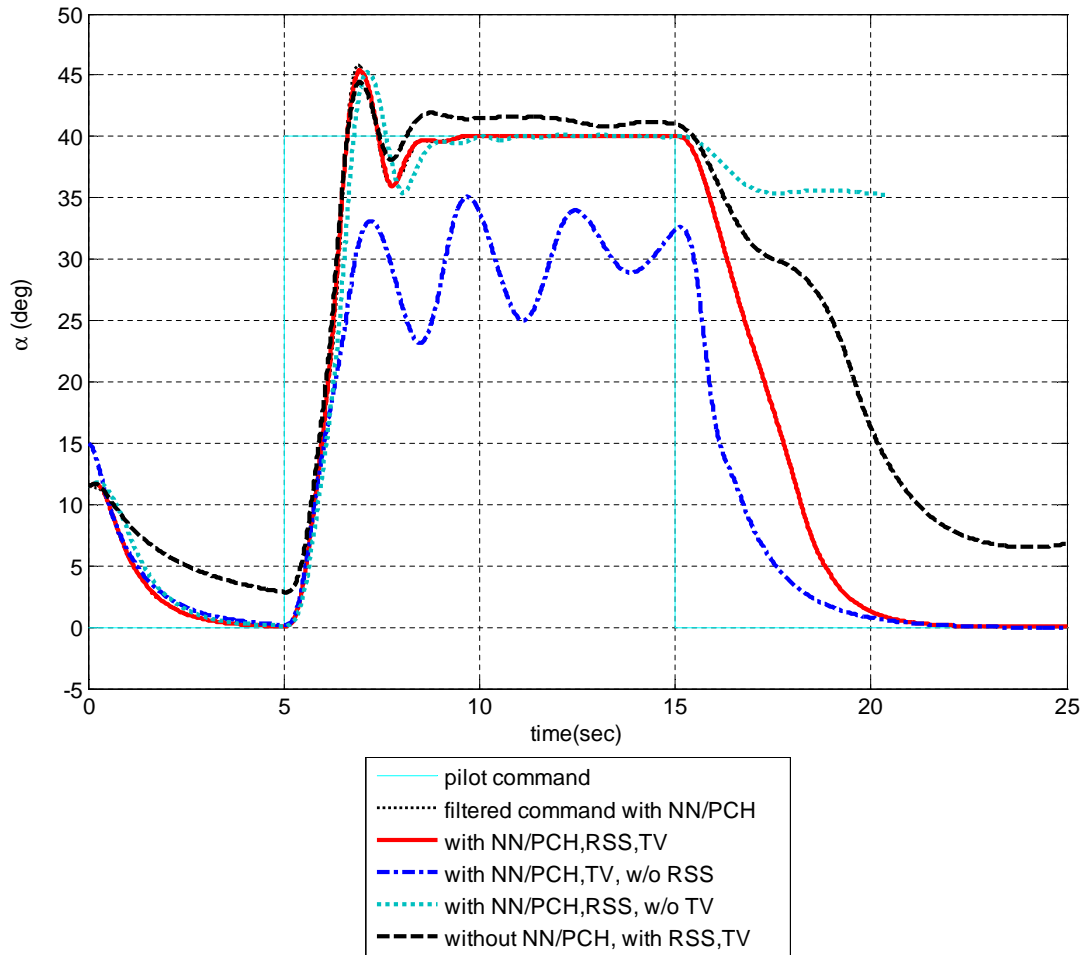
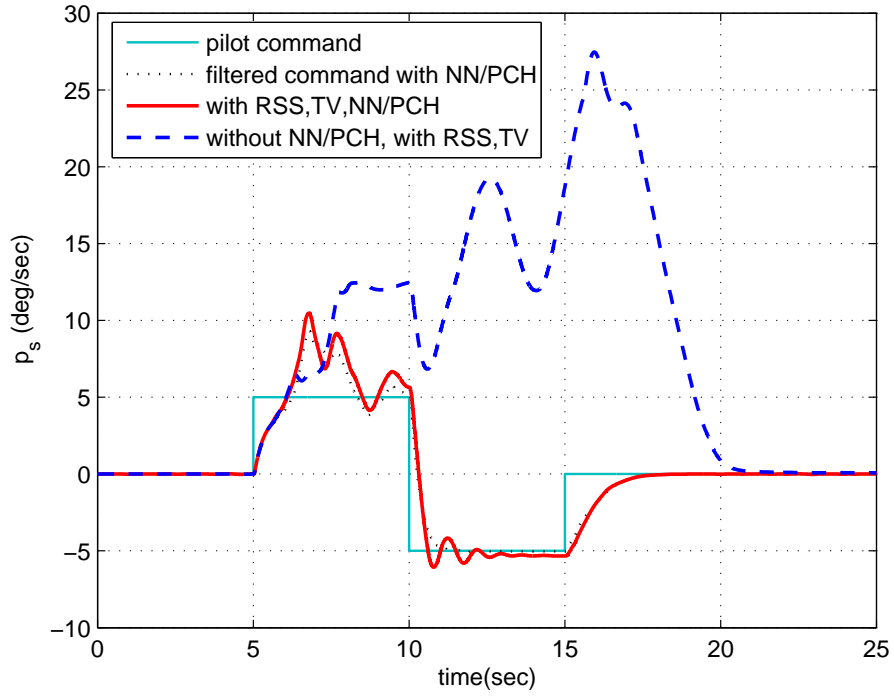
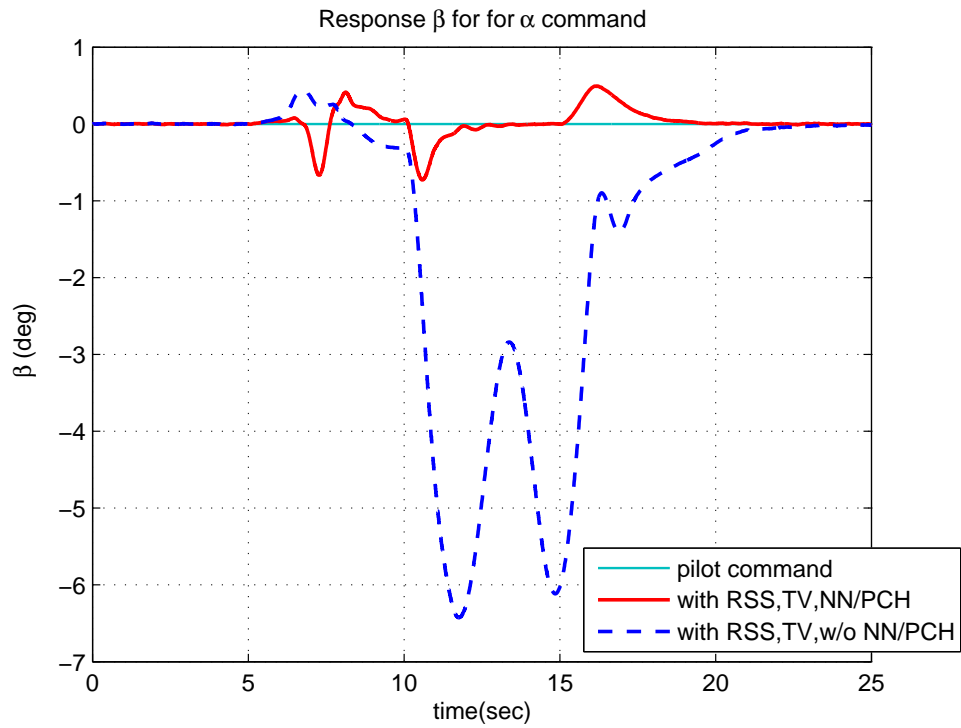


Figure 17: Aircraft α responses for a high α command with/without NN adaptation

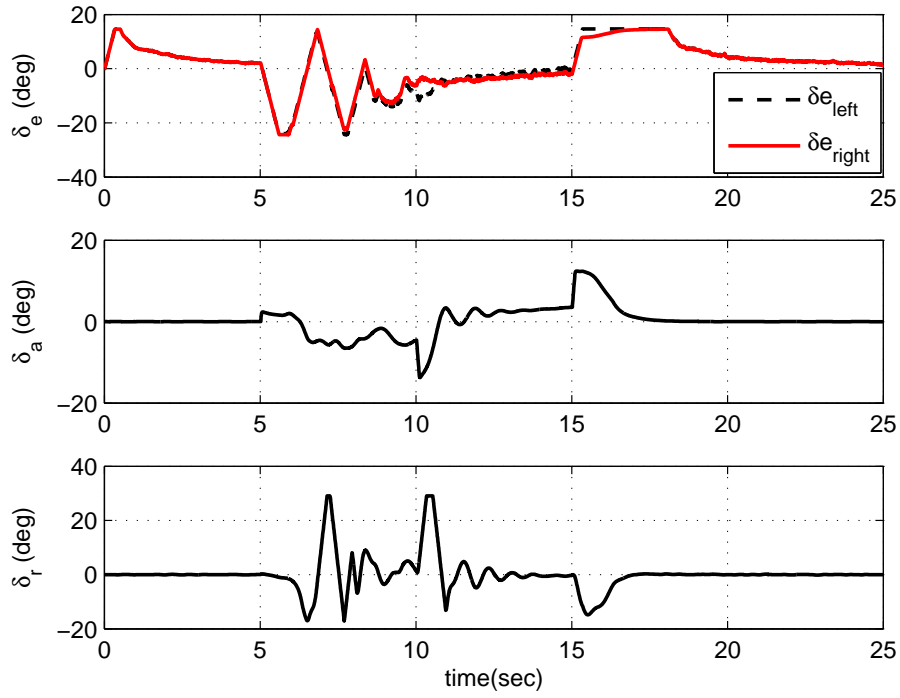


(a) Stability axis roll rate

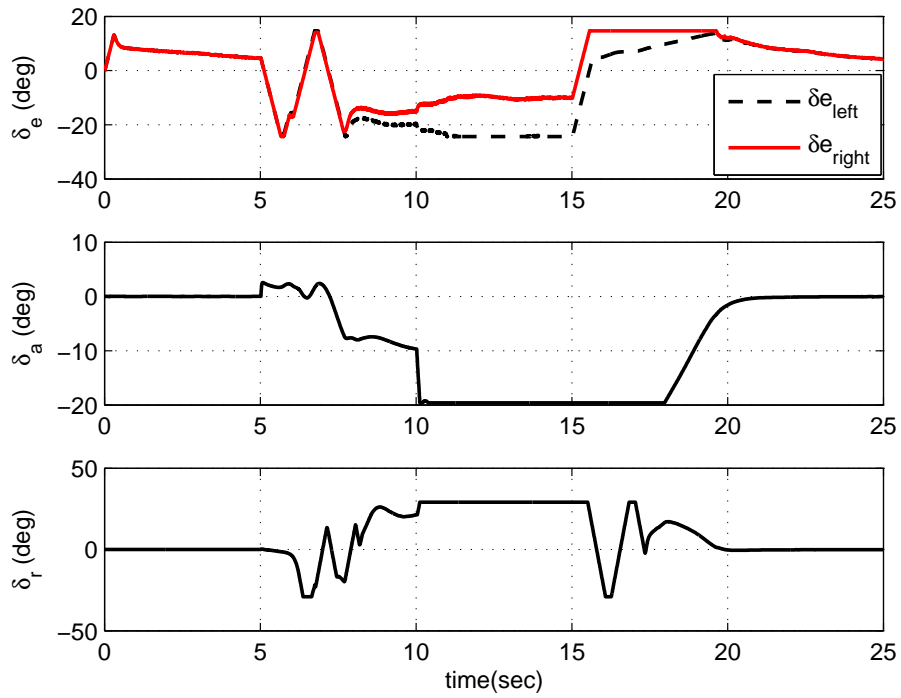


(b) Sideslip angle

Figure 18: Aircraft P_s and β responses for a high α command with/without NN adaptation

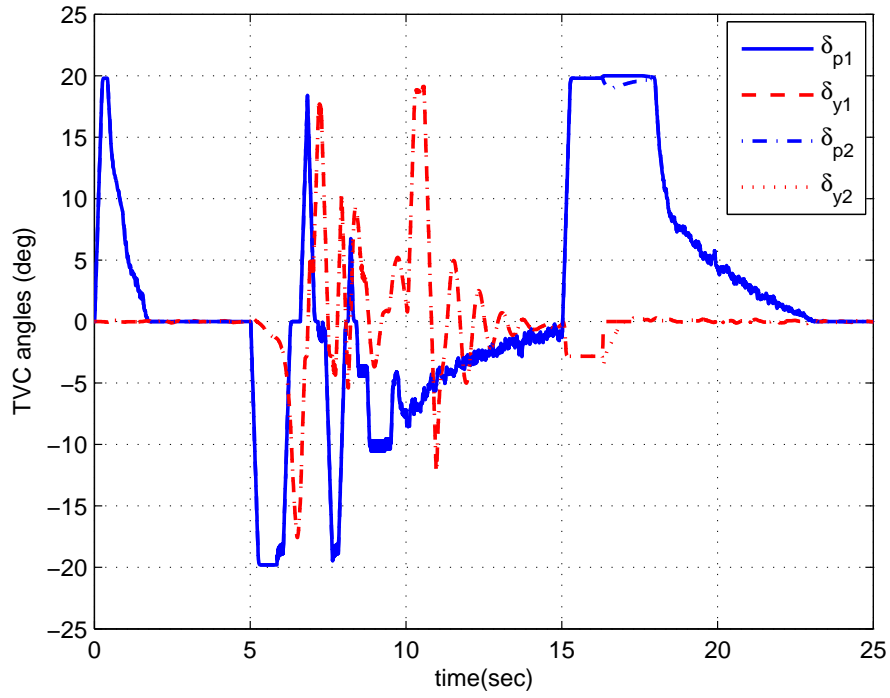


(a) with NN/PCH adaptation

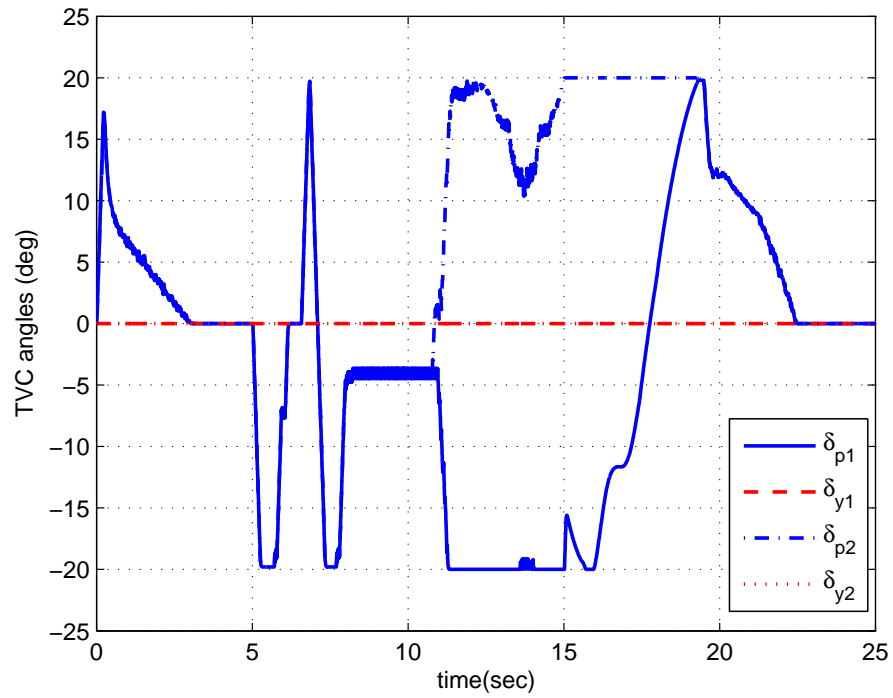


(b) without NN/PCH adaptation

Figure 19: Aerodynamic control deflections for a high α command with/without NN adaptation



(a) with NN/PCH adaptation



(b) without NN/PCH adaptation

Figure 20: Thrust vector controls with/without NN adaptation

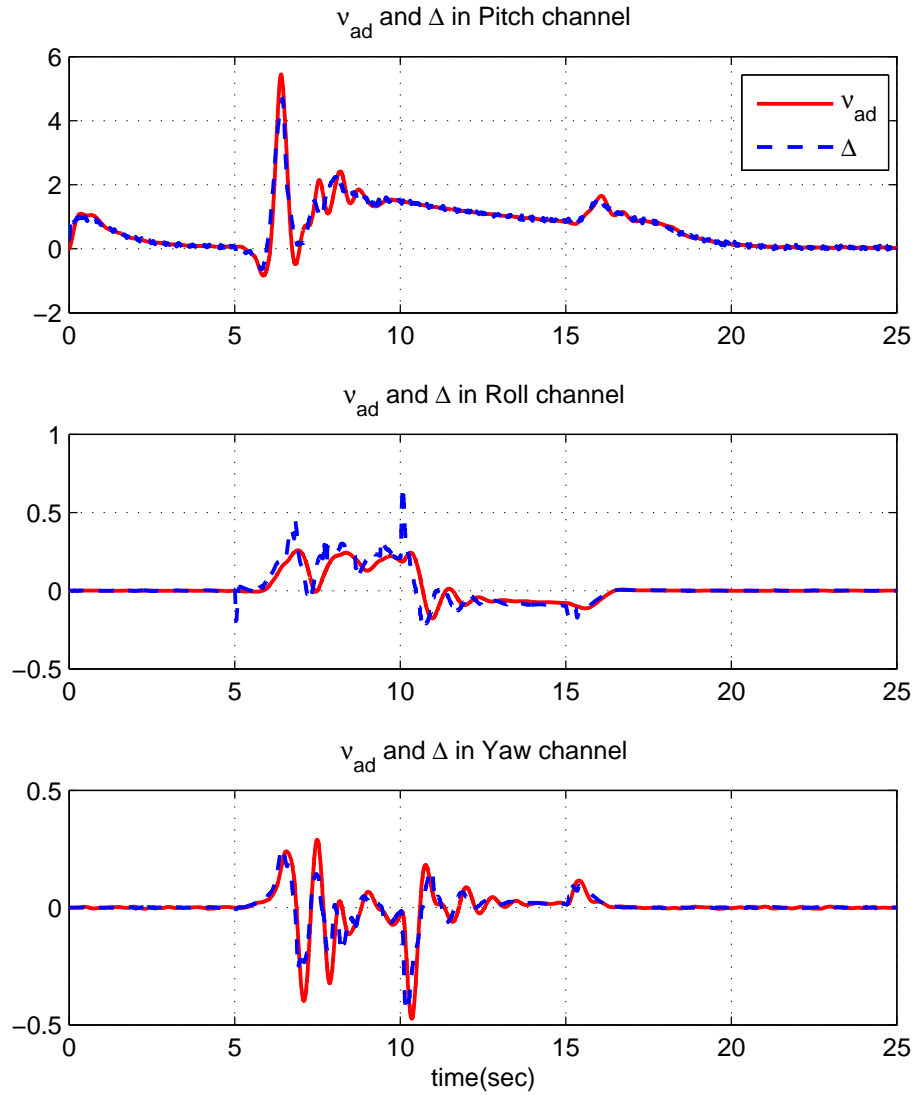


Figure 21: NN adaptation signal $\nu_{ad}(t)$ and $\Delta(t)$ in pitch, roll, and yaw channels

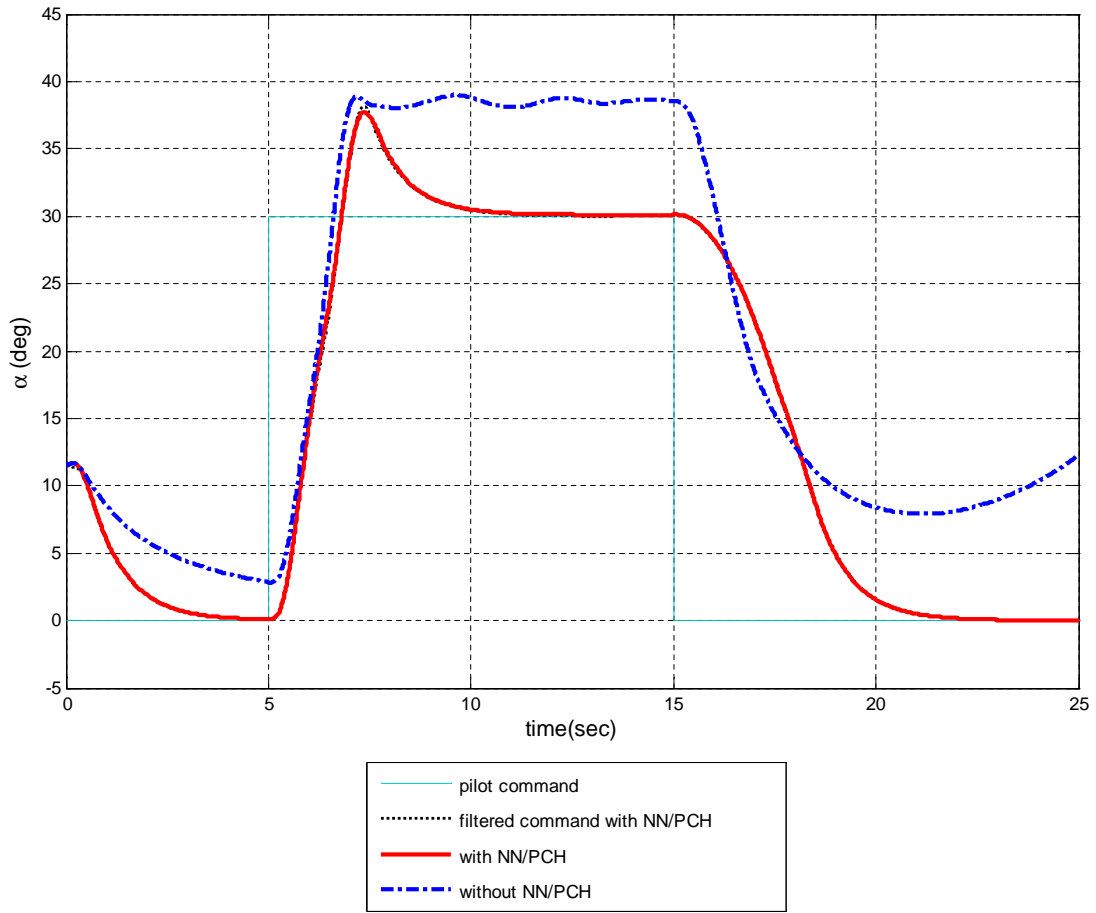
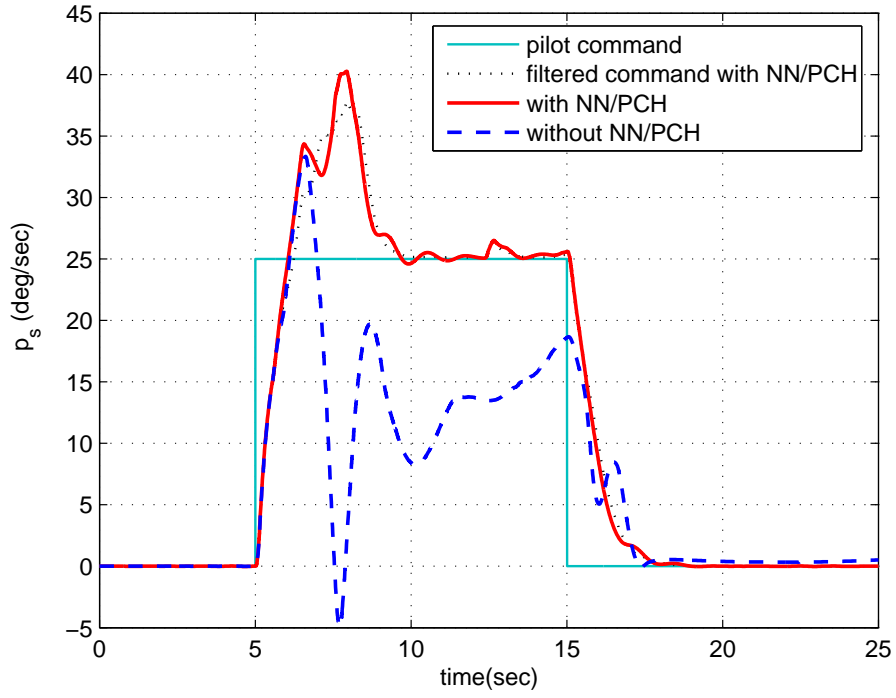
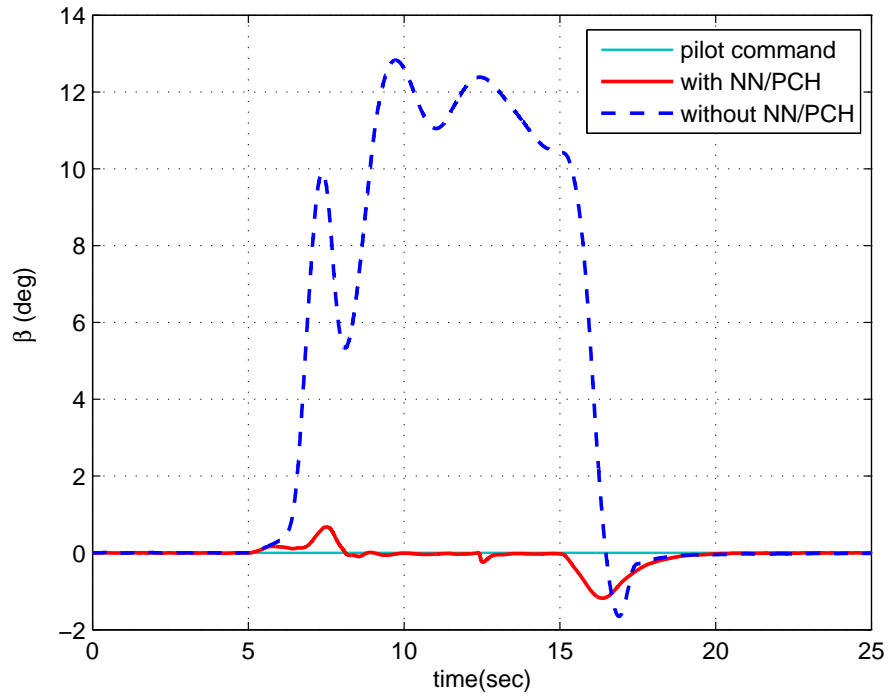


Figure 22: Aircraft α responses for α/p_s command with/without NN adaptation

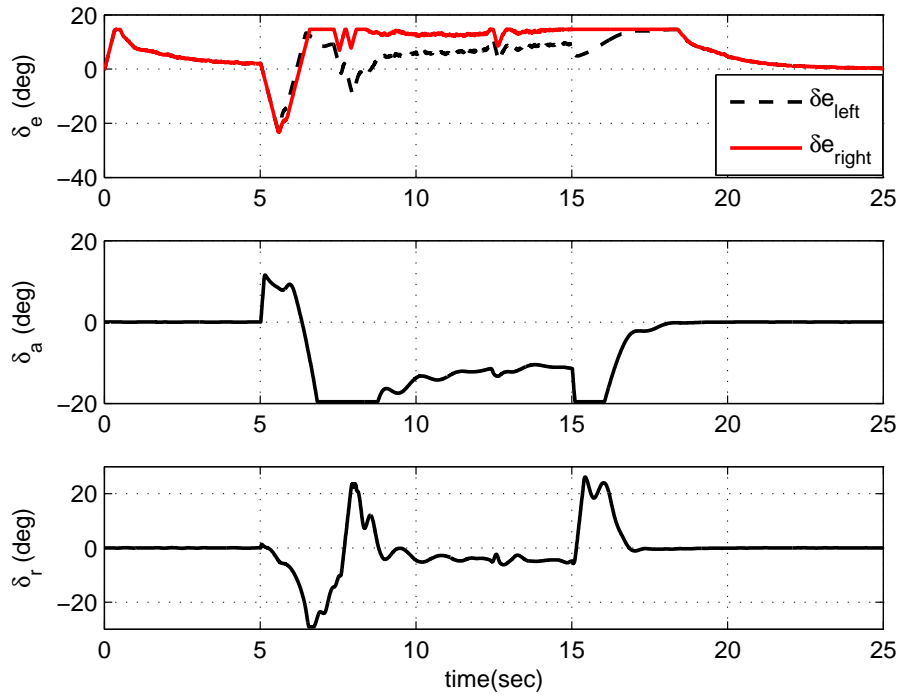


(a) Stability axis roll rate

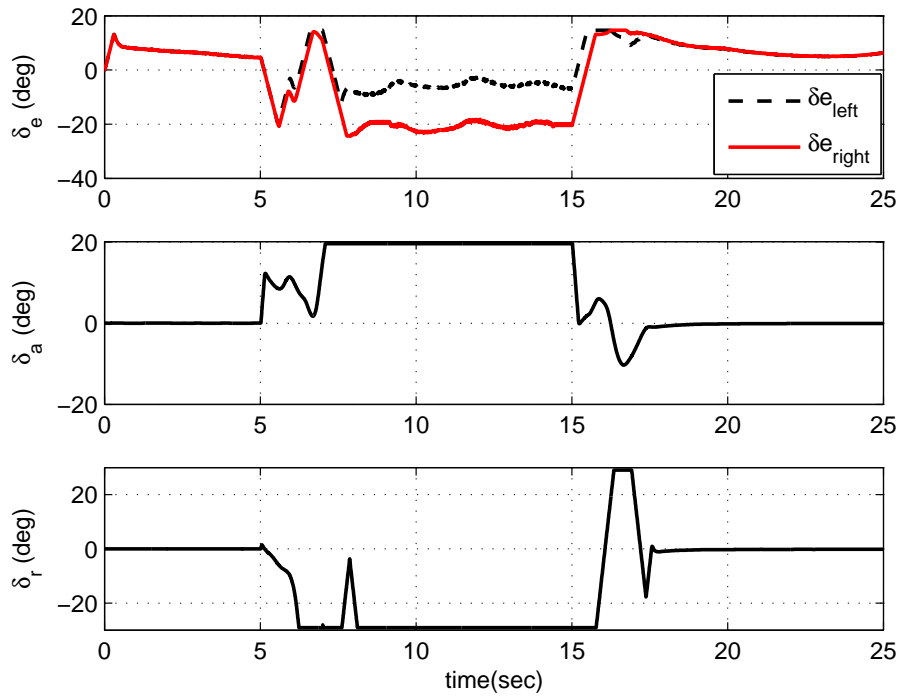


(b) Sideslip angle

Figure 23: Aircraft P_s and β responses for α/p_s command with/without NN adaptation

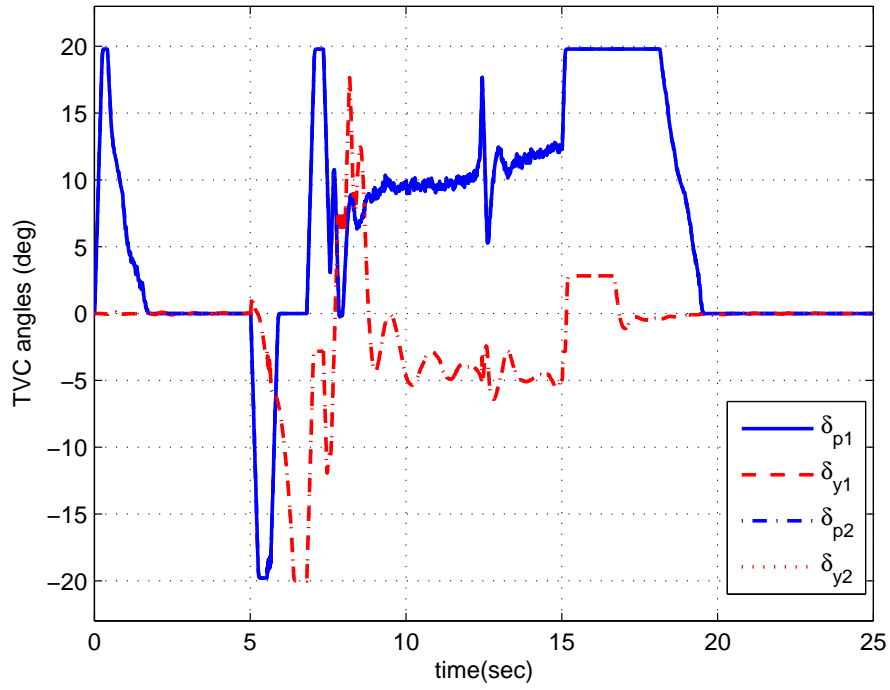


(a) with NN/PCH adaptation

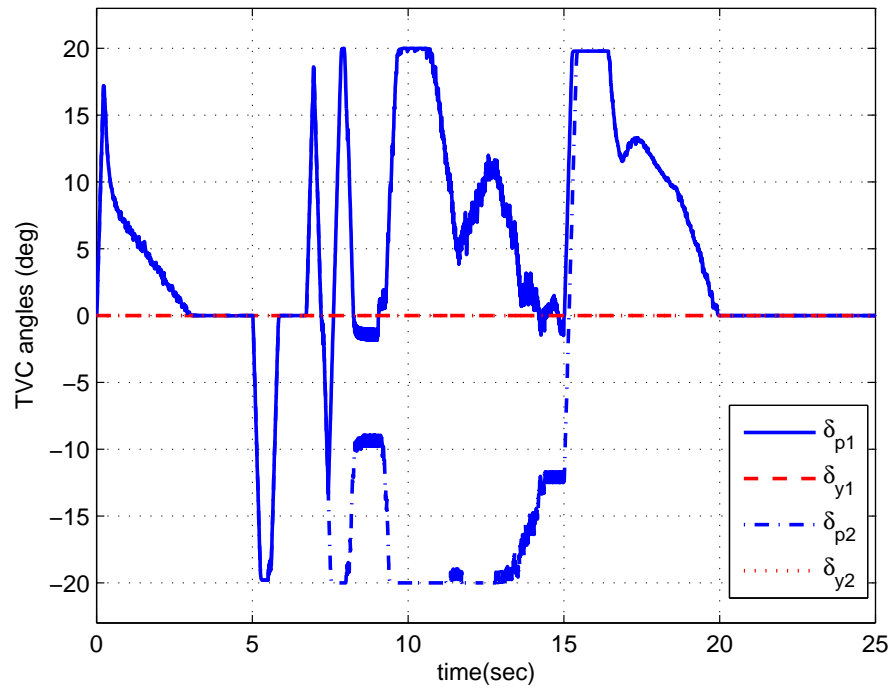


(b) without NN/PCH adaptation

Figure 24: Aerodynamic control deflections for α/p_s command with/without NN adaptation



(a) with NN/PCH adaptation



(b) without NN/PCH adaptation

Figure 25: Thrust vector controls for α/p_s command with/without NN adaptation

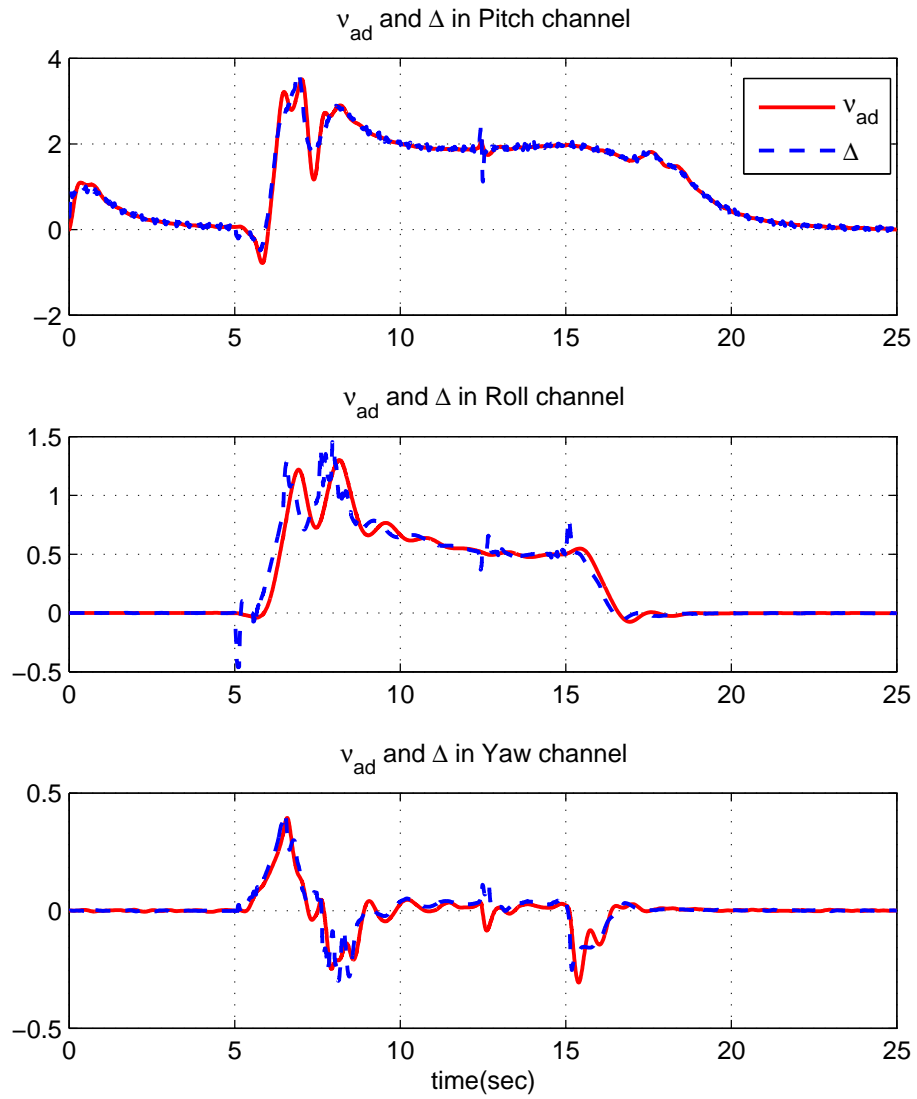


Figure 26: NN adaptation signal $\nu_{ad}(t)$ and $\Delta(t)$ in pitch, roll, and yaw channels for α/p_s command

CHAPTER V

A COMPARISON STUDY OF CLASSICAL AND NEURAL NETWORK-BASED ADAPTIVE CONTROL OF AIRCRAFT WING ROCK

At moderate to high angles of attack, aircraft dynamics can display an oscillatory lateral behavior that manifests itself as a limit cycle known as wing rock. In this chapter, several methods of adaptively stabilizing this oscillatory motion are compared. The main objective is to compare classical and neural NN-based methods of adaptive control. All methods are compared using a model for an 80° swept delta wing.

5.1 Introduction

Wing rock is a lateral-directional instability that occurs in aircraft of varying configurations and aspect ratios. Hsu and Lan [31] describe wing rock as "a phenomenon triggered by flow asymmetries, developed by negative roll damping, and sustained by nonlinear aerodynamic roll damping." Both Hsu and Lan [31] and Nayfeh *et al.* [22, 85] have developed models for wing rock behavior of a slender delta wing. These models exhibit limit cycle behavior for moderate to high angles of attack. Luo and Lan [65] explored controlling this behavior with a controller based on a Hamiltonian formulation. Singh [106] *et al.* investigated two adaptive methods of controlling the phenomenon. The first is a classical method in which the uncertainty is linearly parameterized. In this approach, modeling information is employed to arrive at a linear parametrization. In the second approach the universal approximating property of Radial Basis Function (RBF) Neural Networks (NNs) is used to model the uncertainty, with no *a priori* knowledge of the model error. The performance of the classical adaptive

approach was superior. It was felt by the authors that this was primarily a consequence of the fact that it was designed with knowledge of the form of the system dynamics. The RBF NN was able to stabilize the system, but exhibited very poor transient performance. Adaptation was slow, and the response was highly oscillatory. Only responses to initial conditions were considered.

In this chapter the work of Singh *et al.* is repeated, and compared with a nonlinearly parameterized adaptive controller that employs a Single Hidden Layer (SHL) NN. The objective is to determine if the poor performance of the NN-based controller employed in [106] can be improved by a nonlinear parametrization, and to determine how it compares to the classical adaptive approach. We also consider designs in which all the adaptive controllers augment an inversion-based design [14]. This approach introduces an additional linear controller. Results for all five cases are compared for both responses to initial conditions and in terms of command tracking.

5.2 Aircraft Wing Rock Dynamics

For a flat, thin wing constrained such that it is free only to roll about its x-axis, the differential equation describing the wing rock motion can be modeled as [22, 31]

$$\ddot{\phi} = \left(\frac{\rho U_\infty^2 S b}{2 I_{xx}} \right) C_l + d_0 u \quad (5.2.1)$$

where ϕ is the roll angle and d_0 is the control effectiveness relating the control, u , to angular acceleration. A modified version of the Hsu and Lan model [22] of the rolling moment coefficient is

$$C_l = a_0 + a_1 \phi + a_2 \dot{\phi} + a_3 |\phi| \dot{\phi} + a_4 |\dot{\phi}| \dot{\phi} + a_5 \phi^3 \quad (5.2.2)$$

where

$$\begin{aligned} a_0 &= C_{l0}, & a_1 &= \sin(\alpha_s) \cdot C_{l\beta}, & a_2 &= \frac{b}{2U_\infty} \cdot C_{lp0} \\ a_3 &= \sin(\alpha_s) \cdot \frac{b}{2U_\infty} \cdot C_{lp\beta}, & a_4 &= \left(\frac{b}{2U_\infty} \right)^2 \cdot C_{lpp} \end{aligned} \quad (5.2.3)$$

α_s is the steady state angle of attack. While the $\sin(\alpha_s)$ terms define an explicit dependence on α_s , there is also an implicit dependence that is folded into the values of all the coefficients a_0, \dots, a_5 .

Defining $x_1 = \phi$ and $x_2 = \dot{\phi}$, (5.2.1) becomes

$$\begin{aligned} \dot{x}_1 &= x_2 \\ \dot{x}_2 &= g(\mathbf{x}) + d_0 u \end{aligned} \tag{5.2.4}$$

where

$$g(\mathbf{x}) = b_0 + b_1\phi + b_2\dot{\phi} + b_3|\phi|\dot{\phi} + b_4|\dot{\phi}|\dot{\phi} + b_5\phi^3 \tag{5.2.5}$$

and

$$b_i = \left(\frac{\rho U_\infty^2 S b}{2I_{xx}} \right) a_i \quad i = 1, \dots, 5. \tag{5.2.6}$$

A reference model for the desired response is specified by the linear time invariant differential equation

$$\dot{\mathbf{x}}_m = A_m \mathbf{x}_m \tag{5.2.7}$$

where $\mathbf{x}_m = (x_{m1}, x_{m2})^T$, $\zeta > 0$, $\omega_n > 0$ and

$$A_m = \begin{bmatrix} 0 & 1 \\ -\omega_n^2 & -2\zeta\omega_n \end{bmatrix} \tag{5.2.8}$$

We are interested in the following two wing-rock motion control problems under different assumptions on the function $g(\mathbf{x})$ [106]:

Problem 1 for classical adaptive control : Suppose that in (5.2.4) the parameters b_i , $i = 0, 1, \dots, 5$, and d_0 are unknown, but the sign of d_0 is known. Derive a control law such that

$$\lim_{t \rightarrow \infty} [\mathbf{x}_m(t) - \mathbf{x}(t)] \rightarrow 0$$

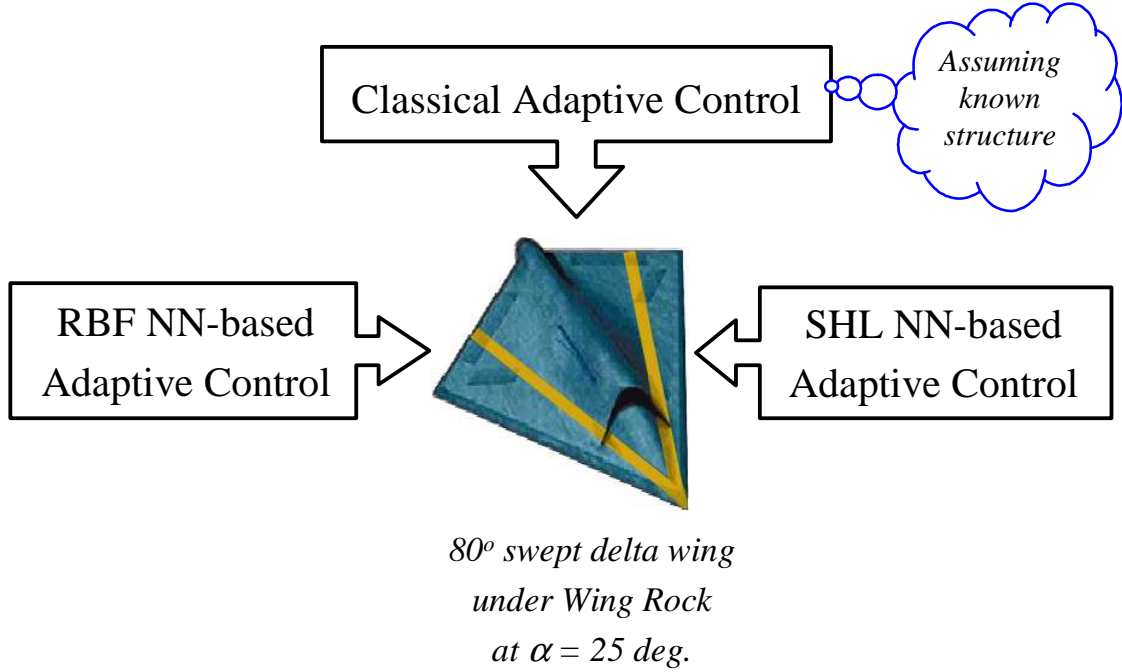


Figure 27: Three Adaptive Control Methods

Problem 2 for NN-based control : Suppose that in (5.2.4) the nonlinear function $g(\mathbf{x})$ is unknown, and d_0 is an unknown constant but its sign is known. Derive a neural control law such that

$$\lim_{t \rightarrow \infty} [\mathbf{x}_m(t) - \mathbf{x}(t)] \rightarrow 0$$

The delta wing and three adaptive control methods are schematically shown in Figure 27. Now classical adaptive control scheme is introduced.

5.3 Classical Adaptive Control

Define the trajectory tracking error

$$\mathbf{E} = \begin{bmatrix} E_1 \\ E_2 \end{bmatrix} = \begin{bmatrix} x_{m1} - x_1 \\ x_{m2} - x_2 \end{bmatrix} \quad (5.3.1)$$

then from equations (5.2.4) and (5.2.7), the error dynamics are given by

$$\dot{\mathbf{E}} = A_m \mathbf{E} + B_m [d_0 u + \Delta(\mathbf{x})] \quad (5.3.2)$$

where $B_m = [0 \ 1]^T$ and

$$\Delta(\mathbf{x}) = b_0 + (b_1 + \omega_n^2)x_1 + (b_2 + 2\zeta\omega_n)x_2 + b_3|x_1|x_2 + b_4|x_2|x_2 + b_5x_1^3 \quad (5.3.3)$$

The adaptive control law is chosen to match the form of the uncertainty in (5.3.3)

$$u = - \left(\theta_0(t) + \theta_1(t)x_1 + \theta_2(t)x_2 + \theta_3(t)|x_1|x_2 + \theta_4(t)|x_2|x_2 + \theta_5(t)x_1^3 \right) \quad (5.3.4)$$

and the adaptation law governing the behavior of the parameter vector $\boldsymbol{\theta} = (\theta_0, \theta_1, \dots, \theta_5)^T$ is

$$\dot{\boldsymbol{\theta}} = -sgn(d_0)\Gamma\mathbf{E}^T P B_m h(\mathbf{x}) \quad (5.3.5)$$

where $\Gamma > 0$, P is the unique and positive definite solution of the Lyapunov equation

$$A_m^T P + P A_m = -Q, \quad Q > 0 \quad (5.3.6)$$

and $h(\mathbf{x}) = [1, x_1, x_2, |x_1|x_2, |x_2|x_2, x_1^3]^T$. The proof of stability is given in [106]. It is apparent from (10) that the ideal goal of the adaptive law is for u to cancel $\Delta(\mathbf{x})/d_0$.

RBF and SHL NNs and their properties are described in Chapter 2 and we use the same formulations described in the chapter.

5.4 Adaptive Augmentation of a Linear Control Law

In this section, we introduce a nominal controller based on the method of feedback inversion. The design approach is taken from [14], and is developed in the setting of command tracking. Hence the reference model in (7) is redefined so that a roll command, ϕ_c , is included.

$$\dot{\mathbf{x}}_m = A_m \mathbf{x}_m + B_m \phi_c \quad (5.4.1)$$

where $B_m = [0 \ \omega_n^2]^T$. Let the dynamics in (5.2.1) be represented by

$$\begin{aligned} \ddot{\mathbf{x}} &= f(\mathbf{x}, \dot{\mathbf{x}}, u) \\ &= \nu \end{aligned} \quad (5.4.2)$$

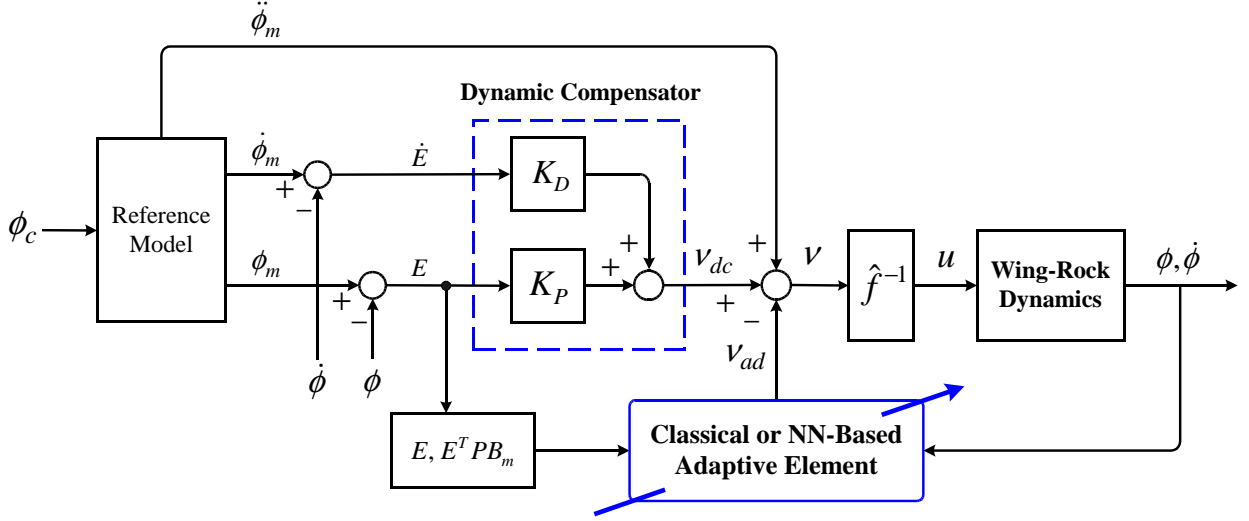


Figure 28: Augmenting adaptive control architecture

The function $f(\mathbf{x}, \dot{\mathbf{x}}, u)$ is not known exactly, and an approximation, $\boldsymbol{\nu} = \hat{f}(\mathbf{x}, \dot{\mathbf{x}}, u)$, is used for inversion, which results in

$$\ddot{\mathbf{x}} = \boldsymbol{\nu} + \Delta(\mathbf{x}, \dot{\mathbf{x}}, u) \quad (5.4.3)$$

where

$$\Delta(\mathbf{x}, \dot{\mathbf{x}}, u) = f(\mathbf{x}, \dot{\mathbf{x}}, u) - \hat{f}(\mathbf{x}, \dot{\mathbf{x}}, u) \quad (5.4.4)$$

The approximation, $\hat{f}(\mathbf{x}, \dot{\mathbf{x}}, u)$, must be chosen such that an inverse with respect to u exists. If we adopt the viewpoint that the dynamics in (5.4.2) are completely unknown to the NN, except for $\text{sign}(d_0)$, then an appropriate choice is $\hat{f}(\mathbf{x}, \dot{\mathbf{x}}, u) = \text{sign}(d_0)$. In this case, the feedback inverting design reduces to the introduction of a dynamic compensator, or linear controller.

The architecture of the augmented inverting control design is shown in Figure 28, where the subscript m denotes a signal coming from the reference model defined in (5.4.1). The pseudo-control signal is made up of three components.

$$\boldsymbol{\nu} = \dot{\mathbf{x}}_{m2} + \boldsymbol{\nu}_{dc} - \boldsymbol{\nu}_{ad} \quad (5.4.5)$$

where ν_{dc} is the output of the dynamic compensator (linear controller), and ν_{ad} is the output generated by the adaptive element. It follows from (5.4.1) that

$$\dot{x}_{m2} = -\omega_n^2 x_{m1} - 2\zeta\omega_n x_{m2} + \omega_n^2 \phi_c \quad (5.4.6)$$

Letting

$$\nu_{dc} = [K_P \ K_D] \cdot \mathbf{E} \quad (5.4.7)$$

and combining (5.2.4), (5.4.1), (5.4.3) and (5.4.5), the error dynamics take the form

$$\dot{\mathbf{E}} = A_{LC} \cdot \mathbf{E} + B_m (\nu_{ad} - \Delta) \quad (5.4.8)$$

where

$$A_{LC} = \begin{bmatrix} 0 & 1 \\ -K_P & -K_D \end{bmatrix} \quad (5.4.9)$$

$$\Delta(\mathbf{x}, u) = b_0 + b_1 x_1 + b_2 x_2 + b_3 |x_1| x_2 + b_4 |x_2| x_2 + b_5 x_1^3 + (d_0 - 1)u \quad (5.4.10)$$

The gains are related to natural frequency and damping ratio by

$$K_P = \omega_{nLC}^2, \quad K_D = 2\zeta_{LC}\omega_{nLC} \quad (5.4.11)$$

The form of the error dynamics in (5.4.8) is similar to (5.3.2). Consequently, in this design approach, the matrix P that appears in the adaptive laws (5.3.5), (2.1.11) or (2.1.12), and (2.2.10) or (2.2.11) is the solution of (5.3.6) with A_m replaced by A_{LC} . In contrast to (5.3.3), it can be seen from (5.4.10) that Δ depends explicitly on both x and u . Since $u = \hat{f}(\mathbf{x}, \nu)$, it follows that Δ is an implicit function of ν , which from (5.4.5) depends explicitly on ν_{ad} . Denoting this functional dependence as $\Delta^*(\mathbf{x}, \nu_{ad})$, and since the role of ν_{ad} is to cancel Δ , it follows that the success of this approach requires that a fixed point solution exists to the equation $\nu_{ad} = \Delta^*(\mathbf{x}, \nu_{ad})$. It has been shown in [11] that the following two conditions are sufficient for existence of a fixed point solution:

$$\begin{aligned} \operatorname{sgn} \left(\frac{\partial f}{\partial u} \right) &= \operatorname{sgn} \left(\frac{\partial \hat{f}}{\partial u} \right) \\ 0 &< \frac{1}{2} \left| \frac{\partial f}{\partial u} \right| < \left| \frac{\partial \hat{f}}{\partial u} \right| < \infty \end{aligned} \quad (5.4.12)$$

Note that this issue is independent of the adaptive approach employed, but it does require that ν be included as an input to the NNs.

To avoid the implied algebraic loop, the implementation is normally done using a one step delayed value of ν . We have verified that this results in nearly an identical solution to that obtained by solving the algebraic loop using the current value of ν as an input to the NN. This further requires that the NN itself also have a fixed point solution with respect to ν_{ad} for all values of the NN weights, which is guaranteed by the fact that the NN basis functions are bounded functions of all its input variables. There is also an alternative approach that avoids the fixed point issue by employing the mean value theorem [45], but that relies on a bound on $d\nu/dt$.

5.5 Simulation Results

Aerodynamic parameters of the delta wing are selected corresponding to $\alpha_s = 25^\circ$ and $U_\infty = 15 \text{ m/sec}$. [106] Nondimensional time t^* is $(4U_\infty/b)t$ and $b = 0.429 \text{ m}$. The parameters b_i and d_0 for the model shown in equation (5.2.4) with t^* as an independent variable are:

$$b_0 = 0, \quad b_1 = -01859521, \quad b_2 = 0.015162375, \quad b_3 = -0.06245153,$$

$$b_4 = 0.00954708, \quad b_5 = 0.02145291, \quad d_0 = 1$$

For these simulations, two initial conditions are used:

1. Small initial condition: $\phi(0) = 6 \text{ deg.}$, $\dot{\phi}(0) = 419.4 \text{ deg/sec.}$
2. Large initial condition: $\phi(0) = 30 \text{ deg.}$, $\dot{\phi}(0) = 1398 \text{ deg/sec.}$

Open loop responses are shown in Figure 29. Note that for the small initial condition a limit cycle results, whereas for the large initial condition the response is unstable.

The reference model parameters in (5.2.8) were selected as $\zeta = 0.707$, $\omega_n = 0.5 \text{ rad/sec}$. The linear controller gains in (5.4.7) were chosen to match the dynamics of the reference model. The adaptation gains and other parameters in the adaptive laws were tuned so as to

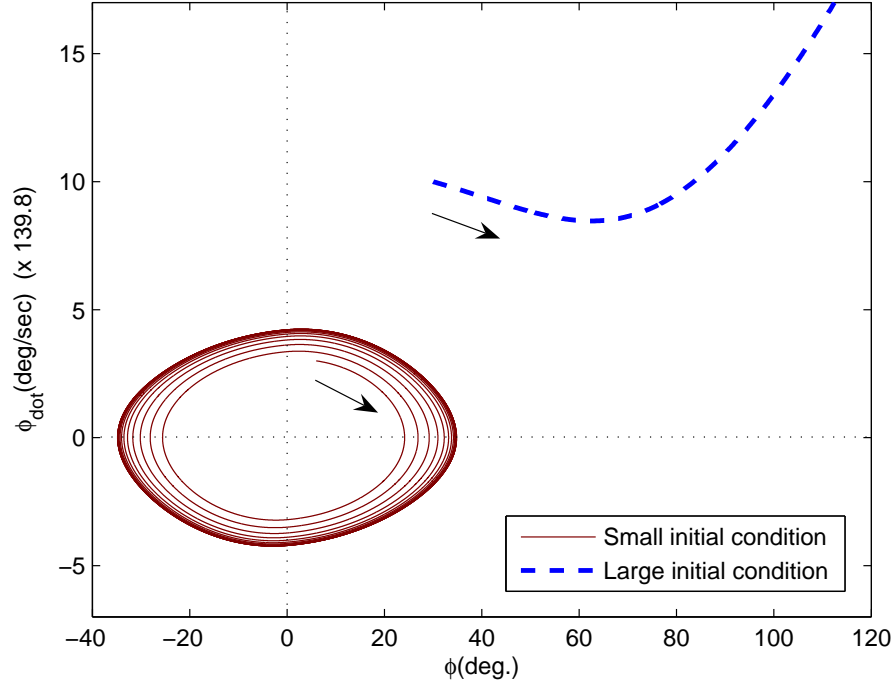


Figure 29: Open loop system dynamics for the two initial conditions

achieve the best possible performance, without any evidence of oscillatory behavior due to adaptation. $Q = I$ was used in solving the Lyapunov equations.

Responses to the two initial conditions, both with and without commands were investigated. Both forms of the three adaptive approaches (without and with the linear controller) were evaluated. A square wave command was used to evaluate tracking performance.

5.5.1 Adaptive Controller Designs

For the classical design, the complete adaptive closed loop system consists of (5.2.4), (5.3.4), (5.3.5), (5.4.6) and (5.4.7). Since $b_0 = 0$, for simplicity, $\theta_0(t)$ was set to zero in the control law (5.3.4). The adaptation gain was set to $\Gamma = 15$ which is the same value used in [106].

For the RBF NN-based design we first used the same parameter settings as those in [106]. The complete closed loop system consists of (5.2.4), (2.1.7), (2.1.11), (5.4.6) and (5.4.7). This consisted of 441 RBF elements that are uniformly spaced in the $\phi - \dot{\phi}$ plane such that

$$\mathbf{c}_i = \begin{bmatrix} j_1 \Delta_1 \\ j_2 \Delta_2 \end{bmatrix} \quad (5.5.1)$$

where $\Delta_1 = 0.2 \text{ rad}$, $\Delta_2 = 0.1 \text{ rad/sec}$, and $j_1, j_2 \in \{-10, -9, \dots, 9, 10\}$. The widths σ_i of the kernel units were set to 1 and the adaptation gains were taken as $\Gamma = 0.05I$, $\kappa = 0$ to repeat the results in [106].

For the SHL NN-based design, the complete closed loop system consists of (5.2.4), (2.2.5), (2.2.10), (5.4.6) and (5.4.7). Adaptation gains $\Gamma_V = 7$ and $\Gamma_W = 10$, and σ -modification gains $\kappa_v = \kappa_w = 5$ were used, with 10 neurons employed in the hidden layer. The values of the activation potentials were evenly distributed between 0.1 and 1.

Note that since $d_0 = 1$, the expression for Δ in (5.4.10) is independent of u , and it was not necessary to use ν as an input to the networks in this case. Also, since the natural frequencies and damping ratios for the reference model and the linear controller design are the same, the solution for P is the same in all designs (with or without the linear controller).

5.5.2 Comparisons

A comparison of the responses for zero command to small and large initial conditions is shown in Figures 30 - 32. The classical and RBF NN-based responses without the linear controller (without LC) are essentially identical to the results obtained in [106], where the conclusion is reached that the response of the classical adaptive controller is superior due to the fact that it employed knowledge of the functional form of the nonlinearity. However, for the results in Figure 30, no modification terms such as those in (20) and (21) were used in the RBF NN-based design. Figures 31 and 32 show that when the σ -modification is employed, the responses are not only improved, but also are superior to the responses obtained using the classical adaptive controller. Similar improvements were obtained using e -modification (not shown). In addition, responses in which a linear controller is augmented with the adaptive designs showed modest improvements in all cases. It should be noted that the responses with LC and without adaptation are all stable, but there is nothing to guarantee that this will be

the case in general.

When employing an RBF NN, the use of kernel units of width 1.0 is not generally the best choice. The widths should be adjusted to achieve an appropriate overlap between neighboring kernels. As an alternative, we employed the following rule

$$\sigma = \frac{p_{max} - p_{min}}{2(\sqrt{N} - 1)} \quad (5.5.2)$$

where p_{max} and p_{min} are the maximum and minimum of input domain ϕ , and N is the number of neurons. An example of the distribution obtained in one axis for $p_{max} = -p_{min} = 2$ and $N = 25$ is illustrated in Figure 33. The effect of N with centers uniformly distributed, and widths defined by (5.5.2) is shown in Figure 34. Figure 35 shows the effect of N in the case of the SHL NNs.

To evaluate the tracking performance of the adaptive control designs, a square wave command with period 4 seconds and amplitude $\phi_c = \pm 10 \text{ deg}$ was applied. The responses shown in Figure 36 are for a reference model with ω_n increased to 4.0 rad/sec . It can be seen that the SHL NN-based design provides much faster adaptation, and thus better tracking than other two designs. Classical adaptive control has difficulty tracking the command even after a long time period. Figure 37 shows a comparison of the adaptation error, $\Delta(t^*) - \nu_{ad}(t^*)$ that corresponds to Figure 36. In the classical case, the error increases in the time period examined. For these results, the adaptation gains were: $\Gamma = 10.0$ for the classical adaptive control, $\Gamma = 10.0I$, $\kappa = 1.0$ with 441 neurons for RBF NN and $\Gamma_V = 7$, $\Gamma_W = 10.0$, $\kappa_v = \kappa_w = 0.3$ with 40 neurons for SHL NN-based design.

Figure 38 shows a 3-dimensional view of ν_{ad} of SHL NN tracking the Δ trajectory on the delta surface for a sinusoidal command. It can be observed from the figure that $\Delta(t^*)$ is moving on the Δ -surface which is determined by (5.4.10) over the $\phi - \dot{\phi}$ domain, while SHL NN output ν_{ad} is tracking and cancelling it out to show good adaptation.

5.5.3 Remarks on Stability

In the case of NN-based adaptive control, since the parameterization is not exact, one can only show that the error response is ultimately bounded. Consequently, with NN-based adaptation it is possible that an equilibrium point that is asymptotically stable without adaptation (or with LC but without adaptation) becomes unstable. However, since the response is ultimately bounded, an unstable response will likely be in the form of a limit cycle. However, if the equilibrium point is asymptotically stable without control, then it is a reasonable expectation that it should remain asymptotically stable with control. As noted earlier, the use of σ -modification provides asymptotic stability in this case because the weights approach zero in equilibrium, whereas this is not necessarily the case with e -modification. The phase plane plot in Figure 39 depicts the final stages of these two adaptive laws on a long time scale. The adaptive law with σ -modification is asymptotically stable, whereas, the adaptive law with e -modification results in a trajectory that first approaches very close to the origin, but later emerges from the origin and approaches a limit cycle. Figures 40 and 41 illustrate the same effect with the states plotted versus time. Both ϕ and $\dot{\phi}$ exhibit bounded oscillations with e -modification. A persistent oscillation emerges even when a square wave command is applied.

As an alternative to both σ - and e -modification, we also implemented the method of projection [88], for both the RBF and SHL NNs. This approach imposes a bound on the norm of the network weights. The bound is adjusted as a network parameter, similar to what was done with the σ - and e -modification gains. After tuning the network adaptation gains and the bound, the best attainable performance for the same case as that depicted in Figure 40, is shown in Figure 42. This figure depicts the response that employs a SHL NN. The response with a RBF NN exhibits a similar behavior. Initially, projection has no effect on the system response, because it does nothing until the weights approach their imposed bound. Thus, the initial part of the response is similar to that shown in Figure 30. Consequently, this approach to avoiding the bursting phenomenon in adaptive control was found to be less

desirable for this example.

5.6 Conclusion

The response of a model for wing rock dynamics of an aircraft at moderate to high angles of attack is examined when regulated by a variety of adaptive controllers. Classical adaptive control is compared to several methods of neural network-based adaptive control, both with and without the introduction of a linear controller. All control systems demonstrate adaptation to the effects of modeling error.

The results show that the single hidden-layer neural network adapts much more rapidly than the radial basis function neural network in command tracking, despite having far fewer neurons, and both neural network based designs significantly out perform the classical adaptive controller in both regulation and tracking, even though the classical adaptive approach employs knowledge of the functional form of the modeling error, while the neural network-based approaches do not. In addition, the inclusion of a linear controller in the architecture improves the response for all the control systems, most noticeably for the classical adaptive design.

Issues related to asymptotic stability versus bounded error response on neural network-based designs have also been addressed. In particular, it has been noted that it is mandatory to implement some means to bound the network weights, otherwise none of the neural network based approaches will provide satisfactory performance.

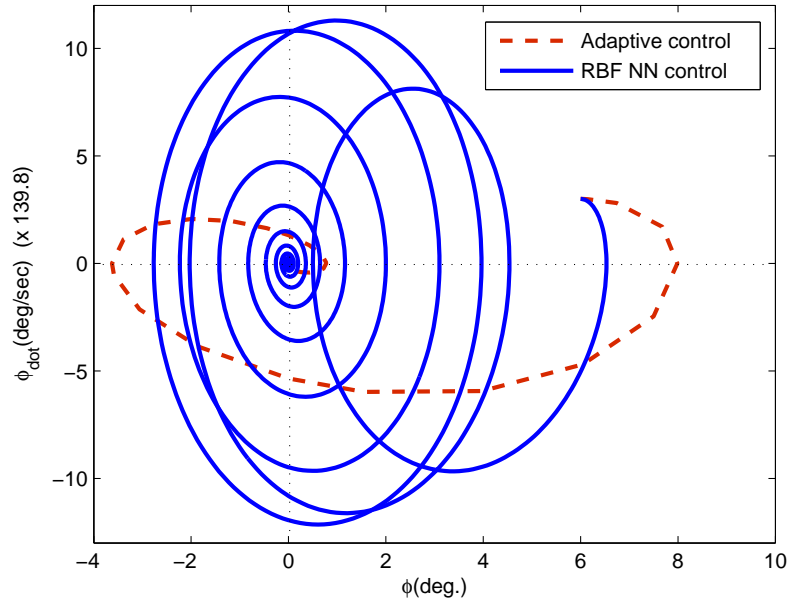


Figure 30: Comparison of responses for a small initial condition

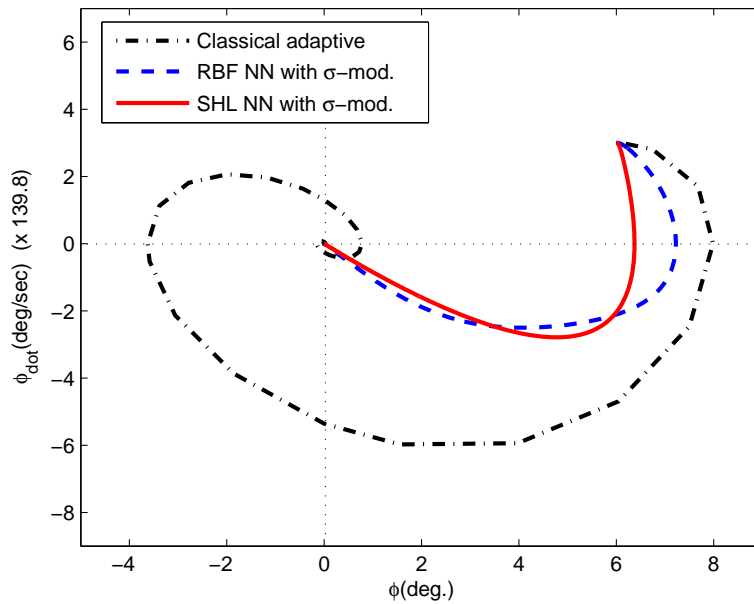


Figure 31: Comparison of classical adaptive and NN-based designs with σ -mod. for a small initial condition

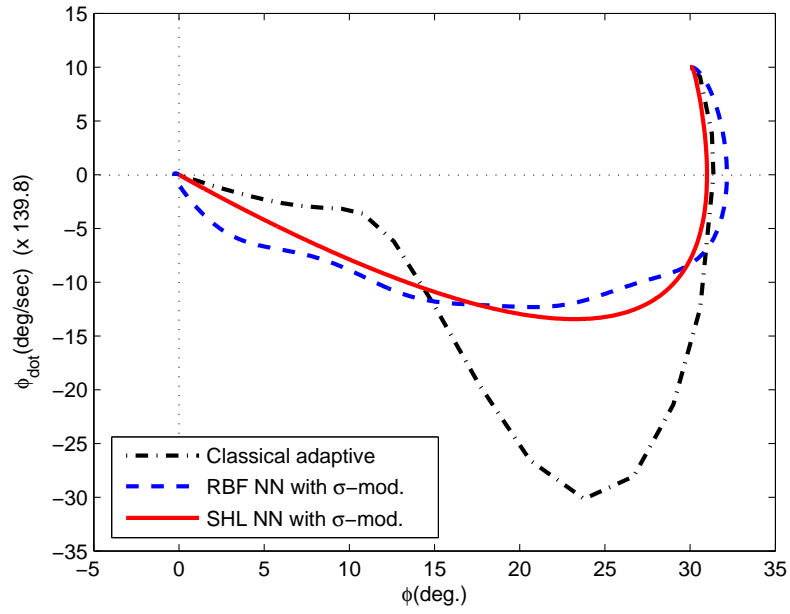


Figure 32: Comparison of classical adaptive and NN-based designs with σ -mod. for a large initial condition

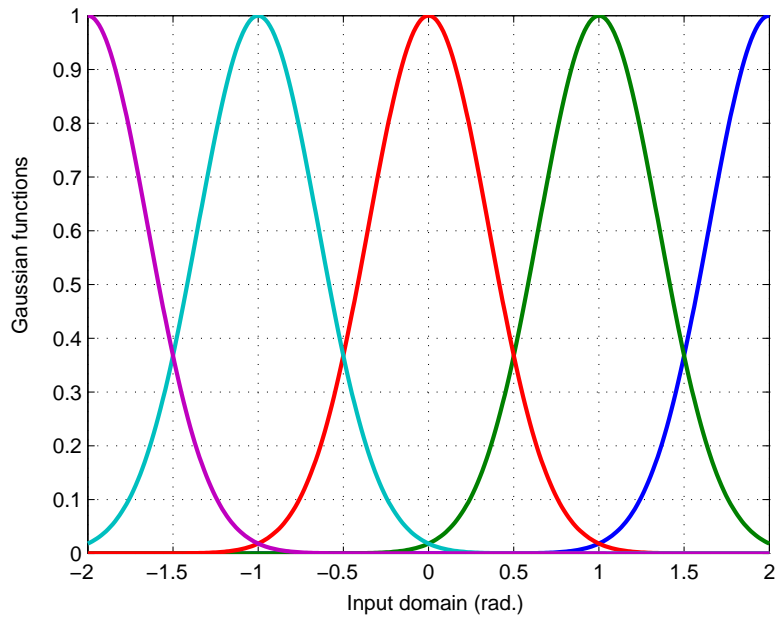


Figure 33: Gaussian basis functions for $N=25$

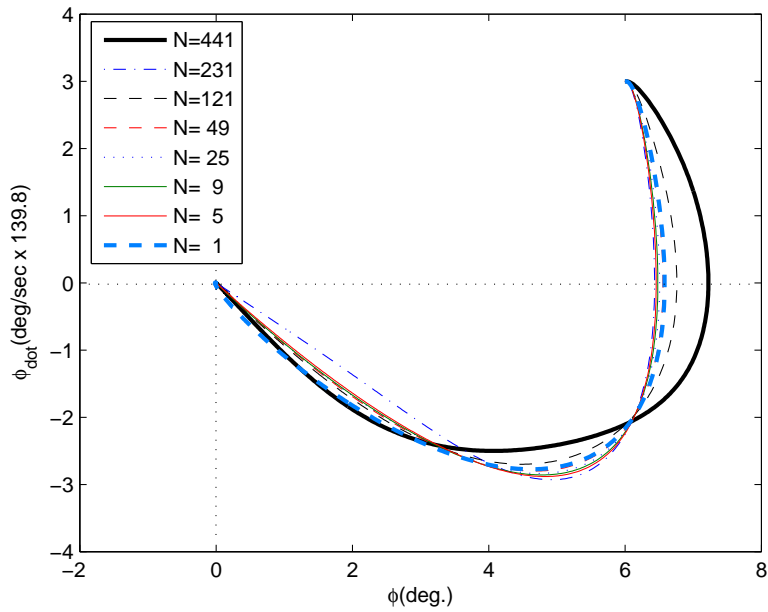


Figure 34: The effect that the number of RBF units has on the response for a small initial condition

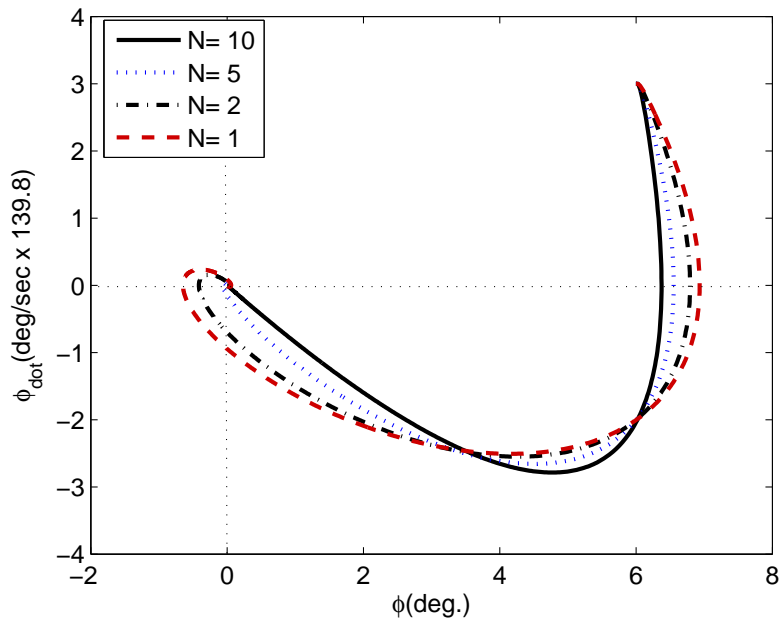


Figure 35: The effect that the number of SHL neurons has on the response for a small initial condition

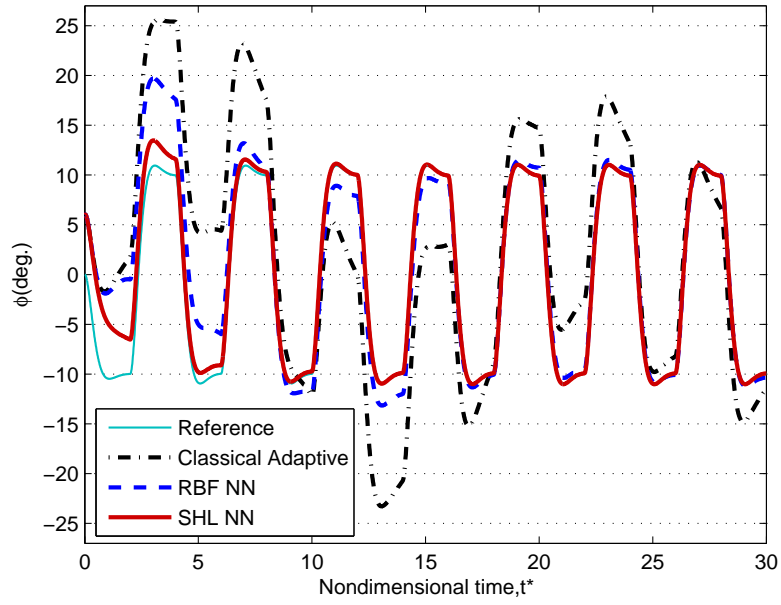


Figure 36: Responses for a square wave command

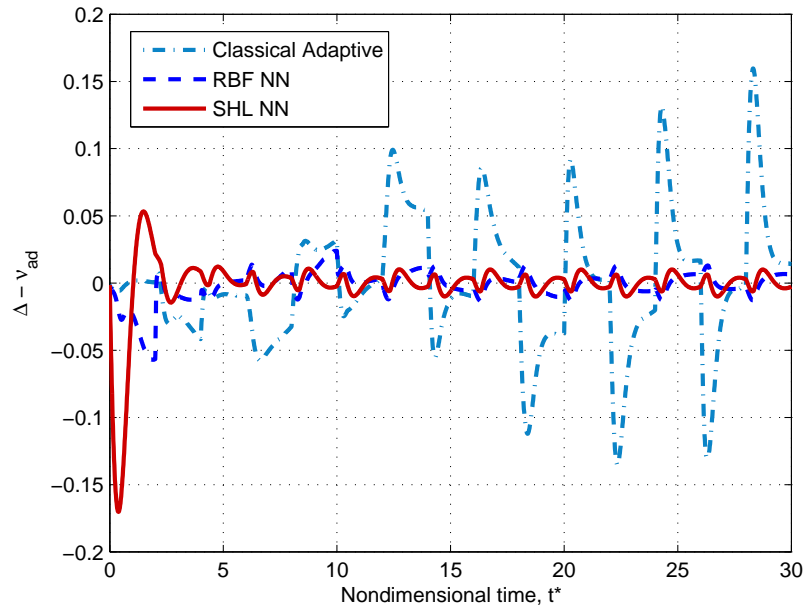


Figure 37: Comparison of ' $\Delta(t^*) - \nu_{ad}(t^*)$ '

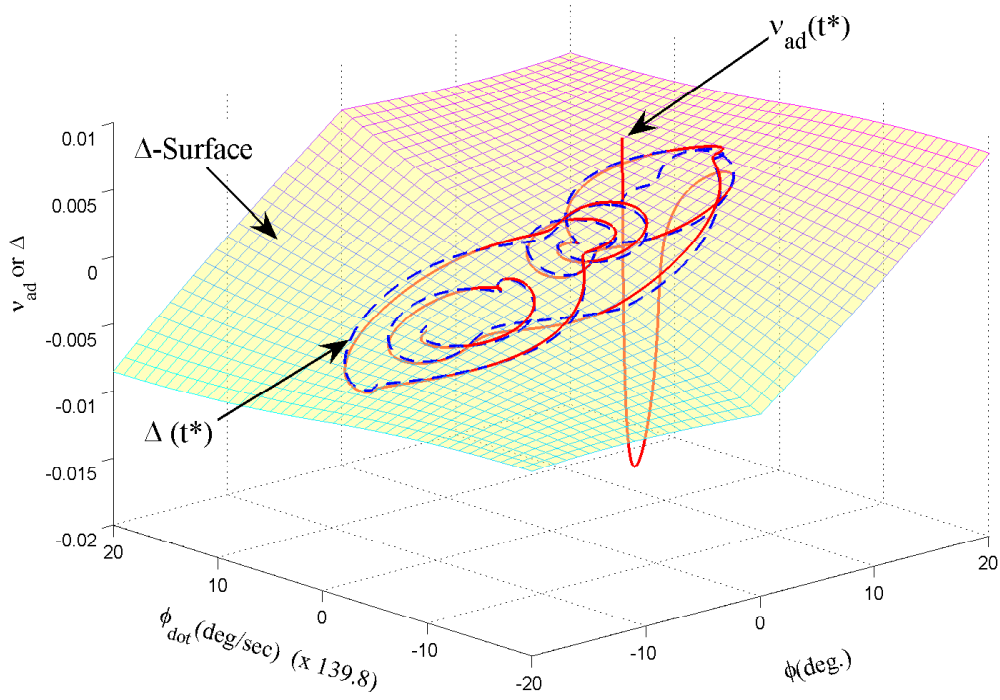


Figure 38: 3-dimensional view of v_{ad} of SHL NN tracking Δ for a sinusoidal command

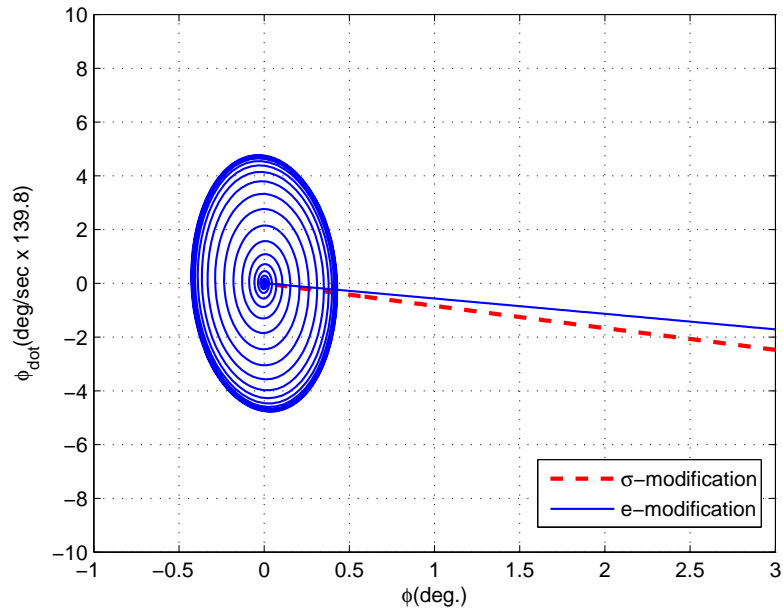


Figure 39: Final stage of σ - and e -modification responses to an initial condition for a zero command

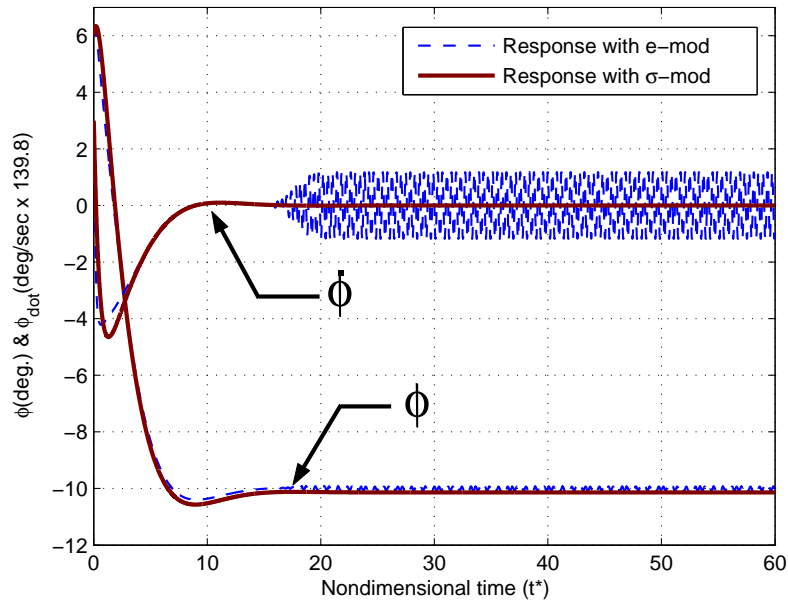


Figure 40: σ - and e -modification responses of SHL NN for a step command of $\phi_c = -10$ degrees

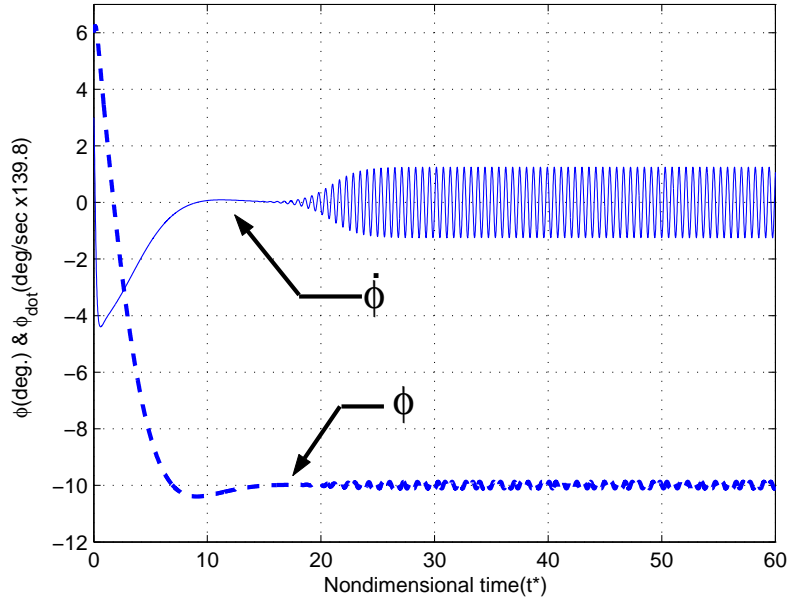


Figure 41: e -modification response of RBF NN for a step command of $\phi_c = -10$ degrees

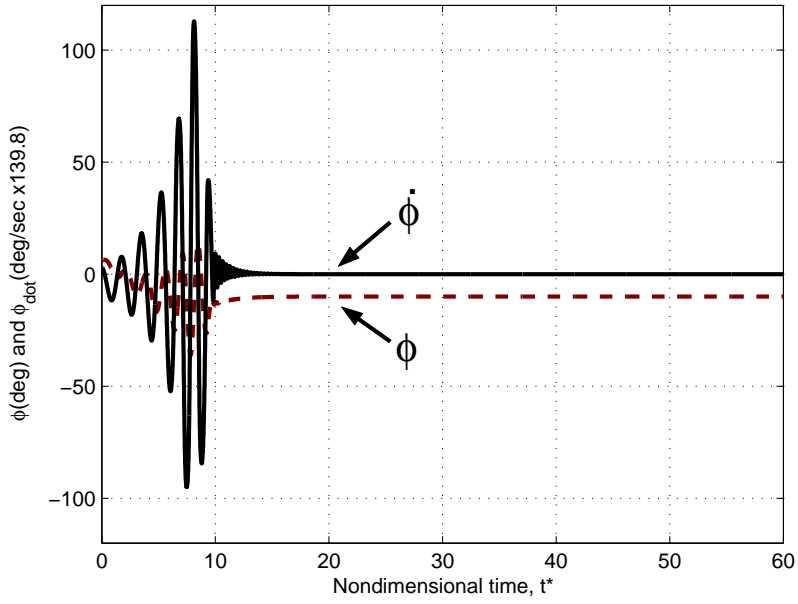


Figure 42: Projection responses for a step command of $\phi_c = -10$ degrees.

CHAPTER VI

ADAPTIVE AUTOPILOT DESIGNS FOR AN UNMANNED AERIAL VEHICLE, FQM-117B

This chapter summarizes the application of two adaptive approaches to autopilot design, and presents an evaluation and comparison of the two approaches in simulation for an unmanned aerial vehicle. One approach employs two-stage dynamic inversion and the other employs feedback dynamic inversions based on a command augmentation system. Both are augmented with neural network-based adaptive elements. The approaches permit adaptation to both parametric uncertainty and unmodeled dynamics, and incorporate a method that permits adaptation during periods of control saturation. Simulation results for an FQM-117B radio controlled miniature aerial vehicle are presented to illustrate the performance of the neural network based adaptation. These designs are currently being implemented at NASA LaRC for purposes of future flight testing [104].

6.1 Introduction

Recent technology developments allow unmanned aerial vehicles (UAVs) to displace manned aircraft in many commercial and military roles. As these roles are expanded from simple reconnaissance missions to more complex missions, there is an increasing need for control systems that are robust to model uncertainty due to incomplete modeling, malfunction, or damage during operation. A challenge to designers of flight control systems is to achieve highly maneuverable UAVs without requiring accurate modeling of these vehicles. Adaptive flight control designs provide a way to deal with the uncertainties in the system and environment, without sacrificing performance.

Most UAV developments are based on simple and inexpensive systems with minimal

mass, having minimal or no aerodynamic data for control design. Therefore, control design for UAVs should take these uncertainties into account. UAV dynamics are also significantly affected by their payloads, which can vary depending upon their mission. Therefore, it is highly desirable to employ an approach to flight control design that is low cost and does not require extensive tuning of gain tables. Adaptive approaches to control system design are ideally suited for this application.

This chapter will illustrate the use of neural network-based adaptive control designs for a UAV. The main objective is to demonstrate adaptation to model uncertainties such as unknown or inaccurate mass properties and unknown aerodynamic derivatives, as well as external aerodynamic disturbances such as wind gusts that can significantly impact UAV flight performance, particularly at the low speeds UAVs typically fly. This chapter presents two NN-based adaptive flight control algorithms that have been successfully utilized for a variety of aerospace applications [14, 18, 105], incorporating recent advances in the area of state/output feedback and adaptation under saturated control conditions. One approach is based on a two-stage dynamic inversion with approximate feedback linearization and synthesis of a fixed-gain linear compensator, and the other approach is a command augmentation system-based dynamic inversion control. Both incorporate NNs as adaptive elements to compensate for the modeling errors such as unmodeled dynamic characteristics of the plant [11, 29]. The effects of control saturation are also directly accounted for in the design of the adaptive controller through pseudo-control hedging (PCH) [39].

The UAV (FQM-117B) used for this study is described in Section 6.2. A two-stage dynamic inversion-based adaptive control design follows in Section 6.3. A command augmentation system-based adaptive control design is presented in Section 6.4. PCH to handle control input nonlinearities is described in Section 6.5, and NNs are briefly discussed in Section 6.6. Simulation results are presented in Section 6.7. Conclusions are given in Section 6.8.

6.2 *The UAV, FQM-117B*

The UAV used for this research is the FQM-117B radio controlled miniature aerial vehicle shown in Figure 43 [32, 75], which is roughly a 1/9 scale version of Russian fighter aircraft MIG-27. This UAV is composed entirely of injection-molded Styrofoam, and has a 1.70 m wingspan, 1.88 m length, and a total vehicle weight of approximately 6.72 kg . It is powered by a 0.60 cubic inch, 1.9 HP glow fuel engine and has elevator, rudder and full-span ailerons. Its moments of inertia are approximately $I_{xx} = 0.2622$, $I_{yy} = 1.2628$, $I_{zz} = 1.5361$, $I_{xz} = -0.0708$, and $I_{xy} = I_{yz} = 0 \text{ kg} \cdot m^2$.

For the control design of the UAV, only simple static wind tunnel test data and mass properties were available. The vehicle employs inexpensive instrumentation, which is noisy and possesses significant amounts of bias, drift and scale factor error. In addition, it is clear that its mass properties change significantly as fuel is consumed, and its flight envelope includes low altitude and low speeds where air disturbances such as gusts are common.

6.3 *Control Design 1: Two-Stage Dynamic Inversion Based Adaptive Control Design*

As in the control design in Chapter 4, angle of attack (α), sideslip angle (β) and stability axis roll rate (p_s) are commanded. As shown in Figure 44, the pilot's command is input to the command filters to generate reference signals, while employing pseudo-control hedging (PCH) to protect the adaptive process from effects due to control saturation. Next, proportional and derivative (PD) controllers are used to follow the reference commands. The control commands are obtained by a two-stage dynamic inversion. Since there are no α and β sensors, the required feedbacks are assumed to be computed by integration of IMU sensor outputs.

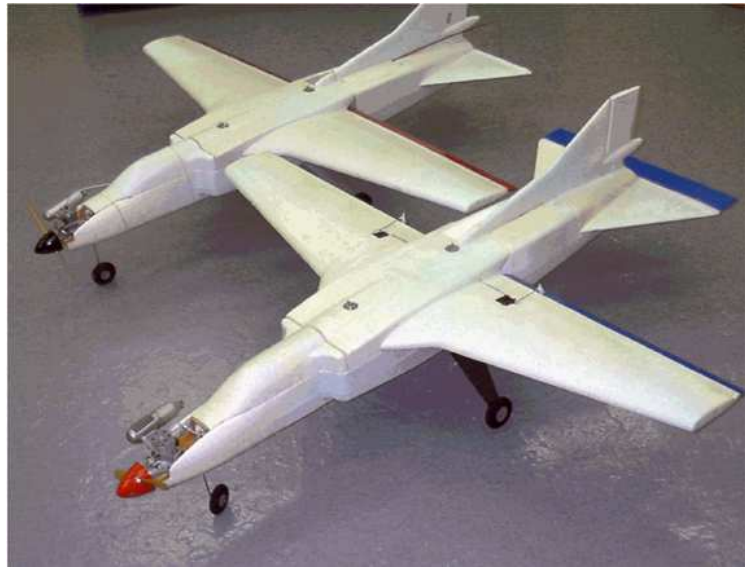
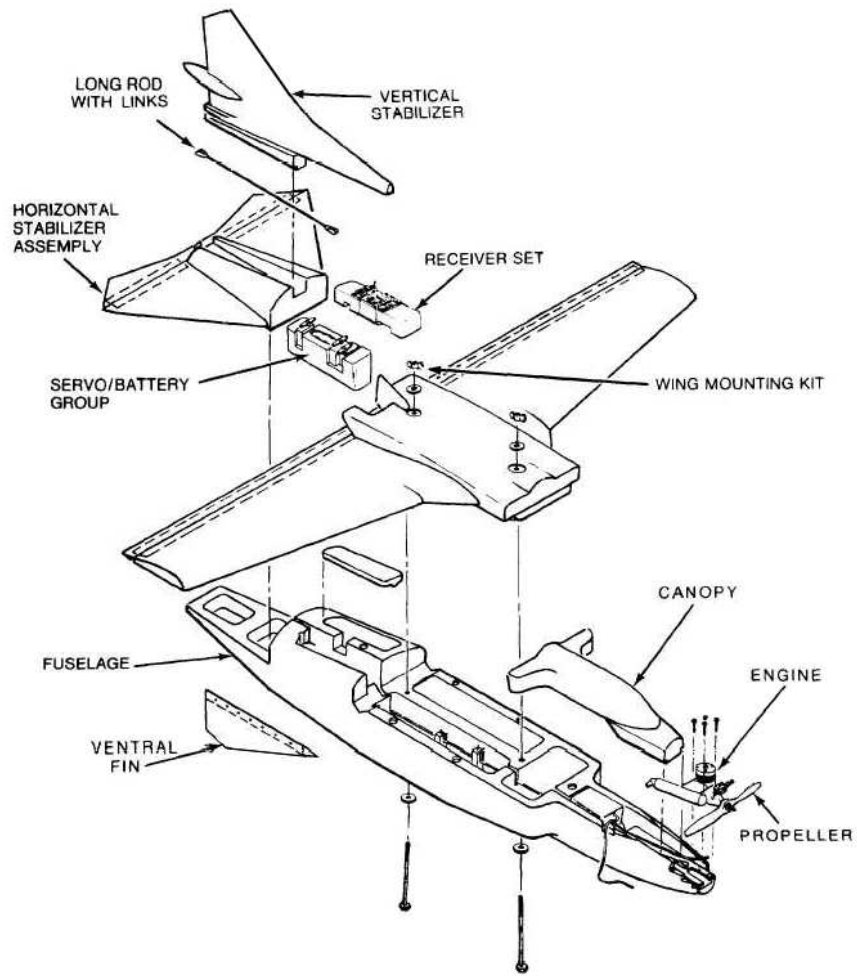


Figure 43: FQM-117B UAV

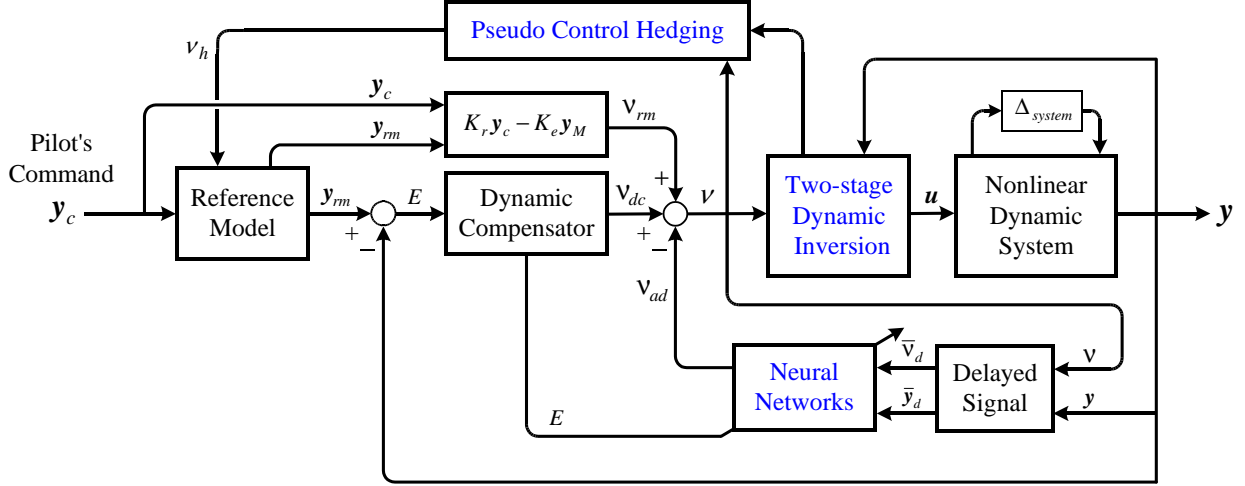


Figure 44: Adaptive feedback control architecture

6.3.1 Two-stage Dynamic Inversion

A two-stage approach for dynamic inversion has been developed for designing a flight control system that regulates $[p_s \ \alpha \ \beta]^T$ [2, 6, 17, 105]. The structure of the inverting law and its implementation is displayed in Figure 45, where the states for the stage 1 dynamics are $\mathbf{x}_1 = [\alpha \ \dot{\alpha} \ \beta \ \dot{\beta} \ \phi \ \theta \ V]^T$ and those for stage 2 dynamics are $\mathbf{x}_2 = [p_s \ q \ r_s]^T$.

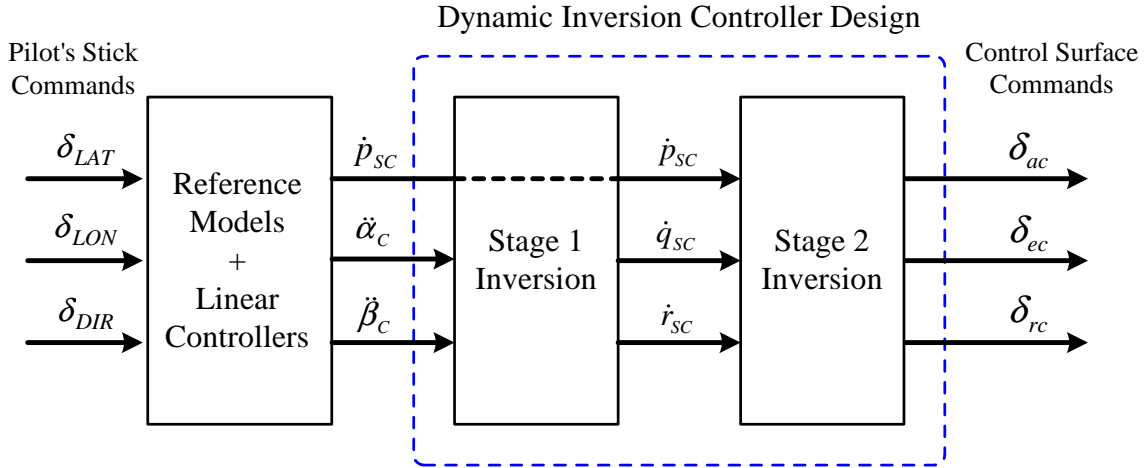


Figure 45: Two-stage dynamic inversion control law structure

The control variables for the stage 1 dynamics are the angular accelerations in the roll, pitch and yaw stability axis frame, $\mathbf{u}_1 = [p_{sc} \ q_c \ r_{sc}]^T$ and the control variables for the stage 2

dynamics are the effective control displacement commands in each axis, $\mathbf{u}_2 = [\delta_{ac} \ \delta_{ec} \ \delta_{rc}]^T$. The regulated variables in each stage are, $\mathbf{y}_1 = [p_s \ \dot{\alpha} \ \dot{\beta}]^T$ and $\mathbf{y}_2 = [p_s \ q \ r_s]^T$. Note that the regulated variables of the stage 1 dynamics are related to regulated variables $[p_s \ \alpha \ \beta]^T$ according to the relative degree of each regulated variable.

Subject to a set of approximations [16] the stage 1 dynamics can be expressed in the following form:

$$\begin{aligned} \begin{bmatrix} \dot{p}_s \\ \ddot{\alpha} \\ \ddot{\beta} \end{bmatrix} &= \begin{bmatrix} 0 \\ f_2(\mathbf{x}, \boldsymbol{\delta}) \\ f_4(\mathbf{x}, \boldsymbol{\delta}) \end{bmatrix} + \begin{bmatrix} 1 & 0 & 0 \\ -\tan(\beta) & 1 & 0 \\ 0 & 0 & -1 \end{bmatrix} \begin{bmatrix} \dot{p}_s \\ \dot{q} \\ \dot{r}_s \end{bmatrix} \\ &= F(\mathbf{x}, \boldsymbol{\delta}) + G(\mathbf{x}) \cdot \mathbf{u}_1 \end{aligned} \quad (6.3.1)$$

where p_s and r_s denote the stability axis roll and yaw rates. Similarly, the stage 2 dynamics can be expressed as:

$$\begin{bmatrix} \dot{p}_s \\ \dot{q} \\ \dot{r}_s \end{bmatrix} = \begin{bmatrix} f_9(\mathbf{x}) \\ f_{10}(\mathbf{x}) \\ f_{11}(\mathbf{x}) \end{bmatrix} + \begin{bmatrix} \overline{L}_{\delta_a} & 0 & 0 \\ 0 & M_{\delta_e} & 0 \\ 0 & 0 & \overline{N}_{\delta_r} \end{bmatrix} \begin{bmatrix} \delta_{ac} \\ \delta_{ec} \\ \delta_{rc} \end{bmatrix} \quad (6.3.2)$$

6.3.2 Computation of the Control

Consider the stage 2 dynamic equation expressed as

$$\dot{\mathbf{x}}_2 = A(\mathbf{x}) + B(\mathbf{x})\mathbf{u}_2 \quad (6.3.3)$$

$$\mathbf{y}_2 = \mathbf{x}_2$$

Then it follows that

$$\begin{aligned} \dot{\mathbf{y}}_2 &= \dot{\mathbf{x}}_2 = A(\mathbf{x}) + B(\mathbf{x})\mathbf{u}_2 \\ &= A(\mathbf{x}) + B(\mathbf{x}) \cdot \mathbf{u}_e \\ &= \mathbf{u}_1 \end{aligned} \quad (6.3.4)$$

The stage 1 dynamic equation is given as

$$\begin{aligned} \dot{\mathbf{y}}_1 &= F(\mathbf{x}) + G(\mathbf{x}) \cdot \mathbf{u}_1 \\ &= \boldsymbol{\nu} \end{aligned} \quad (6.3.5)$$

where $\boldsymbol{\nu}$ is the pseudo-control. Combining (6.3.4) and (6.3.5), we have the commanded control that is applied to the aircraft.

$$\mathbf{u} = (\hat{G}(\mathbf{x})\hat{B}(\mathbf{x})T_a)^{-1} \left[\boldsymbol{\nu} - \{\hat{F}(\mathbf{x}) + \hat{G}(\mathbf{x})\hat{A}(\mathbf{x})\} \right] \quad (6.3.6)$$

where $\hat{G}(\mathbf{x})$, $\hat{B}(\mathbf{x})$, $\hat{F}(\mathbf{x})$ and $\hat{A}(\mathbf{x})$ denote estimates of $G(\mathbf{x})$, $B(\mathbf{x})$, $F(\mathbf{x})$ and $A(\mathbf{x})$.

6.3.3 Control Architecture

The pseudo-control for this state feedback control design has the form:

$$\boldsymbol{\nu} = \mathbf{x}_c^{(r)} + \boldsymbol{\nu}_{dc} - \boldsymbol{\nu}_{ad} \quad (6.3.7)$$

where $\mathbf{x}_c^{(r)}$ is output of an r^{th} -order reference model that is used to define the desired closed loop response, $\boldsymbol{\nu}_{dc}$ is the output of a dynamic compensator, and $\boldsymbol{\nu}_{ad}$ is the adaptive signal.

The error dynamics for the state feedback can be expressed as

$$\begin{aligned} \tilde{\mathbf{x}}_c^{(r)} &= \mathbf{x}_c^{(r)} + \mathbf{x}^{(r)} \\ &= -\boldsymbol{\nu}_{dc} + \boldsymbol{\nu}_{ad} - \boldsymbol{\Delta} \end{aligned} \quad (6.3.8)$$

It is apparent that the dynamic compensator should be designed to stabilize (6.3.8), and that the role of $\boldsymbol{\nu}_{ad}$ is to cancel $\boldsymbol{\Delta}$.

6.4 Control Design 2: Command Augmentation Based Adaptive Control Design

As shown in Figure 46, the acceleration commands to the UAV are first converted to p , q and r commands (p_c , q_c , r_c) through an outer-loop controller, while ensuring the vehicle's stability and maintaining trimmed sideslip angle during maneuvers [72]. Then first-order reference models are inserted in each channel to generate reference signals, while employing PCH to protect the adaptive process from effects due to control saturation. Next, proportional controllers are used to follow the reference commands p_{rm} , q_{rm} and r_{rm} . The output of the controller is a part of the total pseudo-control $\boldsymbol{\nu}$, which is the desired angular acceleration.

The equations for angular acceleration are inverted to obtain the effective control in each axis. Figure 46 also shows the PCH and the NN signals, which are further discussed in Sections 6.5 and 6.6.

6.4.1 Outer-Loop Controller

The outer-loop controller produces a pitch rate command q_c and a yaw rate command r_c such that the lateral acceleration remains close to zero, which provides turn coordination. The dynamic compensator has a proportional plus integral (PI) form:

$$\begin{aligned} q_c &= K_1 \cdot (a_{nc} - a_n) + K_2 \cdot \int_0^t (a_{nc} - a_n) d\tau \\ r_c &= -K_3 \cdot a_y - K_4 \cdot \int_0^t a_y d\tau \end{aligned} \quad (6.4.1)$$

where the feedback gains K_1 , K_2 , K_3 , and K_4 can be selected based on speed of response.

6.4.2 Command Filter (Reference Model)

A first order reference model is introduced to generate reference signals in each channel. For instance, for roll channel it is:

$$\frac{p_{rm}}{p_c} = \frac{1}{\tau s + 1} \quad (6.4.2)$$

where τ is the desired roll mode time constant. In this process, pseudo-control hedging is incorporated to handle control nonlinearities.

6.4.3 Dynamic Compensator and Control

The derivatives of the body angular angles can be described as, designating the approximate mathematical models \hat{p} , \hat{q} , \hat{r} with the pseudo-controls, ν_p , ν_q , ν_r :

$$\begin{bmatrix} \hat{p} \\ \hat{q} \\ \hat{r} \end{bmatrix} = \begin{bmatrix} \nu_p \\ \nu_q \\ \nu_r \end{bmatrix} = \begin{bmatrix} F_1(\mathbf{x}) \\ F_2(\mathbf{x}) \\ F_3(\mathbf{x}) \end{bmatrix} + \begin{bmatrix} G_1 & 0 & 0 \\ 0 & G_2 & 0 \\ 0 & 0 & G_3 \end{bmatrix} \cdot \begin{bmatrix} \delta_a \\ \delta_e \\ \delta_r \end{bmatrix} \quad (6.4.3)$$

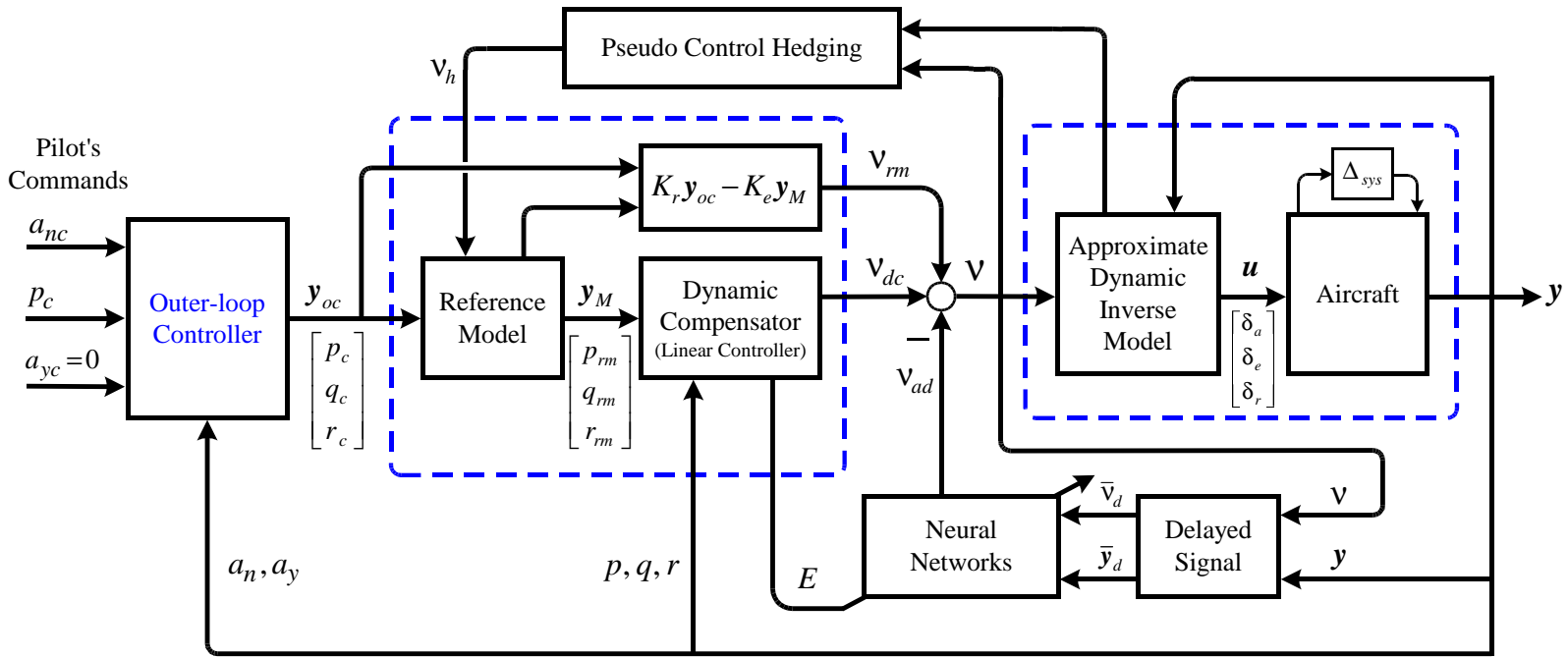


Figure 46: Command augmentation based adaptive control design using neural networks

Inverting (6.4.3) resulting in the control laws:

$$\begin{aligned} \begin{bmatrix} \delta_a \\ \delta_e \\ \delta_r \end{bmatrix} &= \begin{bmatrix} G_1 & 0 & 0 \\ 0 & G_2 & 0 \\ 0 & 0 & G_3 \end{bmatrix}^{-1} \cdot \begin{bmatrix} \nu_p - F_1(\mathbf{x}) \\ \nu_q - F_2(\mathbf{x}) \\ \nu_r - F_3(\mathbf{x}) \end{bmatrix} \\ &= \begin{bmatrix} G_1^{-1} \cdot (\nu_p - F_1(\mathbf{x})) \\ G_2^{-1} \cdot (\nu_q - F_2(\mathbf{x})) \\ G_3^{-1} \cdot (\nu_r - F_3(\mathbf{x})) \end{bmatrix} \end{aligned} \quad (6.4.4)$$

The controls in (6.4.4) are based on the simplified functions $F_i(\mathbf{x})$, $i = 1, 2, 3$, which retain only a few dominate terms:

$$\begin{aligned} F_1(\mathbf{x}) &= \frac{S\bar{q}b}{I_{xx}}C_{lp} \cdot \left(\frac{pb}{2U}\right) + \frac{S\bar{q}b}{I_{xx}}C_{l\beta} \cdot \beta \\ F_2(\mathbf{x}) &= \frac{S\bar{q}\bar{c}}{I_{yy}}C_{mq} \cdot \left(\frac{q\bar{c}}{2U}\right) + \frac{S\bar{q}\bar{c}}{I_{yy}}C_{m\alpha} \cdot \alpha \\ F_3(\mathbf{x}) &= \frac{S\bar{q}b}{I_{zz}}C_{nr} \cdot \left(\frac{rb}{2U}\right) + \frac{S\bar{q}b}{I_{zz}}C_{n\beta} \cdot \beta \end{aligned} \quad (6.4.5)$$

and

$$G_1 = \frac{S\bar{q}b}{I_{xx}}C_{l\delta_a}, \quad G_2 = \frac{S\bar{q}\bar{c}}{I_{yy}}C_{m\delta_e}, \quad G_3 = \frac{S\bar{q}b}{I_{zz}}C_{n\delta_r} \quad (6.4.6)$$

Here the aerodynamic coefficients (C_{lp} , $C_{m\alpha}$, etc) and control effectiveness ($C_{l\delta_a}$, $C_{m\delta_e}$, $C_{n\delta_r}$) are set to constant values. These approximations introduce modeling error.

The exact expression for p can be, for instance, written by:

$$\dot{p} = C_l \frac{S\bar{q}b}{I_{xx}} \quad (6.4.7)$$

where

$$C_l = C_{l0} + C_{l\beta} \cdot \beta + C_{lp} \cdot \frac{pb}{2V} + C_{lr} \cdot \frac{rb}{2V} + C_{l\phi} \cdot \delta\phi + C_{l\delta_a} \cdot \delta_a + C_{l\delta_r} \cdot \delta_r \quad \dots \quad (6.4.8)$$

Because only a few dominant terms among those in (6.4.8) are retained in (6.4.3) and ((6.4.5)), there always exists a modeling error Δ_p defined by

$$\Delta_p = \dot{p} - \hat{\dot{p}} = \dot{p} - \nu_p \quad (6.4.9)$$

Modeling errors Δ_q and Δ_r in pitch and yaw channels, respectively, can also be defined by the same way. Using these definitions, the time derivatives of angular rates can be described by:

$$\begin{aligned}\dot{p} &= \hat{p} + \Delta_p = \nu_p + \Delta_p \\ \dot{q} &= \hat{q} + \Delta_q = \nu_q + \Delta_q \\ \dot{r} &= \hat{r} + \Delta_r = \nu_r + \Delta_r\end{aligned}\tag{6.4.10}$$

The equations in (6.4.3) can be transformed to a linear, time invariant form by designating the pseudo-controls including *only* proportional control laws:

$$\begin{aligned}\nu_p &= A_1 \cdot (p_c - p) - \nu_{adp} \\ \nu_q &= A_2 \cdot (q_c - q) - \nu_{adq} \\ \nu_r &= A_3 \cdot (r_c - r) - \nu_{adr}\end{aligned}\tag{6.4.11}$$

where $(\nu_{adp}, \nu_{adq}, \nu_{adr})$ are adaptive signals which are the output of neural networks as shown in Figure 46. Substitution (6.4.11) into (6.4.10) gives

$$\begin{aligned}\dot{p} &= A_1 \cdot (p_c - p) - \nu_{adp} + \Delta_p \\ \dot{q} &= A_2 \cdot (q_c - q) - \nu_{adq} + \Delta_q \\ \dot{r} &= A_3 \cdot (r_c - r) - \nu_{adr} + \Delta_r\end{aligned}\tag{6.4.12}$$

Hence, if the NN adaptive signals $(\nu_{adp}, \nu_{adq}, \nu_{adr})$ cancel out the modeling errors $(\Delta_p, \Delta_q, \Delta_r)$, then asymptotic tracking in body angular rates can be expected. Consequently, the neural networks play the key role of generating the adaptive signals to compensate for the modeling errors due to the use of approximate models, uncertainties in each channel. Feedback gains A_1, A_1, A_3 are chosen to satisfy the desired handling qualities.

6.4.4 Output Feedback Design

Most UAVs feature simple, fundamental, avionics sensors, so only a limited set of parameters is available for feedback. Thus, an output feedback design of the control system should be considered for such cases.

As a further simplification, angle of attack (α) and sideslip angle (β) dependencies are ignored, and the terms including these values are discarded. In addition, the x -axis speed component, U , may be replaced by the total speed V as shown below:

$$F_1(\mathbf{x}) = \frac{S\bar{q}b}{I_{xx}}C_{lp} \cdot \left(\frac{pb}{2V}\right), \quad F_2(\mathbf{x}) = \frac{S\bar{q}\bar{c}}{I_{yy}}C_{mq} \cdot \left(\frac{q\bar{c}}{2V}\right), \quad F_3(\mathbf{x}) = \frac{S\bar{q}b}{I_{zz}}C_{nr} \cdot \left(\frac{rb}{2V}\right) \quad (6.4.13)$$

According to the theoretical background on the adaptive output feedback design presented in [29], the delayed signals in each channel are input to the NN adaptive elements

6.5 Pseudo-Control Hedging (PCH)

PCH is used to address NN adaptation difficulties arising from various actuation nonlinearities, including actuator position and/or rate saturation, discrete (magnitude quantized) control, time delays and actuator dynamics [40]. NN training difficulties occur when unmodeled actuator characteristics are encountered. For example, the NN adaptive element will attempt to adapt to these nonlinearities, even when it is impossible to do so. The goal of PCH is to prevent the adaptive element from attempting to adapt to these characteristics, while not affecting NN adaptation to other sources of inversion error. Conceptually, PCH "moves the reference model backwards" by an estimate of the amount the controlled system did not move due to selected actuator characteristics (such a position and rate limits, time delays, etc). The reference model is hedged according to an estimate of the difference between the commanded and actually achieved pseudo-control.

The hedge signal is defined as

$$\boldsymbol{\nu}_h = \boldsymbol{\nu} - \hat{\boldsymbol{\nu}} \quad (6.5.1)$$

where $\boldsymbol{\nu}$ is the commanded pseudo-control and $\hat{\boldsymbol{\nu}}$ is an estimate for the achieved pseudo-control. For the design approach in Section 6.3, for example, $\boldsymbol{\nu}$ is defined in (6.3.5) and the estimate is obtained by combining (6.3.3), and (6.3.4) and replacing the elements of \mathbf{u}_2 in (6.3.4) by estimates obtained from actuator models of the form in Figure 47. Thus,

$$\boldsymbol{\nu}_h = \boldsymbol{\nu} - \left[\hat{F}(\mathbf{x}) + \hat{G}(\mathbf{x})\hat{A}(\mathbf{x}) + \hat{G}(\mathbf{x})\hat{B}(\mathbf{x}) \cdot \hat{\mathbf{u}}_2 \right] \quad (6.5.2)$$

The elements of the hedge signal are then subtracted in the reference models for each respective axis (roll, pitch and yaw). The manner in which this is done for a first order reference model is depicted in Figure 48.

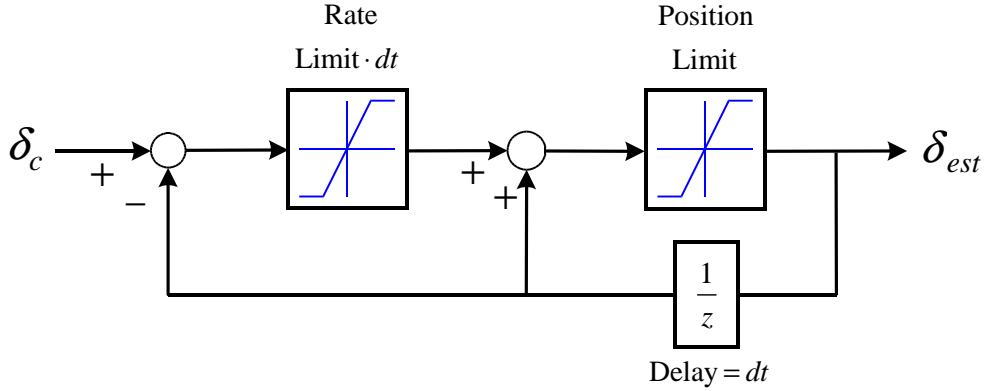


Figure 47: Actuator estimator

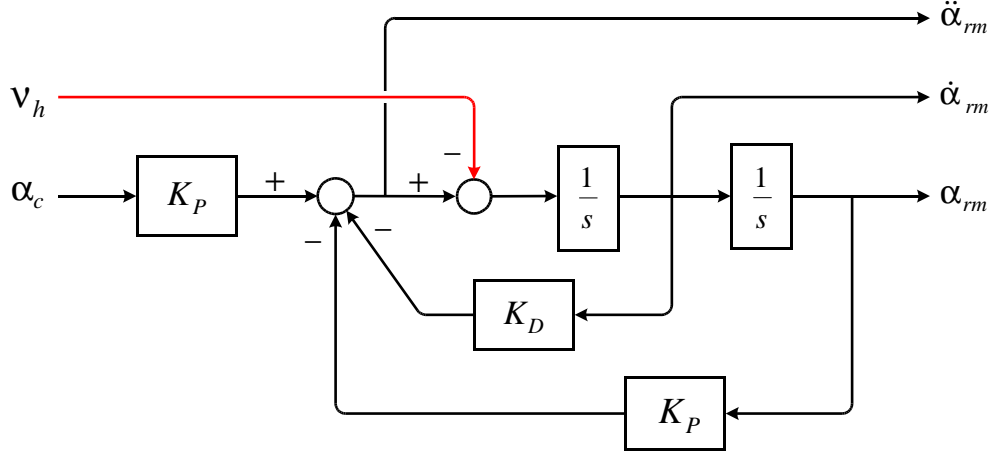


Figure 48: Reference model with hedging in pitch channel

6.6 Neural Network Adaptation

According to (6.4.12) and (6.5.2), Δ depends on the states and the pseudo-control. As described in Chapter 2, this error can be approximated, in a bounded region, to any desired degree of accuracy using a neural network (NN) with a sufficient number of hidden layer

neurons, having the following input vector [11, 20, 29, 87]:

$$\boldsymbol{\mu}(t) = [1 \ \bar{\boldsymbol{\nu}}_d^T(t) \ \bar{\boldsymbol{y}}_d^T(t)] \quad (6.6.1)$$

where

$$\begin{aligned} \bar{\boldsymbol{\nu}}_d(t) &= [\nu(t) \ \nu(t-d) \ \cdots \ \nu(t-(n_1-r-1)d)]^T \\ \bar{\boldsymbol{y}}_d(t) &= [y(t) \ y(t-d) \ \cdots \ y(t-(n_1-r-1)d)]^T \end{aligned} \quad (6.6.2)$$

with $n_1 \geq n$ and $d > 0$ denotes time delay.

In the case of a single hidden-layer (SHL), multi-perceptron NN shown in Figure 3, we have

$$\boldsymbol{\nu}_{ad}(t) = \hat{W}^T \boldsymbol{\sigma} \left(\hat{V}^T \boldsymbol{\mu} \right) \quad (6.6.3)$$

where $\boldsymbol{\sigma}$ is a vector whose elements, $\sigma_i(z_i)$, are the basis functions of the NN. Adaptation laws are used in the form of (2.2.10). See Chapter 2 for more details.

6.7 Simulations

The simulation model was constructed using Matlab/Simulink [90] implementing the UAV's preliminary configuration data, mass properties and static wind tunnel data which covers angles of attack from 6 to 20 degrees and sideslip angles from 16 to 16 degrees, along with the assumed dynamic damping derivatives: $C_{mq} = 1.0$, $C_{lp} = 0.25$, $C_{nr} = 0.1$, $C_{m\dot{\alpha}} = 0$. The aircraft trim conditions are: $V_T = 31.0 \text{ m/s}$, $h_T = 122.0 \text{ m}$, $\alpha_T = 2.816^\circ$, and $\beta_T = 0.541^\circ$. The trimmed throttle setting is 0.44 and is held constant. All aerodynamic control deflections range between 25 to 25 degrees with rate limits of $\pm 120 \text{ deg/sec}$. All simulations begin from the trim condition.

6.7.1 Model of Atmospheric Turbulence

The flight envelope of the UAV involves mostly low altitude where gusts or turbulence are common, hence a model of the turbulence was implemented in control simulations. Turbulence was modeled as a filtered white noise process using the Dryden model.

6.7.2 Control Design 1: Two-Stage Dynamic Inversion Based Adaptive Control Design

The control design was carried out assuming that the pilot commands α , β and p_s . The roll channel is relative degree one ($r = 1$) with respect to the control, while both the α and β channels are relative degree two. The details of this design are described in [17, 105]. Since $r = 1$ in the roll channel, a first order reference model is employed for that channel, with a time constant of 0.3. Likewise, second order reference models are employed in the pitch and directional channels, with $\omega_n = 5 \text{ rad/sec}$ and $\zeta = 1.0$. The values selected for the NN gains, defined in (2.2.10), and the number of hidden layer neurons, n_2 , are given in Table 3. The activation potentials (a_i) were uniformly distributed between 0.1 and 0.5. In addition, the first NN basis function was used to provide a bias term ($a_0 = 0$).

Table 3: FQM-117B neural network parameters for Design 1

Channel	Γ_V	Γ_W	κ_v, κ_w	n_2	n_1	d
p	0.5	0.3	0.1	10	23	0.01
q	1.0	1.5	0.1	10	23	0.01
r	0.5	0.5	0.1	10	23	0.01

6.7.2.1 Angle of Attack Maneuver

Simulation results are presented in Figure 49–51 for a 12° angle of attack with β and p_s set to zero. Figure 49 presents the α , β and $p - s$ responses with and without adaptation. Figure 52(a) shows that with NN/PCH, the α -response follows its reference model response without any overshoot, while β and p_s responses in Figure 52(b) exhibit moderate oscillations. Without adaptation, the α -response goes immediately unstable. It can be clearly seen that good tracking is achieved for the vehicle with adaptation.

Time histories of aerodynamic controls for cases with and without adaptation are depicted in Figure 50. The NN adaptation signal $\nu_{ad}(t)$ and inversion error $\Delta(t)$ for all channels are compared in Figure 51. This represents a measure of the degree that adaptation is able to compensate for the inversion error.

6.7.2.2 Stability Axis Roll Rate (p_s) Maneuver

Simulation results for command of $p_s = 150^\circ/sec$ while maintaining the trim angle of attack are depicted in Figures 52–54. Figure 52 shows the responses with and without adaptation. It can be seen that good tracking is also maintained in this case with adaptation, except for the transient oscillations in roll response at about 8 and 11 seconds. Without adaptation, α -response diverges at the initial phase. Figure 53 depicts time histories of aerodynamic controls for cases with and without adaptation. Figure 54 compares $\boldsymbol{\nu}_{ad}(t)$ and $\boldsymbol{\Delta}(t)$ for all three channels. It can be seen that the NN precisely compensates for the inversion error. The simulation results indicate that the UAV has very agile roll maneuverability, and that it can be greatly enhanced with adaptation.

6.7.3 Control Design 2: Command Augmentation Based Adaptive Control Design

6.7.3.1 State Feedback

The feedback gains K_1, K_2, K_3 , and K_4 in (6.4.1) are chosen in accordance with the following equations:

$$K_2 = K_4 = \frac{\omega_n}{2\zeta}, \quad K_1 = \tau_n K_2, \quad K_3 = \tau_n K_4 \quad (6.7.1)$$

where

$$\tau_n = \frac{2m}{\rho S V_T C_{L\alpha}}, \quad \tau_y = \frac{2m}{\rho S V_T |C_{y\beta}|} \quad (6.7.2)$$

The time constant τ , in (6.4.2), for pitch and roll channels, is set to $\tau = 1/2\zeta\omega_n$, and for the yaw channel it is set to $\tau = 2/\zeta\omega_n$. The natural frequency (ω_n) and damping ratio (ζ) are set to 5 *rad/sec* and 2.0, respectively. The gains A_1, A_2, A_3 in (6.4.11) are chosen as:

$$A_1 = 25, \quad A_2 = 20, \quad A_3 = 10 \quad (6.7.3)$$

The values selected for the NN gains and the number of hidden layer neurons, n_n , are given in Table 4. The activation potentials (a_i) were uniformly distributed between 0.1 and

0.5. In addition, the first NN basis function was used to provide a bias term ($a_0 = 0$).

Normal Acceleration (a_n) Maneuver

Simulation results using state feedback are presented in Figures 55 – 59 for $a_{nc} = 1 \pm 0.8g$ with $a_{yc} = p_c = 0$. Figure 55 presents a_n , a_y and p responses with and without adaptation. As shown in Figure 55, with adaptation a_n closely follows the command with minimal overshoot, while p and a_y are maintained close to zero, except for short transient periods. This is not the case without adaptation. Moreover, Figure 56 shows that the yaw rate response diverges without adaptation. Figure 57 shows that the controller without adaptation has difficulty in restoring α and β to their trim values. Time histories of control deflections are presented in Figure 58, and it is noted that PCH is active in the right elevator channel at right after 4 and 7 seconds due to the actuator rate limits. The NN adaptation signal $\nu_{ad}(t)$ and inversion error $\Delta(t)$ for all channels are compared in Figure 59. It can be seen that NN output, $\nu_{ad}(t)$, satisfactorily cancels out the error $\Delta(t)$ over the entire simulation period.

Roll Rate (p) Maneuver

Simulation results using state feedback for $p_c = \pm 150^\circ/sec$, while maintaining $a_n = 1.0$ and $a_y = 0$, are depicted in Figures 60–64. Figure 60(a) shows the roll rate response for cases with and without adaptation. It can be seen that good tracking is maintained with adaptation, while larger errors occur without adaptation. Normal and lateral accelerations are depicted in Figure 60(b) and they closely follow their commanded values. Figure 61 shows the q and r responses. It can be seen that they also follow the reference command, even without adaptation. Figure 62 shows the α and β responses. Note that β exhibits a slightly larger transient behavior with adaptation. Figure 63 shows time histories of control

Table 4: FQM-117B neural network parameters for Design 2

Channel	Γ_V	Γ_W	λ	n_n	n_l	d
p	3.0	3.0	0.01	10	23	0.01
q	3.0	5.0	0.01	10	23	0.01
r	3.0	1.0	0.01	10	23	0.01

deflections. Figure 64 compares the NN adaptation signal $\boldsymbol{\nu}_{ad}(t)$ and inversion error $\boldsymbol{\Delta}(t)$ for all channels, again demonstrating that $\boldsymbol{\nu}_{ad}(t)$ cancels $\boldsymbol{\Delta}(t)$.

6.7.3.2 Output Feedback

The same parameter settings and NN gains used for state feedback are used for the output feedback case, and (6.4.13) was used instead of (6.4.5) since α and β are treated as not available for feedback.

Normal Acceleration (a_n) Maneuver

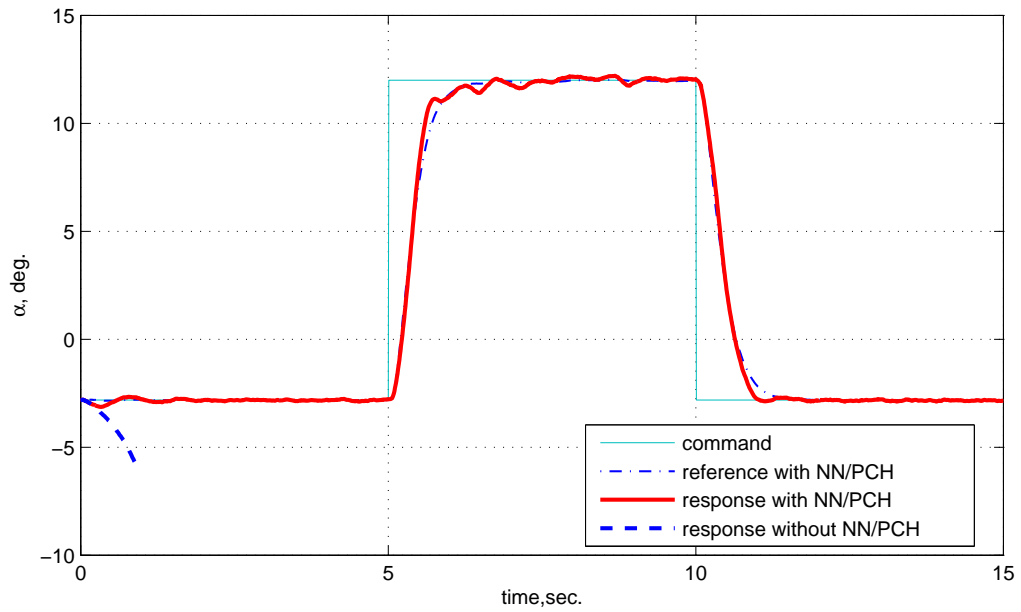
Simulation results using output feedback are presented in Figures 65 – 69 for $a_{nc} = 1 \pm 0.8g$ with $a_{yc} = p_c = 0$. Figure 65 presents a_n , a_y and p responses with and without adaptation. Pitch and roll rates are depicted in Figure 66 and they closely follow their commanded values with adaptation. Figure 67 shows α and β responses. Overall responses for this command are similar to the state feedback case. Figure 68 shows time histories of control deflections. The NN adaptation signal $\boldsymbol{\nu}_{ad}(t)$ and inversion error $\boldsymbol{\Delta}(t)$ for all channels are compared in Figure 69. It can also be seen that NN output, $\boldsymbol{\nu}_{ad}(t)$ shows good adaptation by canceling the error $\boldsymbol{\Delta}(t)$ over the entire simulation period.

Roll Rate (p) Maneuver

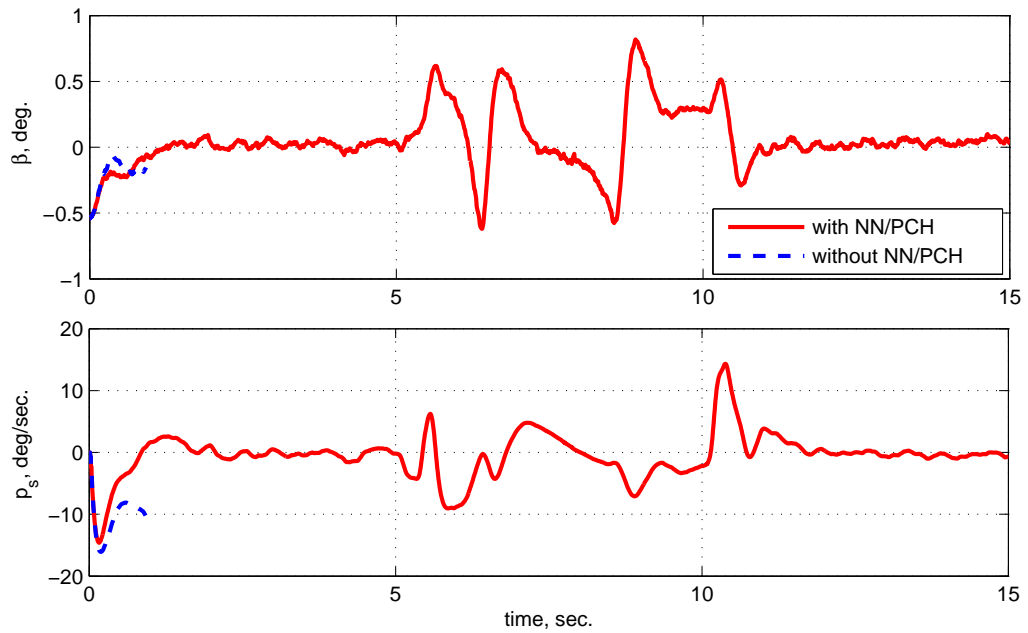
Simulation results using output feedback for $p_c = \pm 150^\circ/sec$, while $a_{nc} = 1.0$ and $a_{yc} = 0$, are depicted in Figures 70–74. Figure 70(a) shows p rate response for cases with and without adaptation. Normal and lateral accelerations are depicted in Figure 70(b), and q and r are presented in Figure 71. Figure 72 shows α and β responses. Figure 73 shows time histories of control deflections. Figure 74 compares the NN adaptation signal $\boldsymbol{\nu}_{ad}(t)$ and inversion error $\boldsymbol{\Delta}(t)$ for all channels, again demonstrating that $\boldsymbol{\nu}_{ad}(t)$ cancels $\boldsymbol{\Delta}(t)$.

6.8 Conclusion

Two NN-based adaptive control designs for the FQM-117B UAV are presented: One with two-stage dynamic inversion and state feedback, and the other with a feedback dynamic inversion based on a command augmentation system with state and output feedback. The tracking performances of both approaches are greatly improved by the NN-based adaptive control design, thereby implying successful adaptation to modeling error and uncertainties. Pseudo-control hedging is implemented to protect the adaptive process during periods of control nonlinearities such as position limits and rate limits. Future efforts will be directed towards flight testing of these algorithms.



(a) Angle of attack



(b) Sideslip angle and stability axis roll rate

Figure 49: Aircraft responses for an α -command with/without NN adaptation

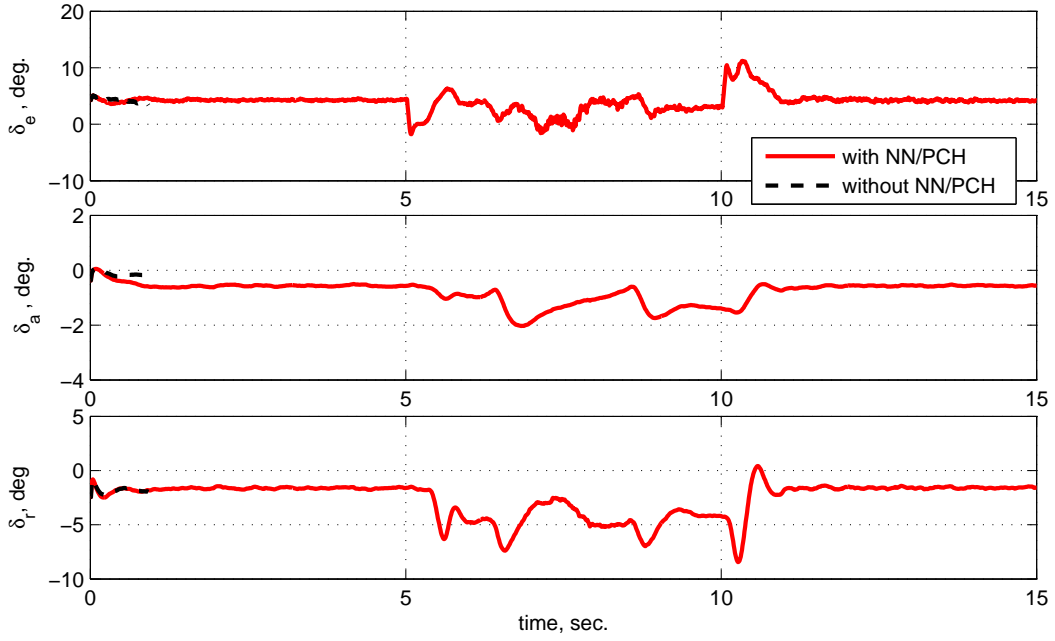


Figure 50: Aerodynamic control deflections

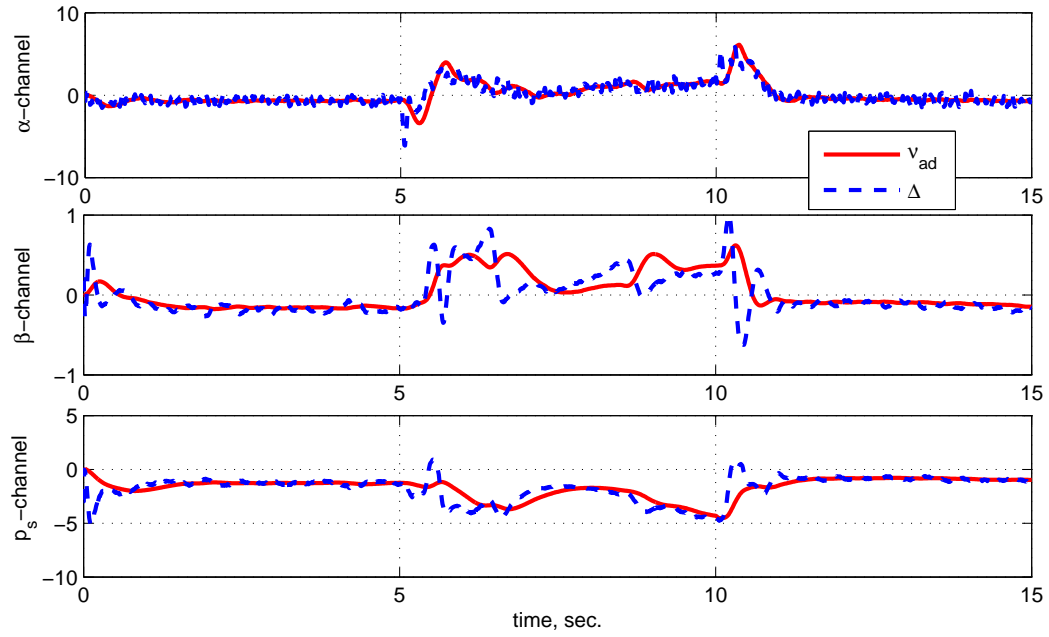
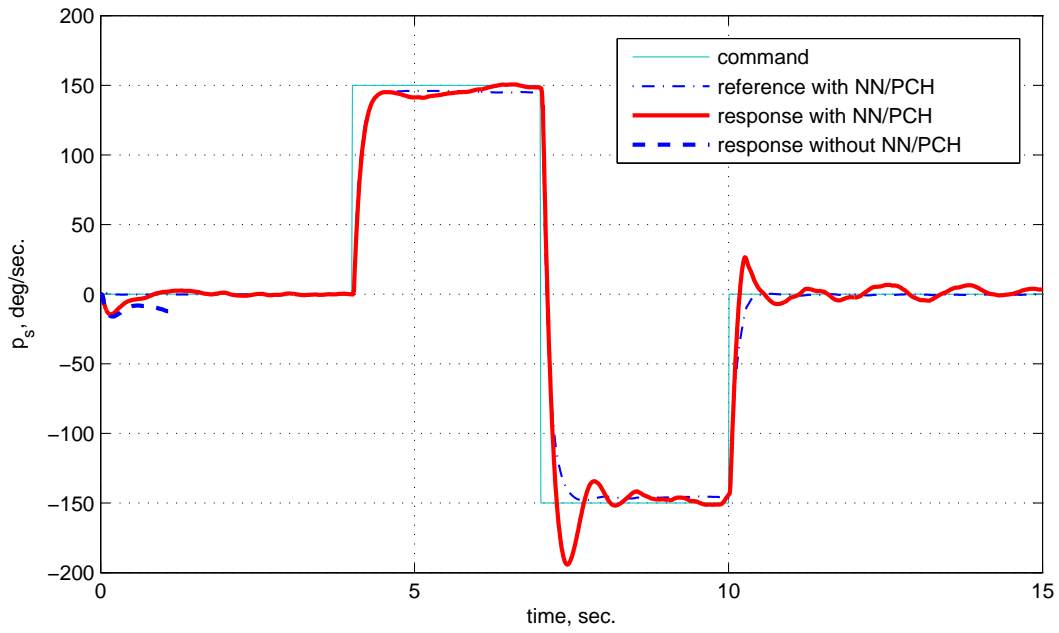
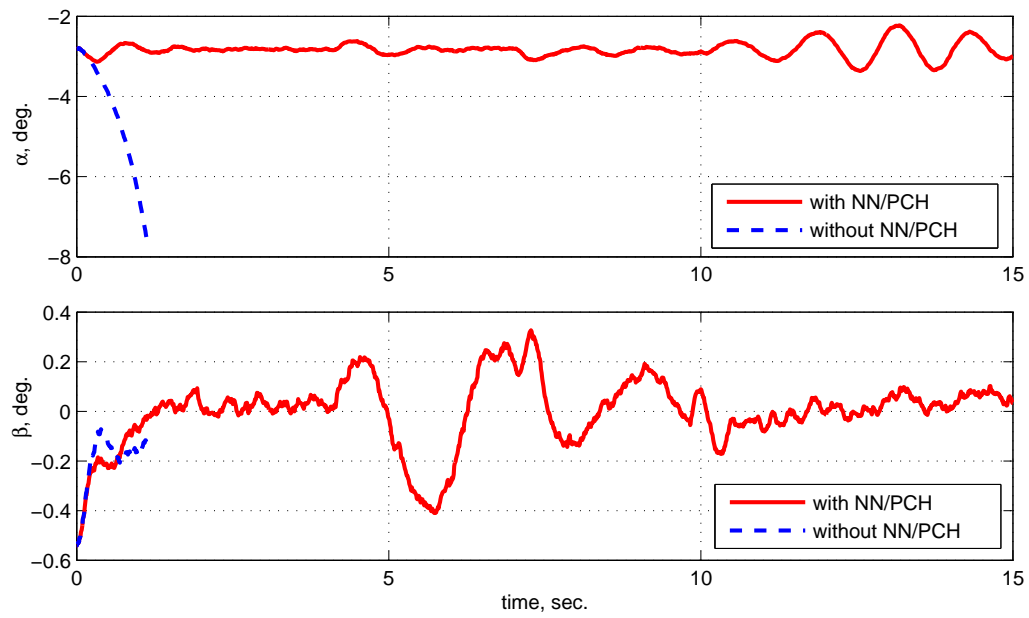


Figure 51: NN adaptation signal $\nu_{ad}(t)$ and $\Delta(t)$



(a) Stability axis roll rate



(b) Angle of attack and sideslip angle

Figure 52: Aircraft responses for a p_s -command with/without NN adaptation

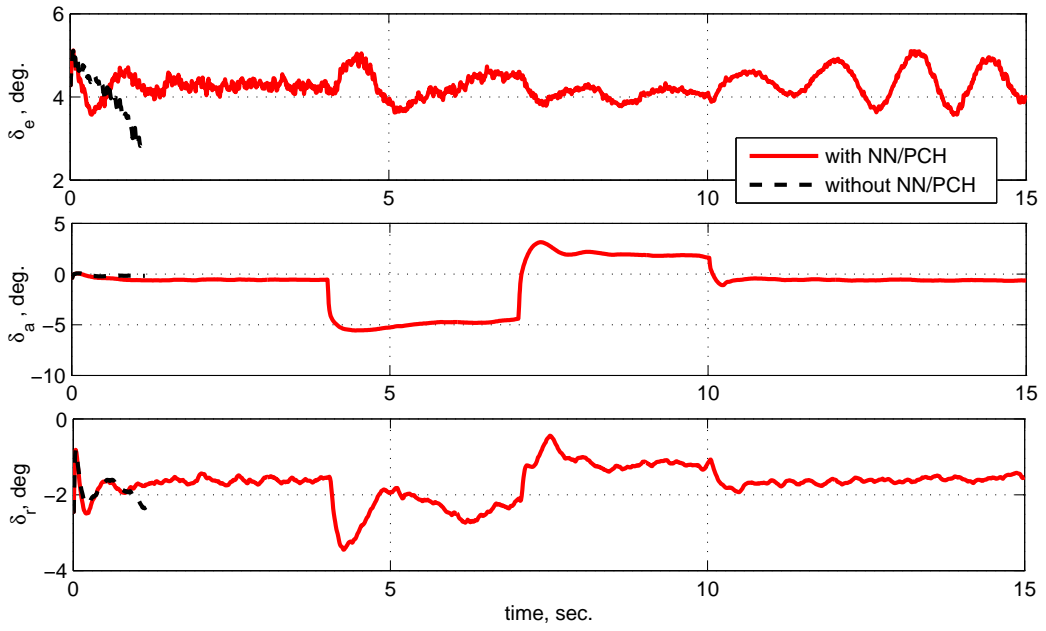


Figure 53: Aerodynamic control deflections

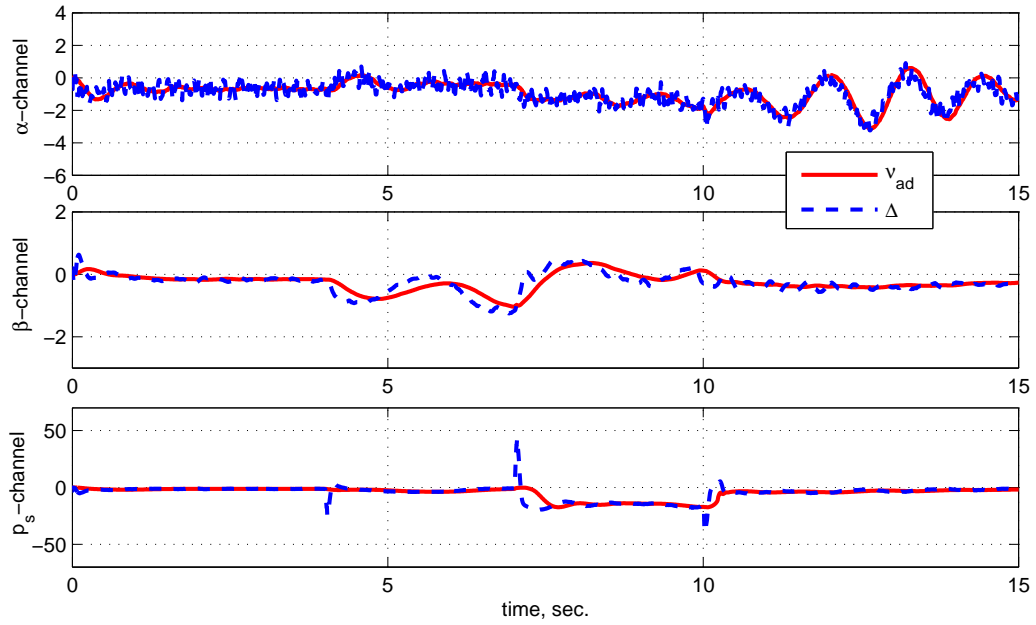
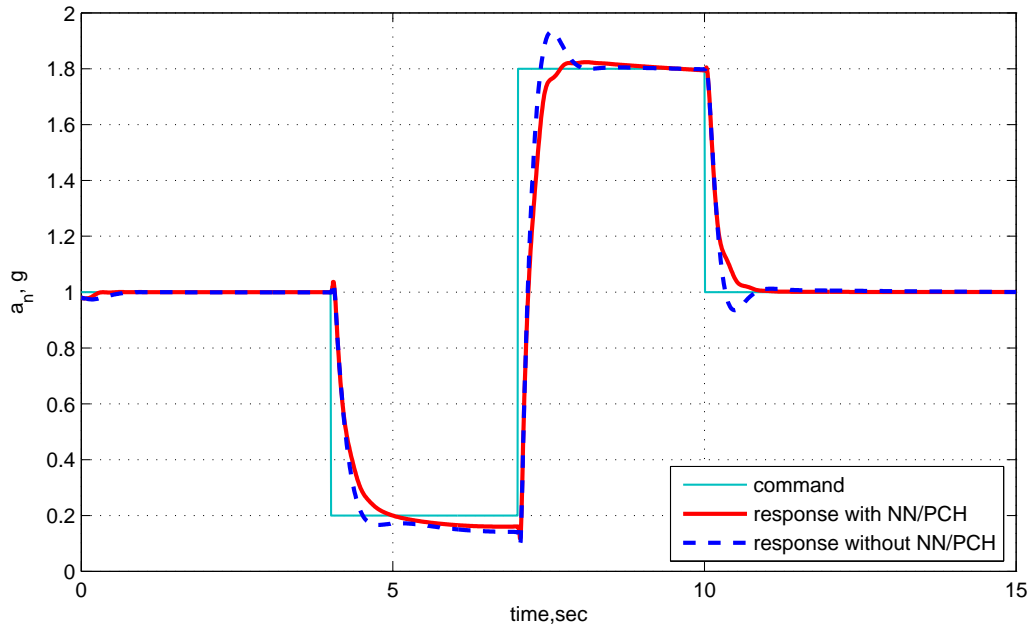
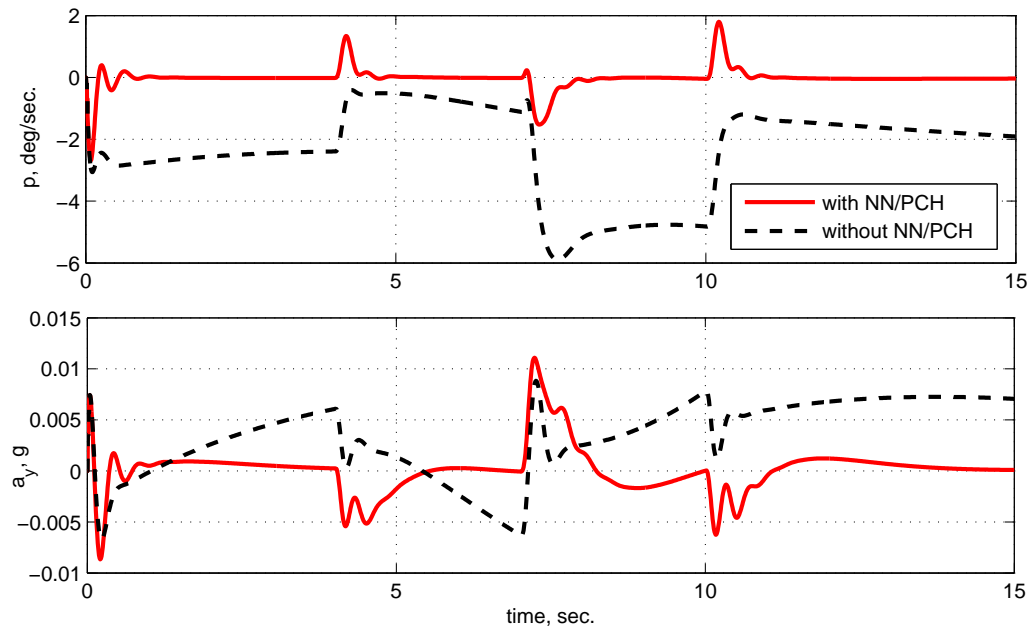


Figure 54: NN adaptation signal $\nu_{ad}(t)$ and $\Delta(t)$



(a) Normal acceleration (a_n)



(b) Roll rate (p) and lateral acceleration (a_y)

Figure 55: Aircraft responses for a normal acceleration (a_n) command using state feedback with/without NN adaptation

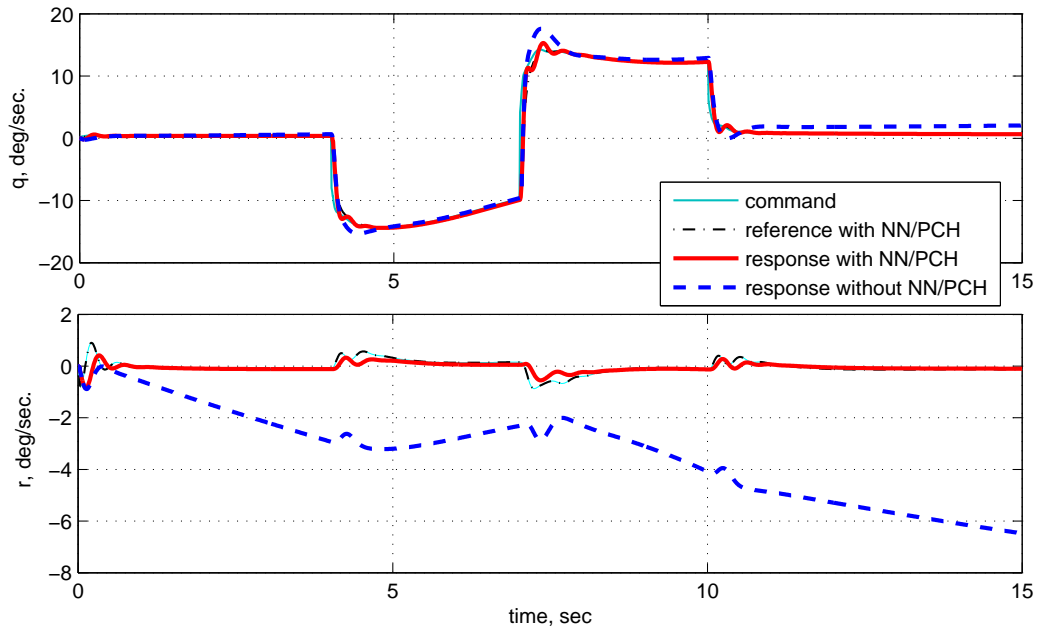


Figure 56: Pitch rate, q and yaw rate, r

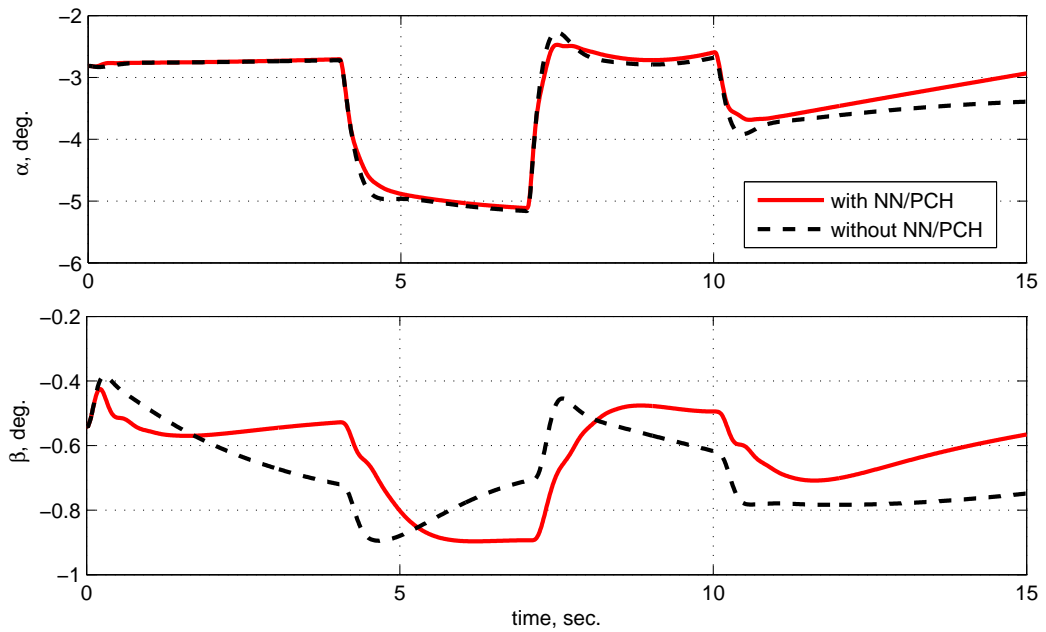


Figure 57: Angle of attack and sideslip angle

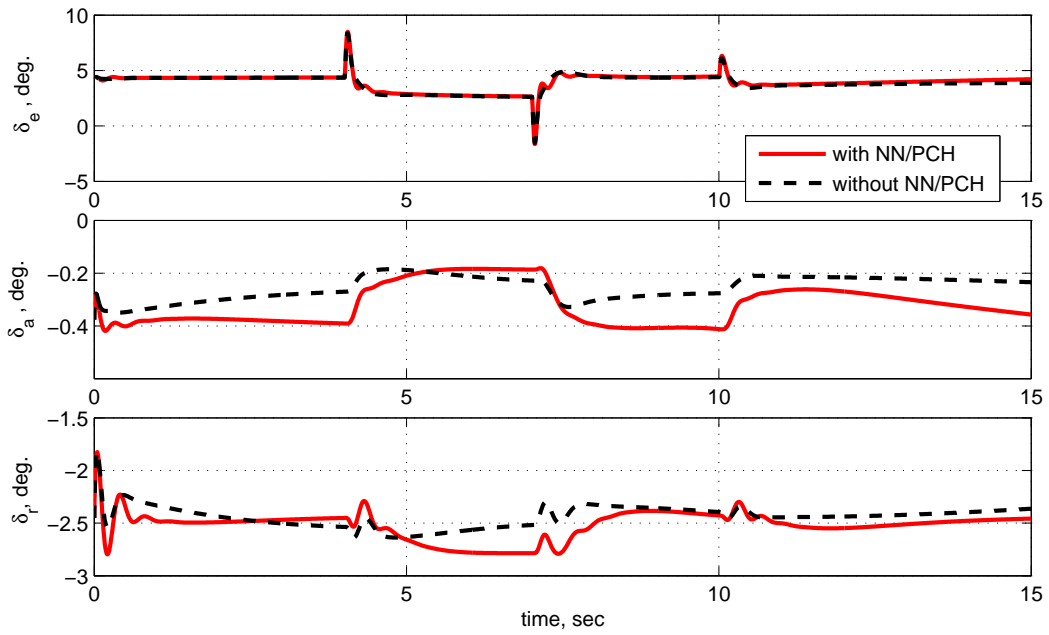


Figure 58: Aerodynamic control deflections

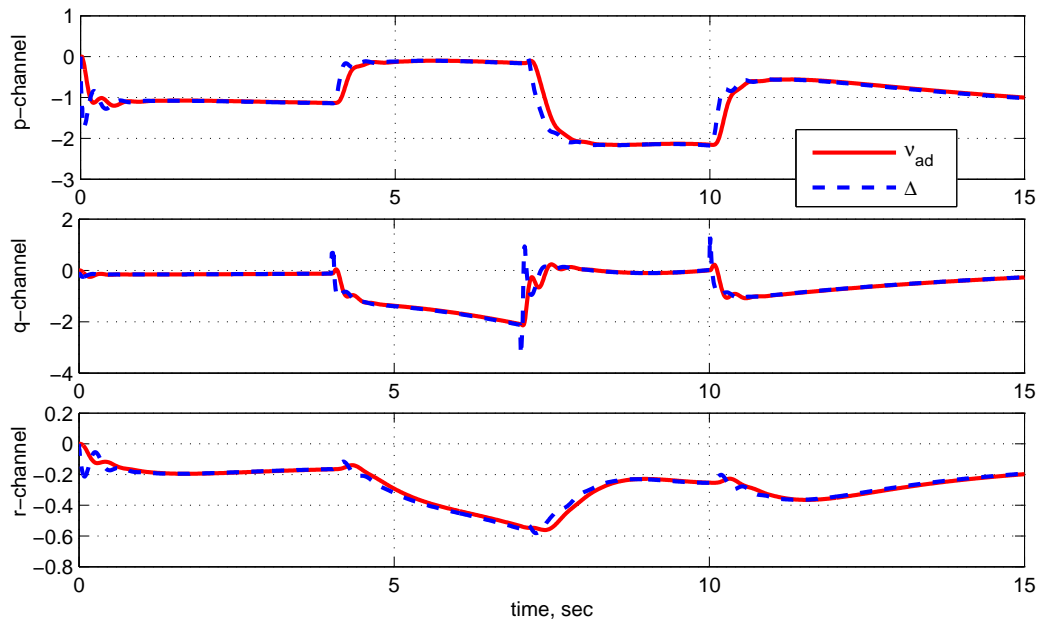
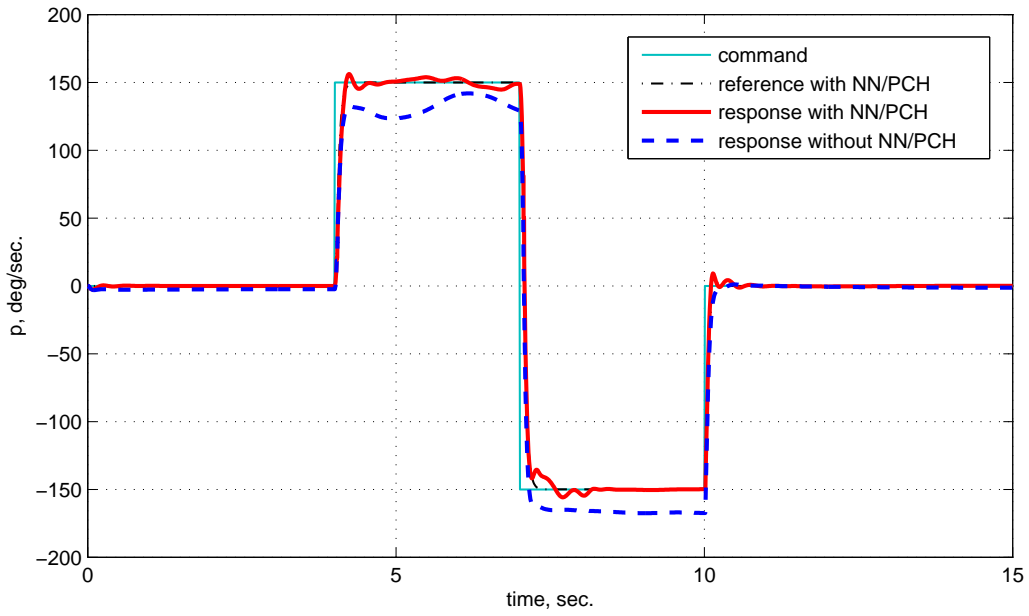
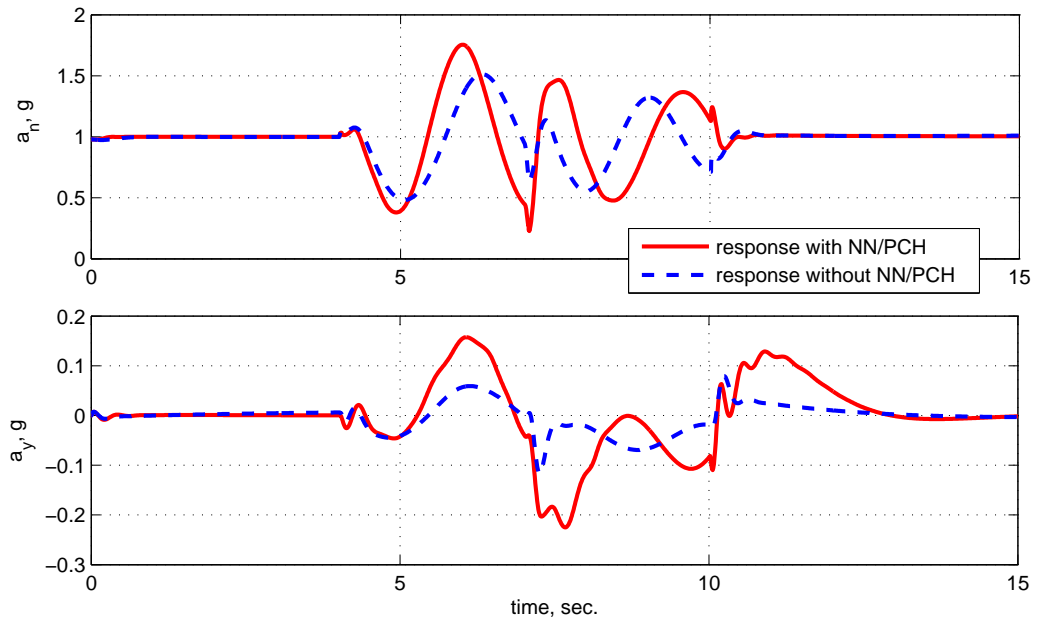


Figure 59: NN adaptation signal $\nu_{ad}(t)$ and $\Delta(t)$



(a) Roll rate (p)



(b) Normal acceleration (a_n) and lateral acceleration (a_y)

Figure 60: Aircraft responses for a roll rate (p) command using state feedback with/without NN adaptation

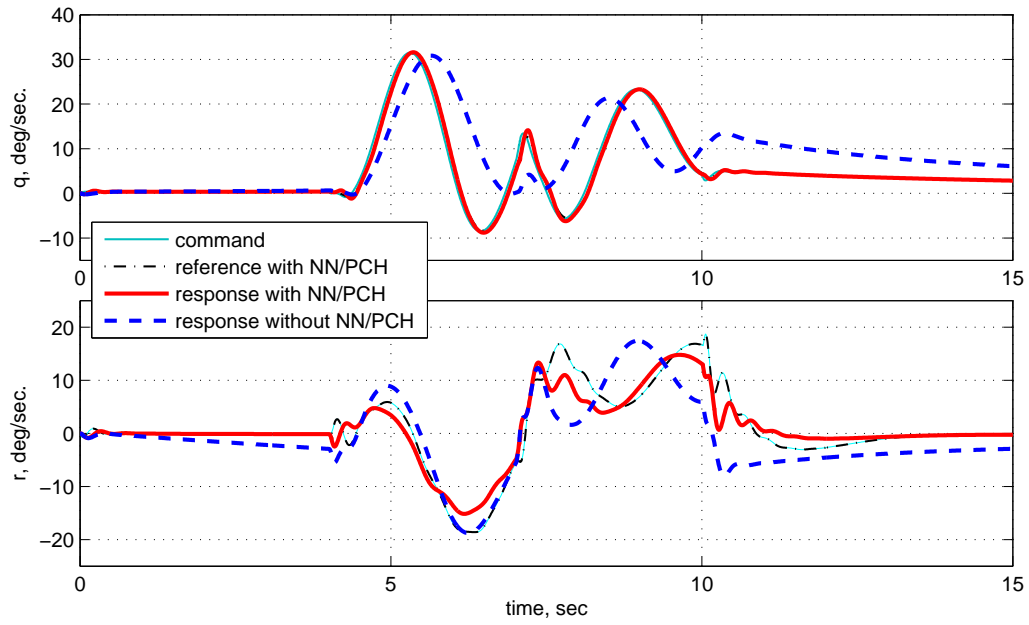


Figure 61: Pitch rate, q and yaw rate, r

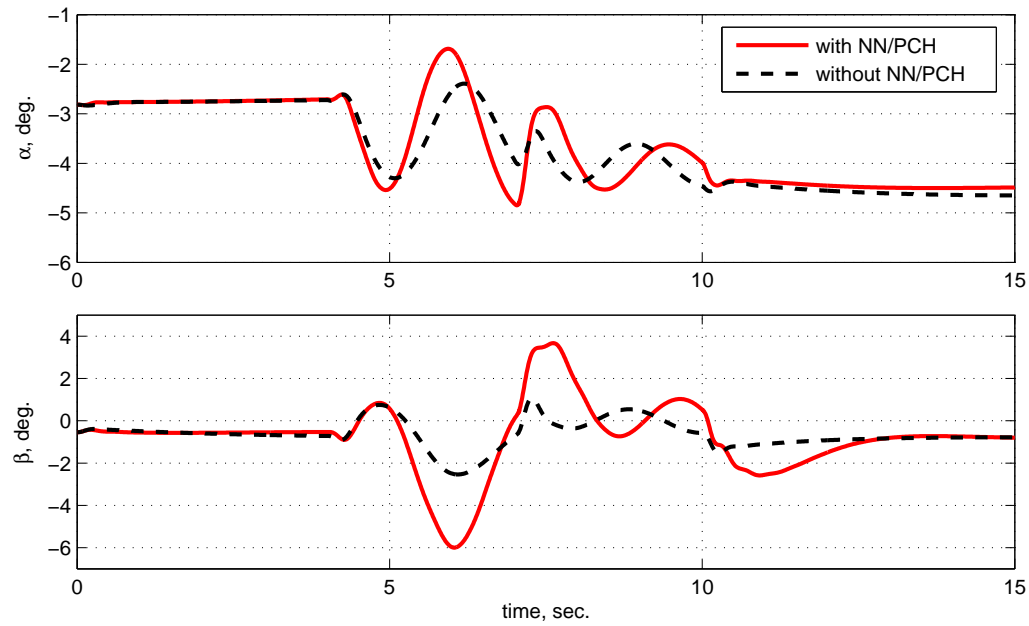


Figure 62: Angle of attack and sideslip angle

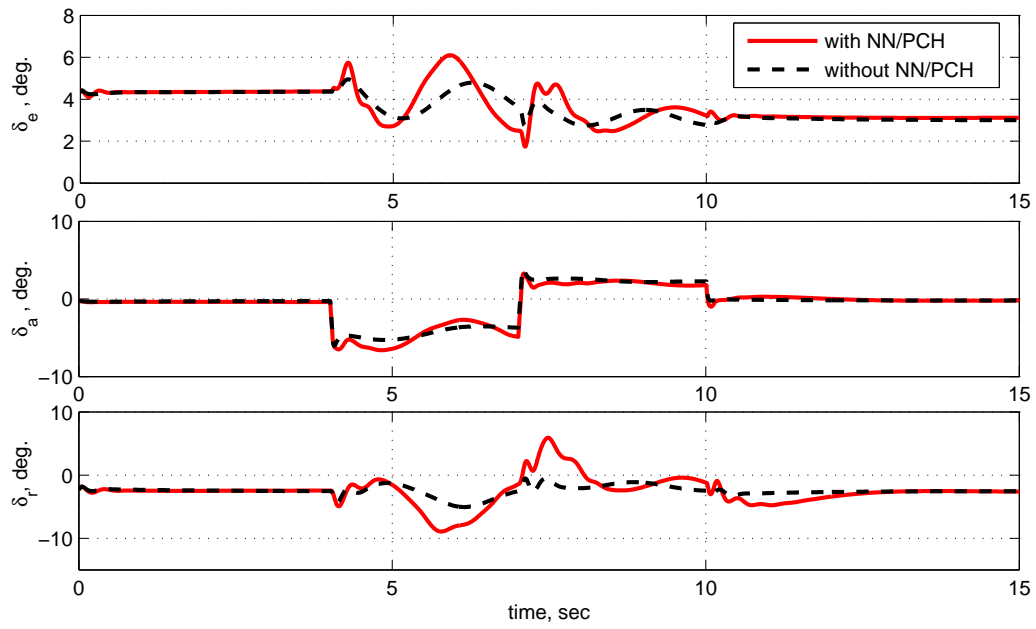


Figure 63: Aerodynamic control deflections

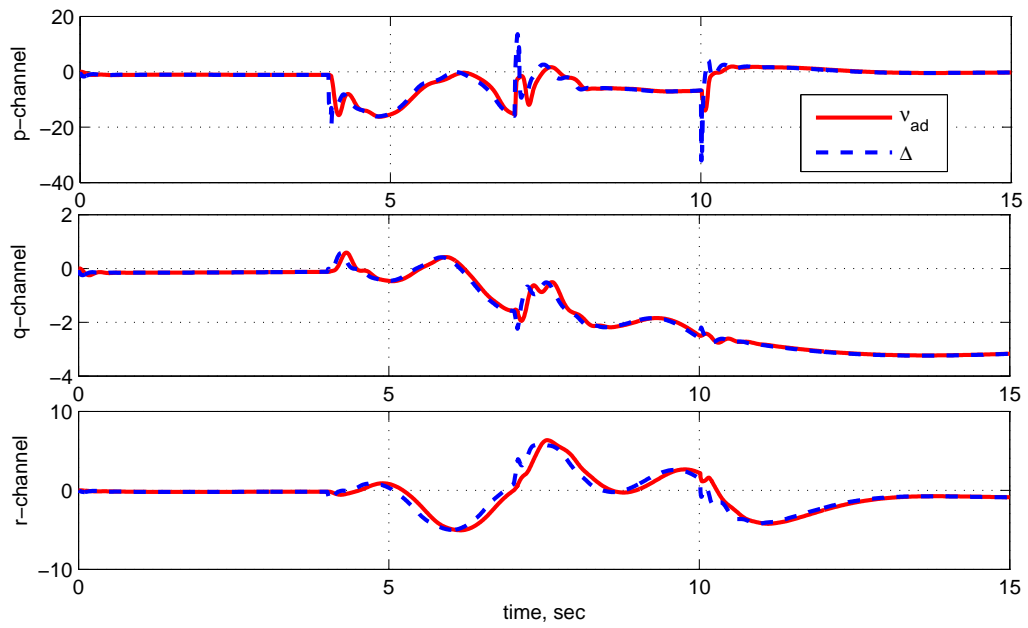
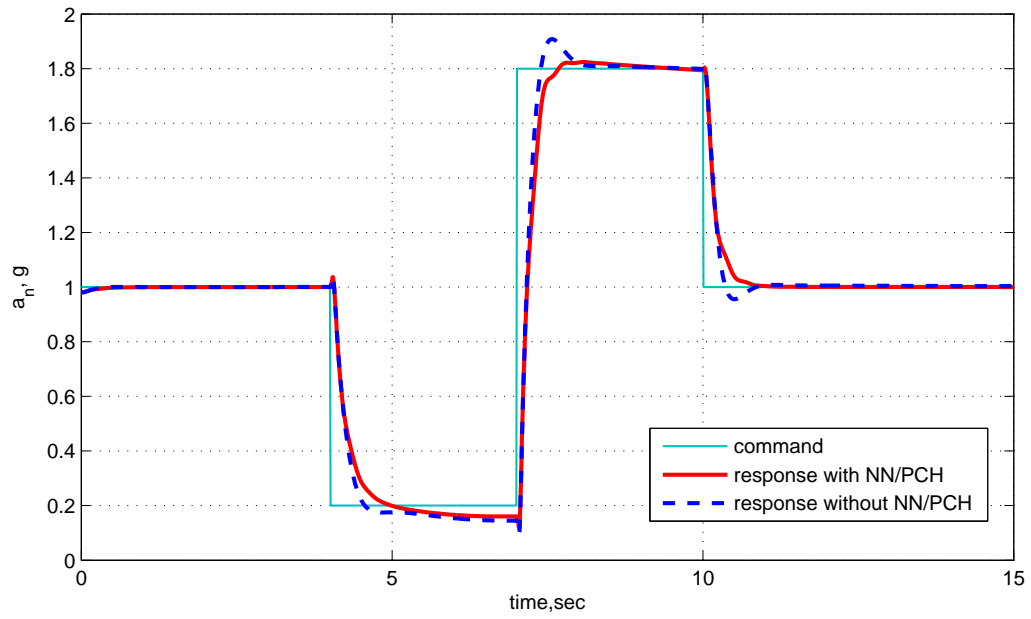
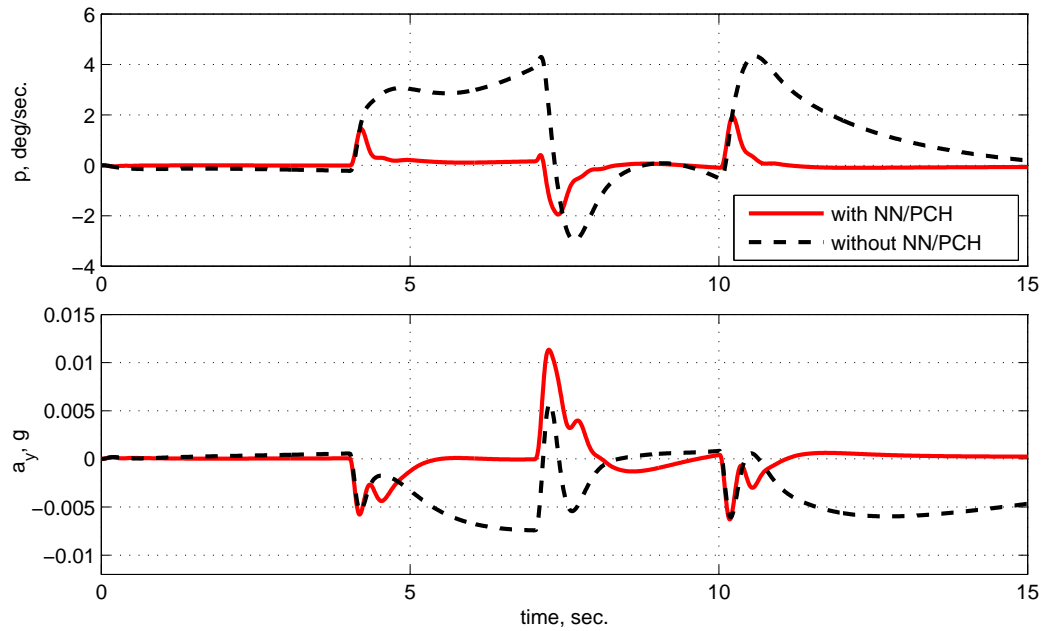


Figure 64: NN adaptation signal $\nu_{ad}(t)$ and $\Delta(t)$



(a) Normal acceleration (a_n)



(b) Roll rate (p) and lateral acceleration (a_y)

Figure 65: Aircraft responses for a normal acceleration (a_n) command using output feedback with/without NN adaptation

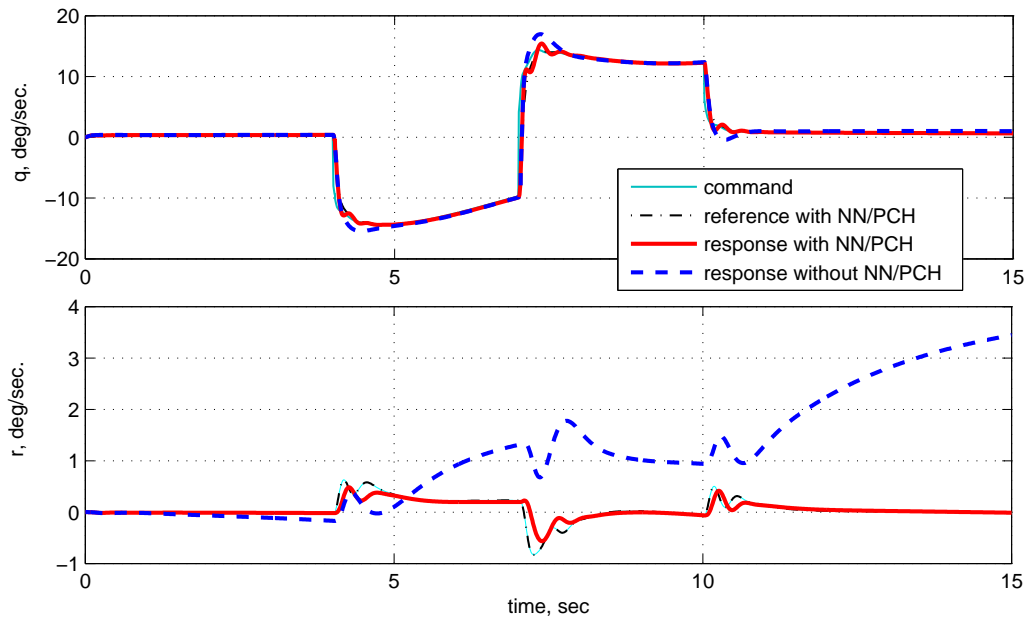


Figure 66: Pitch Rate, q and Yaw Rate, r

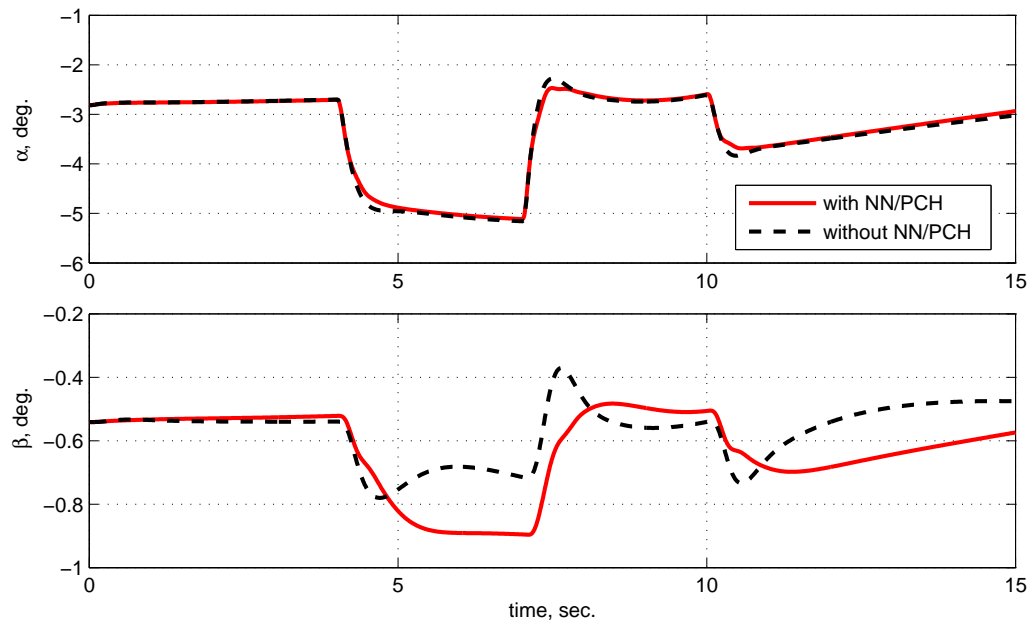


Figure 67: Angle of attack and sideslip angle

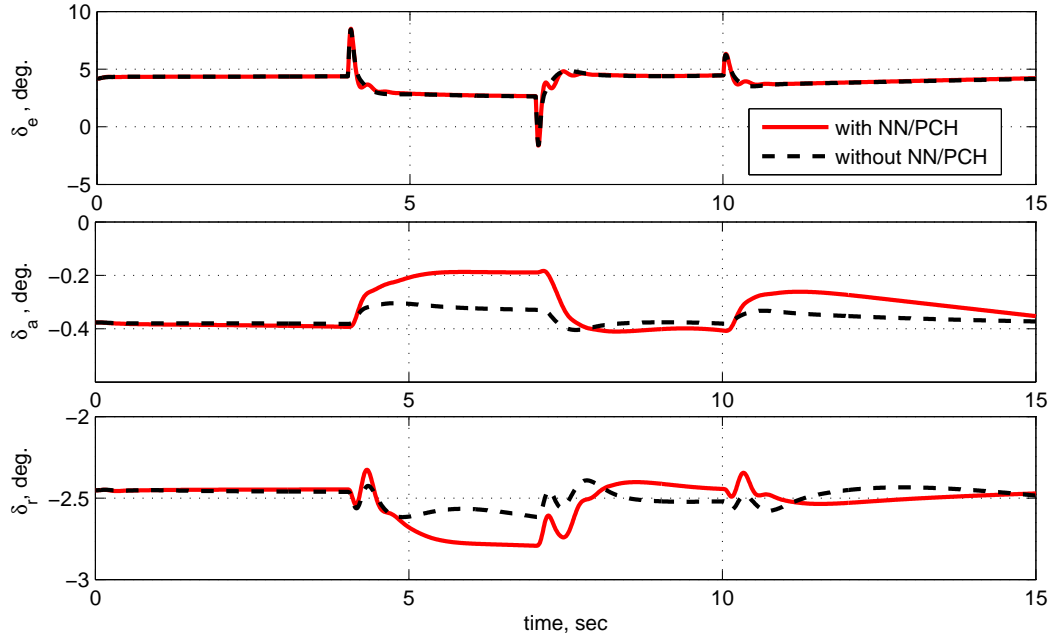


Figure 68: Aerodynamic control deflections

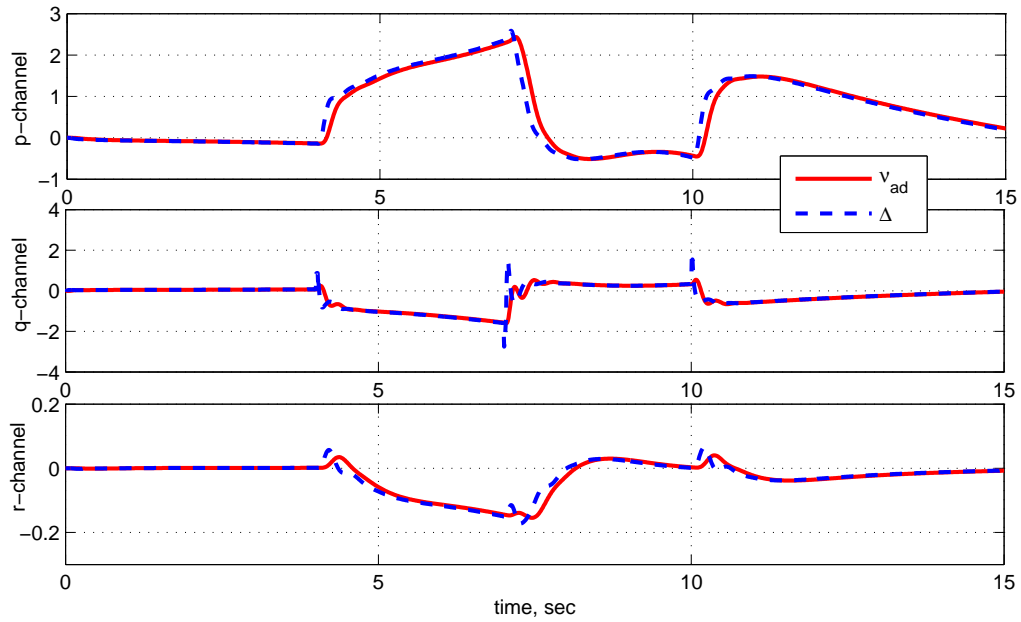
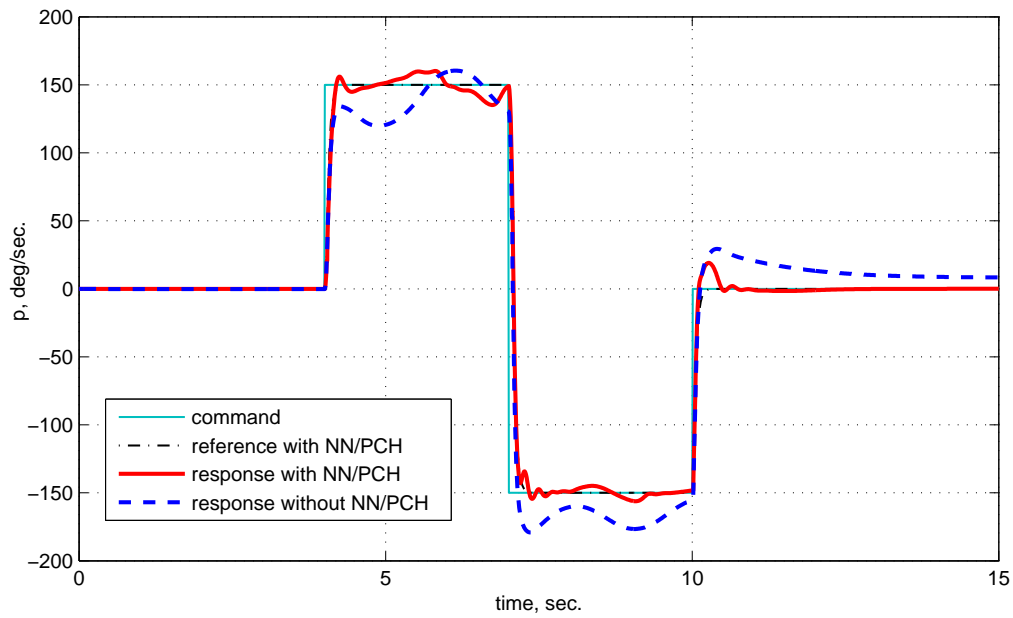
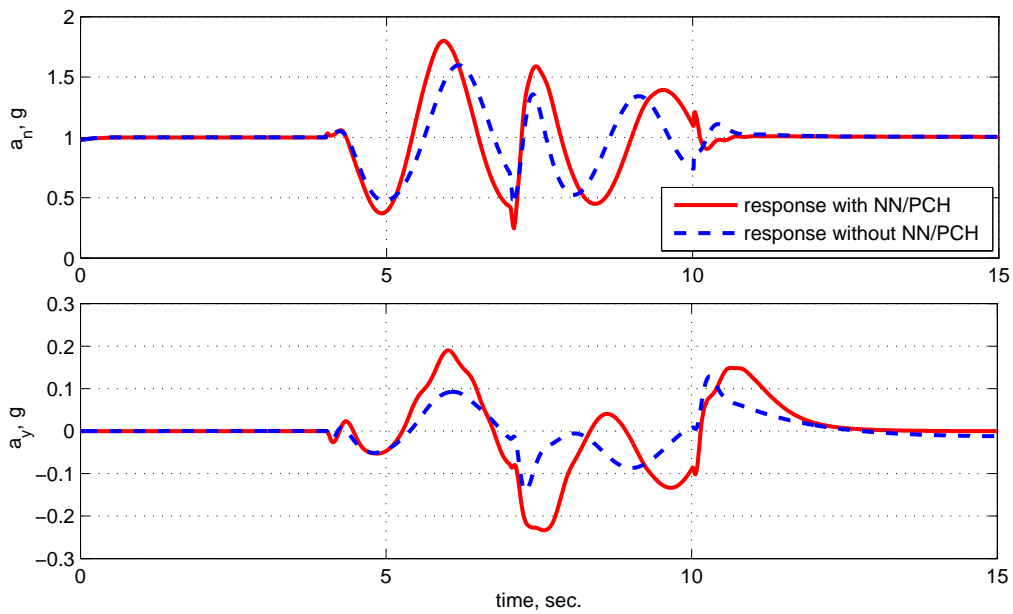


Figure 69: NN adaptation signal $\nu_{ad}(t)$ and $\Delta(t)$



(a) Roll rate (p)



(b) Normal acceleration (a_n) and lateral acceleration (a_y)

Figure 70: Aircraft responses for a roll rate (p) command using output feedback with/without NN adaptation

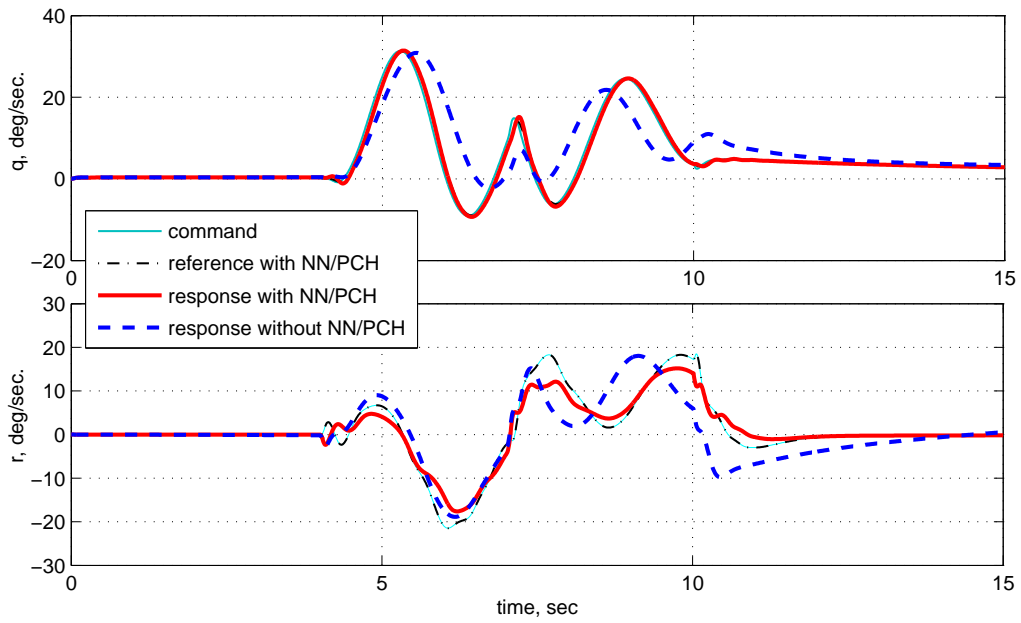


Figure 71: Pitch rate, q and yaw rate, r

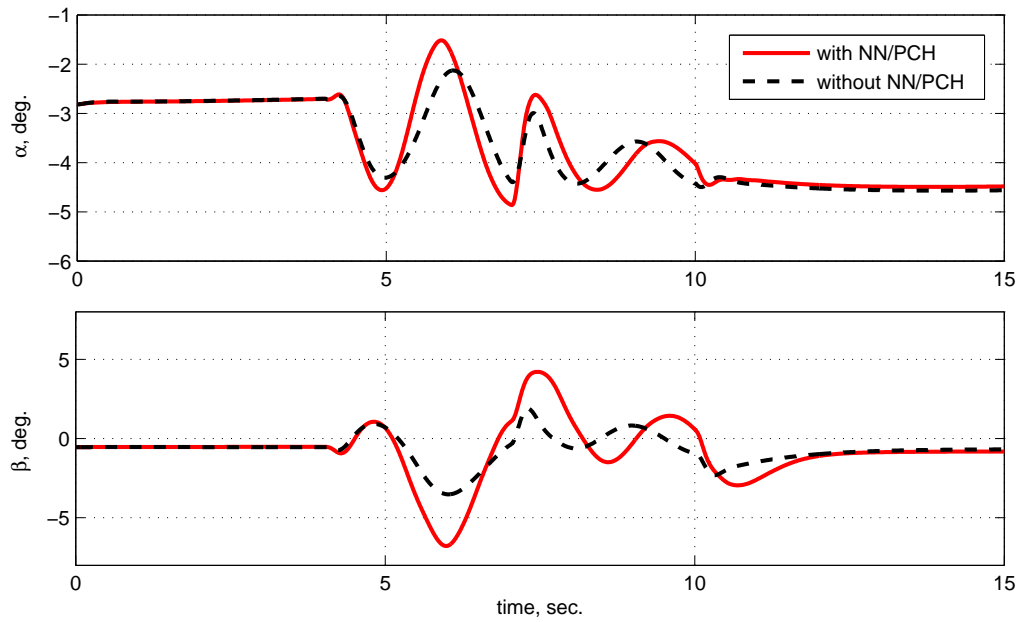


Figure 72: Angle of attack and sideslip angle

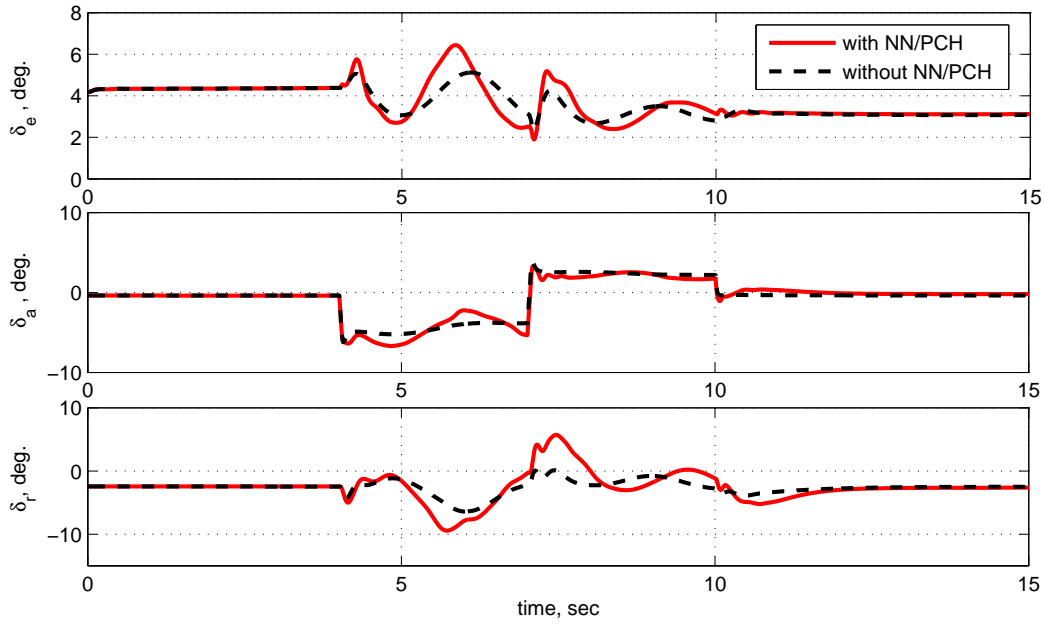


Figure 73: Aerodynamic control deflections

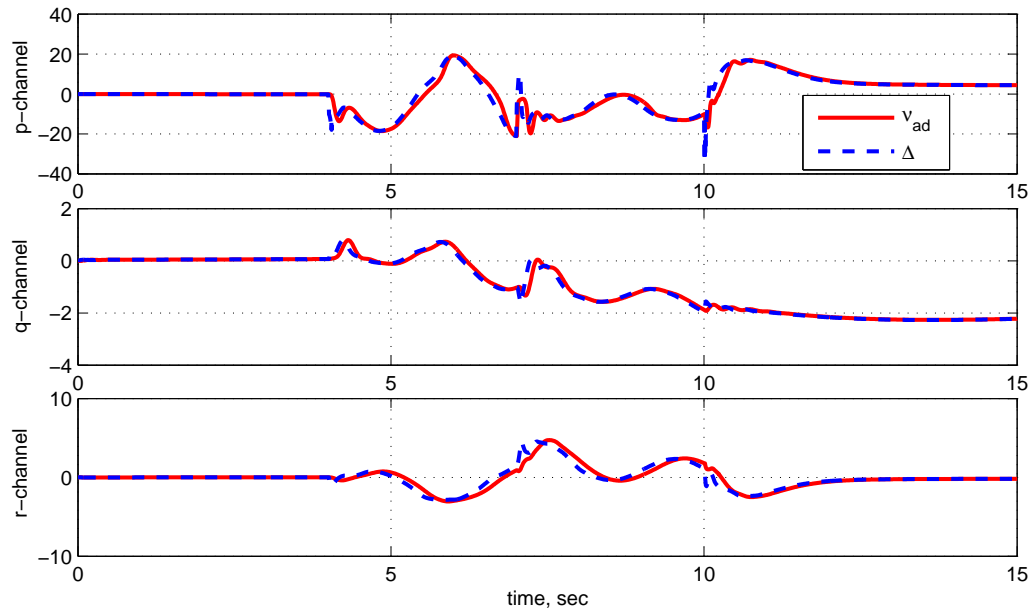


Figure 74: NN adaptation signal $\nu_{ad}(t)$ and $\Delta(t)$

CHAPTER VII

COMPOSITE MODEL REFERENCE ADAPTIVE OUTPUT FEEDBACK CONTROL OF MULTI-INPUT MULTI-OUTPUT NONLINEAR SYSTEMS USING NEURAL NETWORKS

7.1 Introduction

Composite model reference adaptive control (MRAC) was introduced by Slotine and Li [107], and they claim that the advantages of the composite MRAC are:

- The combined use of the tracking error \mathbf{E} and the estimation (or prediction) error $\hat{\mathbf{E}}$ can improve the performance of an adaptive controller, by employing them as training signals in the adaptation laws.
- When multiple unknown parameters are involved, the composite MRAC scheme is more effective than the standard tracking error-based adaptation. In such cases, the former allows high adaptation gain to be used without incurring significant oscillation in the estimated parameters, which is possibly observed for the latter.
- When unmodeled dynamics are present, composite adaptive controllers perform better than standard adaptive controllers. This permits using higher adaptation gain to achieve smaller tracking errors and faster parameter convergence without exciting high-frequency unmodeled dynamics.
- One of the essential benefits of the composite MRAC comes from the smoothness of the results, which has significant implications on the adaptive performance. This comes

from the structure of the adaptation laws, which has a time-varying low-pass filter-like property.

- For parameter oscillation or parameter drift problems mainly associated with non-parametric uncertainties (noise and disturbance), the composite MRAC can be quite helpful.

These claims on the expected properties of the composite MRAC design motivate this research as an extension of the adaptive NDI control design, presented and thoroughly discussed in Chapter 3. In addition, a conventional adaptive control design that augments a dynamic compensator [34, 114] is introduced as an alternative in adaptive control design.

Section 7.2 formulates the control problems of nonlinear control systems, and Section 7.3 introduces feedback linearization of nonlinear MIMO system and nonlinear dynamic inversion. Control system architecture, design processes and stability proofs using Lyapunov theorems are described in Section 7.7. Section 7.8 presents simulation results using F-15 ACTIVE model to demonstrate the performance of the composite MRAC design.

7.2 Control Problem Formulation

We consider n^{th} order nonlinear MIMO dynamic systems that are modeled by:

$$\begin{aligned}\dot{\mathbf{x}} &= \mathbf{f}(\mathbf{x}, u) \\ \mathbf{y} &= \mathbf{g}(\mathbf{x})\end{aligned}\tag{7.2.1}$$

where $\mathbf{x} \in \mathcal{D}_x \subset \mathfrak{R}^n$ is the state vector, $\mathbf{u} \in \mathcal{D}_u \subset \mathfrak{R}^m$ is the system control vector, and $\mathbf{y} \in \mathcal{D}_y \subset \mathfrak{R}^m$ is the system output vector. It is assumed that the system (7.2.1) is stabilizable and observable, and that $\mathbf{f}(\cdot, \cdot)$ and $\mathbf{g}(\cdot)$ are sufficiently smooth, possibly partially known functions.

Assumption 7.2.1. *The dynamical system in (7.2.1) satisfies the conditions for output feedback linearization for the following class of nonlinear uncertain systems with well-defined vector relative degree r .*

This assumption implies that the functions $\mathbf{f} : \mathcal{D}_x \times \mathfrak{R} \rightarrow \mathfrak{R}^n$ and $\mathbf{g} : \mathcal{D}_x \rightarrow \mathfrak{R}^m$ are input-output feedback linearizable, and the output \mathbf{y} has relative degree r for all $(\mathbf{x}, \mathbf{u}) \in \mathcal{D}_x \times \mathcal{D}_u$ such that [30, 35, 43]:

$$\begin{aligned}
\dot{\boldsymbol{\chi}} &= \mathbf{f}_o(\boldsymbol{\chi}, \boldsymbol{\xi}) \\
\dot{\xi}_i^1 &= \xi_{i+1}^2 \\
&\vdots \\
\dot{\xi}_i^{r_i-1} &= \xi_i^{r_i} \\
\dot{\xi}_i^{r_i} &= h_i(\boldsymbol{\xi}, \boldsymbol{\chi}, u_i) \\
y_i &= \xi_i^1, \quad i = 1, \dots, m
\end{aligned} \tag{7.2.2}$$

where $\boldsymbol{\xi} \triangleq [\xi_1^1 \ \xi_1^2 \ \dots \ \xi_1^{r_1} \ \dots \ \xi_m^1 \ \xi_m^2 \ \dots \ \xi_m^{r_m}]^T \in \mathcal{D}_\xi \subset \mathfrak{R}^r$, $h_i(\boldsymbol{\xi}, \boldsymbol{\chi}, u_i) \triangleq L_{\mathbf{f}}^{(r_i)} \mathbf{g}|_{u_i}$, $i = 1, \dots, m$ being the Lie derivatives, $\boldsymbol{\chi} \in \mathcal{D}_\chi \subset \mathfrak{R}^{n-r}$ are the state vector associated with the internal dynamics $\dot{\boldsymbol{\chi}} = \mathbf{f}_o(\boldsymbol{\chi}, \boldsymbol{\xi})$, $\mathcal{D}_\chi, \mathcal{D}_\xi$ are open sets containing their respective origins, r_i is the relative degree of the i^{th} output, and the overall relative degree $r \triangleq r_1 + r_2 + \dots + r_m \leq n$. The function $\mathbf{f}_o(\boldsymbol{\xi}, \boldsymbol{\chi})$ and $h_i(\boldsymbol{\xi}, \boldsymbol{\chi}, u_i)$ are partially known continuous functions. It is noted that control $\mathbf{u} \triangleq [u_1 \ u_2 \ \dots \ u_m]^T$, and output, or controlled variables $\mathbf{y} \triangleq [y_1 \ y_2 \ \dots \ y_m]^T \in \mathcal{D}_y$, where an open set \mathcal{D}_y is defined by continuous mapping $\mathbf{h}(\mathbf{x}, \mathbf{u}) \triangleq [h_1(\mathbf{x}, u_1) \ \dots \ h_m(\mathbf{x}, u_m)]^T$ with an assumption described below.

Assumption 7.2.2. $\partial h_i(\mathbf{x}, u_i) / \partial u_i$ is continuous and non-zero for every $(\mathbf{x}, u_i) \in \mathcal{D}_x \times \mathfrak{R}$.

Introducing $\mathbf{y}_c \triangleq [y_{c1} \ y_{c2} \ \dots \ y_{cm}]^T$ and $\boldsymbol{\xi}_c \triangleq [y_{c1} \ \dot{y}_{c1} \ \dots \ y_{c1}^{(r_1-1)} \ \dots \ y_{cm} \ \dot{y}_{cm} \ \dots \ y_{cm}^{(r_m-1)}]^T$, where the derivatives are generated via asymptotically stable reference model dynamics, we let $\tilde{\mathbf{y}}(t) \triangleq \mathbf{y}_c(t) - \mathbf{y}(t)$, $\tilde{\boldsymbol{\xi}}(t) \triangleq \boldsymbol{\xi}_c(t) - \boldsymbol{\xi}(t)$. In order to address the stability of the internal dynamics, we introduce the following assumption [30, 43].

Assumption 7.2.3. The system $\dot{\boldsymbol{\chi}} = \mathbf{f}_o(\boldsymbol{\chi}, \boldsymbol{\xi})$ has a unique steady-state solution $\boldsymbol{\chi}_s(t)$.

Moreover, with $\tilde{\boldsymbol{\chi}}(t) \triangleq \boldsymbol{\chi}_s(t) - \boldsymbol{\chi}(t)$, the system

$$\begin{aligned}\dot{\tilde{\boldsymbol{\chi}}} &= \mathbf{f}_o(\boldsymbol{\chi}_s, \boldsymbol{\xi}_c) - \mathbf{f}_o(\boldsymbol{\chi}, \boldsymbol{\xi}) \\ &= \mathbf{f}_o(\boldsymbol{\chi}_s, \boldsymbol{\xi}_c) - \mathbf{f}_o(\boldsymbol{\chi}_s - \tilde{\boldsymbol{\chi}}, \boldsymbol{\xi}_c - \tilde{\boldsymbol{\xi}}) \\ &= \tilde{\mathbf{f}}_o(\boldsymbol{\chi}_s, \tilde{\boldsymbol{\chi}}, \boldsymbol{\xi}_c, \tilde{\boldsymbol{\xi}})\end{aligned}\tag{7.2.3}$$

has a continuously differentiable function $V_{\tilde{\boldsymbol{\chi}}}(\tilde{\boldsymbol{\chi}}, t)$ satisfying the following conditions

$$\begin{aligned}c_1\|\tilde{\boldsymbol{\chi}}\|^2 &\leq V_{\tilde{\boldsymbol{\chi}}}(\tilde{\boldsymbol{\chi}}, t) \leq c_2\|\tilde{\boldsymbol{\chi}}\|^2 \\ \dot{V}_{\tilde{\boldsymbol{\chi}}} &\leq -c_3\|\tilde{\boldsymbol{\chi}}\|^2 + c_4\|\tilde{\boldsymbol{\chi}}\|\|\tilde{\boldsymbol{\xi}}\|\end{aligned}\tag{7.2.4}$$

It can be seen from Assumption 7.2.3 that the dynamics (7.2.3) with $\tilde{\boldsymbol{\xi}}$ as input are input-to-state stable. The inequalities (7.2.4) imply that the convergence to the steady state solution $\boldsymbol{\chi}_s$ is exponential. Consequently the zero dynamics in (7.2.2) are exponentially stable with the following upper bound

$$\dot{V}_{\tilde{\boldsymbol{\chi}}} \leq -c_3\|\tilde{\boldsymbol{\chi}}\|^2 + c_4\|\tilde{\boldsymbol{\chi}}\|\|\tilde{\boldsymbol{\xi}}\| \leq -\frac{c_3}{2}\|\tilde{\boldsymbol{\chi}}\|^2 + \frac{c_4^2}{2c_3}\|\tilde{\boldsymbol{\xi}}\|\tag{7.2.5}$$

The objective is to synthesize an output feedback control law that utilizes the available measurements $\mathbf{y}(t)$, so that $y_i(t)$ track bounded smooth reference trajectories $y_{c_i}(t)$, $i = 1, \dots, m$ with bounded errors.

7.3 *Input-Output Feedback Linearization and Nonlinear Dynamic Inversion*

A linearizing feedback control law is approximated by introducing the following signal:

$$u_i = \hat{h}_i^{-1}(\mathbf{y}, \nu_i), \quad i = 1, \dots, m\tag{7.3.1}$$

where ν_i , commonly referred to as pseudo-control, is defined as

$$\nu_i = \hat{\mathbf{h}}(\mathbf{y}, u_i), \quad i = 1, \dots, m\tag{7.3.2}$$

The function $\hat{\mathbf{h}}(\mathbf{y}, \mathbf{u}) = [\hat{h}_1(\mathbf{x}, u_1) \cdots \hat{h}_m(\mathbf{x}, u_m)]^T$ can be determined by using a possibly simplified model of the system dynamics. It is assumed that $\hat{h}_i(\mathbf{x}, u_i)$, an approximation

of $h_i(\boldsymbol{\xi}, \boldsymbol{\chi}, u_i)$, is invertible with respect to its second argument and satisfies the following assumption:

Assumption 7.3.1. $\partial h_i(\mathbf{y}, u_i)/\partial u_i$ is continuous and non-zero for every $(\mathbf{y}, u_i) \in \mathcal{D}_y \times \mathfrak{R}$, and

$$\frac{\partial \hat{h}_i(\mathbf{y}, u_i)}{\partial u_i} \frac{\partial h_i(\mathbf{x}, u_i)}{\partial u_i} > 0, \quad i = 1, \dots, m \quad (7.3.3)$$

for every $(\mathbf{x}, \mathbf{y}, u_i) \in \mathcal{D}_x \times \mathcal{D}_y \times \mathfrak{R}$.

Defining $\boldsymbol{\nu} = [\nu_1 \ \dots \ \nu_m]^T$, we rewrite (7.3.2) in a compact form as

$$\boldsymbol{\nu} = \hat{\mathbf{h}}(\mathbf{y}, \mathbf{u}) \quad (7.3.4)$$

With this definition of pseudo-control (7.3.4), the output dynamics can be expressed as

$$\mathbf{y}^{(r)} = \boldsymbol{\nu} + \boldsymbol{\Delta} \quad (7.3.5)$$

where $\mathbf{y}^{(r)} = [y_1^{(r_1)} \ \dots \ y_m^{(r_m)}]^T$ and

$$\begin{aligned} \boldsymbol{\Delta}(\mathbf{x}, \mathbf{u}) &= \boldsymbol{\Delta}(\boldsymbol{\xi}, \boldsymbol{\chi}, \mathbf{u}) \\ &= \mathbf{h}(\boldsymbol{\xi}, \boldsymbol{\chi}, \hat{\mathbf{h}}^{-1}(\mathbf{y}, \boldsymbol{\nu})) - \hat{\mathbf{h}}(\mathbf{y}, \hat{\mathbf{h}}^{-1}(\mathbf{y}, \boldsymbol{\nu})) \end{aligned} \quad (7.3.6)$$

which is the difference between the function $\mathbf{h}(\mathbf{x}, \mathbf{u})$ and its approximation $\hat{\mathbf{h}}(\mathbf{y}, \mathbf{u})$, and it is usually referred to as modeling error.

The pseudo-control is chosen to have the form

$$\boldsymbol{\nu} = \boldsymbol{\nu}_{dc} + \boldsymbol{\nu}_{rm} - \boldsymbol{\nu}_{ad} \quad (7.3.7)$$

where $\boldsymbol{\nu}_{dc}$ is the output of a linear dynamic compensator, $\boldsymbol{\nu}_{rm} = \mathbf{y}_c^{(r)} = [y_c^{(r_1)} \ \dots \ y_c^{(r_m)}]^T$ is a vector of the r_i^{th} derivative of the command signal $y_{c_i}(t)$, and $\boldsymbol{\nu}_{ad}$ is the adaptive control signal designed to cancel $\boldsymbol{\Delta}(\mathbf{x}, \mathbf{u})$.

Using (7.3.7), the output dynamics in (7.3.5) become

$$\mathbf{y}^{(r)} = \boldsymbol{\nu}_{dc} + \boldsymbol{\nu}_{rm} - \boldsymbol{\nu}_{ad} + \boldsymbol{\Delta} \quad (7.3.8)$$

It can be seen from (7.3.6) that Δ depends on ν_{ad} through ν , whereas ν_{ad} has to be designed to cancel Δ . Throughout the process in Section 3.2, $\nu - \Delta(\mathbf{x}, \mathbf{u})$ can be written in the matrix form as

$$\nu_{ad} - \Delta(\mathbf{x}, \mathbf{u}) = H [\nu_{ad} - \bar{\Delta}(\mathbf{x}, \nu_l)] \quad (7.3.9)$$

where

$$H = \begin{bmatrix} h_{\bar{\nu}_1} & 0 & \cdots & 0 & 0 \\ 0 & h_{\bar{\nu}_2} & \cdots & 0 & 0 \\ \vdots & \vdots & \ddots & \vdots & \vdots \\ 0 & 0 & \cdots & h_{\bar{\nu}_{m-1}} & 0 \\ 0 & 0 & \cdots & 0 & h_{\bar{\nu}_m} \end{bmatrix} \in \mathfrak{R}^{m \times m} \quad (7.3.10)$$

It is noted that this matrix H is positive because its diagonal components are all positive by Assumption 7.2.2 and 7.3.1. Now using (7.3.9) the dynamics in (7.3.8) can be rewritten as

$$\tilde{\mathbf{y}}^{(r)} = -\nu_{dc} + H [\nu_{ad} - \bar{\Delta}(\mathbf{x}, \nu_l)] \quad (7.3.11)$$

The main difference between the dynamics in (7.3.8) and (7.3.11) lies in the functional structure of the modeling error. In (7.3.11) the modeling error is independent of the actual control variable.

It is noted that either of the cases when ν_{ad} ideally cancels out non-zero $\bar{\Delta}$ in (7.3.11), or when $\bar{\Delta} = 0$ (thus the adaptive term ν_{ad} is not required), results in the integrator-decoupled form of the error dynamics of (7.3.11) as

$$\tilde{\mathbf{y}}^{(r)} = -\nu_{dc} \quad (7.3.12)$$

This means that in such a case the resultant control problem becomes a control design for a system having r -poles at the origin. Usually the dynamic controller for ν_{dc} is designed to achieve an asymptotically stable closed-loop system of (7.3.12) and its own dynamics are also asymptotically stable.

7.4 Nonlinear System and its Reference Model

In order to design an adaptive control architecture for a nonlinear dynamic system, we also consider the external disturbance as well as modeling error. Considering (7.2.2), (7.3.1) and (7.3.2), we write the system dynamics (7.3.5) in the matrix form:

$$\dot{\mathbf{y}}(t) = A\mathbf{y}(t) + B[\boldsymbol{\nu}(t) + \boldsymbol{\Delta}(\mathbf{x}, \mathbf{u}) + \mathbf{d}(t)] \quad (7.4.1)$$

where

$$\begin{aligned} \mathbf{y} &\triangleq [\mathbf{y}_1^T \ \mathbf{y}_2^T \ \cdots \ \mathbf{y}_m^T]^T \in \mathfrak{R}^r \\ \mathbf{y}_i &\triangleq [y_i \ \dot{y}_i \ \cdots \ y_i^{(r_i-1)}]^T \in \mathfrak{R}^{r_i}, \quad i = 1, \dots, m \\ A &\triangleq \text{block-diag}(A_1 \ A_2 \ \cdots \ A_m) \in \mathfrak{R}^{r \times r} \\ B &\triangleq \text{block-diag}(B_1 \ B_2 \ \cdots \ B_m) \in \mathfrak{R}^{r \times m} \end{aligned} \quad (7.4.2)$$

and

$$A_i = \begin{bmatrix} 0 & 1 & 0 & \cdots & 0 & 0 \\ 0 & 0 & 1 & \cdots & 0 & 0 \\ \vdots & \vdots & \vdots & \ddots & \vdots & \vdots \\ 0 & 0 & 0 & \cdots & 0 & 1 \\ 0 & 0 & 0 & \cdots & 0 & 0 \end{bmatrix} \in \mathfrak{R}^{r_i \times r_i}, \quad B_i = \begin{bmatrix} 0 \\ 0 \\ \vdots \\ 0 \\ b_i \end{bmatrix} \in \mathfrak{R}^{r_i \times 1} \quad (7.4.3)$$

where b_i , $i = 1, \dots, m$ are control effectiveness terms, and $\mathbf{d}(t) \in \mathfrak{R}^{m \times 1}$ is the bounded external disturbance such that

$$\|\mathbf{d}(t)\| \leq d_m \quad (7.4.4)$$

Assumption 7.4.1. *For a clear derivation of the composite output feedback NDI-based model reference adaptive control design containing complicated elements, we assume that the output is available for control design. If this case is not exactly applicable for a specific nonlinear system, then we further assume that we get closely approximated output values using a nominal nonlinear observer.*

A reference model is described by an equation which is composed of m -ordinary differential equations having $r_i^{th}, i = 1, \dots, m$ order, respectively. The equation can be written in a compact state space form as:

$$\dot{\mathbf{y}}_M(t) = A_M \mathbf{y}_M(t) + B_M \cdot \mathbf{y}_c(t) \quad (7.4.5)$$

where

$$\begin{aligned} \mathbf{y}_M &\triangleq [\mathbf{y}_{M_1}^T \ \mathbf{y}_{M_2}^T \ \cdots \ \mathbf{y}_{M_m}^T]^T \in \mathfrak{R}^r \\ \mathbf{y}_{M_i} &\triangleq [y_{M_i} \ \dot{y}_{M_i} \ \cdots \ y_{M_i}^{(r_i-1)}]^T \in \mathfrak{R}^{r_i}, \quad i = 1, \dots, m \\ \mathbf{y}_c &\triangleq [y_{c_1} \ y_{c_2} \ \cdots \ y_{c_m}]^T \in \mathfrak{R}^m \\ A_M &\triangleq \text{block - diag}(A_{M_1} \ A_{M_2} \ \cdots \ A_{M_m}) \in \mathfrak{R}^{r \times r} \\ B_M &\triangleq \text{block - diag}(B_{M_1} \ B_{M_2} \ \cdots \ B_{M_m}) \in \mathfrak{R}^{r \times m} \end{aligned} \quad (7.4.6)$$

and

$$A_{M_i} = \begin{bmatrix} 0 & 1 & 0 & \cdots & 0 & 0 \\ 0 & 0 & 1 & \cdots & 0 & 0 \\ \vdots & \vdots & \vdots & \ddots & \vdots & \vdots \\ 0 & 0 & 0 & \cdots & 0 & 1 \\ -a_{i1} & -a_{i2} & -a_{i3} & \cdots & -a_{i(r_i-1)} & -a_{ir_i} \end{bmatrix} \in \mathfrak{R}^{r_i \times r_i}, \quad B_{M_i} = \begin{bmatrix} 0 \\ 0 \\ \vdots \\ 0 \\ a_{i1} \end{bmatrix} \in \mathfrak{R}^{r_i \times 1} \quad (7.4.7)$$

and $\mathbf{y}_M \in \mathfrak{R}^r$ is the reference model state vector, $\mathbf{y}_c(t) \in \mathfrak{R}^m$ is bounded piecewise continuous reference command, and A_M is Hurwitz.

Now it is desired to design a control law such that the output tracking error

$$\mathbf{E}(t) = \mathbf{y}_M(t) - \mathbf{y}(t) \quad (7.4.8)$$

tends to zero and all the signals in the system remain bounded as $t \rightarrow \infty$.

7.5 Composite Adaptive Control Architecture

In this section we design an adaptive control based on the Lyapunov theorems for the nonlinear system described in previous sections. First we define an ideal control solution, as if all

the unknown parameters were known. The ideal pseudo-control is chosen to have feedback and feedforward elements, considering (7.3.7), such that

$$\begin{aligned}\boldsymbol{\nu}_{ideal}(t) &\triangleq (\boldsymbol{\nu}_{dc} + \boldsymbol{\nu}_{rm} - \boldsymbol{\nu}_{ad})_{ideal} \\ &\triangleq \underbrace{K_e \cdot \mathbf{E}(t)}_{\boldsymbol{\nu}_{dc}} + \underbrace{K_r \cdot \mathbf{y}_c(t) - K_e \cdot \mathbf{y}_M(t)}_{\boldsymbol{\nu}_{rm}} - \boldsymbol{\nu}_{ad}\end{aligned}\quad (7.5.1)$$

where $K_e \in \mathfrak{R}^{m \times r}$ and $K_r \in \mathfrak{R}^{m \times m}$, which is adopted for command tracking, are assumed to be bounded:

$$\begin{aligned}\|K_e\| &< k_{em} \\ \|K_r\| &< k_{rm}\end{aligned}\quad (7.5.2)$$

with positive numbers k_{em} and k_{rm} , respectively. Substituting (7.5.1) into (7.4.1), ignoring the disturbance term, the ideal closed-loop dynamics become:

$$\dot{\mathbf{y}}(t) = (A - BK_e) \mathbf{y}(t) + BK_r \mathbf{y}_c(t) \quad (7.5.3)$$

Assumption 7.5.1. *There exist ideal gains K_e and K_r satisfying the model matching conditions defined by [34, 55, 114]:*

$$\begin{aligned}A - BK_e &= A_M \\ BK_r &= B_M\end{aligned}\quad (7.5.4)$$

Comparing (7.5.3) with the desired reference model dynamics in (7.4.5), it can be immediately seen that the ideal gains K_e and K_r must satisfy the model matching conditions in (7.5.4). It is noted that the existence of ideal gains K_e and K_r is assumed without any knowledge of them. In this case with appropriate forms of each element of the equation (7.5.4) and (7.4.5), it is clear that the ideal constant gains always exist.

Based on the structure of (7.5.1), the actual tracking pseudo-control is formed as:

$$\boldsymbol{\nu}(t) = \hat{K}_e \cdot \mathbf{E}(t) + \hat{K}_r \cdot \mathbf{y}_c(t) - \hat{K}_e \cdot \mathbf{y}_M(t) - \boldsymbol{\nu}_{ad} \quad (7.5.5)$$

where the feedback gain \hat{K}_e , the feedforward gain \hat{K}_r , and the estimated vector of parameters \hat{W} will be found to achieve the desired tracking performance. The overall architecture of this composite model reference control design is presented in Figure 75.

Substituting (7.5.5) into the system dynamics (7.4.1) results in the closed-loop system

$$\dot{\mathbf{y}}(t) \triangleq A\mathbf{y}(t) + B \left(\hat{K}_e \mathbf{E}(t) + \hat{K}_r \mathbf{y}_c(t) - \hat{K}_e \mathbf{y}_M(t) + \Delta - \boldsymbol{\nu}_{ad} + \mathbf{d} \right) \quad (7.5.6)$$

which yields, by adding and subtracting corresponding terms,

$$\begin{aligned} \dot{\mathbf{y}}(t) &= (A - BK_e) \mathbf{y}(t) + BK_r \mathbf{y}_c(t) + B \left(K_e - \hat{K}_e \right) \mathbf{y}(t) - B \left(K_r - \hat{K}_r \right) \mathbf{y}_c(t) \\ &\quad + B(\Delta - \boldsymbol{\nu}_{ad} + \mathbf{d}) \end{aligned} \quad (7.5.7)$$

Using matching conditions (7.5.4), equation (7.5.7) is written in a compact form,

$$\dot{\mathbf{y}}(t) = A_M \mathbf{y}(t) + B_M \mathbf{y}_c(t) + B \left(\tilde{K}_e \mathbf{y}(t) - \tilde{K}_r \mathbf{y}_c(t) + \Delta - \boldsymbol{\nu}_{ad} + \mathbf{d} \right) \quad (7.5.8)$$

where \tilde{K}_e, \tilde{K}_r are the parameter estimation errors defined by:

$$\begin{aligned} \tilde{K}_e &= K_e - \hat{K}_e \\ \tilde{K}_r &= K_r - \hat{K}_r \end{aligned} \quad (7.5.9)$$

Then the closed-loop dynamics of the tracking error signal $\mathbf{E}(t)$ in (7.4.8) can be obtained by subtracting (7.5.8) from (7.4.5)

$$\dot{\mathbf{E}}(t) = A_M \mathbf{E}(t) - B \left(\tilde{K}_e \mathbf{y}(t) - \tilde{K}_r \mathbf{y}_c(t) + \Delta - \boldsymbol{\nu}_{ad} + \mathbf{d} \right) \quad (7.5.10)$$

Since A_M is Hurwitz, there exists a unique and positive definite matrix $P = P^T > 0$ for an arbitrary matrix $Q = Q^T > 0$ satisfying the Lyapunov equation

$$A_M^T P + P A_M = -Q \quad (7.5.11)$$

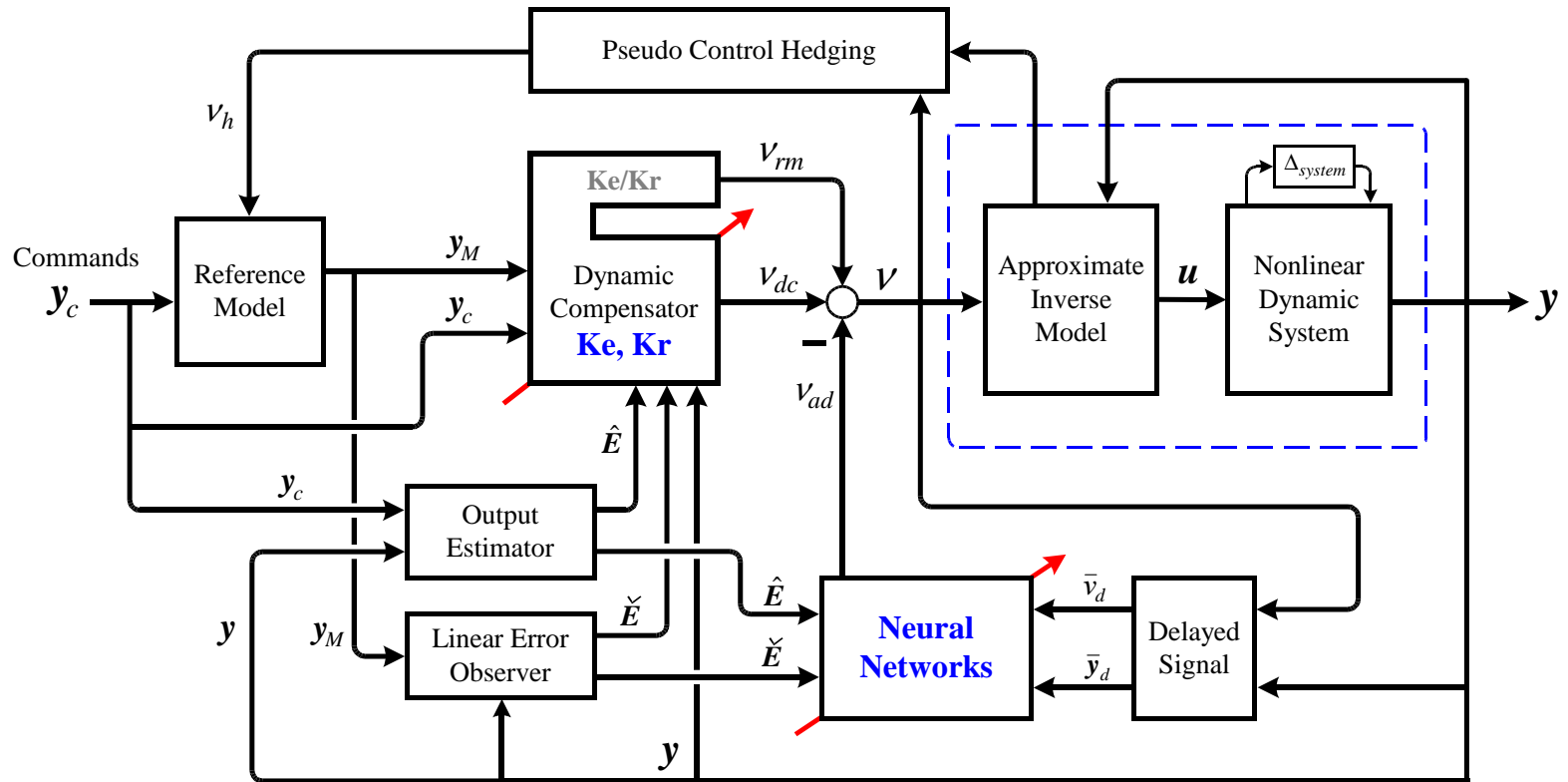


Figure 75: Composite model reference adaptive control architecture

7.6 The System State Estimator

Next, consider the system state estimator dynamics [54, 107]:

$$\dot{\hat{\mathbf{y}}}(t) = A_P (\hat{\mathbf{y}}(t) - \mathbf{y}(t)) + A_M \mathbf{y}(t) + B_M \mathbf{y}_c(t) \quad (7.6.1)$$

where $\hat{\mathbf{y}}$ is the estimator state vector, and the constant matrix A_P is Hurwitz.

Let

$$\hat{\mathbf{E}}(t) = \hat{\mathbf{y}}(t) - \mathbf{y}(t) \quad (7.6.2)$$

denote the state estimation error. Subtracting (7.4.1) from (7.6.1), the state estimation error dynamics can be written as:

$$\dot{\hat{\mathbf{E}}}(t) = A_P \hat{\mathbf{E}}(t) - B \left(\tilde{K}_e \mathbf{y}(t) - \tilde{K}_r \mathbf{y}_c(t) + \Delta - \nu_{ad} + \mathbf{d} \right) \quad (7.6.3)$$

Since A_P is Hurwitz, there exists a unique and positive definite matrix $\hat{P} = \hat{P}^T > 0$ for an arbitrary matrix $\hat{Q} = \hat{Q}^T > 0$ satisfying the Lyapunov equation

$$A_P^T \hat{P} + \hat{P} A_P = -\hat{Q} \quad (7.6.4)$$

7.7 Stability Analysis using Lyapunov Theorems

In this section using Lyapunov's direct method we show that all the errors are ultimately bounded. They are the tracking error \mathbf{E} , the state estimation error $\hat{\mathbf{E}}$, the control estimation errors \tilde{K}_e and \tilde{K}_r , and the NN weight errors. To this end we consider one of following vectors:

a) RBF NN:

$$\zeta = \left[\mathbf{E}^T \quad \hat{\mathbf{E}}^T \quad \tilde{K}_e^T \quad \tilde{K}_r^T \quad \tilde{W}^T \right]^T \quad (7.7.1)$$

b) SHL NN:

$$\zeta = \left[\mathbf{E}^T \quad \hat{\mathbf{E}}^T \quad \tilde{K}_e^T \quad \tilde{K}_r^T \quad \tilde{W}^T \quad \tilde{V}^T \right]^T \quad (7.7.2)$$

and one of following positive definite Lyapunov function candidates:

a) RBF NN:

$$V(\zeta) = \mathbf{E}^T P \mathbf{E} + \hat{\mathbf{E}}^T \hat{P} \hat{\mathbf{E}} + tr \left(\tilde{K}_e^T \Gamma_e^{-1} \tilde{K}_e + \tilde{K}_r^T \Gamma_r^{-1} \tilde{K}_r + H \cdot \tilde{W}^T \Gamma_w^{-1} \tilde{W} \right) \quad (7.7.3)$$

b) SHL NN:

$$\mathcal{L}(\zeta) = \mathbf{E}^T P \mathbf{E} + \hat{\mathbf{E}}^T \hat{P} \hat{\mathbf{E}} + tr \left(\tilde{K}_e^T \Gamma_e^{-1} \tilde{K}_e + \tilde{K}_r^T \Gamma_r^{-1} \tilde{K}_r + \tilde{W}^T \Gamma_w^{-1} \tilde{W} + \tilde{V}^T \Gamma_v^{-1} \tilde{V} \right) \quad (7.7.4)$$

In the expanded space of the compound error variable, consider the largest level set of $V(\zeta)$ or $\mathcal{L}(\zeta)$ in \mathcal{D}_ζ such that its projection on the subspace of the NN input variables completely lies in \mathcal{D}_l . As shown in figure 76, define the largest ball that lies inside that level set as

$$B_R \triangleq \{\zeta \mid \|\zeta\| \leq R\} \quad (7.7.5)$$

and let α be the minimum value of $V(\zeta)$ or $\mathcal{L}(\zeta)$ on the boundary of B_R

$$\begin{aligned} \alpha &\triangleq \min_{\|\zeta\|=R} V(\zeta) \quad \text{for RBF NN} \\ \text{or } \alpha &\triangleq \min_{\|\zeta\|=R} \mathcal{L}(\zeta) \quad \text{for SHL NN} \end{aligned} \quad (7.7.6)$$

Introduce the set

$$\begin{aligned} \Omega_\alpha &\triangleq \{\zeta \in B_R \mid V(\zeta) \leq \alpha\} \quad \text{for RBF NN} \\ \text{or } \Omega_\alpha &\triangleq \{\zeta \in B_R \mid \mathcal{L}(\zeta) \leq \alpha\} \quad \text{for SHL NN} \end{aligned} \quad (7.7.7)$$

7.7.1 Composite RBF NN Adaptation

In this section we show that \mathbf{E} , $\hat{\mathbf{E}}$, \tilde{K}_e , \tilde{K}_r , and \tilde{W} are all uniformly bounded using RBF NNs with σ -modification.

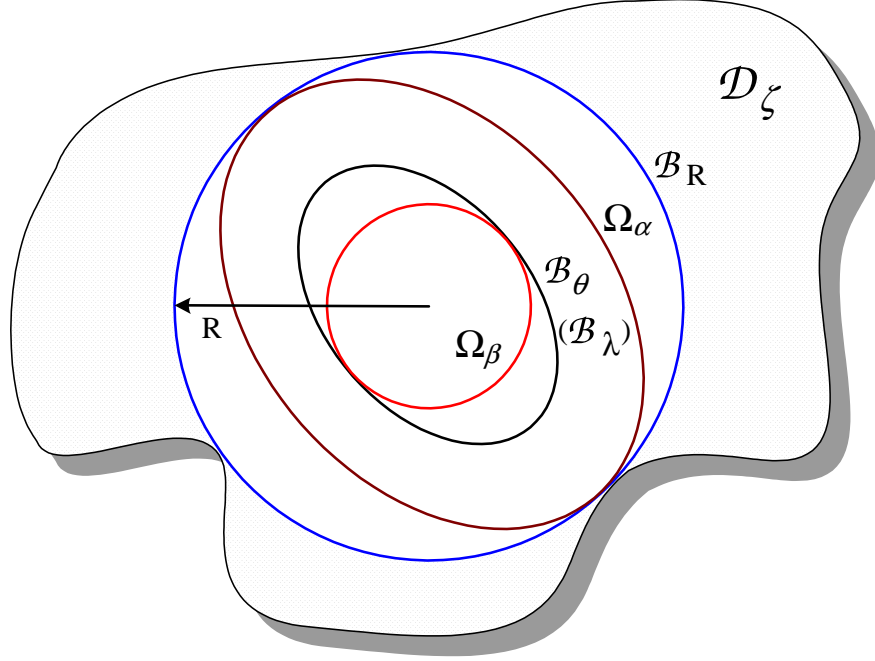


Figure 76: Geometric representation of sets in the error space

Since $h_{\bar{\nu}_i}, i = 1, \dots, m$ in (3.2.13) are positive continuous functions over the compact set \mathcal{D}_l , we can define the minimum/maximum values of the functions as

$$\begin{aligned} \underline{h} &\triangleq \min \left[\min_{(\mathbf{x}, \boldsymbol{\nu}_1) \in \mathcal{D}_1} h_{\bar{\nu}_1}, \min_{(\mathbf{x}, \boldsymbol{\nu}_1) \in \mathcal{D}_1} h_{\bar{\nu}_2}, \dots, \min_{(\mathbf{x}, \boldsymbol{\nu}_1) \in \mathcal{D}_1} h_{\bar{\nu}_m} \right] \\ \bar{h} &\triangleq \max \left[\max_{(\mathbf{x}, \boldsymbol{\nu}_1) \in \mathcal{D}_1} h_{\bar{\nu}_1}, \max_{(\mathbf{x}, \boldsymbol{\nu}_1) \in \mathcal{D}_1} h_{\bar{\nu}_2}, \dots, \max_{(\mathbf{x}, \boldsymbol{\nu}_1) \in \mathcal{D}_1} h_{\bar{\nu}_m} \right] \end{aligned} \quad (7.7.8)$$

Assumption 7.7.1. *It is assumed that the time derivative of the control effectiveness matrix H in (7.3.10) is bounded such that [25, 30, 45]:*

$$\|\dot{H}\| \leq h_m \quad (7.7.9)$$

From the definition of the candidate Lyapunov function in (7.7.3), there exist class \mathcal{K} functions η_1 and η_2 such that

$$\eta_1(\zeta) \leq V(\|\zeta\|) \leq \eta_2(\zeta) \quad (7.7.10)$$

where

$$\begin{aligned}
\eta_1(\|\zeta\|) &= \lambda_{\min}(P)\|\mathbf{E}\|^2 + \lambda_{\min}(\hat{P})\|\hat{\mathbf{E}}\|^2 + \lambda_{\min}(\Gamma_e^{-1})\|\tilde{K}_e\|^2 \\
&\quad + \lambda_{\min}(\Gamma_r^{-1})\|\tilde{K}_r\|^2 + \lambda_{\min}(\Gamma_w^{-1})\underline{h}\|\tilde{W}\|^2 \\
\eta_2(\|\zeta\|) &= \lambda_{\max}(P)\|\mathbf{E}\|^2 + \lambda_{\max}(\hat{P})\|\hat{\mathbf{E}}\|^2 + \lambda_{\max}(\Gamma_e^{-1})\|\tilde{K}_e\|^2 \\
&\quad + \lambda_{\max}(\Gamma_r^{-1})\|\tilde{K}_r\|^2 + \lambda_{\max}(\Gamma_w^{-1})\bar{h}\|\tilde{W}\|^2
\end{aligned} \tag{7.7.11}$$

Assumption 7.7.2. *Assume that*

$$R > \eta_1^{-1}(\eta_2(\theta)) \tag{7.7.12}$$

where θ is defined as

$$\theta \triangleq \frac{\sqrt{\Pi_1 + \Pi_2}}{\min\left(\sqrt{\lambda_{\min}(Q)} - 1, \sqrt{\lambda_{\min}(\hat{Q})} - 1, \sqrt{\rho_e}, \sqrt{\rho_r}, \sqrt{\kappa\bar{h}}\right)} \tag{7.7.13}$$

where

$$\begin{aligned}
\Pi_1 &\triangleq \rho_e\|K_e - K_{e0}\|_F^2 + \rho_r\|K_r - K_{r0}\|_F^2 + \kappa\bar{h}\|W - W_0\|_F^2 \\
\Pi_2 &\triangleq \left(\|PB\|^2 + \|\tilde{P}B\|^2 + \|\hat{P}B\|^2\right) (2w_m p_m \bar{h} + \varepsilon_m \bar{h} + d_m)^2
\end{aligned} \tag{7.7.14}$$

Remark 7.7.1 (Boundedness of RBF NN with Backpropagation *alone*). It is noted that the update laws of adaptive control elements with *back-propagation* alone, shown below, result in the proof of the boundedness of \mathbf{E} , $\hat{\mathbf{E}}$ only.

$$\begin{aligned}
\dot{K}_e &= -\Gamma_e \left(\mathbf{E}^T PB + \hat{\mathbf{E}}^T \hat{P}B \right)^T \cdot \mathbf{y}^T \\
\dot{K}_r &= \Gamma_r \left(\mathbf{E}^T PB + \hat{\mathbf{E}}^T \hat{P}B \right)^T \cdot \mathbf{y}_c^T \\
\dot{W} &= -\Gamma_w \Psi(\boldsymbol{\mu}) \left(\mathbf{E}^T PB + \hat{\mathbf{E}}^T \hat{P}B \right)
\end{aligned} \tag{7.7.15}$$

where $\Gamma_e = \Gamma_e^T > 0$, $\Gamma_r = \Gamma_r^T > 0$, $\Gamma_w = \Gamma_w^T > 0$ are the rates of adaptation, or adaptation gains. Hence, in order to prove the boundedness of all parameters including \tilde{K}_e , \tilde{K}_r , and \tilde{W} , we need to introduce a modification such as σ -modification or e -modification to the adaptation laws (7.7.15). A similar remark is applicable to SHL NNs in Section 7.7.2. \diamond

Theorem 7.7.1. *Let assumptions 7.2.1 - 7.7.2 hold. Then, if the initial error $\zeta(0) \in \Omega_\alpha$, the control law given by (7.5.5), along with σ -modifications shown below, guarantees that the signals \mathbf{E} , $\hat{\mathbf{E}}$, \tilde{K}_e , \tilde{K}_r , and \tilde{W} in the closed loop system are all ultimately bounded.*

$$\begin{aligned}\dot{\hat{K}}_e &= -\Gamma_e \left[\left(\mathbf{E}^T P B + \hat{\mathbf{E}}^T \hat{P} B \right)^T \cdot \mathbf{y}^T + \rho_e \cdot \left(\hat{K}_e - K_{eo} \right) \right] \\ \dot{\hat{K}}_r &= \Gamma_r \left[\left(\mathbf{E}^T P B + \hat{\mathbf{E}}^T \hat{P} B \right)^T \cdot \mathbf{y}_c^T - \rho_r \cdot \left(\hat{K}_r - K_{ro} \right) \right] \\ \dot{\hat{W}} &= -\Gamma_w \left[\Psi(\boldsymbol{\mu}) \left(\mathbf{E}^T P B + \hat{\mathbf{E}}^T \hat{P} B \right) + \kappa \cdot \left(\hat{W} - W_0 \right) \right]\end{aligned}\quad (7.7.16)$$

where the matrices $\Gamma_e = \Gamma_e^T > 0$, $\Gamma_r = \Gamma_r^T > 0$ and $\Gamma_w = \Gamma_w^T > 0$, the constants $\rho_e > 0$, $\rho_r > 0$ and $\kappa > 0$ are the adaptation gains, and K_{eo} , K_{ro} , and W_0 are initial guesses (or guesses).

Proof. See Appendix C □

From the result of Theorem 7.7.1, we can see that the overall control architecture of the *composite* adaptive NDI scheme using RBF NNs developed in this chapter results in stable closed-loop systems for output feedback, NDI-based MIMO nonlinear systems.

7.7.2 Composite SHL NN Adaptation

In this section, through Lyapunov theorems, we show that \mathbf{E} , $\hat{\mathbf{E}}$, \tilde{K}_e , \tilde{K}_r , \tilde{V} , and \tilde{W} are all uniformly bounded using SHL NNs with σ -modification.

From the definition of the candidate Lyapunov function \mathcal{L} in (7.7.4), there exist class \mathcal{K} functions φ_1 and φ_2 such that

$$\varphi_1(\|\zeta\|) \leq \mathcal{L}(\|\zeta\|) \leq \varphi_2(\|\zeta\|) \quad (7.7.17)$$

where

$$\begin{aligned}\varphi_1(\|\zeta\|) &= \lambda_{\min}(P) \|\mathbf{E}\|^2 + \lambda_{\min}(\hat{P}) \|\hat{\mathbf{E}}\|^2 + \lambda_{\min}(\Gamma_e^{-1}) \|\tilde{K}_e\|^2 \\ &\quad + \lambda_{\min}(\Gamma_r^{-1}) \|\tilde{K}_r\|^2 + \lambda_{\min}(\Gamma_w^{-1}) \|\tilde{W}\|^2 \\ \varphi_2(\|\zeta\|) &= \lambda_{\max}(P) \|\mathbf{E}\|^2 + \lambda_{\max}(\hat{P}) \|\hat{\mathbf{E}}\|^2 + \lambda_{\max}(\Gamma_e^{-1}) \|\tilde{K}_e\|^2 \\ &\quad + \lambda_{\max}(\Gamma_r^{-1}) \|\tilde{K}_r\|^2 + \lambda_{\max}(\Gamma_w^{-1}) \|\tilde{W}\|^2\end{aligned}\quad (7.7.18)$$

Assumption 7.7.3. Assume that

$$R > \varphi_1^{-1}(\varphi_2(\lambda)) \quad (7.7.19)$$

where λ is defined as

$$\lambda \triangleq \frac{\sqrt{\Omega_1 + \Omega_2}}{\min(C_1, C_2, \sqrt{\rho_e}, \sqrt{\rho_r}, \sqrt{\kappa_b - 2\gamma_1 p_b})} \quad (7.7.20)$$

where

$$\begin{aligned} \Omega_1 &\triangleq \kappa_b - 2\gamma_1 p_b \\ \Omega_2 &\triangleq \rho_e \|K_e - K_{eo}\|_F^2 + \rho_r \|K_r - K_{ro}\|_F^2 + \kappa_v \|V - V_0\|_F^2 + \kappa_w \|W - W_0\|_F^2 \\ C_1 &\triangleq \sqrt{\lambda_{\min}(Q) - p_b(\gamma_1 + \gamma_2 + d_m)} \\ C_2 &\triangleq \sqrt{\lambda_{\min}(\hat{Q}) - p_b(\gamma_1 + \gamma_2 + d_m)} \end{aligned} \quad (7.7.21)$$

Theorem 7.7.2. Let assumptions 7.2.1 - 7.7.3 hold. Then, if the initial error $\zeta(0) \in \Omega_\alpha$, the control law given by (7.5.5), along with SHL NN shown below, guarantees that the signals \mathbf{E} , $\hat{\mathbf{E}}$, \tilde{K}_e , \tilde{K}_r , \tilde{V} , and \tilde{W} in the closed loop system are all ultimately bounded.

$$\begin{aligned} \dot{\hat{K}}_e &= -\Gamma_e \left[\left(\mathbf{E}^T P B + \hat{\mathbf{E}}^T \hat{P} B \right)^T \cdot \mathbf{y}^T + \rho_e \cdot \left(\hat{K}_e - K_{eo} \right) \right] \\ \dot{\hat{K}}_r &= \Gamma_r \left[\left(\mathbf{E}^T P B + \hat{\mathbf{E}}^T \hat{P} B \right)^T \cdot \mathbf{y}_c^T - \rho_r \cdot \left(\hat{K}_r - K_{ro} \right) \right] \\ \dot{\hat{V}} &= -\Gamma_v \cdot \left[\boldsymbol{\mu} \left(\mathbf{E}^T P B + \hat{\mathbf{E}}^T \hat{P} B \right) \hat{W}^T \boldsymbol{\sigma}' + \kappa_v \cdot \left(\hat{V} - V_0 \right) \right] \\ \dot{\hat{W}} &= -\Gamma_w \cdot \left[\left(\hat{\boldsymbol{\sigma}} - \hat{\boldsymbol{\sigma}}' \hat{V}^T \boldsymbol{\mu} \right) \left(\mathbf{E}^T P B + \hat{\mathbf{E}}^T \hat{P} B \right) + \kappa_w \cdot \left(\hat{W} - W_0 \right) \right] \end{aligned} \quad (7.7.22)$$

where $\hat{\boldsymbol{\sigma}} = \boldsymbol{\sigma} \left(\hat{V}^T \boldsymbol{\mu} \right)$ and $\boldsymbol{\sigma}' = \text{diag} \left(d\sigma_i / dz_i \right)$ denotes the Jacobian matrix. Γ_v , Γ_w , κ_v , and $\kappa_w > 0$ are adaptation gains. K_{eo} , K_{ro} , W_0 and V_0 are initial guesses (or guesses),

Proof. See Appendix D □

From the result of Theorem 7.7.1, we can conclude that the overall control architecture of the *composite* adaptive NDI scheme using SHL NNs developed in this chapter results in stable closed-loop systems for output feedback, NDI-based MIMO nonlinear systems.

7.8 Simulations and Evaluations

As we see in Chapter 4, the adaptive NDI control design in Chapter 3 is shown to provide good adaptation using the vehicle NASA F-15 ACTIVE performing nonlinear maneuvers in highly nonlinear regimes. The vehicle is shown in Figure 77. Theoretically the newly-suggested composite adaptive NDI MRAC design of this chapter is expected to exhibit better performance over a wider operational range by providing quicker and/or better adaptation utilizing more adaptive elements.

This section contains composite adaptive control design processes for the setup of the adaptive dynamic compensator part and the NN-based adaptation part, and simulation results using the same vehicle, F-15 ACTIVE, used for adaptive NDI simulation in Chapter 4.

7.8.1 Control Design Parameters

As shown in Chapters 3 and 4, dynamic compensators ν_{dc} and ν_{rm} of the adaptive NDI design have *fixed* gains, and then in (3.5.4) we set them to force the tracking error dynamics in (3.5.6) to have the same pole locations as those of the reference model, while in the composite adaptive design we have *non-constant* adapted dynamic compensator gains K_e , K_r updated by adaptation laws in (7.7.16) or (7.7.22). In addition, output estimator/predictor values are involved for NN update laws.

In Chapters 4 – 6, we saw that the pole locations of error dynamics are defined by fixed gains K_e and K_r , while in the composite adaptive design only their existence satisfying the matching condition (7.5.4) is assumed in Assumption 7.5.1. However if we set those parameters free during the control process, the closed-loop performance could be unsatisfactory especially in transient response phases. That comes from the fact that there is no element or device in the design process to enforce the matching condition. Ideally we want the estimates \hat{K}_e , \hat{K}_r to play closely around the ideal values K_e , K_r , if known, satisfying the matching condition, and thus we want the pole locations of error dynamics to be close to those of the



Figure 77: NASA F-15 ACTIVE in flight

reference model during simulation period.

To this end we use a property of σ -modification laws in (7.7.22) such as: when tracking and estimation errors become small, \hat{K}_e , \hat{K}_r in σ -modifications are driven toward K_{eo} , K_{ro} . Hence if we set K_{eo} , K_{ro} such that, for the second order sub-system,

$$\begin{aligned}
 K_{eo}(1, 1) &= \omega_n^2 \\
 K_{eo}(1, 2) &= 2\zeta\omega_n \\
 K_{ro} &= \omega_n^2
 \end{aligned} \tag{7.8.1}$$

where ω , ζ are assumed values as design parameters, then \hat{K}_e , \hat{K}_r are forced to stay around where we set in (7.8.1). This approach is also applied for the first order sub-system by setting its parameters such that

$$\begin{aligned}
 K_{eo} &= 1/\tau \\
 K_{ro} &= 1/\tau
 \end{aligned} \tag{7.8.2}$$

where τ is an assumed value. It is noted that this process can be accelerated by choosing a bigger value of ρ_e , ρ_r in (7.7.22).

7.8.2 Simulation Results

7.8.2.1 High- α Maneuver

As the first simulation, we command a high angle of attack maneuver similar to that of Chapter 4. For simulations in this section, SHL NNs in (7.7.22) are implemented, and the same NN adaptation gains for adaptive NDI design are used for composite adaptive design as shown in Table 5. Gains for adaptive compensators Γ_e , Γ_r , ρ_e , ρ_r in (7.7.22) are shown in Table 6.

Table 5: Neural network parameters for F-15 ACTIVE simulation

Channel	Γ_V	Γ_W	κ_v, κ_w	n_1	n_2	d
p_s	3.0	3.0	0.5	24	10	0.01
α	5.0	4.0	0.1	24	10	0.01
β	3.0	3.0	0.5	24	10	0.01

Table 6: Adaptation gains for adaptive dynamic compensators

Channel	Γ_e	Γ_r	ρ_e	ρ_r
p_s	3.0	3.0	10.0	10.0
α	3.0	3.0	10.0	10.0
β	3.0	3.0	10.0	10.0

Simulation results are presented in Figures 78–82 for a 45° angle of attack command with a small amplitude ($5^\circ/\text{sec}$) doublet in p_s . Figure 78 presents the α , p_s and β responses for various conditions: adaptive NDI, composite adaptive control with addition only $\hat{\mathbf{E}}$, or with addition only \hat{K}_e , \hat{K}_r , or both. As shown in the figure, α -responses are almost identical, while p_s and β responses are a little different. It is not easy to determine whether composite adaptive design yields a significant improvement..

Aerodynamic and TV control deflections are shown in Figures 79 and 80, respectively. It can be seen that composite adaptive design exhibits frequent control movement with less

control saturation.

The NN adaptation signal $\nu_{ad}(t)$ and inversion error $\Delta(t)$ for both adaptive NDI and composite design are compared in Figure 81. The figures show that both algorithms result in satisfactory adaptation.

Time histories of \hat{K}_e , \hat{K}_r in each channel are presented in Figure 82. As we intended the parameters remain near the values we desire. It is noted that even though not clearly visible, they change slightly whenever command are changed.

7.8.2.2 Simultaneous High- α and p_s Maneuver

In order to make obvious the performance differences between the two designs, we command a much more difficult, nonlinear maneuver featuring high angle of attack and higher stability axis roll rate.

Simulation results for simultaneous commands of $\alpha = 40^\circ$ and $p_s = 30^\circ/sec$ are depicted in Figures 83–87. Figure 83 shows the vehicles’s angle of attack, p_s and β responses. It can be seen that the composite adaptive design yields better responses than adaptive NDI design. Angle of attack responses are not much different, while p_s and β responses differ greatly, especially in a time period from 12 sec to 21 sec. As shown in Figure 83(b), composite adaptive design exhibits smaller overshoots with fewer oscillations in p_s responses. A similar difference is observed in the β response of Figure 83(c). The adaptive NDI results feature larger overshoots and large-amplitude oscillations. The composite adaptive design features results with smoother transient responses as a result of its architecture, as noted in Section 7.1.

Aerodynamic and TV control deflections are shown in Figures 84 and 85, respectively. Similar to the previous simulation, it can be seen that composite adaptive design exhibits frequent control movement with less control saturation.

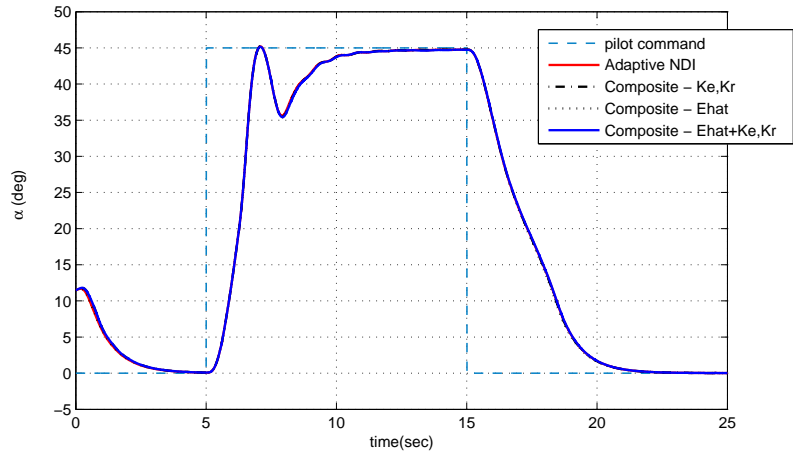
Both designs depict good adaptation as shown in Figure 86, and the time histories of \hat{K}_e , \hat{K}_r are depicted in Figure 87.

7.9 *Conclusions*

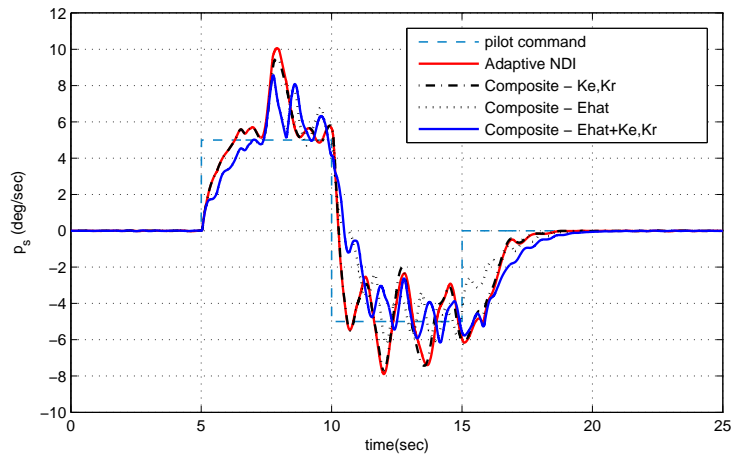
Through a systematic approach we set up the NN-based composite model reference adaptive control design architecture for output feedback control of MIMO nonlinear systems. The new design has more adaptive elements than the adaptive NDI design of Chapter 3. Both employ NNs, while the composite adaptive controller also features an adaptive dynamic compensator.

Using Lyapunov's theorem we investigate the stability analysis of the overall composite adaptive control system, and prove the boundedness of all the error signals.

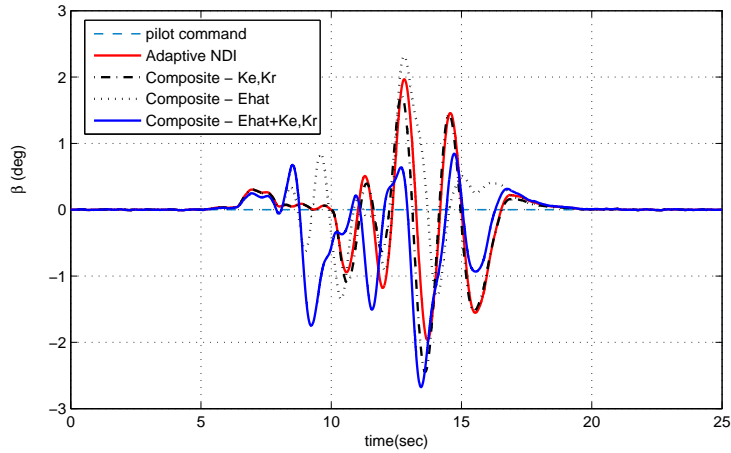
Simulation results using an advanced vehicle, NASA F-15 ACTIVE, show better responses than the adaptive NDI of Chapter 3 during highly nonlinear maneuvers at nonlinear dynamic regimes. As a result we can observe that this composite MRAC design using NNs has the potential for improving the performance of the adaptive control systems.



(a) Angle of attack

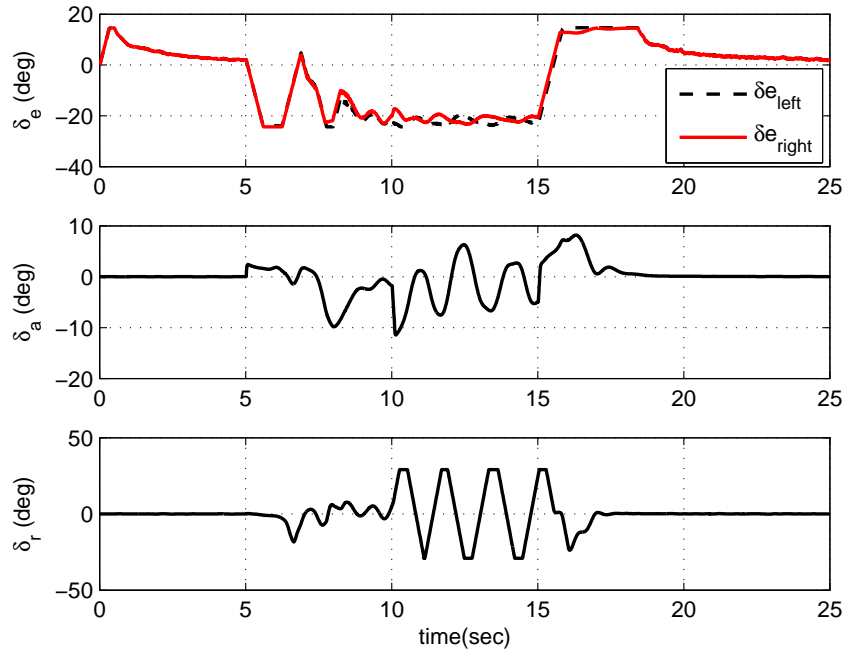


(b) Stability axis roll rate

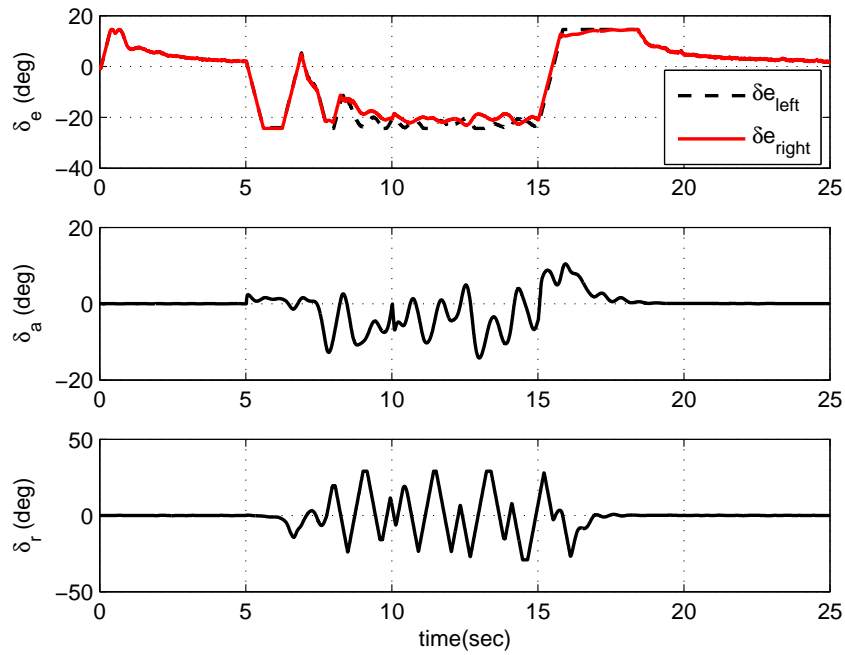


(c) Sideslip angle

Figure 78: Aircraft responses for a high α command with Adaptive NDI and Composite adaptive control

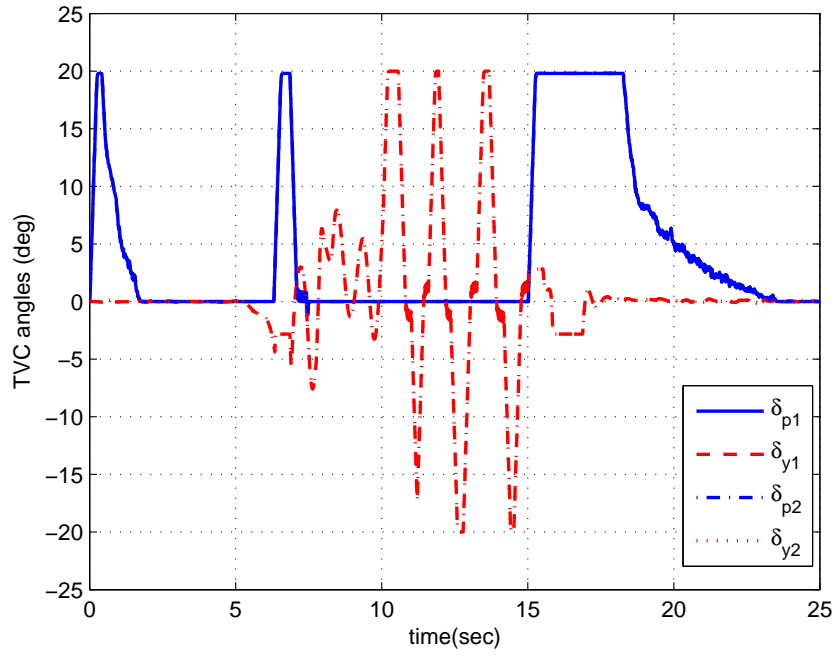


(a) with Adaptive NDI Control

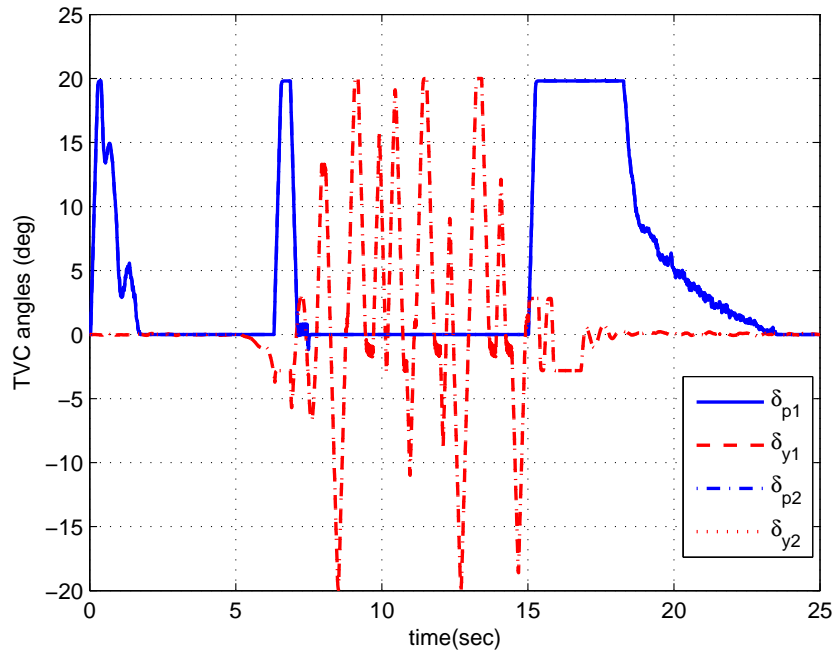


(b) with Composite Adaptive Control

Figure 79: Aerodynamic control deflections for a high α command with Adaptive NDI and Composite adaptive control

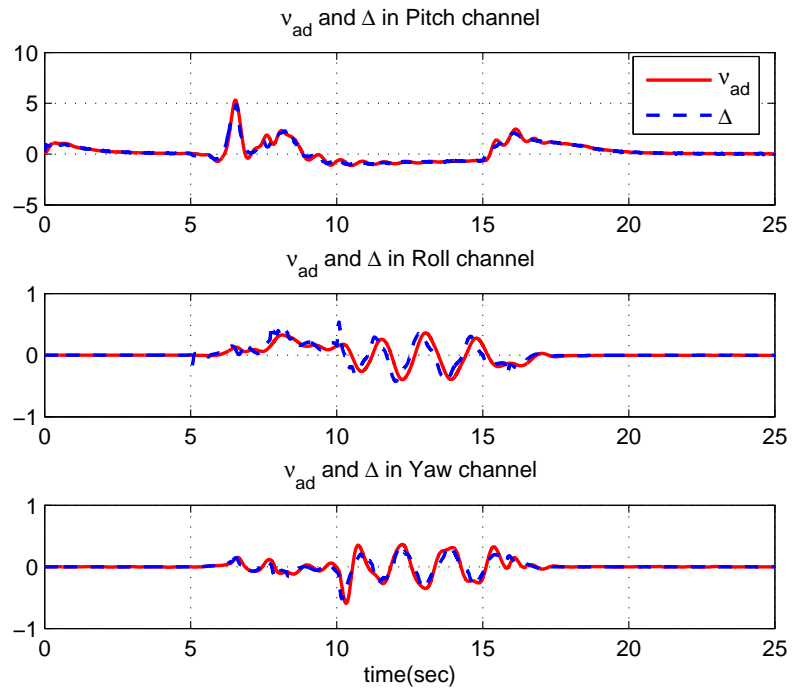


(a) with Adaptive NDI Control

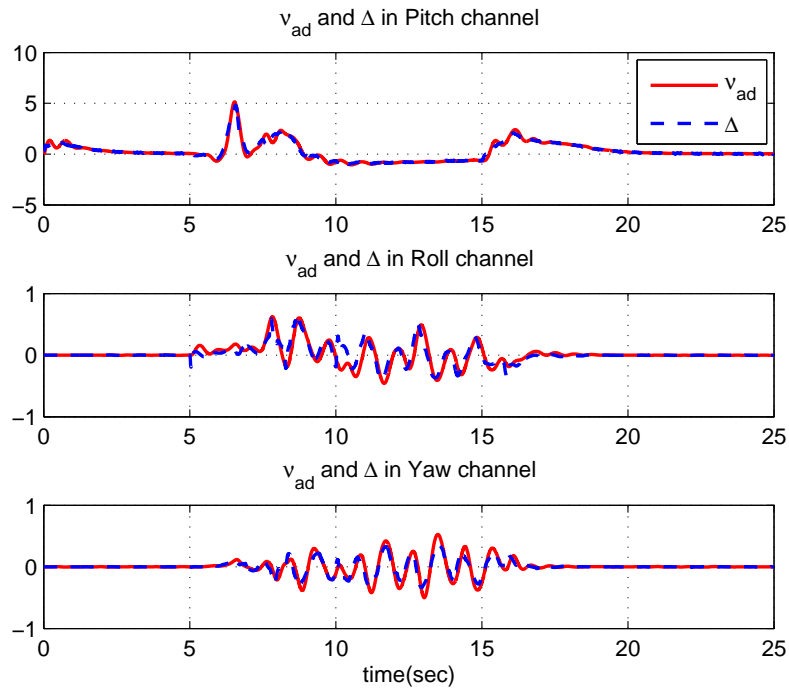


(b) with Composite Adaptive Control

Figure 80: Thrust vector controls with Adaptive NDI and Composite adaptive control

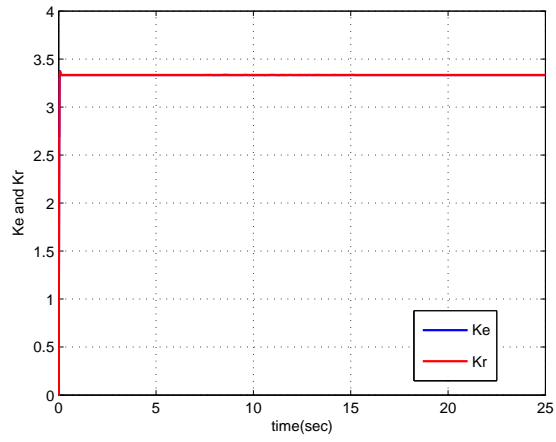


(a) with Adaptive NDI Control

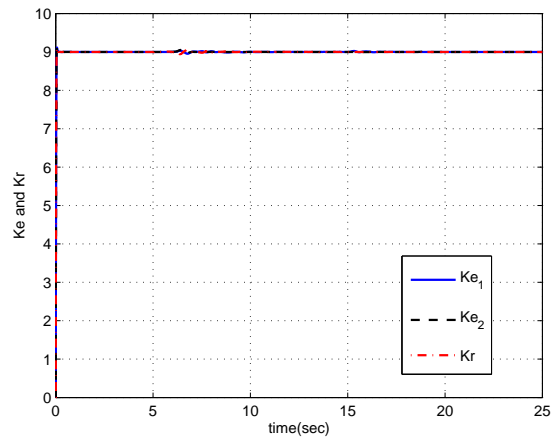


(b) with Composite Adaptive Control

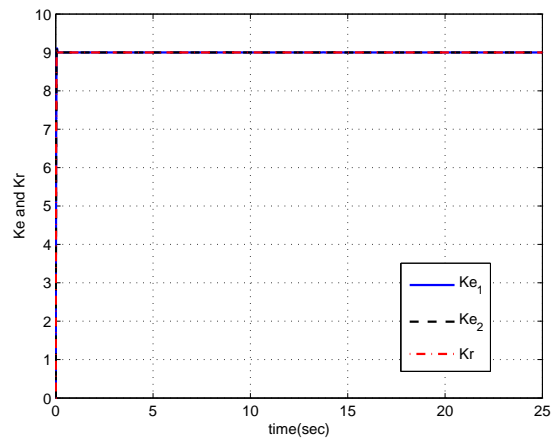
Figure 81: NN adaptation signal $\nu_{ad}(t)$ and $\Delta(t)$ in each channel with Adaptive NDI and Composite adaptive control



(a) Roll channel

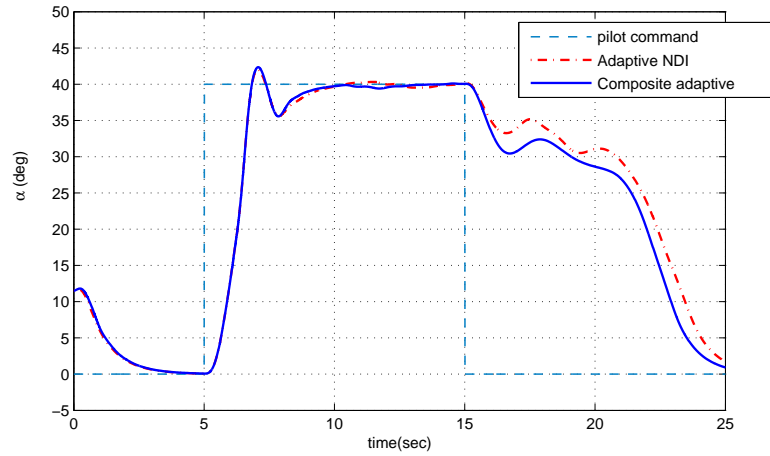


(b) Pitch channel

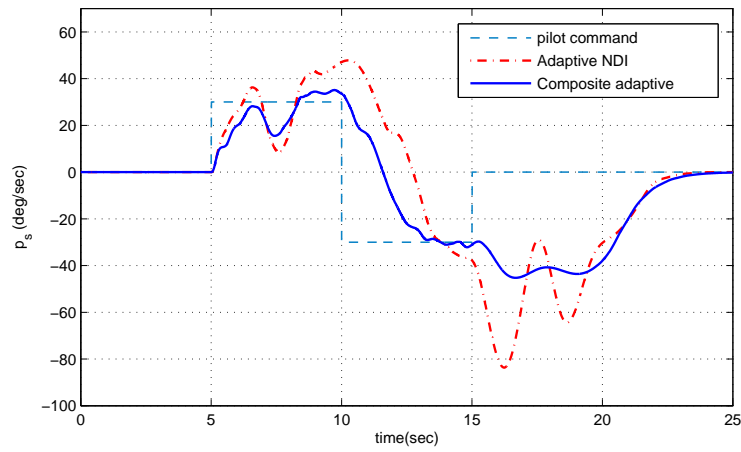


(c) Yaw channel

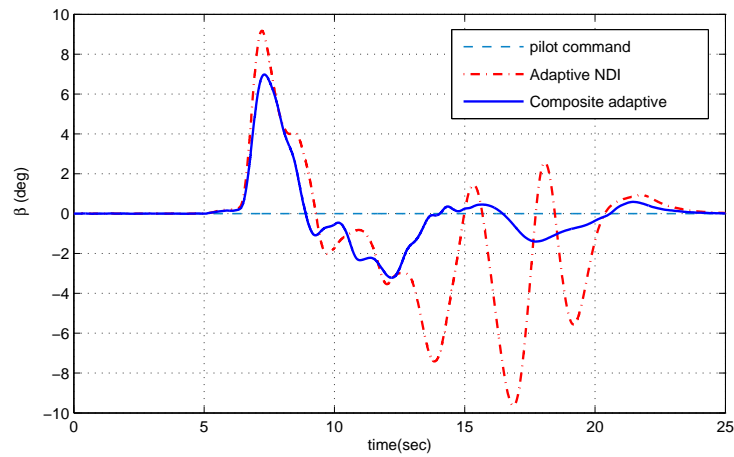
Figure 82: Time history of adaptive DC gains \hat{K}_e , \hat{K}_r in each channel of Composite adaptive control



(a) Angle of attack

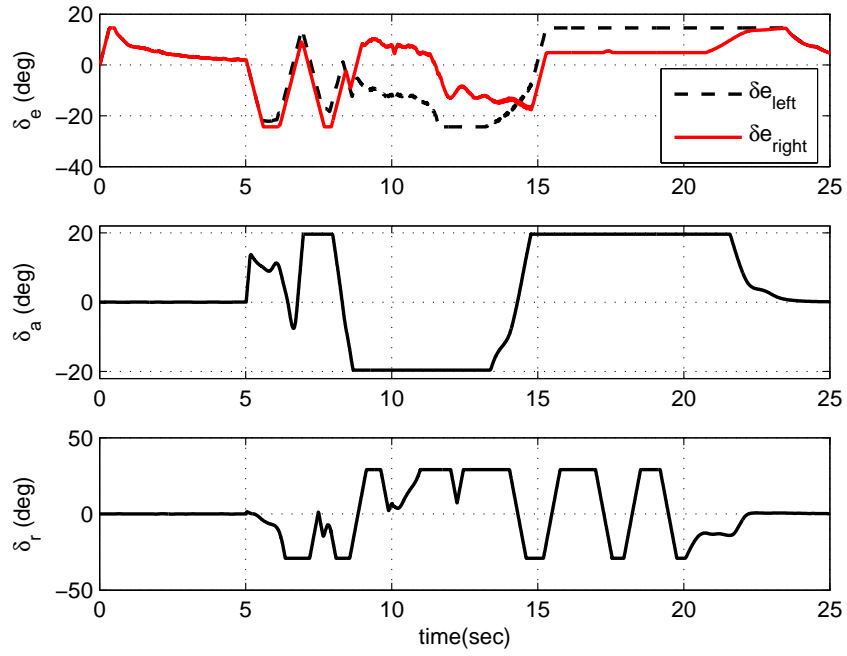


(b) Stability axis roll rate

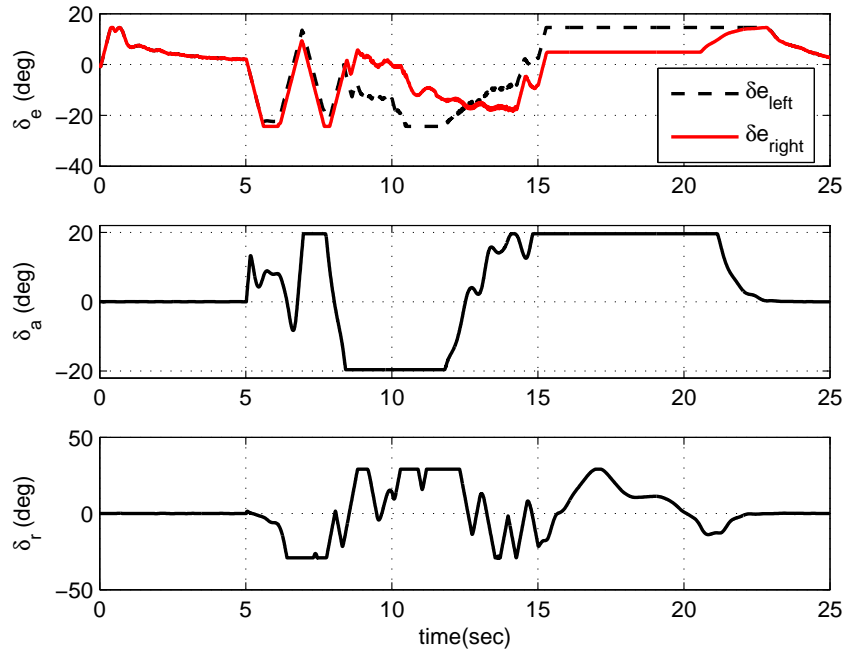


(c) Sideslip angle

Figure 83: Aircraft responses for a high α command with Adaptive NDI and Composite adaptive control

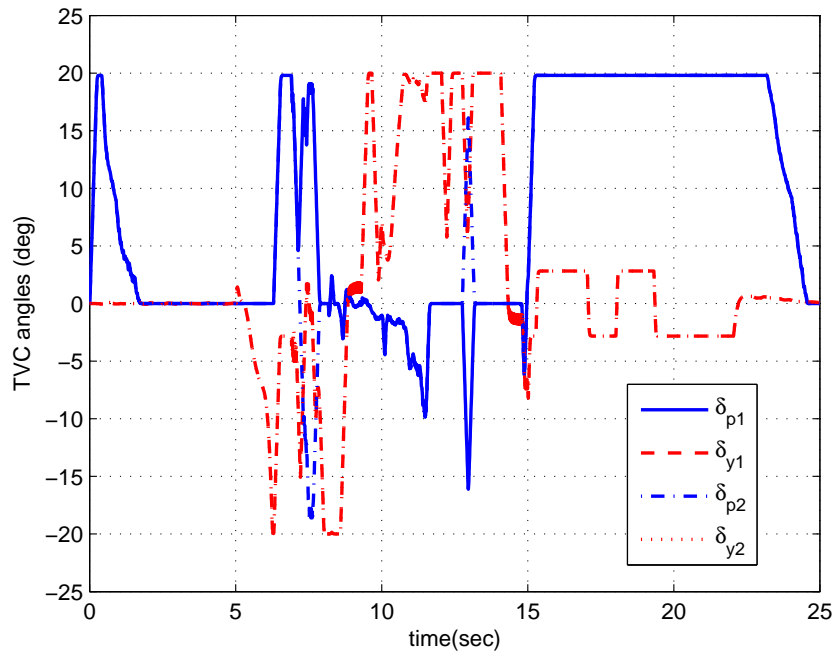


(a) with Adaptive NDI Control

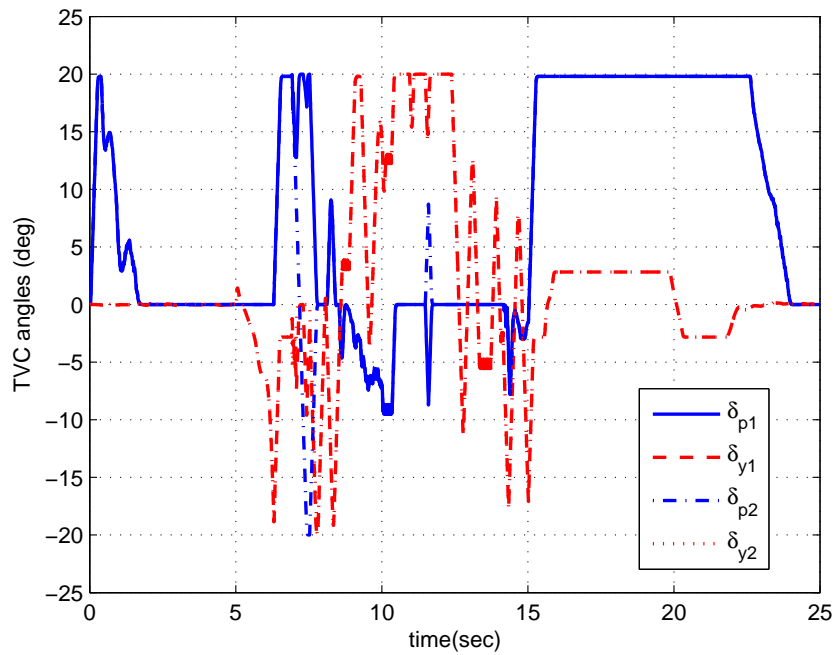


(b) with Composite Adaptive Control

Figure 84: Aerodynamic control deflections for a high α command with Adaptive NDI and Composite adaptive control

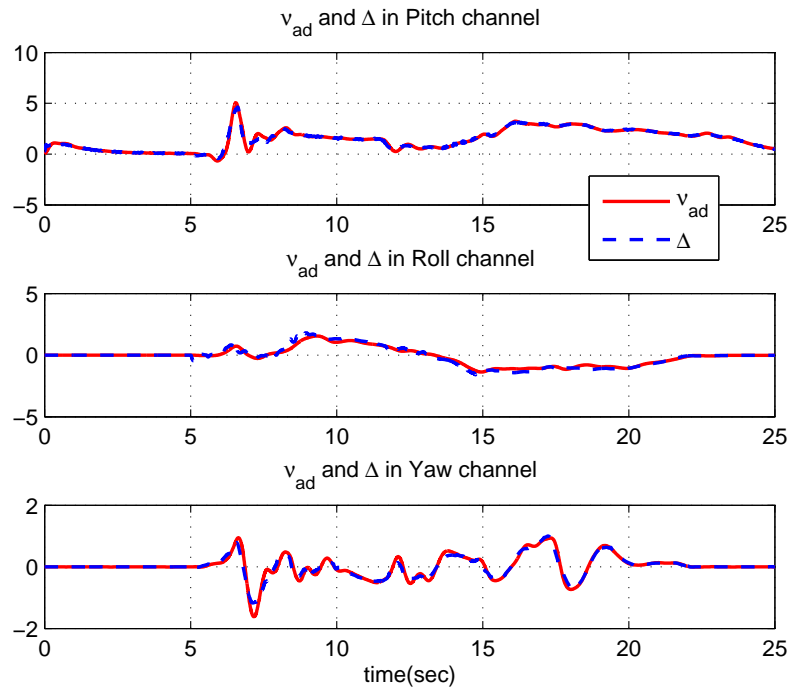


(a) with Adaptive NDI Control

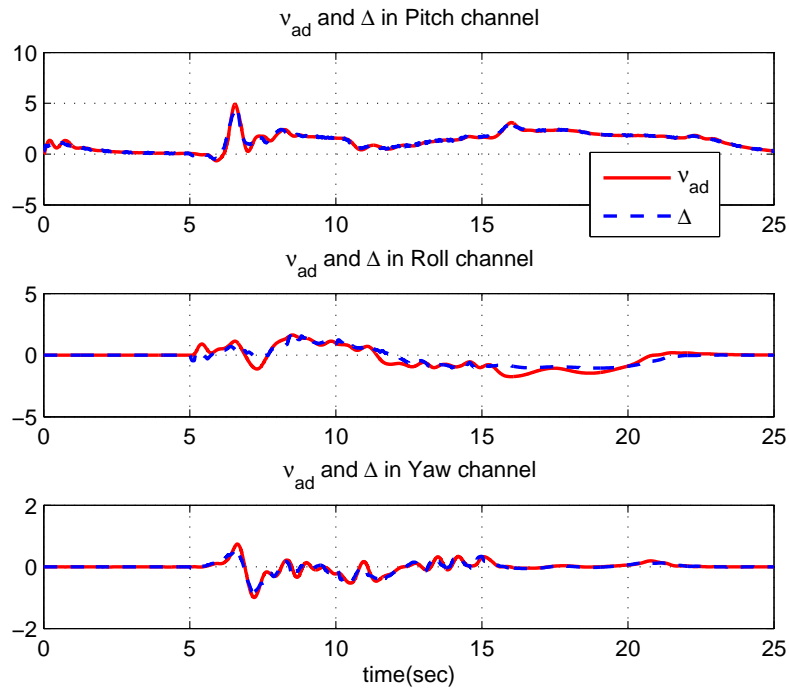


(b) with Composite Adaptive Control

Figure 85: Thrust vector controls with Adaptive NDI and Composite adaptive control

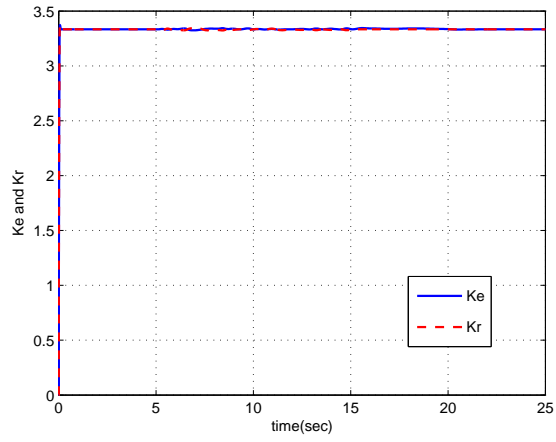


(a) with Adaptive NDI Control

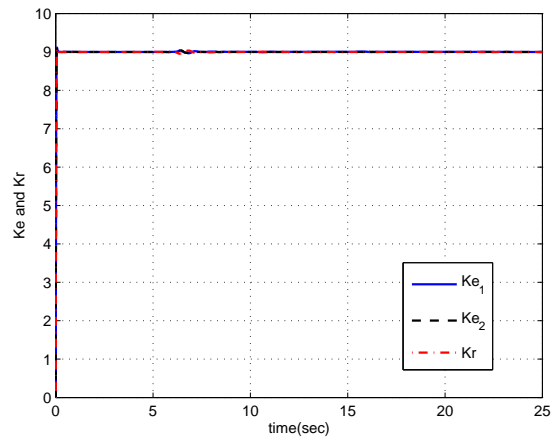


(b) with Composite Adaptive Control

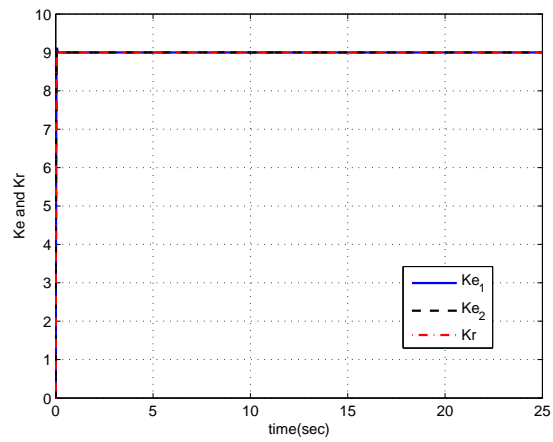
Figure 86: NN adaptation signal $\nu_{ad}(t)$ and $\Delta(t)$ in each channel with Adaptive NDI and Composite adaptive control



(a) Roll channel



(b) Pitch channel



(c) Yaw channel

Figure 87: Time history of adaptive DC gains \hat{K}_e , \hat{K}_r in each channel of Composite adaptive control

CHAPTER VIII

CONCLUSIONS

The research in this thesis is focused on NN-based adaptive control designs for aircraft operating in highly nonlinear dynamic regimes. This thesis contains nonlinear dynamic inversion-based output feedback adaptive control design methodologies using neural networks as adaptive elements. Three aerial vehicles operating in highly nonlinear, uncertain regimes are simulated in order to validate the performance of adaptive designs which are systematically introduced and developed for MIMO nonlinear systems. Simulation results verify that the NN-based adaptive nonlinear dynamic inversion control design methodologies are highly effective and powerful for adaptive control of aerial vehicles.

The design was successfully implemented and demonstrated for an accurate nonlinear model of NASA F-15 ACTIVE (Advanced Control Technology for Integrated Vehicles), equipped with thrust vectored nozzles [16, 105], which is operated at extremely nonlinear dynamic regimes where there exist unmodeled parameter variations and unmodeled vehicle dynamics such as highly nonlinear, unsteady aerodynamic effects, saturation of aerodynamic effectors, and highly coupled vehicle dynamics [17, 105].

A PCH technique was implemented to protect NN adaptation from various actuation nonlinearities such as actuator position and rate saturation, while not interfering with NN adaptation to other sources of inversion error. Thrust vector and differential stabilator are successfully implemented to increase control authority at high angles of attack, and the vehicle's static stability was relaxed in order to achieve more pitch maneuverability. A control allocation methodology was introduced and implemented for effective operation of the redundant control effectors of F-15 ACTIVE.

A thorough comparison study was completed on the performance of a classical adaptive

control design and two different classes of NNs: linearly parameterized RBF NN and nonlinearly parameterized SHL NN for stabilizing an unsteady lateral dynamics, or wing rock, of a delta wing [17, 18].

A command augmentation based adaptive control design using NNs was developed and implemented for a vehicle, FQM-117B UAV which was built with simple and inexpensive subsystems, with access to little aerodynamic data for control design. Its control system was designed to achieve high maneuverability without requiring accurate modeling of the vehicle, and the UAV's adaptive flight control design provided a way to deal with the uncertainties in the system and environment [104].

Further, the composite model reference adaptive design methodology was developed for output feedback MIMO nonlinear systems by introducing additional adaptive elements into the traditional dynamic compensators and additional terms into both the NN adaptation laws and the adaptive dynamic compensators. The new adaptive control design scheme was systematically developed and its stability was proved. Its performance was demonstrated by using an advanced fighter aircraft model to show improved capability.

8.1 Future Research

8.1.1 Relaxation of Assumption 7.2.3

During feedback linearization and nonlinear dynamic inversion, the internal dynamics or zero dynamics are assumed to be stable, which means that the process is restricted to minimum phase systems. Even though widely used in aerospace control designs, this assumption is not quite applicable for the control of aircraft pitch axis. Any theoretical development to extend the methods to non-minimum phase systems is desirable.

8.1.2 Relaxation of Assumption 7.4.1

The introduction of Assumption 7.4.1 in the composite MRAC design of Chapter 7 comes from the fact that utilization of observer error instead tracking error causes triple or higher order terms, coupled with estimation errors of adaptive dynamic compensator gains K_e , K_r ,

in the Lyapunov function for the stability analysis. This condition becomes worse with e -modification of adaptive elements. Actually such condition is common in output feedback control design problems because of availability of the output signal itself. Mathematical or theoretical development to overcome this complexity could be a good topic for a future work.

APPENDIX A

PROOF OF THEOREM 3.7.1

Adaptive Nonlinear Dynamic Inversion Control Using RBF Neural Networks

Proof. Consider the following Lyapunov function candidate:

$$V(\mathbf{E}, \tilde{\mathbf{E}}, \tilde{W}) = \mathbf{E}^T P \mathbf{E} + \tilde{\mathbf{E}}^T \tilde{P} \tilde{\mathbf{E}} + tr\left(H \cdot \tilde{W}^T \Gamma_w^{-1} \tilde{W}\right) \quad (\text{A.0.1})$$

The time derivative of V along the trajectories of (3.5.6) and (3.6.3) implies

$$\begin{aligned} \dot{V} &= 2\mathbf{E}^T P \dot{\mathbf{E}} + 2\tilde{\mathbf{E}}^T \tilde{P} \dot{\tilde{\mathbf{E}}} - 2tr\left(H \cdot \tilde{W}^T \Gamma_w^{-1} \dot{\tilde{W}}\right) + tr\left(\dot{H} \cdot \tilde{W}^T \Gamma_w^{-1} \tilde{W}\right) \\ &= 2\mathbf{E}^T P A_M \mathbf{E} - 2\mathbf{E}^T P B \left(\Delta - \nu_{ad} + \mathbf{d} - K_e \tilde{\mathbf{E}}\right) \\ &\quad + 2\tilde{\mathbf{E}}^T \tilde{P} \tilde{A} \tilde{\mathbf{E}} - 2\tilde{\mathbf{E}}^T \tilde{P} B \left(\Delta - \nu_{ad} + \mathbf{d} - K_e \tilde{\mathbf{E}}\right) \\ &\quad - 2tr\left(H \cdot \tilde{W}^T \Gamma_w^{-1} \dot{\tilde{W}}\right) + tr\left(\dot{H} \cdot \tilde{W}^T \Gamma_w^{-1} \tilde{W}\right) \end{aligned} \quad (\text{A.0.2})$$

Substituting the σ -modification laws in (3.7.16) with recalling $\tilde{\mathbf{E}} = \mathbf{E} - \check{\mathbf{E}}$, the relation (3.2.15), (3.3.6), and the fact that, if M_1, M_2, M_3 are matrices such that $M_1 M_2 M_3$ is a square matrix, then $tr(M_1 M_2 M_3) = tr(M_3^T M_2^T M_1^T) = tr(M_1^T M_3^T M_2^T)$, the equation \dot{V} in (A.0.2) becomes

$$\begin{aligned} \dot{V} &= 2\mathbf{E}^T P A_M \mathbf{E} + 2\tilde{\mathbf{E}}^T \tilde{P} \tilde{A} \tilde{\mathbf{E}} - 2\tilde{\mathbf{E}}(PB + \tilde{P}B)H\tilde{W}^T \Psi(\mathbf{x}) + tr\left(\dot{H} \cdot \tilde{W}^T \Gamma_w^{-1} \tilde{W}\right) \\ &\quad - 2(\mathbf{E}^T P B + \tilde{\mathbf{E}}^T \tilde{P} B) \left(HW^T(\Psi(\boldsymbol{\mu}) - \Phi(\mathbf{x}, \nu_l)) + H\boldsymbol{\varepsilon} - K_e \tilde{\mathbf{E}} + \mathbf{d}\right) \\ &\quad + 2\kappa \cdot tr\left(H\tilde{W}^T(\hat{W} - W_0)\right) \end{aligned} \quad (\text{A.0.3})$$

Considering (3.3.7), (3.5.7), (3.6.4), and (3.7.9), this results in

$$\begin{aligned}
\dot{V} \leq & -\lambda_{\min}(Q)\|\mathbf{E}\|^2 - \lambda_{\min}(\tilde{Q})\|\tilde{\mathbf{E}}\|^2 + 2p_m\bar{h}\|\tilde{\mathbf{E}}\|(\|PB\| + \|\tilde{P}B\|)\|\tilde{W}\|_F + \frac{h_m}{\lambda_{\min}(\Gamma_w)}\|\tilde{W}\|_F^2 \\
& + 2(\|\mathbf{E}\|\|PB\| + \|\tilde{\mathbf{E}}\|\|\tilde{P}B\|)(2w_m p_m \bar{h} + \varepsilon_m \bar{h} + d_m) \\
& + 2(\|\mathbf{E}\|\|PB\| + \|\tilde{\mathbf{E}}\|\|\tilde{P}B\|)(k_{em}\|\tilde{\mathbf{E}}\|) + 2\kappa \cdot \text{tr}\left(H\tilde{W}^T(\hat{W} - W_0)\right)
\end{aligned} \tag{A.0.4}$$

Using completion of squares yields

$$\begin{aligned}
\dot{V} \leq & -(\lambda_{\min}(Q) - 1 - k_{em}^2\|PB\|^2)\|\mathbf{E}\|^2 \\
& - \left(\lambda_{\min}(\tilde{Q}) - 3 - 2k_{em}\|\tilde{P}B\|\right)\|\tilde{\mathbf{E}}\|^2 \\
& - \left(\kappa\bar{h} - p_m^2\bar{h}^2(\|PB\| + \|\tilde{P}B\|)^2 - \frac{h_m}{\lambda_{\min}(\Gamma_w)}\right)\|\tilde{W}\|_F^2 \\
& + (\|PB\|^2 + \|\tilde{P}B\|^2)(2w_m p_m \bar{h} + \varepsilon_m \bar{h} + d_m)^2 + \kappa\bar{h}\|W - W_0\|_F^2
\end{aligned} \tag{A.0.5}$$

where the following trace inequality of matrices was used.

$$\begin{aligned}
\text{tr}\left(\tilde{W}^T(\hat{W} - W_0)\right) & \leq \|\tilde{W}\|_F\|W - W_0\|_F - \|\tilde{W}\|_F^2 \\
& \leq -\frac{1}{2}\|\tilde{W}\|_F^2 + \frac{1}{2}\|W - W_0\|_F^2
\end{aligned} \tag{A.0.6}$$

Consequently the time derivative of the Lyapunov function V in (A.0.1) becomes negative outside of the sets, S_E , $S_{\tilde{E}}$, and S_W defined by:

$$\begin{aligned}
S_E & \triangleq \left\{ \mathbf{E} : \|\mathbf{E}\| \leq \sqrt{\frac{(\|PB\|^2 + \|\tilde{P}B\|^2)(2w_m p_m \bar{h} + \varepsilon_m \bar{h} + d_m)^2 + \kappa\bar{h}\|W - W_0\|_F^2}{\lambda_{\min}(Q) - 1 - k_{em}^2\|PB\|^2}} \right\} \\
S_{\tilde{E}} & \triangleq \left\{ \tilde{\mathbf{E}} : \|\tilde{\mathbf{E}}\| \leq \sqrt{\frac{(\|PB\|^2 + \|\tilde{P}B\|^2)(2w_m p_m \bar{h} + \varepsilon_m \bar{h} + d_m)^2 + \kappa\bar{h}\|W - W_0\|_F^2}{\lambda_{\min}(\tilde{Q}) - 3 - 2k_{em}\|\tilde{P}B\|}} \right\} \\
S_W & \triangleq \left\{ \tilde{W} : \|\tilde{W}\|_F \leq \sqrt{\frac{(\|PB\|^2 + \|\tilde{P}B\|^2)(2w_m p_m \bar{h} + \varepsilon_m \bar{h} + d_m)^2 + \kappa\bar{h}\|W - W_0\|_F^2}{\kappa\bar{h} - p_m^2\bar{h}^2(\|PB\| + \|\tilde{P}B\|)^2 - \frac{h_m}{\lambda_{\min}(\Gamma_w)}}}} \right\}
\end{aligned} \tag{A.0.7}$$

Therefore it can be concluded that $\dot{V}(\zeta)$ is negative outside a compact set.

$$B_\theta \triangleq \{ \zeta \in B_R \mid \|\zeta\| \leq \theta \} \tag{A.0.8}$$

where $\zeta = [\mathbf{E}^T \ \tilde{\mathbf{E}}^T \ \tilde{W}^T]^T$. It can be seen from (3.7.12) that $B_\theta \subset B_R$. Let β be the maximum value of the Lyapunov function $V(\zeta)$ on the boundary of B_θ as

$$\beta \triangleq \max_{\|\zeta\|=\theta} V(\zeta) \quad (\text{A.0.9})$$

Defining the set

$$\Omega_\beta \triangleq \{ \zeta \mid V(\zeta) \leq \beta \} \quad (\text{A.0.10})$$

the conditions (3.7.6), (3.7.7) and (3.7.12) ensures $\Omega_\beta \subset \Omega_\alpha$ and thus ultimate boundedness of ζ with ultimate boundedness equal to $\eta_1^{-1}(\eta_2(\theta))$. Consequently, according to Lyapunov's direct theorem, this proof demonstrates the ultimate uniform boundedness of $(\mathbf{E}, \tilde{\mathbf{E}}, \tilde{W})$ with RBF NNs. \square

APPENDIX B

PROOF OF THEOREM 3.7.2

Adaptive Nonlinear Dynamic Inversion Control Using SHL Neural Networks

Proof. Consider the following Lyapunov function candidate:

$$\mathcal{L}(\mathbf{E}, \tilde{\mathbf{E}}, \tilde{V}, \tilde{W}) = \mathbf{E}^T P \mathbf{E} + \tilde{\mathbf{E}}^T \tilde{P} \tilde{\mathbf{E}} + tr(\tilde{W}^T \Gamma_w^{-1} \tilde{W}) + tr(\tilde{V}^T \Gamma_v^{-1} \tilde{V}) \quad (\text{B.0.1})$$

The time derivative of V along the trajectories of (3.5.6) and (3.6.3) implies

$$\begin{aligned} \dot{\mathcal{L}} &= 2\mathbf{E}^T P \dot{\mathbf{E}} + 2\tilde{\mathbf{E}}^T \tilde{P} \dot{\tilde{\mathbf{E}}} - 2tr(\tilde{W}^T \Gamma_w^{-1} \dot{\tilde{W}}) - 2tr(\tilde{V}^T \Gamma_v^{-1} \dot{\tilde{V}}) \\ &= 2\mathbf{E}^T P A_M \mathbf{E} - 2\mathbf{E}^T P B (\Delta - \nu_{ad} + \mathbf{d} - K_e \tilde{\mathbf{E}}) \\ &\quad + 2\tilde{\mathbf{E}}^T \tilde{P} \tilde{A} \tilde{\mathbf{E}} - 2\tilde{\mathbf{E}}^T \tilde{P} B (\Delta - \nu_{ad} + \mathbf{d} - K_e \tilde{\mathbf{E}}) \\ &\quad - 2tr(\tilde{W}^T \Gamma_w^{-1} \dot{\tilde{W}}) - 2tr(\tilde{V}^T \Gamma_v^{-1} \dot{\tilde{V}}) \end{aligned} \quad (\text{B.0.2})$$

Substituting the σ -modification laws in (3.7.22) with recalling $\tilde{\mathbf{E}} = \mathbf{E} - \check{\mathbf{E}}$, the relation (3.3.14), and the fact that, if M_1, M_2, M_3 are matrices such that $M_1 M_2 M_3$ is a square matrix, then $tr(M_1 M_2 M_3) = tr(M_3^T M_2^T M_1^T) = tr(M_1^T M_3^T M_2^T)$, the equation $\dot{\mathcal{L}}$ in (B.0.2) becomes

$$\begin{aligned} \dot{\mathcal{L}} &= 2\mathbf{E}^T P A_M \mathbf{E} + 2\tilde{\mathbf{E}}^T \tilde{P} \tilde{A} \tilde{\mathbf{E}} - 2\tilde{\mathbf{E}}(PB + \tilde{P}B) \left(\tilde{W}^T (\hat{\sigma} - \hat{\sigma}' \hat{V}^T \boldsymbol{\mu}) + \hat{W}^T \hat{\sigma}' \tilde{V}^T \boldsymbol{\mu} \right) \\ &\quad - 2(\mathbf{E}PB + \tilde{\mathbf{E}}\tilde{P}B)(\boldsymbol{\varepsilon} - \mathbf{w} + \mathbf{d}) + 2(\mathbf{E}PB + \tilde{\mathbf{E}}\tilde{P}B)K_e \tilde{\mathbf{E}} \\ &\quad + 2\kappa_w \cdot tr(\tilde{W}^T (\hat{W} - W_0)) + 2\kappa_v \cdot tr(\tilde{V}^T (\hat{V} - V_0)) \end{aligned} \quad (\text{B.0.3})$$

Considering (3.5.7) and (3.6.4) yields

$$\begin{aligned}
\dot{\mathcal{L}} &\leq -\lambda_{\min}(Q)\|\mathbf{E}\|^2 - \lambda_{\min}(\hat{Q})\|\hat{\mathbf{E}}\|^2 - 2\tilde{\mathbf{E}}(PB + \tilde{P}B)(\Delta - \boldsymbol{\nu}_{ad}) \\
&\quad + 2(\tilde{\mathbf{E}} - \mathbf{E})PB(\boldsymbol{\varepsilon} - \mathbf{w} + \mathbf{d}) + 2(\mathbf{E}PB + \tilde{\mathbf{E}}\tilde{P}B)K_e\tilde{\mathbf{E}} \\
&\quad - \kappa_w\|\tilde{W}\|_F^2 + \kappa_w\|W - W_0\|_F^2 - \kappa_v\|\tilde{V}\|_F^2 + \kappa_v\|V - V_0\|_F^2
\end{aligned} \tag{B.0.4}$$

where the following trace inequality of matrices was used.

$$\begin{aligned}
tr\left(\tilde{W}^T(\hat{W} - W_0)\right) &\leq \|\tilde{W}\|_F\|W - W_0\|_F - \|\tilde{W}\|_F^2 \\
&\leq -\frac{1}{2}\|\tilde{W}\|_F^2 + \frac{1}{2}\|W - W_0\|_F^2
\end{aligned} \tag{B.0.5}$$

Considering (3.3.15) and (3.3.17) results in

$$\begin{aligned}
\dot{\mathcal{L}} &\leq -\lambda_{\min}(Q)\|\mathbf{E}\|^2 - \lambda_{\min}(\hat{Q})\|\hat{\mathbf{E}}\|^2 + 2\|\tilde{\mathbf{E}}\|\left(\|PB\| + \|\tilde{P}B\|\right)\left(\alpha_1\|\tilde{Z}\|_F + \alpha_2\right) \\
&\quad + 2\left(\|\tilde{\mathbf{E}}\| + \|\mathbf{E}\|\right)\|PB\|\left(\gamma_1\|\tilde{Z}\|_F + \gamma_2 + d_m\right) + 2k_{em}\left(\|\mathbf{E}\|\|PB\| + \|\tilde{\mathbf{E}}\|\|\tilde{P}B\|\right)\|\tilde{\mathbf{E}}\| \\
&\quad - \kappa_w\|\tilde{W}\|_F^2 + \kappa_w\|W - W_0\|_F^2 - \kappa_v\|\tilde{V}\|_F^2 + \kappa_v\|V - V_0\|_F^2
\end{aligned} \tag{B.0.6}$$

Assigning $p_a = \max\{\|PB\|, \|\tilde{P}B\|\}$, $\kappa_a = \min\{\kappa_v, \kappa_w\}$, and using completion of squares yield

$$\begin{aligned}
\dot{\mathcal{L}} &\leq -(\lambda_{\min}(Q) - \gamma_1\|PB\|(1 + \gamma_2 + d_m) - 2p_ak_{em})\|\mathbf{E}\|^2 \\
&\quad - \left(\lambda_{\min}(\tilde{Q}) - 2p_a(\alpha_1 + \alpha_2) - \gamma_1\|PB\|(1 + \gamma_2 + d_m) - 6p_ak_{em}\right)\|\tilde{\mathbf{E}}\|^2 \\
&\quad - (\kappa_a - 2\alpha_1p_a - 2\gamma_1\|PB\|)\|\tilde{Z}\|_F^2 \\
&\quad + 2\alpha_1p_a + 2\gamma_1(\gamma_2 + d_m)\|PB\| + \kappa_w\|W - W_0\|_F^2 + \kappa_v\|V - V_0\|_F^2
\end{aligned} \tag{B.0.7}$$

Consequently, recalling

$$\|\tilde{Z}\|_F = \left\| \begin{bmatrix} \tilde{W} & 0 \\ 0 & \tilde{V} \end{bmatrix} \right\|_F = \|\tilde{W}\|_F + \|\tilde{V}\|_F$$

the time derivative of the Lyapunov function \mathcal{L} in (B.0.1) becomes negative outside of the sets, $S_E, S_{\tilde{E}}, S_Z$ defined by:

$$\begin{aligned}
S_E &\triangleq \left\{ \mathbf{E} : \|\mathbf{E}\| \leq \sqrt{\frac{2\alpha_1 p_a + 2\gamma_1(\gamma_2 + d_m)\|PB\| + \kappa_w\|W - W_0\|_F^2 + \kappa_v\|V - V_0\|_F^2}{\lambda_{\min}(Q) - \gamma_1\|PB\|(1 + \gamma_2 + d_m) - 2p_a k_{em}}} \right\} \\
S_{\tilde{E}} &\triangleq \left\{ \tilde{\mathbf{E}} : \|\tilde{\mathbf{E}}\| \leq \sqrt{\frac{2\alpha_1 p_a + 2\gamma_1(\gamma_2 + d_m)\|PB\| + \kappa_w\|W - W_0\|_F^2 + \kappa_v\|V - V_0\|_F^2}{\lambda_{\min}(\tilde{Q}) - 2p_a(\alpha_1 + \alpha_2) - \gamma_1\|PB\|(1 + \gamma_2 + d_m) - 6p_a k_{em}}} \right\} \\
S_{\tilde{Z}} &\triangleq \left\{ \tilde{Z} : \|\tilde{Z}\|_F \leq \sqrt{\frac{2\alpha_1 p_a + 2\gamma_1(\gamma_2 + d_m)\|PB\| + \kappa_w\|W - W_0\|_F^2 + \kappa_v\|V - V_0\|_F^2}{\kappa_a - 2\alpha_1 p_a - 2\gamma_1\|PB\|}} \right\}
\end{aligned} \tag{B.0.8}$$

Therefore it can be concluded that $\dot{\mathcal{L}}(\zeta)$ is negative outside a compact set.

$$B_\lambda \triangleq \{ \zeta \in B_R \mid \|\zeta\| \leq \lambda \} \tag{B.0.9}$$

where $\zeta = [\mathbf{E}^T \ \tilde{\mathbf{E}}^T \ \tilde{W}^T \ \tilde{V}^T]^T$. It can be seen from (3.7.19) that $B_\lambda \subset B_R$. Let β be the maximum value of the Lyapunov function $\mathcal{L}(\zeta)$ on the boundary of B_λ as

$$\beta \triangleq \max_{\|\zeta\|=\lambda} \mathcal{L}(\zeta) \tag{B.0.10}$$

Defining the set

$$\Omega_\beta \triangleq \{ \zeta \mid \mathcal{L}(\zeta) \leq \beta \} \tag{B.0.11}$$

the conditions (3.7.6), (3.7.7) and (3.7.19) ensures $\Omega_\beta \subset \Omega_\alpha$ and thus ultimate boundedness of ζ with ultimate boundedness equal to $\varphi_1^{-1}(\varphi_2(\lambda))$. Consequently, according to Lyapunov's direct theorem, this proof demonstrates the ultimate uniform boundedness of $(\mathbf{E}, \tilde{\mathbf{E}}, \tilde{Z})$, or $(\mathbf{E}, \tilde{\mathbf{E}}, \tilde{V}, \tilde{W})$ with SHL NNs. \square

APPENDIX C

PROOF OF THEOREM 7.7.1

Composite Model Reference Adaptive NDI Control Using RBF Neural Networks

Proof. Consider the following Lyapunov function candidate:

$$V(\mathbf{E}, \hat{\mathbf{E}}, \tilde{K}_e, \tilde{K}_r, \tilde{W}) = \mathbf{E}^T P \mathbf{E} + \hat{\mathbf{E}}^T \hat{P} \hat{\mathbf{E}} + tr \left(\tilde{K}_e^T \Gamma_e^{-1} \tilde{K}_e + \tilde{K}_r^T \Gamma_r^{-1} \tilde{K}_r + H \cdot \tilde{W}^T \Gamma_w^{-1} \tilde{W} \right) \quad (\text{C.0.1})$$

The time derivative of V along the trajectories of (7.5.10) and (7.6.3) implies

$$\begin{aligned} \dot{V} &= 2\mathbf{E}^T P \dot{\mathbf{E}} + 2\hat{\mathbf{E}}^T \hat{P} \dot{\hat{\mathbf{E}}} - 2tr \left(\tilde{K}_e^T \Gamma_e^{-1} \dot{\tilde{K}}_e + \tilde{K}_r^T \Gamma_r^{-1} \dot{\tilde{K}}_r + H \cdot \tilde{W}^T \Gamma_w^{-1} \dot{\tilde{W}} \right) + 2tr \left(\dot{H} \cdot \tilde{W}^T \Gamma_w^{-1} \tilde{W} \right) \\ &= 2\mathbf{E}^T P A_M \mathbf{E} - 2\mathbf{E}^T P B \left(\tilde{K}_e \mathbf{y} - \tilde{K}_r \mathbf{y}_c + \Delta - \boldsymbol{\nu}_{ad} + \mathbf{d} \right) \\ &\quad + 2\hat{\mathbf{E}}^T \hat{P} A_P \hat{\mathbf{E}} - 2\hat{\mathbf{E}}^T \hat{P} B \left(\tilde{K}_e \mathbf{y} - \tilde{K}_r \mathbf{y}_c + \Delta - \boldsymbol{\nu}_{ad} + \mathbf{d} \right) \\ &\quad - 2tr \left(\tilde{K}_e^T \Gamma_e^{-1} \dot{\tilde{K}}_e + \tilde{K}_r^T \Gamma_r^{-1} \dot{\tilde{K}}_r + H \cdot \tilde{W}^T \Gamma_w^{-1} \dot{\tilde{W}} \right) + 2tr \left(\dot{H} \cdot \tilde{W}^T \Gamma_w^{-1} \tilde{W} \right) \end{aligned} \quad (\text{C.0.2})$$

Substituting the σ -modification laws in (7.7.16) with recalling the relations (3.3.6) and (7.3.9), and the fact that, if M_1, M_2, M_3 are matrices such that $M_1 M_2 M_3$ is a square matrix, then $tr(M_1 M_2 M_3) = tr(M_3^T M_2^T M_1^T) = tr(M_1^T M_3^T M_2^T)$, the equation \dot{V} in (C.0.2) becomes

$$\begin{aligned} \dot{V} &= 2\mathbf{E}^T P A_M \mathbf{E} + 2\hat{\mathbf{E}}^T \hat{P} A_P \hat{\mathbf{E}} + 2\rho_e \cdot tr \left(\tilde{K}_e^T (\hat{K}_e - K_{eo}) \right) + 2\rho_r \cdot tr \left(\tilde{K}_r^T (\hat{K}_e - K_{eo}) \right) \\ &\quad + 2\rho_w \kappa \cdot tr \left(H \tilde{W}^T (\hat{W} - W_o) \right) + 2tr \left(\dot{H} \cdot \tilde{W}^T \Gamma_w^{-1} \tilde{W} \right) \\ &\quad + 2 \left(\mathbf{E}^T P B + \hat{\mathbf{E}}^T \hat{P} B \right) \cdot \{ HW^T (\Psi(\boldsymbol{\mu}) - \Psi(\mathbf{x}, \boldsymbol{\nu}_l)) - H\boldsymbol{\varepsilon} - \mathbf{d} \} \end{aligned} \quad (\text{C.0.3})$$

Considering (3.3.7), (7.5.11), (7.6.4), and (7.7.9), this results in

$$\begin{aligned}
\dot{V} \leq & -\lambda_{\min}(Q)\|\mathbf{E}\|^2 - \lambda_{\min}(\hat{Q})\|\hat{\mathbf{E}}\|^2 + \frac{h_m}{\lambda_{\min}(\Gamma_w)}\|\tilde{W}\|_F^2 \\
& + \rho_e \left(\|K_e - K_{eo}\|_F^2 - \|\tilde{K}_e\|_F^2 \right) + \rho_r \left(\|K_r - K_{ro}\|_F^2 - \|\tilde{K}_r\|_F^2 \right) + \kappa\bar{h} \left(\|W - W_0\|_F^2 - \|\tilde{W}\|_F^2 \right) \\
& + 2 \left(\|\mathbf{E}\| \|PB\| + \|\hat{\mathbf{E}}\| \|\tilde{P}B\| + \|\hat{\mathbf{E}}\| \|\hat{P}B\| \right) (2w_m p_m \bar{h} + \varepsilon_m \bar{h} + d_m)
\end{aligned} \tag{C.0.4}$$

where the following trace inequality of matrices was used.

$$\begin{aligned}
\text{tr} \left(\tilde{W}^T (\hat{W} - W_0) \right) & \leq \|\tilde{W}\|_F \|W - W_0\|_F - \|\tilde{W}\|_F^2 \\
& \leq -\frac{1}{2} \|\tilde{W}\|_F^2 + \frac{1}{2} \|W - W_0\|_F^2
\end{aligned} \tag{C.0.5}$$

Using completion of squares yields

$$\begin{aligned}
\dot{V} \leq & -(\lambda_{\min}(Q) - 1)\|\mathbf{E}\|^2 - \left(\lambda_{\min}(\hat{Q}) - 1 \right) \|\hat{\mathbf{E}}\|^2 - \rho_e \|\tilde{K}_e\|_F^2 - \rho_r \|\tilde{K}_r\|_F^2 - \kappa\bar{h} \|\tilde{W}\|_F^2 \\
& + \rho_e \|K_e - K_{eo}\|_F^2 + \rho_r \|K_r - K_{ro}\|_F^2 + \kappa\bar{h} \|W - W_0\|_F^2 \\
& + \left(\|PB\|^2 + \|\tilde{P}B\|^2 + \|\hat{P}B\|^2 \right) (2w_m p_m \bar{h} + \varepsilon_m \bar{h} + d_m)^2
\end{aligned} \tag{C.0.6}$$

Consequently the time derivative of the Lyapunov function V in (C.0.1) becomes negative outside of the sets, S_E , $S_{\hat{E}}$, S_{K_e} , S_{K_r} , and S_W defined by:

$$\begin{aligned}
S_E & \triangleq \left\{ \mathbf{E} : \|\mathbf{E}\| \leq \sqrt{\frac{\Pi_1 + \Pi_2}{\lambda_{\min}(Q) - 1}} \right\} \\
S_{\hat{E}} & \triangleq \left\{ \hat{\mathbf{E}} : \|\hat{\mathbf{E}}\| \leq \sqrt{\frac{\Pi_1 + \Pi_2}{\lambda_{\min}(\hat{Q}) - 1}} \right\} \\
S_{K_e} & \triangleq \left\{ \tilde{K}_e : \|\tilde{K}_e\|_F \leq \sqrt{\frac{\Pi_1 + \Pi_2}{\rho_e}} \right\} \\
S_{K_r} & \triangleq \left\{ \tilde{K}_r : \|\tilde{K}_r\|_F \leq \sqrt{\frac{\Pi_1 + \Pi_2}{\rho_r}} \right\} \\
S_W & \triangleq \left\{ \tilde{W} : \|\tilde{W}\|_F \leq \sqrt{\frac{\Pi_1 + \Pi_2}{\kappa\bar{h}}} \right\}
\end{aligned} \tag{C.0.7}$$

where

$$\begin{aligned}\Pi_1 &\triangleq \rho_e \|K_e - K_{e0}\|_F^2 + \rho_r \|K_r - K_{r0}\|_F^2 + \kappa \bar{h} \|W - W_0\|_F^2 \\ \Pi_2 &\triangleq \left(\|PB\|^2 + \|\tilde{P}B\|^2 + \|\hat{P}B\|^2 \right) (2w_m p_m \bar{h} + \varepsilon_m \bar{h} + d_m)^2\end{aligned}\tag{C.0.8}$$

Therefore it can be concluded that $\dot{V}(\zeta)$ is negative outside a compact set.

$$B_\theta \triangleq \{ \zeta \in B_R \mid \|\zeta\| \leq \theta \}\tag{C.0.9}$$

where $\zeta = \left[\mathbf{E}^T \ \hat{\mathbf{E}}^T \ \tilde{K}_e^T \ \tilde{K}_r^T \ \tilde{W}^T \right]^T$. It can be seen from (7.7.12) that $B_\theta \subset B_R$. Let β be the maximum value of the Lyapunov function $V(\zeta)$ on the boundary of B_θ as

$$\beta \triangleq \max_{\|\zeta\|=\theta} V(\zeta)\tag{C.0.10}$$

Defining the set

$$\Omega_\beta \triangleq \{ \zeta \mid V(\zeta) \leq \beta \}\tag{C.0.11}$$

the conditions (7.7.6), (7.7.7) and (7.7.12) ensures $\Omega_\beta \subset \Omega_\alpha$ and thus ultimate boundedness of ζ with ultimate boundedness equal to $\eta_1^{-1}(\eta_2(\theta))$. Consequently, according to Lyapunov's direct theorem, this proof demonstrates the ultimate uniform boundedness of $(\mathbf{E}, \hat{\mathbf{E}}, \tilde{K}_e, \tilde{K}_r, \tilde{W})$ with RBF NNs. \square

APPENDIX D

PROOF OF THEOREM 7.7.2

Composite Model Reference Adaptive NDI Control Using SHL Neural Networks

Proof. Consider the following Lyapunov function candidate:

$$\begin{aligned} \mathcal{L} \left(\mathbf{E}, \hat{\mathbf{E}}, \tilde{K}_e, \tilde{K}_r, \tilde{V}, \tilde{W} \right) &= \mathbf{E}^T P \mathbf{E} + \hat{\mathbf{E}}^T \hat{P} \hat{\mathbf{E}} \\ &+ tr \left(\tilde{K}_e^T \Gamma_e^{-1} \tilde{K}_e + \tilde{K}_r^T \Gamma_r^{-1} \tilde{K}_r + \tilde{V}^T \Gamma_v^{-1} \tilde{V} + \tilde{W}^T \Gamma_w^{-1} \tilde{W} \right) \end{aligned} \quad (\text{D.0.1})$$

The time derivative of V along the trajectories of (7.5.10) and (7.6.3) implies

$$\begin{aligned} \dot{\mathcal{L}} &= 2\mathbf{E}^T P \dot{\mathbf{E}} + 2\hat{\mathbf{E}}^T \hat{P} \dot{\hat{\mathbf{E}}} - 2tr \left(\tilde{K}_e^T \Gamma_e^{-1} \dot{\tilde{K}}_e + \tilde{K}_r^T \Gamma_r^{-1} \dot{\tilde{K}}_r + \tilde{V}^T \Gamma_v^{-1} \dot{\tilde{V}} + \tilde{W}^T \Gamma_w^{-1} \dot{\tilde{W}} \right) \\ &= 2\mathbf{E}^T P A_M \mathbf{E} - 2\mathbf{E}^T P B \left(\tilde{K}_e \mathbf{y} - \tilde{K}_r \mathbf{y}_c + \Delta - \boldsymbol{\nu}_{ad} + \mathbf{d} \right) \\ &+ 2\hat{\mathbf{E}}^T \hat{P} A_P \hat{\mathbf{E}} - 2\hat{\mathbf{E}}^T \hat{P} B \left(\tilde{K}_e \mathbf{y} - \tilde{K}_r \mathbf{y}_c + \Delta - \boldsymbol{\nu}_{ad} + \mathbf{d} \right) \\ &- 2tr \left(\tilde{K}_e^T \Gamma_e^{-1} \dot{\tilde{K}}_e + \tilde{K}_r^T \Gamma_r^{-1} \dot{\tilde{K}}_r + \tilde{V}^T \Gamma_v^{-1} \dot{\tilde{V}} + \tilde{W}^T \Gamma_w^{-1} \dot{\tilde{W}} \right) \end{aligned} \quad (\text{D.0.2})$$

Substituting the σ -modification laws in (7.7.22) with recalling the relation (2.2.13), and the fact that, if M_1, M_2, M_3 are matrices such that $M_1 M_2 M_3$ is a square matrix, then $tr(M_1 M_2 M_3) = tr(M_3^T M_2^T M_1^T) = tr(M_1^T M_3^T M_2^T)$, the equation \dot{V} in (D.0.2) becomes

$$\begin{aligned} \dot{\mathcal{L}} &= 2\mathbf{E}^T P A_M \mathbf{E} + 2\hat{\mathbf{E}}^T \hat{P} A_P \hat{\mathbf{E}} + 2\rho_e \cdot tr \left(\tilde{K}_e^T (\hat{K}_e - K_{eo}) \right) + 2\rho_r \cdot tr \left(\tilde{K}_r^T (\hat{K}_e - K_{eo}) \right) \\ &+ 2\kappa_v \cdot tr \left(\tilde{V}^T (\hat{V} - V_o) \right) + 2\kappa_w \cdot tr \left(\tilde{W}^T (\hat{W} - W_o) \right) \\ &- 2 \left(\mathbf{E}^T P B + \hat{\mathbf{E}}^T \hat{P} B \right) (\Delta - \boldsymbol{\nu}_{ad} + \mathbf{d}) - 2 \left(\mathbf{E}^T P B + \hat{\mathbf{E}}^T \hat{P} B \right) (\boldsymbol{\varepsilon} - \mathbf{w}) \\ &+ 2 \left(\mathbf{E}^T P B + \hat{\mathbf{E}}^T \hat{P} B \right) \left(\tilde{W}^T \left(\hat{\boldsymbol{\sigma}} - \hat{\boldsymbol{\sigma}}' \hat{V}^T \boldsymbol{\mu} \right) + \hat{W}^T \hat{\boldsymbol{\sigma}}' \tilde{V}^T \boldsymbol{\mu} + \boldsymbol{\varepsilon} - \mathbf{w} \right) \end{aligned} \quad (\text{D.0.3})$$

Considering (3.3.15), (7.5.11), and (7.6.4), this yields

$$\begin{aligned}
\dot{\mathcal{L}} &\leq -\lambda_{\min}(Q)\|\mathbf{E}\|^2 - \lambda_{\min}(\hat{Q})\|\hat{\mathbf{E}}\|^2 + \left(\|\mathbf{E}\|\|PB\| + \|\hat{\mathbf{E}}\|\|\hat{P}B\|\right) d_m \\
&\quad + \left(\|\mathbf{E}\|\|PB\| + \|\hat{\mathbf{E}}\|\|\hat{P}B\|\right) \left(\gamma_1\|\tilde{Z}\|_F + \gamma_2\right) \\
&\quad - \rho_e\|\tilde{K}_e\|_F^2 + \rho_e\|K_e - K_{eo}\|_F^2 - \rho_r\|\tilde{K}_r\|_F^2 + \rho_r\|K_r - K_{ro}\|_F^2 \\
&\quad - \kappa_v\|\tilde{V}\|_F^2 + \kappa_v\|V - V_0\|_F^2 - \kappa_w\|\tilde{W}\|_F^2 + \kappa_w\|W - W_0\|_F^2
\end{aligned} \tag{D.0.4}$$

where the following trace inequality of matrices was used.

$$\begin{aligned}
tr\left(\tilde{K}_e^T(\hat{K}_e - K_{eo})\right) &\leq \|\tilde{K}_e\|_F\|K_e - K_{eo}\|_F - \|\tilde{K}_e\|_F^2 \\
&\leq -\frac{1}{2}\|\tilde{K}_e\|_F^2 + \frac{1}{2}\|K_e - K_{eo}\|_F^2
\end{aligned} \tag{D.0.5}$$

Assigning $p_b = \max\{\|PB\|, \|\hat{P}B\|\}$, $\kappa_b = \min\{\kappa_v, \kappa_w\}$, and using completion of squares result in

$$\begin{aligned}
\dot{\mathcal{L}} &\leq -(\lambda_{\min}(Q) - p_b(\gamma_1 + \gamma_2 + d_m))\|\mathbf{E}\|^2 - \left(\lambda_{\min}(\hat{Q}) - p_b(\gamma_1 + \gamma_2 + d_m)\right)\|\hat{\mathbf{E}}\|^2 \\
&\quad - (\kappa_b - 2\gamma_1 p_b)\|\tilde{Z}\|_F^2 - \rho_e\|\tilde{K}_e\|_F^2 - \rho_r\|\tilde{K}_r\|_F^2 \\
&\quad + 2p_b(\gamma_2 + d_m) + \rho_e\|K_e - K_{eo}\|_F^2 + \rho_r\|K_r - K_{ro}\|_F^2 + \kappa_v\|V - V_0\|_F^2 + \kappa_w\|W - W_0\|_F^2
\end{aligned} \tag{D.0.6}$$

Consequently, recalling

$$\|\tilde{Z}\|_F = \left\| \begin{bmatrix} \tilde{W} & 0 \\ 0 & \tilde{V} \end{bmatrix} \right\|_F = \|\tilde{W}\|_F + \|\tilde{V}\|_F$$

the time derivative of the Lyapunov function \mathcal{L} in (D.0.1) becomes negative outside of the sets, S_E , $S_{\hat{E}}$, S_{K_e} , S_{K_r} , and $S_{\tilde{Z}}$ defined by:

$$\begin{aligned}
S_E &\triangleq \left\{ \mathbf{E} : \|\mathbf{E}\| \leq \sqrt{\frac{\Omega_1 + \Omega_2}{\lambda_{\min}(Q) - p_b(\gamma_1 + \gamma_2 + d_m)}} \right\} \\
S_{\hat{\mathbf{E}}} &\triangleq \left\{ \hat{\mathbf{E}} : \|\hat{\mathbf{E}}\| \leq \sqrt{\frac{\Omega_1 + \Omega_2}{\lambda_{\min}(\hat{Q}) - p_b(\gamma_1 + \gamma_2 + d_m)}} \right\} \\
S_{K_e} &\triangleq \left\{ \tilde{K}_e : \|\tilde{K}_e\|_F \leq \sqrt{\frac{\Omega_1 + \Omega_2}{\rho_e}} \right\} \\
S_{K_r} &\triangleq \left\{ \tilde{K}_r : \|\tilde{K}_r\|_F \leq \sqrt{\frac{\Omega_1 + \Omega_2}{\rho_r}} \right\} \\
S_{\tilde{Z}} &\triangleq \left\{ \tilde{Z} : \|\tilde{Z}\|_F \leq \sqrt{\frac{\Omega_1 + \Omega_2}{\kappa_b - 2\gamma_1 p_b}} \right\}
\end{aligned} \tag{D.0.7}$$

where

$$\begin{aligned}
\Omega_1 &\triangleq \kappa_b - 2\gamma_1 p_b \\
\Omega_2 &\triangleq \rho_e \|K_e - K_{eo}\|_F^2 + \rho_r \|K_r - K_{ro}\|_F^2 + \kappa_v \|V - V_0\|_F^2 + \kappa_w \|W - W_0\|_F^2
\end{aligned} \tag{D.0.8}$$

Therefore it can be concluded that $\dot{\mathcal{L}}(\zeta)$ is negative outside a compact set.

$$B_\lambda \triangleq \{ \zeta \in B_R \mid \|\zeta\| \leq \lambda \} \tag{D.0.9}$$

where $\zeta = [\mathbf{E}^T \ \hat{\mathbf{E}}^T \ \tilde{K}_e^T \ \tilde{K}_r^T \ \tilde{W}^T \ \tilde{V}^T]^T$. It can be seen from (7.7.19) that $B_\lambda \subset B_R$. Let β be the maximum value of the Lyapunov function $\mathcal{L}(\zeta)$ on the boundary of B_λ as

$$\beta \triangleq \max_{\|\zeta\|=\lambda} \mathcal{L}(\zeta) \tag{D.0.10}$$

Defining the set

$$\Omega_\beta \triangleq \{ \zeta \mid \mathcal{L}(\zeta) \leq \beta \} \tag{D.0.11}$$

the conditions (7.7.6), (7.7.7) and (7.7.19) ensures $\Omega_\beta \subset \Omega_\alpha$ and thus ultimate boundedness of ζ with ultimate boundedness equal to $\varphi_1^{-1}(\varphi_2(\lambda))$. Consequently, according to Lyapunov's direct theorem, this proof demonstrates the ultimate uniform boundedness of $(\mathbf{E}, \hat{\mathbf{E}}, \tilde{K}_e, \tilde{K}_r, \tilde{Z})$, or $(\mathbf{E}, \hat{\mathbf{E}}, \tilde{K}_e, \tilde{K}_r, \tilde{V}, \tilde{W})$ with SHL NNs. \square

APPENDIX E

AIRCRAFT EQUATIONS OF MOTION

The aircraft dynamic equations used in this thesis for nonlinear dynamic inversion are given in this Appendix. The aircraft dynamics are divided into slow and fast dynamics. First accurate expressions are presented for the slow and fast dynamics [5, 108, 121]. Then a set of assumptions are introduced to simplify these expressions needed for the inversion process outlined in Chapters 4 and 6.

E.1 The Slow Dynamics

The slow dynamics can be written in the following form

$$\begin{bmatrix} \dot{\alpha} \\ \ddot{\alpha} \\ \dot{\beta} \\ \ddot{\beta} \\ \dot{\phi} \\ \dot{\theta} \\ \dot{V} \\ \ddot{V} \end{bmatrix} = \begin{bmatrix} f_1(\mathbf{x}) \\ f_2(\mathbf{x}, \boldsymbol{\delta}) \\ f_3(\mathbf{x}) \\ f_4(\mathbf{x}, \boldsymbol{\delta}) \\ f_5(\mathbf{x}, \boldsymbol{\delta}) \\ f_6(\mathbf{x}, \boldsymbol{\delta}) \\ f_7(\mathbf{x}, \boldsymbol{\delta}) \\ f_8(\mathbf{x}, \boldsymbol{\delta}, \dot{\boldsymbol{\delta}}) \end{bmatrix} + \begin{bmatrix} 0 & 0 & 0 \\ -\tan(\beta) & 1 & 0 \\ 0 & 0 & 0 \\ 0 & 0 & -1 \\ 0 & 0 & 0 \\ 0 & 0 & 0 \\ 0 & 0 & 0 \\ 0 & 0 & 0 \end{bmatrix} \begin{bmatrix} \dot{p}_s \\ \dot{q} \\ \dot{r}_s \end{bmatrix} \quad (\text{E.1.1})$$

where

$$\begin{aligned}
 \dot{\alpha} &= q - [p \cos(\alpha) + r \sin(\alpha)] \tan(\beta) + \frac{1}{V \cos(\beta)} [-\sin(\alpha)(A_X + G_x + A_{T_x}) + \cos(\alpha)(A_Z + G_z + A_{T_z})] \\
 &= q - p_s \tan(\beta) + \frac{1}{V \cos(\beta)} [-a_x \sin(\alpha) + a_z \cos(\alpha)] \\
 &= f_1(\mathbf{x})
 \end{aligned}$$

(E.1.2)

$$\begin{aligned}
\ddot{\alpha} &= \dot{q} - \dot{p}_s \tan(\beta) - \frac{\sin(\alpha)}{V \cos(\beta)} \cdot \dot{a}_x + \frac{\cos(\alpha)}{V \cos(\beta)} \cdot \dot{a}_z - \frac{1}{V^2 \cos(\beta)} [-a_x \sin(\alpha) + a_z \cos(\alpha)] \cdot \dot{V} \\
&\quad - \frac{1}{V \cos(\beta)} [a_x \cos(\alpha) + a_z \sin(\alpha)] \cdot \dot{\alpha} + \left[-\frac{p_s}{\cos^2(\beta)} + \frac{\tan(\beta)}{V \cos(\beta)} (-a_x \sin(\alpha) + a_z \cos(\alpha)) \right] \cdot \dot{\beta} \\
&= f_2(\mathbf{x}) - \dot{p}_s \tan(\beta) + \dot{q}
\end{aligned} \tag{E.1.3}$$

$$\begin{aligned}
\dot{\beta} &= -r_s + \frac{1}{V} [-\cos(\alpha) \sin(\beta)(A_X + G_x + A_{T_x}) + \cos(\beta)(A_Y + G_y + A_{T_y}) \\
&\quad - \sin(\alpha) \sin(\beta)(A_Z + G_z + A_{T_z})] \\
&= -r_s + \frac{1}{V} [-a_x \cos(\alpha) \sin(\beta) + a_y \cos(\beta) - a_z \sin(\alpha) \sin(\beta)] \\
&= f_3(\mathbf{x})
\end{aligned} \tag{E.1.4}$$

$$\begin{aligned}
\ddot{\beta} &= -\dot{r}_s - \frac{1}{V} \cos(\alpha) \sin(\beta) \cdot \dot{a}_x + \frac{1}{V} \cos(\beta) \cdot \dot{a}_y - \frac{1}{V} \sin(\alpha) \sin(\beta) \cdot \dot{a}_z \\
&\quad - \frac{1}{V^2} [-a_x \cos(\alpha) \sin(\beta) + a_y \cos(\beta) - a_z \sin(\alpha) \sin(\beta)] \cdot \dot{V} \\
&\quad + \frac{1}{V} [a_x \sin(\alpha) \sin(\beta) - a_z \cos(\alpha) \sin(\beta)] \cdot \dot{\alpha} \\
&\quad - \frac{1}{V} [a_x \cos(\alpha) \cos(\beta) + a_y \sin(\beta) + a_z \sin(\alpha) \cos(\beta)] \cdot \dot{\beta} \\
&= f_4(\mathbf{x}) - \dot{r}_s
\end{aligned} \tag{E.1.5}$$

$$\begin{aligned}
\dot{\phi} &= p + q \cdot \tan(\theta) \sin(\phi) + r \cdot \tan(\theta) \cos(\phi) \\
&= f_5(\mathbf{x})
\end{aligned} \tag{E.1.6}$$

$$\begin{aligned}
\dot{\theta} &= q \cdot \cos(\phi) - r \cdot \sin(\phi) \\
&= f_6(\mathbf{x})
\end{aligned} \tag{E.1.7}$$

$$\begin{aligned}
\dot{V} &= \cos(\alpha) \cos(\beta)(A_X + G_x + A_{T_x}) + \sin(\beta)(A_Y + G_y + A_{T_y}) + \sin(\alpha) \cos(\beta)(A_Z + G_z + A_{T_z}) \\
&= a_x \cos(\alpha) \cos(\beta) + a_y \sin(\beta) + a_z \sin(\alpha) \cos(\beta) \\
&= f_7(\mathbf{x})
\end{aligned} \tag{E.1.8}$$

$$\begin{aligned}
\ddot{V} &= \dot{a}_x \cdot \cos(\alpha) \cos(\beta) + \dot{a}_y \cdot \sin(\beta) + \dot{a}_z \cdot \sin(\alpha) \cos(\beta) \\
&+ [-a_x \sin(\alpha) \cos(\beta) + a_z \cos(\alpha) \cos(\beta)] \cdot \dot{\alpha} \\
&+ [-a_x \cos(\alpha) \sin(\beta) + a_y \cos(\beta) - a_z \sin(\alpha) \sin(\beta)] \cdot \dot{\beta} \\
&= f_{\mathcal{S}}(\mathbf{x})
\end{aligned} \tag{E.1.9}$$

In the above equations, a_x, a_y, a_z are the total accelerations along the body x,y,z axes due to aerodynamic forces, gravity and thrust:

$$\begin{aligned}
a_x &= A_X + G_x + A_{Tx} \\
a_y &= A_Y + G_y + A_{Ty} \\
a_z &= A_Z + G_z + A_{Tz}
\end{aligned} \tag{E.1.10}$$

where, A_X, A_Y, A_Z are the accelerations due to aerodynamic forces along the body x,y,z axes. These can be written using wind axis forces, drag(D), sideforce(Y) and lift(L). It is noted that this is necessary because F-15 database consists of these wind axis components [8]:

$$\begin{aligned}
\begin{bmatrix} A_X \\ A_Y \\ A_Z \end{bmatrix} &= \frac{1}{m} \cdot \begin{bmatrix} \cos(\alpha) \cos(\beta) & -\cos(\alpha) \sin(\beta) & -\sin(\alpha) \\ \sin(\beta) & \cos(\beta) & 0 \\ \sin(\alpha) \cos(\beta) & -\sin(\alpha) \sin(\beta) & \cos(\alpha) \end{bmatrix} \begin{bmatrix} -D \\ Y \\ -L \end{bmatrix}_{WIND} \\
&= \frac{1}{m} \cdot \begin{bmatrix} -D \cos(\alpha) \cos(\beta) - Y \cos(\alpha) \sin(\beta) + L \sin(\alpha) \\ -D \sin(\beta) + Y \cos(\beta) \\ -D \sin(\alpha) \cos(\beta) - Y \sin(\alpha) \sin(\beta) - L \cos(\alpha) \end{bmatrix}
\end{aligned} \tag{E.1.11}$$

where

$$\begin{aligned}
D &= D_0 + D_\alpha \cdot \alpha + D_{\delta e} \cdot \delta e \\
Y &= Y_\beta \cdot \beta + Y_{\delta a} \cdot \delta a + Y_{\delta r} \cdot \delta r \\
L &= L_0 + L_\alpha \cdot \alpha + L_{\delta e} \cdot \delta e
\end{aligned} \tag{E.1.12}$$

G_x, G_y, G_z are the components of gravity along the body x,y,z axes:

$$\begin{aligned} G_x &= -g \cdot \sin(\theta) \\ G_y &= g \cdot \cos(\theta) \sin(\phi) \\ G_z &= g \cdot \cos(\theta) \cos(\phi) \end{aligned} \tag{E.1.13}$$

Including the thrust vectoring nozzles, the control vector has a total of seven elements

$$\boldsymbol{\delta} = [\delta e \quad \delta a \quad \delta r \quad \delta p_1 \quad \delta y_1 \quad \delta p_2 \quad \delta y_2]^T \tag{E.1.14}$$

where δp_1 and δy_1 are the pitch and yaw vectoring of left engine, and δp_2 and δy_2 are the pitch and yaw vectoring of right engine.

The forces produced by thrust vectored engines along three axes are described as follows.

$$\begin{aligned} F_{Tx} &= T_p \cdot \{\cos(\delta p_1) \cos(\delta y_1) + \cos(\delta p_2) \cos(\delta y_2)\} \\ F_{Ty} &= T_p \cdot \{\sin(\delta y_1) + \sin(\delta y_2)\} \\ F_{Tz} &= -T_p \cdot \{\sin(\delta p_1) \cos(\delta y_1) + \sin(\delta p_2) \cos(\delta y_2)\} \end{aligned} \tag{E.1.15}$$

where T_p denotes the thrust of a single engine, i.e. $T = 2T_p$.

If small TVC angles are assumed, these equations for the forces can be simplified to:

$$\begin{aligned} F_{Tx} &\cong T = 2 \cdot T_p \\ F_{Ty} &\cong T_p \cdot \{\delta y_1 + \delta y_2\} \\ F_{Tz} &\cong -T_p \cdot \{\delta p_1 + \delta p_2\} \end{aligned} \tag{E.1.16}$$

The accelerations due to thrust and TVC along the body x,y,z axes, A_{Tx}, A_{Ty} and A_{Tz} in (E.1.10) can thus be approximated by:

$$\begin{aligned} A_{Tx} &= \frac{F_{Tx}}{m} \cong \frac{T}{m} \\ A_{Ty} &= \frac{F_{Ty}}{m} \cong \frac{T_p}{m} \cdot \{\delta y_1 + \delta y_2\} \\ A_{Tz} &= \frac{F_{Tz}}{m} \cong -\frac{T_p}{m} \cdot \{\delta p_1 + \delta p_2\} \end{aligned} \tag{E.1.17}$$

The jerk terms in (E.1.9) can be expressed in the following form:

$$\begin{aligned}
\begin{bmatrix} \dot{a}_x \\ \dot{a}_y \\ \dot{a}_z \end{bmatrix} &= \begin{bmatrix} \dot{G}_x + \dot{A}_{Tx} \\ \dot{G}_y + \dot{A}_{Ty} \\ \dot{G}_z + \dot{A}_{Tz} \end{bmatrix} + \begin{bmatrix} A_{X\delta_e} & A_{X\delta_a} & A_{X\delta_r} \\ A_{Y\delta_e} & A_{Y\delta_a} & A_{Y\delta_r} \\ A_{Z\delta_e} & A_{Z\delta_a} & A_{Z\delta_r} \end{bmatrix} \begin{bmatrix} \dot{\delta}_e \\ \dot{\delta}_a \\ \dot{\delta}_r \end{bmatrix} \\
&+ \frac{1}{V} \begin{bmatrix} 2A_X & A_{X\alpha} & A_{X\beta} \\ 2A_Y & A_{Y\alpha} & A_{Y\beta} \\ 2A_Z & A_{Z\alpha} & A_{Z\beta} \end{bmatrix} \cdot C(\alpha, \beta) \cdot \begin{bmatrix} a_x \\ a_y \\ a_z \end{bmatrix} + V \cdot \begin{bmatrix} r \sin(\beta) - q \sin(\alpha) \cos(\beta) \\ p \sin(\alpha) \cos(\beta) - r \cos(\alpha) \cos(\beta) \\ q \cos(\alpha) \cos(\beta) - p \sin(\beta) \end{bmatrix}
\end{aligned} \tag{E.1.18}$$

where

$$C(\alpha, \beta) = \begin{bmatrix} \cos(\alpha) \cos(\beta) & \sin(\beta) & \sin(\alpha) \cos(\beta) \\ -\sin(\alpha) / \cos(\beta) & 0 & \cos(\alpha) / \cos(\beta) \\ -\cos(\alpha) \sin(\beta) & \cos(\beta) & -\sin(\alpha) \sin(\beta) \end{bmatrix} \tag{E.1.19}$$

and

$$\begin{aligned}
\dot{G}_x &= -g \cdot \cos(\theta) \cdot \dot{\theta} \\
\dot{G}_y &= -g \cdot \sin(\theta) \sin(\phi) \cdot \dot{\theta} + g \cdot \cos(\theta) \cos(\phi) \cdot \dot{\phi} \\
\dot{G}_z &= -g \cdot \sin(\theta) \cos(\phi) \cdot \dot{\theta} - g \cdot \cos(\theta) \sin(\phi) \cdot \dot{\phi}
\end{aligned} \tag{E.1.20}$$

E.2 The Fast Dynamics

The fast dynamics can be written as:

$$\begin{bmatrix} \dot{p}_s \\ \dot{q} \\ \dot{r}_s \end{bmatrix} = \begin{bmatrix} f_9(\mathbf{x}) \\ f_{10}(\mathbf{x}) \\ f_{11}(\mathbf{x}) \end{bmatrix} + \begin{bmatrix} \bar{L}_{\delta_a} & 0 & \bar{L}_{\delta_r} \\ 0 & M_{\delta_e} & 0 \\ \bar{N}_{\delta_a} & 0 & \bar{N}_{\delta_r} \end{bmatrix} \begin{bmatrix} \delta_a \\ \delta_e \\ \delta_r \end{bmatrix} \tag{E.2.1}$$

where

$$\begin{aligned}
f_9(\mathbf{x}) &= [E_{pq} \cos(\alpha) + H_{pq} \sin(\alpha)] pq + [E_{qr} \cos(\alpha) + H_{qr} \sin(\alpha)] qr + \bar{L}_\beta \cdot \beta + \bar{L}_p \cdot p_s + \bar{L}_r \cdot r_s \\
&\quad + \bar{L}_T \cos(\alpha) + \bar{N}_T \sin(\alpha) \\
f_{10}(\mathbf{x}) &= F_{pr} pr + F_{rr}(r^2 - p^2) + M_\alpha \cdot \alpha + M_q \cdot q + \bar{M}_T \\
&= F_{pr} pr + F_{rr}(r^2 - p^2) + W_M \cdot C_{m\alpha} \cdot \alpha + W_M \cdot \left(\frac{\bar{c}}{2V}\right) \cdot C_{mq} \cdot q + \bar{M}_T \\
f_{11}(\mathbf{x}) &= [H_{pq} \cos(\alpha) - E_{pq} \sin(\alpha)] pq + [H_{qr} \cos(\alpha) - E_{qr} \sin(\alpha)] qr + \bar{N}_\beta \cdot \beta + \bar{N}_p \cdot p_s + \bar{N}_r \cdot r_s \\
&\quad - \bar{L}_T \sin(\alpha) + \bar{N}_T \cos(\alpha)
\end{aligned} \tag{E.2.2}$$

and

$$\begin{aligned}
\bar{L}_{\delta_a} &= (J_L C_{l\delta_a} + J_N C_{n\delta_a}) \cos(\alpha) + (K_N C_{n\delta_a} + K_L C_{l\delta_a}) \sin(\alpha) \\
\bar{L}_{\delta_r} &= (J_L C_{l\delta_r} + J_N C_{n\delta_r}) \cos(\alpha) + (K_N C_{n\delta_r} + K_L C_{l\delta_r}) \sin(\alpha) \\
\bar{L}_\beta &= (J_L C_{l\beta} + J_N C_{n\beta}) \cos(\alpha) + (K_N C_{n\beta} + K_L C_{l\beta}) \sin(\alpha) \\
M_{\delta_e} &= W_M C_{m\delta_e} \\
\bar{N}_{\delta_a} &= (K_N C_{n\delta_a} + K_L C_{l\delta_a}) \cos(\alpha) - (J_L C_{l\delta_a} + J_N C_{n\delta_a}) \sin(\alpha) \\
\bar{N}_{\delta_r} &= (K_N C_{n\delta_r} + K_L C_{l\delta_r}) \cos(\alpha) - (J_L C_{l\delta_r} + J_N C_{n\delta_r}) \sin(\alpha) \\
\bar{N}_\beta &= (K_N C_{n\beta} + K_L C_{l\beta}) \cos(\alpha) - (J_L C_{l\beta} + J_N C_{n\beta}) \sin(\alpha)
\end{aligned} \tag{E.2.3}$$

and

$$\begin{aligned}
\begin{bmatrix} \bar{L}_p & \bar{L}_r \\ \bar{N}_p & \bar{N}_r \end{bmatrix} &= \begin{bmatrix} \cos(\alpha) & \sin(\alpha) \\ -\sin(\alpha) & \cos(\alpha) \end{bmatrix} \begin{bmatrix} L_p & L_r \\ N_p & N_r \end{bmatrix} \begin{bmatrix} \cos(\alpha) & -\sin(\alpha) \\ \sin(\alpha) & \cos(\alpha) \end{bmatrix} \\
&= \begin{bmatrix} \cos(\alpha) & \sin(\alpha) \\ -\sin(\alpha) & \cos(\alpha) \end{bmatrix} \left(\frac{\bar{q} S b^2}{2V}\right) \begin{bmatrix} I_{xx} & -I_{xz} \\ -I_{xz} & I_{zz} \end{bmatrix}^{-1} \begin{bmatrix} C_{lp} & C_{lr} \\ C_{np} & C_{nr} \end{bmatrix} \begin{bmatrix} \cos(\alpha) & -\sin(\alpha) \\ \sin(\alpha) & \cos(\alpha) \end{bmatrix}
\end{aligned} \tag{E.2.4}$$

and

$$\begin{aligned}
J_L &= \frac{\bar{q}SbI_{zz}}{I_{xx}I_{zz} - I_{xz}^2}, & J_N &= \frac{\bar{q}SbI_{xz}}{I_{xx}I_{zz} - I_{xz}^2} \\
W_M &= \frac{\bar{q}S\bar{c}}{I_{yy}}, \\
K_N &= \frac{\bar{q}SbI_{xx}}{I_{xx}I_{zz} - I_{xz}^2}, & K_L &= \frac{\bar{q}SbI_{xz}}{I_{xx}I_{zz} - I_{xz}^2}
\end{aligned} \tag{E.2.5}$$

and

$$\begin{aligned}
E_{pq} &= \frac{I_{xz}(I_{xx} - I_{yy} + I_{zz})}{I_{xx}I_{zz} - I_{xz}^2}, & E_{qr} &= \frac{I_{zz}(I_{yy} - I_{zz}) - I_{xz}^2}{I_{xx}I_{zz} - I_{xz}^2} \\
F_{pr} &= \frac{I_{zz} - I_{xx}}{I_{yy}}, & F_{rr} &= \frac{I_{xz}}{I_{yy}} \\
H_{pq} &= \frac{I_{xx}(I_{xx} - I_{yy}) + I_{xz}^2}{I_{xx}I_{zz} - I_{xz}^2}, & H_{qr} &= \frac{-I_{xz}(I_{xx} - I_{yy} + I_{zz})}{I_{xx}I_{zz} - I_{xz}^2}
\end{aligned} \tag{E.2.6}$$

All the aerodynamic derivatives in the fast dynamic equations are described in body axis.

The moments produced by thrust vectored engines along three axes, L_T, M_T, N_T are described as follows:

$$\begin{aligned}
L_T &= T_p \cdot l_y \cdot \{\sin(\delta p_1) \cos(\delta y_1) - \sin(\delta p_2) \cos(\delta y_2)\} \\
M_T &= -T_p \cdot l_x \cdot \{\sin(\delta p_1) \cos(\delta y_1) + \sin(\delta p_2) \cos(\delta y_2)\} \\
N_T &= -T_p \cdot l_x \cdot \{\sin(\delta y_1) + \sin(\delta y_2)\} + T_p \cdot l_y \{\cos(\delta p_1) \cos(\delta y_1) - \cos(\delta p_2) \cos(\delta y_2)\}
\end{aligned} \tag{E.2.7}$$

where l_x is the distance from the aircraft's center of gravity to the nozzle, and l_y is the distance from the center line of the aircraft to one engine.

If small TVC angles are assumed, these equations for moments can be written by:

$$\begin{aligned}
L_T &\cong T_p \cdot l_y \cdot (\delta p_1 - \delta p_2) \\
M_T &\cong -T_p \cdot l_x \cdot (\delta p_1 + \delta p_2) \\
N_T &\cong -T_p \cdot l_x \cdot (\delta y_1 + \delta y_2)
\end{aligned} \tag{E.2.8}$$

Thus \overline{L}_T , \overline{M}_T and \overline{N}_T in equation (E.2.2) are:

$$\begin{aligned}\overline{L}_T &= \frac{L_T \cdot I_{zz}}{I_{xx}I_{zz} - I_{xz}^2} = \frac{T_p \cdot l_y \cdot I_{zz} \cdot (\delta p_1 - \delta p_2)}{I_{xx}I_{zz} - I_{xz}^2} \\ \overline{M}_T &= \frac{M_T}{I_{yy}} = \frac{-T_p \cdot l_x \cdot (\delta p_1 + \delta p_2)}{I_{yy}} \\ \overline{N}_T &= \frac{N_T \cdot I_{xx}}{I_{xx}I_{zz} - I_{xz}^2} = \frac{-T_p \cdot l_x \cdot I_{xx} \cdot (\delta y_1 + \delta y_2)}{I_{xx}I_{zz} - I_{xz}^2}\end{aligned}\tag{E.2.9}$$

E.3 Simplified Dynamic Equations

It is possible to simplify the equations using the following assumptions:

Assumption E.3.1. In order to simplify the full scale nonlinear equations of motion of the aircraft, we introduce reasonable assumptions such as:

1. In the fast dynamics the time derivatives of the slow states are ignored because they are regarded as slow variables. Also, in the slow dynamics, the time derivatives of the actual controls are ignored, and the time derivatives of the fast states are treated as control variables.
2. Sideslip angle, β , is small, hence

$$\sin(\beta) \cong 0, \quad \cos(\beta) \cong 1, \quad \tan(\beta) \cong 0\tag{E.3.1}$$

3. I_{xz} is negligible.
4. Directional acceleration change due to thrust vectoring is negligible.

$$A_{T_x} \cong \text{constant}, \quad A_{T_y} = A_{T_z} \cong 0, \quad \dot{A}_{T_x} = \dot{A}_{T_y} = \dot{A}_{T_z} \cong 0.\tag{E.3.2}$$

5. A_{X0} , $A_{X\delta a}$, $A_{X\delta r}$, $A_{Y\delta e}$, $A_{Y\delta a}$, $A_{Z\delta a}$, $A_{Z\delta r}$, $A_{X\beta}$, $A_{Y\alpha}$, $A_{Z\beta}$ are negligible.
6. The rate of change of velocity is negligible.
7. $C_{n\delta a}$, $C_{l\delta r}$, $\overline{L}_{\delta r}$, \overline{L}_r , $\overline{N}_{\delta a}$, \overline{N}_p are negligible.

E.3.1 Simplified Slow Dynamics

With the above assumptions, the accelerations in (E.1.10) can be simplified to:

$$\begin{aligned}
 a_x &= A_X + G_x + T/m \\
 a_y &= A_Y + G_y \\
 a_z &= A_Z + G_z
 \end{aligned} \tag{E.3.3}$$

where the simplified A_X, A_Y, A_Z of (E.1.11) and G_x, G_y, G_z in (E.1.13) are:

$$\begin{aligned}
 A_X &= -\frac{1}{m} \cdot [D \cos(\alpha) - L \sin(\alpha)] \\
 &= -\frac{\bar{q}S}{m} \cdot (C_{D0} + C_{D\alpha} \cdot \alpha + C_{D\delta e} \cdot \delta e) \cos(\alpha) + \frac{\bar{q}S}{m} \cdot (C_{L0} + C_{L\alpha} \cdot \alpha + C_{L\delta e} \cdot \delta e) \sin(\alpha) \\
 A_Y &= \frac{\bar{q}S}{m} \cdot (C_{Y\beta} \cdot \beta + C_{Y\delta r} \cdot \delta r) \\
 A_Z &= -\frac{1}{m} \cdot [D \sin(\alpha) + L \cos(\alpha)] \\
 &= -\frac{\bar{q}S}{m} \cdot (C_{D0} + C_{D\alpha} \cdot \alpha + C_{D\delta e} \cdot \delta e) \sin(\alpha) - \frac{\bar{q}S}{m} \cdot (C_{L0} + C_{L\alpha} \cdot \alpha + C_{L\delta e} \cdot \delta e) \cos(\alpha)
 \end{aligned} \tag{E.3.4}$$

and

$$\begin{aligned}
 \dot{G}_x &= -g \cdot \cos(\theta) \cdot \dot{\theta} \\
 &\cong -g \cdot \cos(\theta) \cdot q \\
 \dot{G}_y &= -g \cdot \sin(\theta) \sin(\phi) \cdot \dot{\theta} + g \cdot \cos(\theta) \cos(\phi) \cdot \dot{\phi} \\
 &\cong g \cdot \cos(\theta) \cos(\phi) \cdot p \\
 \dot{G}_z &= -g \cdot \sin(\theta) \cos(\phi) \cdot \dot{\theta} - g \cdot \cos(\theta) \sin(\phi) \cdot \dot{\phi} \\
 &\cong -g \cdot \cos(\theta) \sin(\phi) \cdot p
 \end{aligned} \tag{E.3.5}$$

The equations for $\dot{a}_x, \dot{a}_y, \dot{a}_z$ in (E.1.18) are expressed by:

$$\begin{aligned}
\begin{bmatrix} \dot{a}_x \\ \dot{a}_y \\ \dot{a}_z \end{bmatrix} &\cong \begin{bmatrix} \dot{G}_x \\ \dot{G}_y \\ \dot{G}_z \end{bmatrix} + \begin{bmatrix} A_{X\delta e} & 0 & 0 \\ 0 & 0 & A_{Y\delta r} \\ A_{Z\delta e} & 0 & 0 \end{bmatrix} \begin{bmatrix} \dot{\delta e} \\ \dot{\delta a} \\ \dot{\delta r} \end{bmatrix} = \begin{bmatrix} \dot{G}_x + A_{X\delta e} \cdot \dot{\delta e} \\ \dot{G}_y + A_{Y\delta r} \cdot \dot{\delta r} \\ \dot{G}_z + A_{Z\delta e} \cdot \dot{\delta e} \end{bmatrix} \\
&\cong \begin{bmatrix} -g \cdot \cos(\theta) \cdot q + \frac{1}{m} \bar{q} S \cdot [-C_{D\delta e} \cos(\alpha) + C_{L\delta e} \sin(\alpha)] \cdot \dot{\delta e} \\ g \cdot \cos(\theta) \cos(\phi) \cdot p + \frac{1}{m} \bar{q} S \cdot C_{Y\delta r} \cdot \dot{\delta r} \\ -g \cdot \cos(\theta) \sin(\phi) \cdot p - \frac{1}{m} \bar{q} S \cdot [C_{D\delta e} \sin(\alpha) + C_{L\delta e} \cos(\alpha)] \cdot \dot{\delta e} \end{bmatrix} \quad (\text{E.3.6}) \\
&\cong \begin{bmatrix} -g \cdot \cos(\theta) \cdot q + \frac{1}{m} \bar{q} S \cdot C_{L\delta e} \sin(\alpha) \cdot \dot{\delta e} \\ g \cdot \cos(\theta) \cos(\phi) \cdot p + \frac{1}{m} \bar{q} S \cdot C_{Y\delta r} \cdot \dot{\delta r} \\ -g \cdot \cos(\theta) \sin(\phi) \cdot p - \frac{1}{m} \bar{q} S \cdot C_{L\delta e} \cos(\alpha) \cdot \dot{\delta e} \end{bmatrix}
\end{aligned}$$

The functions from $f_1(\mathbf{x})$ to $f_8(\mathbf{x})$ given in (E.1.2) ~ (E.1.9) are expressed in much simpler forms:

$$\begin{aligned}
\dot{\alpha} &= q + \frac{1}{V} [-a_x \sin(\alpha) + a_z \cos(\alpha)] \\
&= q + \frac{g}{V} \cdot \cos(\theta) \cos(\phi) \cos(\alpha) - \frac{T}{mV} \sin(\alpha) - \frac{\bar{q}S}{mV} C_{L\alpha} \cdot \alpha \\
&= f_1(\mathbf{x})
\end{aligned} \quad (\text{E.3.7})$$

$$\begin{aligned}
\ddot{\alpha} &= \dot{q} - \dot{p}_s \tan(\beta) - p_s \cdot \dot{\beta} - \frac{\sin(\alpha)}{V} \cdot \dot{a}_x + \frac{\cos(\alpha)}{V} \cdot \dot{a}_z \\
&= \dot{q} - \dot{p}_s \tan(\beta) - p_s \cdot \dot{\beta} + \frac{g}{V} \cdot \{q \cos(\theta) \sin(\alpha) - p \cos(\alpha) \cos(\theta) \sin(\phi)\} \\
&\cong \dot{q} - \dot{p}_s \tan(\beta) - p_s \cdot \dot{\beta} - \frac{g}{V} \cdot p_s \cdot \cos(\theta) \sin(\phi) \\
&= \dot{q} + f_2(\mathbf{x})
\end{aligned} \quad (\text{E.3.8})$$

$$\begin{aligned}
\dot{\beta} &= -r_s + \frac{a_y}{V} \\
&\cong -r_s + \frac{g}{V} \cos(\theta) \sin(\phi) + \frac{\bar{q}S}{mV} C_{Y\delta r} \cdot \delta r + \frac{\bar{q}S}{mV} C_{Y\beta} \cdot \beta \\
&= f_3(\mathbf{x})
\end{aligned} \quad (\text{E.3.9})$$

$$\begin{aligned}
\ddot{\beta} &= -\dot{r}_s + \frac{1}{V} \cdot \dot{a}_y \\
&\cong -\dot{r}_s + \frac{g}{V} \cdot p \cdot \cos(\theta) \cos(\phi) + \frac{\bar{q}S}{mV} C_{Y\beta} \cdot \dot{\beta} \\
&= -\dot{r}_s + f_4(\mathbf{x})
\end{aligned} \tag{E.3.10}$$

$$\begin{aligned}
\dot{\phi} &= p + q \cdot \tan(\theta) \sin(\phi) + r \cdot \tan(\theta) \cos(\phi) \\
&= f_5(\mathbf{x})
\end{aligned} \tag{E.3.11}$$

$$\begin{aligned}
\dot{\theta} &= q \cdot \cos(\phi) - r \cdot \sin(\phi) \\
&= f_6(\mathbf{x})
\end{aligned} \tag{E.3.12}$$

$$\begin{aligned}
\dot{V} &= a_x \cos(\alpha) + a_z \sin(\alpha) \\
&\cong g \cdot \{ \cos(\theta) \cos(\phi) \sin(\alpha) - \sin(\theta) \cos(\alpha) \} + \frac{T}{m} \cos(\alpha) - \frac{\bar{q}S}{mV} C_{D\alpha} \cdot \alpha \\
&= f_7(\mathbf{x})
\end{aligned} \tag{E.3.13}$$

$$\begin{aligned}
\ddot{V} &= \dot{a}_x \cdot \cos(\alpha) + \dot{a}_z \cdot \sin(\alpha) \\
&\cong -g \cdot \{ q \cos(\theta) \cos(\alpha) + p \cos(\theta) \sin(\phi) \sin(\alpha) \} \\
&\cong -g \cdot q \cos(\theta) \cos(\alpha) \\
&= f_8(\mathbf{x})
\end{aligned} \tag{E.3.14}$$

E.3.2 Simplified Fast Dynamics

Using Assumptions 1 ~ 6 reduces (E.2.1) to

$$\begin{bmatrix} \dot{p}_s \\ \dot{q} \\ \dot{r}_s \end{bmatrix} = \begin{bmatrix} f_9(\mathbf{x}) \\ f_{10}(\mathbf{x}) \\ f_{11}(\mathbf{x}) \end{bmatrix} + \begin{bmatrix} \bar{L}_{\delta_a} & 0 & 0 \\ 0 & M_{\delta_e} & 0 \\ 0 & 0 & \bar{N}_{\delta_r} \end{bmatrix} \begin{bmatrix} \delta_a \\ \delta_e \\ \delta_r \end{bmatrix} \tag{E.3.15}$$

where

$$\begin{aligned}
f_9(\mathbf{x}) &= E_{qr} \cos(\alpha) \cdot qr + H_{pq} \sin(\alpha) \cdot pq + \bar{L}_\beta \cdot \beta + \bar{L}_p \cdot p_s \\
f_{10}(\mathbf{x}) &= F_{pr} \cdot pr + W_M \cdot C_{m\alpha} \cdot \alpha + W_M \cdot \left(\frac{\bar{c}}{2V}\right) C_{mq} \cdot q \\
f_{11}(\mathbf{x}) &= -E_{qr} \sin(\alpha) \cdot qr + H_{pq} \cos(\alpha) \cdot pq + \bar{N}_\beta \cdot \beta + \bar{N}_r \cdot r_s
\end{aligned} \tag{E.3.16}$$

Also, (E.2.3) reduces to:

$$\begin{aligned}
\bar{L}_{\delta_a} &= J_L C_{l\delta_a} \cos(\alpha) \\
\bar{L}_\beta &= J_L C_{l\beta} \cos(\alpha) + K_N C_{n\beta} \sin(\alpha) \\
M_{\delta_e} &= W_M C_{m\delta_e} \\
\bar{N}_{\delta_r} &= K_N C_{n\delta_r} \cos(\alpha) \\
\bar{N}_\beta &= K_N C_{n\beta} \cos(\alpha) - J_L C_{l\beta} \sin(\alpha)
\end{aligned} \tag{E.3.17}$$

and (E.2.4) simplifies to:

$$\begin{aligned}
\bar{L}_p &= J_L \left(\frac{b}{2V}\right) C_{lp} \cos^2(\alpha) \\
\bar{N}_r &= K_N \left(\frac{b}{2V}\right) C_{nr} \cos^2(\alpha)
\end{aligned} \tag{E.3.18}$$

and (E.2.5) and (E.2.6) become:

$$J_L = \frac{\bar{q} S b}{I_{xx}}, \quad W_M = \frac{\bar{q} S \bar{c}}{I_{yy}}, \quad K_N = \frac{\bar{q} S b}{I_{zz}}, \quad J_N = K_L = 0 \tag{E.3.19}$$

$$E_{qr} = \frac{I_{yy} - I_{zz}}{I_{xx}}, \quad F_{pr} = \frac{I_{zz} - I_{xx}}{I_{yy}}, \quad H_{pq} = \frac{I_{xx} - I_{yy}}{I_{zz}}, \quad E_{pq} = F_{rr} = H_{qr} = 0 \tag{E.3.20}$$

REFERENCES

- [1] ADAMS, R. J. and BANDA, S. S., “Robust flight control design using dynamic inversion and structured singular value synthesis,” *IEEE Transactions on Control Systems Technology*, vol. 1, pp. 80–92, June 1993.
- [2] ADAMS, R. J., BUFFINGTON, J. M., and BANDA, S. S., “Design of nonlinear control laws for high angle of attack flight,” *Journal of Guidance, Control, and Dynamics*, vol. 17, pp. 737–746, July-Aug. 1994.
- [3] ASTROM, K. and WITTENMARK, B., *Adaptive Control*. New York: Addison-Wesley Publishing Company, 2nd ed., 1995.
- [4] BAKER, W. L. and FARELL, J. A., “Learning augmented flight control for high performance aircraft,” in *AIAA Guidance, Navigation and Control Conference*, pp. 347–358, AIAA-1991-2836, 1991.
- [5] BLAKELOCK, J. H., *Automatic Control of Aircraft and Missiles*. New York, NY: Wiley-Interscience, John Wiley & Sons, 2nd ed., 1991.
- [6] BRINKER, J. S. and WISE, K. A., “Stability and flying qualities robustness of a dynamic inversion aircraft control law,” *Journal of Guidance, Control, and Dynamics*, vol. 19, pp. 1270–1277, Nov.-Dec. 1996.
- [7] BRINKER, J. S. and WISE, K. A., “Flight testing of a reconfigurable flight control law on the X-36 tailless fighter aircraft,” in *AIAA Guidance, Navigation and Control Conference*, AIAA-2000-3941, Aug. 2000.
- [8] BRUMBAUGH, R. W., “Aircraft model for the AIAA controls design challenge,” *Journal of Guidance, Control, and Dynamics*, vol. 17, pp. 747–752, July-Aug. 1994. NASA-CR-186019.
- [9] BUFFINGTON, J. M., ADAMS, R. J., and BANDA, S. S., “Robust, nonlinear, high angle of attack control design for a supermaneuverable vehicle,” in *AIAA Guidance, Navigation and Control Conference*, pp. 690–700, Aug. 1993.
- [10] BUGAJSKI, D. J., ENNS, D. F., and ELGERSMA, M. R., “A dynamic inversion based control law with application to the high angle of attack research vehicle,” in *AIAA Guidance, Navigation and Control Conference*, (Portland, OR), pp. 826–839, AIAA-1990-3407, Aug. 1990.
- [11] CALISE, A. J., HOVAKIMYAN, N., and IDAN, M., “Adaptive output feedback control of nonlinear systems using neural networks,” *Automatica*, vol. 37, pp. 1201–1211, Aug. 2001.

- [12] CALISE, A. J., LEE, H., and KIM, N., “High bandwidth adaptive flight control,” in *AIAA Guidance, Navigation and Control Conference*, AIAA-2000-4551, Aug. 2000.
- [13] CALISE, A. J., LEE, S., and SHARMA, M., “Development of a reconfigurable flight control law for the X-36 tailless fighter aircraft,” in *AIAA Guidance, Navigation and Control Conference*, AIAA-2000-3940, Aug. 2000.
- [14] CALISE, A. J., LEE, S., and SHARMA, M., “Development of a reconfigurable flight control law for tailless aircraft,” *Journal of Guidance, Control, and Dynamics*, vol. 24, pp. 896–902, Sept.-Oct. 2001.
- [15] CALISE, A. J., PRASAD, J. V. R., and CORBAN, J. E., “Flight evaluation of an adaptive neural network flight controller of an unmanned helicopter,” in *Proceedings 25th European Rotorcraft Forum*, (Rome, Italy), Sept. 1999.
- [16] CALISE, A. J., SHIN, Y., and JOHNSON, M., *Neural Network-Based Adaptive Control for Nonlinear Flight Regimes*. NASA Technical Report, NASA Langley Research Center, Hampton, VA, Aug. 2002.
- [17] CALISE, A. J., SHIN, Y., and JOHNSON, M., *Neural Network-Based Adaptive Control for Nonlinear Flight Regimes*. NASA Technical Report, NASA Langley Research Center, Hampton, VA, Aug. 2003.
- [18] CALISE, A. J., SHIN, Y., and JOHNSON, M., “A comparison study of classical and neural network based adaptive control of wing rock,” in *AIAA Guidance, Navigation and Control Conference*, (Providence, RI), AIAA-2004-5320, Aug. 2004.
- [19] CORBAN, J. E., CALISE, A. J., and PRASAD, J. V. R., “Flight test of an adaptive control system for unmanned helicopter trajectory following,” in *AIAA Guidance, Navigation and Control Conference*, AIAA-2000-4058, Aug. 2000.
- [20] CYBENKO, G., “Approximation by superpositions of a sigmoidal function,” *Mathematics of Control, Signals and Systems*, vol. 2, pp. 303–314, 1989.
- [21] DEVASIA, S., CHEN, D., and PADEN, B., “Nonlinear inversion-based output tracking,” *IEEE Transactions on Automatic Control*, vol. 41, no. 7, pp. 930–942, 1996.
- [22] ELZEBDA, J. M., NAYFEH, A. H., and MOOK, D. T., “Development of an analytical model of wing rock for slender delta wings,” *Journal of Aircraft*, vol. 26, pp. 737–743, Aug. 1989.
- [23] ENNS, D., BUGAJSKI, D., HENDRICK, R., and STEIN, G., “Dynamic inversion: an evolving methodology for flight control design,” *International Journal of Control*, vol. 59, no. 1, pp. 71–91, 1994.
- [24] FUNAHASHI, K.-I., “On the approximate realization of continuous mappings by neural networks,” *Neural Networks*, vol. 2, pp. 183–192, Aug. 1989.

- [25] GE, S. S., HANG, C. C., H., T., and ZHANG, T., *Stable Adaptive Neural Network Control*. Norwell, Massachusetts: Kluwer Academic Publishers, 2002.
- [26] GILI, P. A. and BATTIPEDE, M., “Adaptive neurocontroller for a nonlinear combat aircraft model,” *Journal of Guidance, Control, and Dynamics*, vol. 24, pp. 910–917, Sept.-Oct. 2001.
- [27] HORNIK, K., “Multilayer feedforward networks are universal approximators,” *Neural Networks*, vol. 2, pp. 359–366, 1989.
- [28] HORNIK, K., STINCHCOMBE, M., and WHITE, H., “Universal approximation of an unknown mapping and its derivatives using multilayer feedforward networks,” *Neural Networks*, vol. 3, no. 8, pp. 551–560, 1990.
- [29] HOVAKIMYAN, N., CALISE, A. J., and KIM, N., “Adaptive output feedback control of uncertain nonlinear systems using single-hidden-layer neural networks,” *IEEE Transactions on Neural Networks*, vol. 13, pp. 1420–1431, Nov. 2002.
- [30] HOVAKIMYAN, N., CALISE, A. J., and KIM, N., “Adaptive output feedback control of a class of multi-input multi-output systems using neural networks,” *International Journal of Control*, vol. 77, no. 15, pp. 1318–1329, 2004.
- [31] HSU, C.-H. and LAN, C. E., “Theory of wing rock,” *Journal of Aircraft*, vol. 22, pp. 920–924, Oct. 1985.
- [32] INTEGRATED PUBLISHING, “Operator, unit and intermediate direct and general support maintenance manual including repair parts and special tools LIS for FQM-117 B-1 and C-1 Radio Controlled Miniature Aerial Target (RCMAT) ground support equipment, and auxiliary equipment,” TM-9-1550-416-14P, Aviation Flight Manuals and Accessories, 2004. <http://www.tpub.com/content/aviationandaccessories/TM-9-1550-416-14P/>.
- [33] IOANNOU, P. A. and KOKOTOVIC, P. V., “Instability analysis improvement of robustness of adaptive control,” *Automatica*, vol. 20, no. 5, pp. 583–594, 1984.
- [34] IOANNOU, P. A. and SUN, J., *Robust Adaptive Control*. New Jersey: Prentice Hall, 1996.
- [35] ISIDORI, A., *Nonlinear Control Systems: An Introduction*. Berlin, Germany: Springer-Verlag, 2nd ed., 1989.
- [36] ISIDORI, A., *Nonlinear Control Systems*. London, UK: Springer-Verlag, 3rd ed., 1995.
- [37] ISIDORI, A., ARHUR, J. K., CLAUDIO, G., and SALVATORE, M., “Nonlinear decoupling via feedback: A differential geometric approach,” *IEEE Transactions on Automatic Control*, vol. 26, pp. 331–345, Apr. 1981.
- [38] JOHNSON, E. N., *Limited Authority Adaptive Flight Control*. Ph.D dissertation, Georgia Institute of Technology, School of Aerospace Engineering, Atlanta, GA, Dec. 2000.

- [39] JOHNSON, E. N. and CALISE, A. J., “Neural network adaptive control of systems with input saturation,” in *American Control Conference*, (Arlington, VA), June 2001.
- [40] JOHNSON, E. N., CALISE, A. J., RYSDYK, R. T., and EL-SHIRBINY, H., “Feedback linearization with neural network augmentation applied to X-33 attitude control,” in *AIAA Guidance, Navigation and Control Conference*, AIAA-2000-4157, Aug. 2000.
- [41] KALMAN, R. E. and BERTRAM, J. E., “Control system analysis and design via the second method of Lyapunov, I & II,” *Transaction of the ASME, Journal Of of Basic Engineering*, pp. 371–400, June 1960.
- [42] KANELLAKOPOULOS, I., KOKOTOVIC, P. V., and MORSE, A. S., “Systematic design of adaptive controller for feedback linearizable systems,” *IEEE Transactions on Automatic Control*, vol. 36, no. 11, pp. 1241–1253, 1991.
- [43] KHALIL, H. K., *Nonlinear Systems*. New Jersey: Prentice-Hall, 2nd ed., 1996.
- [44] KIM, B. S. and CALISE, A. J., “Nonlinear flight control using neural networks,” *Journal of Guidance, Control, and Dynamics*, vol. 20, pp. 26–33, Jan.-Feb. 1997.
- [45] KIM, N., *Improved Methods in Neural Network-Based Adaptive Output Feedback Control, with Applications to Flight Control*. Ph.D dissertation, Georgia Institute of Technology, School of Aerospace Engineering, Atlanta, GA, Nov. 2003.
- [46] KLEIN, V. and NODERER, K. D., *Modeling of Aircraft Unsteady Aerodynamic Characteristics: Part 1 - Postulated Models*. NASA-TM-109120, NASA Langley Research Center, May 1994.
- [47] KOKOTOVIC, P. V., “The joy of feedback: Nonlinear and adaptive,” *IEEE Control Systems*, pp. 7–17, June 1992.
- [48] KRSTIC, M., SUN, J., and KOKOTOVIC, V., “Robust control of nonlinear systems with input unmodeled dynamics,” *IEEE Transactions on Automatic Control*, vol. 41, pp. 913–920, June 1996.
- [49] KRSTIC, M., KANELLAKOPOULOS, I., and KOKOTOVIC, P., *Nonlinear and Adaptive Control Design*. New York, NY: John Wiley & Sons, 1995.
- [50] LALLMAN, F. J., DAVIDSON, J. B., and MURPHY, P. C., *A method for Integrating Thrust-Vectoring and Actuated Forebody Strakes with Conventional Aerodynamic Controls on a High-Performance Fighter Airplane*. NASA-TP-208464, NASA Langley Research Center, Sept. 1998.
- [51] LANE, S. H. and STENGEL, R. F., “Flight control design using nonlinear inverse dynamics,” *Automatica*, vol. 24, no. 4, pp. 471–483, 1988.
- [52] LASALLE, J. P., “Some extensions of Liapunov’s second method,” *IRE Transactions of Circuit Theory*, vol. CT-7, no. 4, pp. 520–527, 1960.

- [53] LASALLE, J. P., *The Stability of Dynamical Systems*. Bristol, England: Society for Industrial and Applied Mathematics, 1976.
- [54] LAVRETSKY, E., “Composite model reference adaptive control.” A technical note, May 2005.
- [55] LAVRETSKY, E., HOVAKIMYAN, N., and CALISE, A., “Upper bounds for approximation of continuous-time dynamics using delayed outputs and feedforward neural networks,” *IEEE Transactions on Automatic Control*, vol. 48, pp. 1606–1610, Sept. 2003.
- [56] LEE, T. and KIM, Y., “Nonlinear adaptive flight control using backstepping and neural networks controller,” *Journal of Guidance, Control, and Dynamics*, vol. 24, pp. 910–917, July-Aug. 2001.
- [57] LEITNER, J., CALISE, A. J., and PRASAD, J. V. R., “Analysis of adaptive neural networks for helicopter flight controls,” *Journal of Guidance, Control, and Dynamics*, vol. 20, pp. 972–979, Sept.-Oct. 1997.
- [58] LEITNER, J., CALISE, A. J., and PRASAD, J. V. R., “Analysis of adaptive neural networks for helicopter flight control,” *Journal of Guidance, Control, and Dynamics*, vol. 20, no. 5, pp. 972–979, 1997.
- [59] LEITNER, J., CALISE, A. J., and PRASAD, J. V. R., “A full authority helicopter adaptive neuro-controller,” in *Proceeding of IEEE Aerospace Conference*, pp. 117–126, Mar. 1998.
- [60] LEWIS, F. L., LIU, K., and YESILDIREK, A., “Neural net robot controller with guaranteed tracking performance,” *IEEE Transactions on Neural Networks*, vol. 6, pp. 703–715, May 1995.
- [61] LEWIS, F. L., YESILDIREK, A., and LIU, K., “Multilayer neural-net robot controller with guaranteed tracking performance,” *IEEE Transactions on Neural Networks*, vol. 7, pp. 388–399, Mar. 1996.
- [62] LEWIS, F. L., “Nonlinear network structures for feedback control,” *Asian Journal of Control*, vol. 1, pp. 205–228, Dec. 1999.
- [63] LI, Y., SUNDARARAJAN, N., and SARATCHANDRAN, P., “Neuro-controller design for nonlinear fighter aircraft maneuver using fully tuned RBF networks,” *Automatica*, vol. 37, pp. 1293–1301, 2001.
- [64] LI, Y., SUNDARARAJAN, N., and SARATCHANDRAN, P., “Stable neuro-flight-controller design using fully tuned radial based function neural networks,” *Journal of Guidance, Control, and Dynamics*, vol. 24, pp. 665–674, July-Aug. 2001.
- [65] LUO, J. and LAN, E. C., “Control of wing-rock motion of slender delta wings,” *Journal of Guidance, Control, and Dynamics*, vol. 16, pp. 225–231, Mar.-Apr. 1993.

- [66] MACKALL, D., NELSON, S., and SCHUMANN, J., *Verification and validation of neural networks for aerospace systems*. NASA/CR-2002-211409, NASA Ames Research Center, July 2002.
- [67] MCDOWELL, D. M., IRWIN, G. W., and MCCONNELL, G., “Online neural control applied to a bank-to-turn missile autopilot,” in *AIAA Guidance, Navigation and Control Conference*, (Baltimore, MD), pp. 1286–1294, AIAA-1995-3316, Aug. 1995.
- [68] MCFARLAND, M. B., *Adaptive Nonlinear Control of Missiles Using Neural Networks*. Ph.D dissertation, Georgia Institute of Technology, School of Aerospace Engineering, Atlanta, GA, 1997.
- [69] MCFARLAND, M. B. and CALISE, A. J., “Neural-adaptive nonlinear autopilot design for an agile anti-air missile,” in *AIAA Guidance, Navigation and Control Conference*, (San Diego, CA), AIAA-1996-3941, July 1996.
- [70] MCFARLAND, M. B. and CALISE, A. J., “Nonlinear adaptive control of agile anti-air missiles using neural networks,” in *AIAA Missile Sciences Conference*, (Monterey, CA), Dec. 1996.
- [71] MCFARLAND, M. B. and CALISE, A. J., “Multilayer neural networks and adaptive nonlinear control of agile anti-air missiles,” in *AIAA Guidance, Navigation and Control Conference*, pp. 401–410, AIAA-1997-3540, Aug. 1997.
- [72] MENON, P. K. A., “Nonlinear command augmentation system for a high performance fighter aircraft,” in *AIAA Guidance, Navigation and Control Conference*, (Monterey, CA), pp. 720–730, 1993.
- [73] MENON, P. K. A., CHATTERJI, G. B., and CHENG, V. H. L., “Two-time-scale autopilot for high performance aircraft,” in *AIAA Guidance, Navigation and Control Conference*, (New Orleans, LA), AIAA-1991-2674, Aug. 1991.
- [74] MORSE, A. S., “Global stability of parameter adaptive systems,” *IEEE Transactions on Automatic Control*, vol. 25, pp. 433–439, 1980.
- [75] MOTTER, M. A., *Autonomous Flight Tests of a Small Unmanned Aerial Vehicle*. NASA Langley Research Center, Virginia, 2004.
- [76] NAIK, S. M., KUMAR, P. R., and YDSTIE, B. E., “Robust continuous-time adaptive control by parameter projection,” *IEEE Transactions on Automatic Control*, vol. 37, pp. 182–197, Feb. 1992.
- [77] NARENDRA, K. S. and ANNASWAMY, A. M., *Stable Adaptive Systems*. New Jersey: Prentice Hall, 1989.
- [78] NARENDRA, K. S. and ANNASWAYMY, A. M., “A new adaptive law for robust adaptation without persistent excitation,” *IEEE Transactions on Automatic Control*, vol. 32, no. 2, pp. 134–145, 1987.

- [79] NARENDRA, K. S. and LIN, Y. H., “Stable discrete adaptive control,” *IEEE Transactions on Automatic Control*, vol. 25, pp. 456–461, 1980.
- [80] NARENDRA, K. S., LIN, Y. H., and VALAVANI, L. S., “Stable adaptive controller design - part II : Proof of stability,” *IEEE Transactions on Automatic Control*, vol. 25, pp. 440–448, 1980.
- [81] NARENDRA, K. S. and MUKHOPADHYAY, S., “Adaptive control of nonlinear multi-variable systems using neural networks,” *Neural Networks*, vol. 7, no. 5, pp. 737–752, 1994.
- [82] NARENDRA, K. S. and MUKHOPADHYAY, S., “Adaptive control using neural networks and approximate models,” *IEEE Transactions on Neural Networks*, vol. 8, pp. 475–485, May 1997.
- [83] NARENDRA, K. S. and PARTHASARATHY, K., “Identification and control of dynamical systems using neural networks,” *IEEE Transactions on Neural Networks*, vol. 1, pp. 4–27, Mar. 1990.
- [84] NARENDRA, K. S. and LEWIS, F. L., “Introduction to the special issue on neural network feedback control,” *Automatica*, vol. 37, pp. 1147–1148, Aug. 2001.
- [85] NAYFEH, A. H., ELZEBDA, J. M., and MOOK, D. T., “Analytical study of the subsonic wing-rock phenomenon for slender delta wings,” *Journal of Aircraft*, vol. 26, pp. 805–809, Sept. 1989.
- [86] ORME, J. S., HATHAWAY, R., and FERGUSON, M. D., *Initial Flight Test Evaluation of the F-15 ACTIVE Axisymmetric Vectoring Nozzle Performance*. NASA Technical Memorandum, NASA/TM-1998-206558, NASA Dryden Flight Research Center, July 1998.
- [87] PARK, J. and SANDBERG, I., “Universal approximation using radial-basis-function networks,” *Neural Computation*, vol. 3, no. 2, pp. 246–257, 1991.
- [88] POMET, J. and PRALY, L., “Adaptive nonlinear regulation: Estimation from the lyapunov equation,” *IEEE Transactions on Automatic Control*, vol. 37, pp. 729–740, June 1992.
- [89] PRASAD, J. V. R., CALISE, A. J., PEI, Y., and CORBAN, J. E., “Adaptive nonlinear controller synthesis and flight test evaluation on an unmanned helicopter,” in *Proceeding of IEEE International Conference on Control Applications*, 1999.
- [90] RAUW, M., *FDC 1.2. A Simulink Toolbox for Flight Dynamics and Control Analysis*. AIAA Educational Series, AIAA, 2nd ed., 2000.
- [91] REINER, J., BALAS, G. J., and GARRARD, W. L., “Robust dynamic inversion for control of highly maneuverable aircraft,” *Journal of Guidance, Control, and Dynamics*, vol. 18, pp. 18–24, Jan.-June 1995.

- [92] REINER, J., BALAS, G. J., and GARRARD, W. L., “Flight control design using robust dynamic inversion and time-scale separation,” *Automatica*, vol. 32, no. 11, pp. 1493–1504, 1996.
- [93] ROKHSAZ, K., STECK, J. E., and SHUE, S.-P., “Longitudinal flight control decoupling using artificial neural networks,” in *AIAA Aerospace Sciences Meeting and Exhibit, 32nd*, AIAA-94-0274, Jan. 1994.
- [94] RYSZYK, R. T. and CALISE, A. J., “Adaptive model inversion flight control for tilt-rotor aircraft,” *Journal of Guidance, Control, and Dynamics*, vol. 22, no. 3, pp. 402–407, 1999.
- [95] SADEGH, N., “Nonlinear identification and control via neural networks,” in *Control Systems with Inexact Dynamic Models, DSC-Vol.33, ASME Winter Annual Meeting*, (Atlanta, GA), Dec. 1991.
- [96] SADEGH, N., “A perceptron network for functional identification and control of nonlinear systems,” *IEEE Transactions on Neural Networks*, vol. 4, pp. 982–988, Nov. 1993.
- [97] SANNER, R. M. and SLOTINE, J. J., “Stable adaptive control and recursive identification using radial gaussian networks,” in *Proceeding of the 30th Conference on Decision and Control*, pp. 2116–2123, Dec. 1991.
- [98] SANNER, R. M. and SLOTINE, J. J., “Gaussian networks for direct adaptive control,” *IEEE Transactions on Neural Networks*, vol. 3, no. 6, pp. 837–863, 1992.
- [99] SASTRY, S. S. and ISIDORI, A., “Adaptive control of linearizable systems,” *IEEE Transactions on Automatic Control*, vol. 34, pp. 1123–1131, Nov. 1989.
- [100] SASTRY, S., *Nonlinear Systems: Analysis, Stability, and Control*. New York: Springer-Verlag, 1999.
- [101] SCARSELLI, F. and TSOI, A., “Universal approximation using feedforward neural networks: A survey of some existing methods, and some new results,” *Neural Networks*, vol. 11, pp. 15–37, Jan. 1987.
- [102] SCHUMACHER, C. and KHARGONEKAR, P. P., “Stability analysis of a missile control system with a dynamic inversion controller,” *Journal of Guidance, Control, and Dynamics*, vol. 21, pp. 12–19, May-June 2005.
- [103] SHARMA, M. and CALISE, A. J., “Neural-network augmentation of existing linear controllers,” *Journal of Guidance, Control, and Dynamics*, vol. 28, pp. 12–19, Sept.-Oct. 2005.
- [104] SHIN, Y., CALISE, A. J., and MOTTER, M. A., “Application of adaptive autopilot designs for an unmanned aerial vehicle,” in *AIAA Guidance, Navigation and Control Conference*, (San Francisco, CA), AIAA-2005-6166, An invited paper, Aug. 2005.

- [105] SHIN, Y., JOHNSON, M., and CALISE, A. J., “Neural network-based adaptive control for nonlinear flight regimes,” in *AIAA Guidance, Navigation and Control Conference*, (Austin, TX), AIAA-2003-5717, Aug. 2003.
- [106] SINGH, S. N., YIM, W., and WELLS, W. R., “Direct adaptive control of wing-rock motion of slender delta wings,” *Journal of Guidance, Control, and Dynamics*, vol. 18, pp. 25–30, Mar.-Apr. 1995.
- [107] SLOTINE, J. J. and LI, W., *Applied Nonlinear Control*. Englewood Cliffs, New Jersey: Prentice-Hall, 1991.
- [108] SNELL, S. A., *Nonlinear Dynamic-Inversion Flight Control of Supermaneuverable Aircraft*. Ph.D dissertation, University of Minnesota, Dept. of Aerospace Engineering, Minneapolis, MN, Oct. 1991.
- [109] SNELL, S. A., ENNS, D. F., and GARRARD, W. L., “Nonlinear inversion flight control for a supermaneuverable aircraft,” *Journal of Guidance, Control, and Dynamics*, vol. 15, pp. 976–984, July-Aug. 1992.
- [110] STECK, J. E. and ROKHSAZ, K., “Use of neural networks in control of high alpha maneuvers,” in *AIAA Aerospace Sciences Meeting and Exhibit, 30th*, AIAA-92-0048, Jan. 1992.
- [111] STEINBERG, M., “Potential role of neural networks and fuzzy logic in flight control design and development,” in *Proceeding of AIAA Aerospace Design Conference*, AIAA-1992-0999, Feb. 1992.
- [112] STEINBERG, M., “An initial assessment of neural network and fuzzy logic technology for flight control systems,” in *Proceeding of American Control Conference*, vol. 1, pp. 173–177, June-July 1994.
- [113] STENGEL, R. F., “Toward intelligent flight control,” *IEEE Transactions on Systems, Man, and Cybernetics*, vol. 23, no. 6, pp. 1699–1717, 1993.
- [114] TAO, G., *Adaptive Control Design and Analysis*. Hoboken, New Jersey: Wiley-Interscience, John Wiley & Sons, 2003.
- [115] VIDYASAGAR, M., *Nonlinear Systems Analysis*. New Jersey: Prentice-Hall, 2nd ed., 1993.
- [116] WANG, Q. and STENGEL, R. F., “Robust nonlinear flight control of a high-performance aircraft,” *IEEE Transactions on Control Systems Technology*, vol. 13, no. 1, pp. 15–26, 2005.
- [117] WERBOS, P. J., “Neural networks and flight control - overview of capabilities and emerging applications,” in *AIAA Guidance, Navigation and Control Conference*, pp. 912–919, AIAA-1995-3272, Aug. 1995.

- [118] WERBOS, P. J., “Neural networks for flight control - a strategic and scientific assessment,” in *Virtual intelligence; Workshops on Virtual Intelligence: Neural Networks, Fuzzy Systems, Evolutionary Systems, and Virtual Reality, 6th, 7th, and 8th*, pp. 10–20, SPIE Proceedings. Vol. 2878, Jan. 1996.
- [119] WIDROW, B. and LEHR, M. A., “30 years of adaptive neural networks: Peceptron, madaline, and backpropagation,” *Proceeding of the IEEE*, vol. 78, pp. 1415–1442, Sept. 1990.
- [120] WILLIAMS-HAYES, P. S., *Selected Flight Test Results for Online Learning Neural Network-Based Flight Control System*. NASA Technical Memorandum, NASA/TM-2004-212857, NASA Dryden Flight Research Center, Feb. 2005.
- [121] WISE, K. A. and BROY, J. B., “Agile missile dynamics and control,” *Journal of Guidance, Control, and Dynamics*, vol. 21, pp. 441–449, May-June 1998.
- [122] WISE, K. A., BRINKER, J. S., CALISE, A. J., ENNS, D. F., ELGERSMA, M. R., and VOULGARIS, P., “Direct adaptive reconfigurable flight control for a tailless advanced fighter aircraft,” *International Journal of Robust and Nonlinear Control*, vol. 9, pp. 999–1012, 1999.
- [123] YOSHIZAWA, T., *Stability Theory by Liapunov’s Second Method*. Tokyo, Japan: The Mathematical Society of Japan, 1966.
- [124] ZHANG, Y. and IOANNOU, P. A., “Stability and performance of nonlinear robust adaptive control,” in *Proceeding of the 34th Conference on Decision and Control*, pp. 3941–3946, Dec. 1995.

VITA

Yoonghyun Shin was born in Young-am, Korea on October 1, 1967. He received the B.Sc. and M.Sc. degrees in Aerospace Engineering at Inha University, Korea, in 1992 and 1994, respectively. Since 1994, he has been with the Korean Agency for Defense Development (ADD) as a research engineer and later as a senior research engineer. He has worked for the enhancement of spin characteristics of the Korean KT-1 Turbo-prop military trainer aircraft, and he is very proud of the world's best class spin performance of the vehicle.

In Spring 2001, he began his studies for a Ph.D degree at Georgia Institute of Technology, Atlanta, Georgia, USA. Since September 2001, he worked with Professor Anthony J. Calise for a NASA Langley project titled "Neural Network Based Adaptive Control for Non-linear Flight Regimes," and all the research associated with this project has been included in his Ph.D dissertation. He received another M.Sc. degree in Aerospace Engineering at Georgia Institute of Technology in 2004.

His current research interests include adaptive control design methodologies using neural networks, advanced flight control technologies, supermaneuvers of aerial vehicles at high angle of attack, digital fly-by-wire/light (DFBW or DFBL) control systems, and control designs and applications of nonlinear systems in various fields.